

## 11. SITE 918<sup>1</sup>

### Shipboard Scientific Party<sup>2</sup>

#### HOLE 918A

**Date occupied:** 26 October 1993  
**Date departed:** 28 October 1993  
**Time on hole:** 1 day, 20 hr, 15 min  
**Position:** 63°5.569'N, 38°38.336'W  
**Bottom felt (drill-pipe measurement from rig floor, m):** 1879.7  
**Distance between rig floor and sea level (m):** 11.2  
**Water depth (drill-pipe measurement from sea level, m):** 1868.5  
**Total depth (from rig floor, m):** 2212.4  
**Penetration (m):** 332.7  
**Number of cores (including cores having no recovery):** 38  
**Total length of cored section (m):** 332.7  
**Total core recovered (m):** 260.27  
**Core recovery (%):** 78.2  
**Oldest sediment cored:**  
Depth (mbsf): 332.7  
Nature: micritic mudstone and quartz silt with clay and gravel  
Age: Pliocene  
Measured velocity (km/s): 1.75

#### HOLE 918B

**Date occupied:** 28 October 1993  
**Date departed:** 28 October 1993  
**Time on hole:** 4 hr, 45 min  
**Position:** 63°5.568'N, 38°38.339'W  
**Bottom felt (drill-pipe measurement from rig floor, m):** 1879.4  
**Distance between rig floor and sea level (m):** 11.2  
**Water depth (drill-pipe measurement from sea level, m):** 1868.2  
**Total depth (from rig floor, m):** 1905.2  
**Penetration (m):** 25.8  
**Number of cores (including cores having no recovery):** 3  
**Total length of cored section (m):** 25.8  
**Total core recovered (m):** 25.48  
**Core recovery (%):** 98.8  
**Oldest sediment cored:**  
Depth (mbsf): 25.8  
Nature: silt with sand  
Age: Quaternary  
Measured velocity (km/s): 1.6

#### HOLE 918C

**Date occupied:** 28 October 1993  
**Date departed:** 28 October 1993  
**Time on hole:** 9 hr, 30 min  
**Position:** 63°5.575'N, 38°38.328'W  
**Bottom felt (drill-pipe measurement from rig floor, m):** 1879.4  
**Distance between rig floor and sea level (m):** 11.2  
**Water depth (drill-pipe measurement from sea level, m):** 1868.2  
**Total depth (from rig floor, m):** 1914.8  
**Penetration (m):** 35.4  
**Number of cores (including cores having no recovery):** 2  
**Total length of cored section (m):** 9.6  
**Total core recovered (m):** 9.64  
**Core recovery (%):** 100.4  
**Oldest sediment cored:**  
Depth (mbsf): 35.4  
Nature: gravel  
Age: Quaternary  
Measured velocity (km/s): 1.6  
**Comments:** Drilled from 0.0 to 25.8 mbsf

#### HOLE 918D

**Date occupied:** 28 October 1993  
**Date departed:** 13 November 1993  
**Time on hole:** 15 days, 4 hr, 45 min  
**Position:** 63°5.572'N, 38°38.334'W  
**Bottom felt (drill-pipe measurement from rig floor, m):** 1879.4  
**Distance between rig floor and sea level (m):** 11.2  
**Water depth (drill-pipe measurement from sea level, m):** 1868.2  
**Total depth (from rig floor, m):** 3189.50  
**Penetration (m):** 1310.1  
**Number of cores (including cores having no recovery):** 113  
**Total length of cored section (m):** 1012.8  
**Total core recovered (m):** 254.58  
**Core recovery (%):** 25.1  
**Oldest sediment cored:**  
Depth (mbsf): 1189.4  
Nature: glauconitic sandy silt  
Age: early Eocene  
Measured velocity (km/s): 2.1  
**Hard rock:**  
Depth (mbsf): 1310.1  
Nature: basalt  
Measured velocity (km/s): 4.0

<sup>1</sup> Larsen, H.C., Saunders, A.D., Clift, P.D., et al., 1994. *Proc. ODP, Init. Repts.*, 152: College Station, TX (Ocean Drilling Program).

<sup>2</sup> Shipboard Scientific Party is as given in the list of participants preceding the contents.

**Basement:**

Depth (mbsf): 1310.1  
 Nature: basalt  
 Measured velocity (km/s): 4.0

**Comments:** Drilled 0–253.2, 279.9–324; sill, 1168.2–1180.4 mbsf

**Principal results:** Site 918 is located near the center of the seaward-dipping reflector sequences (SDRS) on the upper continental rise of the Southeast Greenland Margin, approximately 130 km from the Greenland coast. The site was selected to study the age and emplacement environment of the SDRS, the history of East Greenland glaciation, the subsidence history of the Irminger Basin, and the early formation of North Atlantic Deep Water.

The principal drilling results from Site 918 are summarized in Figure 1. The 1189.4-m-thick sedimentary section has been divided into five lithologic units. Lithologic Unit I (0–600.0 mbsf; Holocene to Miocene) is predominantly dark gray silt with both volcanoclastic and continentally derived components. The unit is divided into five subunits, based on the presence of turbidites and the proportion of ice-rafted debris. Unit II (600–806.5 mbsf; upper Miocene to lower Miocene) is 206.5 m thick, composed of nannofossil chalk and silt and is moderately to heavily burrowed. Frequent micritic and glauconitic hardgrounds occur at the base and top of this unit. The silt bands contain a mixed suite of minerals derived from both volcanic and continental terrains.

Lithologic Unit III (806.5–1108.2) mbsf; lower Miocene to upper Oligocene) is made up of sand, silt, and nannofossil chalk and is divided into two subunits. Subunit IIIA constitutes interbedded sands and nannofossil chalk; Subunit IIIB comprises massive, quartz-rich turbiditic sands that are intermittently heavily bioturbated. Dolomite is a common constituent in the lower subunit, and glauconite pellets increase downcore. A layer of unconsolidated gravel occurs at the base of Unit III.

Lithologic Unit IV (1108.2–1157.9 mbsf; middle to lower Eocene) is 49.7 m thick and comprises interbeds of nannofossil chalk and volcanoclastic silt with nannofossils.

Lithologic Unit V (1157.9–1189.4 mbsf; lower Eocene) is 31.5 m thick and consists of glauconitic sandy silt with interbeds of calcareous sand.

A diverse nannofossil assemblage is present in Sample 152-918D-93R-CC (1168 mbsf), which can be assigned to Zones CP96 through CP10 (early Eocene). Slightly older sediment from Sample 152-918D-95R-CC (1183 mbsf) yielded only a few nannofossil specimens. Although these specimens did not allow a useful age determination, they did indicate that the sediment was deposited in open-marine conditions. Lower Eocene benthic foraminifers from Samples 152-918D-92R-CC and -93R-CC indicate a paleowater depth of between 75 and 200 m for the interval between 1160 and 1168 mbsf.

Eighteen biostratigraphic data points were used to construct an age-vs.-depth diagram and to calculate accumulation rates for the sedimentary sequence at Site 918. The sedimentation rate for the Pleistocene–Holocene interval is on the order of 8 cm/k.y. This is comparable to that estimated for Site 914 on the continental shelf. The Pliocene section has a high sedimentation rate (20 cm/k.y.), which suggests a significant contribution of ice-rafted material during that time. The Miocene has a sedimentation rate of about 2 cm/k.y. The upper Oligocene turbidite sequence also has a high sedimentation rate (5 cm/k.y.). An unconformity separates the upper Oligocene and middle Eocene. A very low sedimentation rate (0.4 cm/k.y.) characterizes the middle and lower Eocene interval.

Basalt was first encountered in Core 152-918D-93R at 1168.2 mbsf. Although only 2.8 m was recovered, this unit may have been as much as 12 m thick. It constitutes dark gray, holocrystalline basalt with glomerocrysts of plagioclase and clinopyroxene and less than 1% olivine micropheocrysts. Secondary alteration has been restricted to slight clay development in the mesostasis and in the rims of olivines. Compositionally, the rock is an evolved tholeiite, with 5.1% MgO and 66 ppm Ni, and 3 wt% TiO<sub>2</sub>. The high Zr/Y (6.7) and low Zr/Nb (6.5) values of this basalt indicate affinities with Icelandic tholeiites. The unit may represent a sill or a flow; no contacts were recovered. Below this unit, a further 9.3 m of sedimentary rocks lies above the main basaltic basement.

Hole 918D reached basaltic basement at 1189.4 mbsf. Deep (17.7 m), subaerial weathering has affected the top three flow units, which have been

completely oxidized and altered to clay (lithologic Unit VI, 1189.4–1204.4 mbsf). The first rock preserving any original minerals was encountered at 1206.0 mbsf (Core 152-918D-98R-2, 65 cm). From there to the bottom of the hole (at 1310.1 mbsf), 18 flow units were identified. The upper units were separated by altered basaltic breccia, which was generally severely disturbed by drilling and, in places, had been reduced to gravel. Therefore, the breccia is of indeterminate origin, although some of it may be hyaloclastite.

The proportion of breccia decreases with depth and is last seen beneath Unit 12 at 1264.8 mbsf. Units 13 to 19 are separated by reddened flow tops, where these have been recovered. No evidence for submarine eruption was found, although the upper flow units may have been erupted into shallow water or across a wet substrate.

All of the flow units consist of aphyric tholeiite, with little mineralogical or compositional variation. They contain 7.1% to 8.8% MgO, 70 to 84 ppm Ni, and are highly depleted in incompatible elements (K<sub>2</sub>O < 0.1%, Nb < 3 ppm). High Zr/Nb values (16–30), and low Zr/Y values (1.6–2.2) are similar to depleted mid-ocean ridge basalts (MORB). Low concentrations of Ba, K<sub>2</sub>O, and Sr are consistent with derivation from a depleted MORB source.

Hole 918A reveals a detailed record of normal and reversed magnetozones. The normal polarity sediment in the interval between Interval 152-918A-1H-1, 0 cm, and -7H-3, 60 cm, have been correlated mainly with the Brunhes Chron; the predominantly reversely magnetized interval below this is correlated with the Matuyama Chron. A marked hiatus may occur in the sedimentary record between these two events, which has led to the omission of the Jaramillo Event. The Interval 152-918A-10H-3, 30 cm, to -11H-6, 90 cm, has been tentatively correlated with the Olduvai Event, and the interval from 152-918A-16H-1, 0 cm, to -18H-4, 150 cm, contains normal polarities associated with the Réunion event. For much of the succession in Hole 918D, and particularly the Miocene, firm magnetochron assignments were not possible. Lower Eocene (CP9b–CP10) sediments immediately overlying basement are reversely magnetized and possibly correlate with Chron C24r. All of the measured basalts from the volcanic basement are reversely magnetized. From the biostratigraphic evidence, this interval is likely to be Chron C24r, but radiometric data will be needed to confirm this.

Monitoring of light hydrocarbons C1 to C3 showed a significant increase of methane (up to 80,000 ppm) in the sediments between 80 and 470 mbsf. Above and below this interval, very low values occur. This increase is consistent with a zone of low sulfate concentrations and indicates methane generation from the in situ decay of organic matter, rather than migration from lower parts of the sequence. The content of organic matter within the sediments is low. The correlation between organic carbon and the organic carbon/nitrogen ratios indicates a marine background sedimentation enhanced by an episodic supply of terrigenous organic matter, causing elevated organic carbon spikes. Carbonate contents vary between 0 and 10 wt% in the upper 600 m and increase dramatically (up to 40 wt%) in the lower parts of the succession.

Initial results from the interstitial-water chemistry reveal: (1) concentrations of dissolved chloride in the upper 100 mbsf show a maximum at about 50 mbsf, most likely imprinted by a higher salinity seawater during the glacial maximum; (2) concentrations in calcium, magnesium, and chloride show extremes in their concentration/depth profiles at about 550 mbsf, related to the alteration of volcanic matter at this level; (3) below 825 mbsf (i.e., in the zone characterized by the occurrence of sandy and silty deposits), chloride concentrations decline as much as 5% below seawater values. Some of these lower chloride fluids may have undergone lateral transport along sand horizons.

The water sampling and temperature probe (WSTP) was deployed in Hole 918A, with two successful runs for temperature and three successful runs for interstitial water. Temperatures at 142 and 198 mbsf suggest a linear gradient in the top 200 m of Site 918, with a gradient of 5.6°C/100 m and a heat flow of 75 ± 8 mW/m<sup>2</sup>. This heat flux is similar to other observations in the Irminger Basin.

Based principally on MST and index property data, 12 mechanical units can be defined for Site 918. Few of the boundaries between these units

correspond with the lithologic units described above, but MST and discrete property measurements do reveal and corroborate detailed sedimentary features, such as glauconitic hardgrounds, diamictons, and fining-upward sequences. GRAPE bulk density data, natural gamma, and magnetic susceptibility measurements proved particularly useful for detecting these features. Mean thermal conductivity in the sediments ranges from 1.1 to 1.70 W/(m·K). In the basalts, thermal conductivity ranges from 1.5 to 1.8 W/(m·K).

## BACKGROUND AND SCIENTIFIC OBJECTIVES

### Introduction

Site 918 is located in 1868.5 m of water on the upper continental rise of southeast Greenland within the western part of the Irminger Basin. The site is located within the middle of the planned EG63 transect (planned Site EG63-2, see Figs. 5 and 6, "Introduction" chapter, this volume). Our primary objective at Site 918 was to sample the volcanic basement within the SDRS in a position where the process of the anomalously thick, igneous crustal accretion represented by the SDRS is likely to have operated in a steady-state mode, and with a minimum of influence from the continental lithosphere. To this end, a location within the central part of the approximately 150-km-wide SDRS was chosen. The site was selected away from areas of late, post-SDRS volcanic activity, which would represent off-axis volcanism and which can be observed on the seismic profiles.

The volcanic basement is covered with approximately 1200 m of sediments at Site 918. Site objectives within the sediments were to determine (1) the age and subsidence history of the SDRS; (2) the overflow history of cold, oxygenated water from the Norwegian-Greenland Sea across the Faeroe-Iceland-Greenland Ridge into the Irminger Basin; (3) the evolution of Icelandic and breakup volcanism recorded in the basin by tephra and ash layers, and (4) the history of glaciation in southern Greenland. With respect to the last of these, Site 918 is ideally located close to the margin and has a thick, potentially high-resolution Quaternary section.

Site 918 is located approximately 70 km seaward of the shelf Site 914. The crust at Site 918 is assumed to be entirely of igneous ("oceanic") origin. It is located within a broad magnetic low landward of seafloor spreading anomalies 24n.1n through 24n.3n (Fig. 7, "Introduction" chapter, this volume). This broad magnetic low is considered to be of magnetic chron C24r age. However, a number of positive, low-amplitude anomalies can be recognized and also partly correlated from line to line. As the top surface of the SDRS is essentially flat, nonfaulted, and only shows sparse evidence of late volcanism, the low-amplitude anomalies are likely to reflect primary variations in the magnetic field during deposition of the SDRS. These anomalies can represent true and, hence, pre-anomaly Chron 24n.3n normals, or they may have resulted from short field excursions and/or intensity variations, such as the cryptochrons of Cande and Kent (1992).

No specific underway geophysical survey was done to locate Site 918. The position of the site was determined by coordinates from the preexisting site-survey data (see "Pre-cruise Site Surveys" chapter, this volume). Correlation of 12.5-kHz precision depth recorder data with the seabed topography was done during the approach to the site. The site is located at the intersection of high-resolution seismic Lines GGU/EG92-24 and GGU/EG92-14 (Fig. 2). The drill site is very close to the deep seismic Line GGU81-08 that was used for original planning of the site.

The depths and thicknesses referred to in the following section were derived from a preliminary two-way traveltime-vs.-depth relationship (Fig. 3), established from seismic velocities measured in the cores recovered at Site 918.

### Seismic Stratigraphy

#### Volcanic Basement

Within the central part of the SDRS, the top of the volcanic basement generally forms a smooth and, in most cases, well-defined

seismic stratigraphic boundary. The boundary is generally defined by strong seismic reflections. However, the best and most reliable definition is obtained by applying seismic stratigraphic principles. The characteristic upward termination of the internal reflectors within the SDRS tends to form an unconformity between the SDRS and the overlying sediments and, possibly, some late-stage volcanic rocks (Fig. 4). This surface may not be a true unconformity in a strict chronostratigraphic sense, because sediments almost coeval with the very last volcanism may be present right on top of the volcanic basement, or between the upper lava flows. In most areas, a thin (75–150 m) layer of high-amplitude reflections is present between the seismic stratigraphically defined unconformity and the overlying, lower-amplitude reflecting sediments. The reflection pattern within this zone was difficult to interpret as it most likely comprised strongly contrasting lithologies, such as sediments, lavas, and hyaloclastics (Sequence 4 of Fig. 4). Reflections can vary from one or two fairly continuous, horizontal reflections, to more hummocky type reflectors and can also include diffractions (Fig. 4). In some places, this boundary layer can develop to several hundred meters in thickness and, clearly, may have the characteristics of a late, volcanic mound. An example of this is present 3.5 km west of Site 918.

At Site 918, the transition zone of high-amplitude reflectors between the main SDRS and the overlying main sediment column is 100 m thick. The zone is characterized by high-amplitude reflectors, which form regular mounds with a spacing of about 500 m and heights of 15 to 30 m. The thickness of the zone is increasing to about 170 m on the flank of the volcanic hill southeast of Site 918. Northwest of the site, the thickness decreases, and the zone pinches out at the volcanic basement below the flank of the volcanic hill northwest of Site 918 (Fig. 4).

#### Sediments

High-resolution and deep reflection-seismic profiles show that the slope fill at Site 918 on the continental rise is composed of a number of seismic stratigraphic sequences. Thus, the approximately 1200-m-thick sediment column over the volcanic basement at Site 918 can be divided into four seismic stratigraphic sequences, which, in a general sense, can be correlated with the sequences found on the shelf transect through Sites 914 to 917 (Fig. 2, and "Shelf Stratigraphic Summary" chapter, this volume).

The lower boundary of the lowermost sequence (Sequence 4) is defined by the low-angle unconformity at the top of the SDRS. Thus, Sequence 4 embraces the volcanic elements included in the transition zone below the mounded reflector described above. The upper boundary is marked by a high-amplitude reflector that interdigitates with the supposedly volcanic mounds on either side of Site 918. At Site 918, Sequence 4 is found in the interval from 1115 to 1265 mbsf. The internal reflectors in Sequence 4 have strong amplitudes and high continuity. In the lowermost part of the sequence, the internal reflectors either are concordant with the surface of the volcanic basement or they form regular mounds, as described above. The reflectors in the upper part of Sequence 4 drape over the mounds and, to a certain degree, level off the topography of the mounds. Though somewhat wavy, the surface of Sequence 4 is nearly concordant with the surface of the volcanic basement. Laterally, Sequence 4 interdigitates with the volcanic mounds in the vicinity of Site 918 (Fig. 4).

Sequence 3 rests partly on Sequence 4 and partly on the volcanic mounds. Internal reflectors overlap the flanks of the volcanic mounds and downlap onto the top of Sequence 4. The upper boundary of Sequence 3 is defined by a coherent, high-amplitude reflector onto which the internal reflectors of the overlying Sequence 2 downlap. Toplap or truncation of the internal reflectors in Sequence 3 at the top of Sequence 3 is indicated at a few places. The total thickness of Sequence 3 at Site 918 is about 650 m (465–1115 mbsf). Thus, this sequence constitutes more than one-half of the sedimentary column at Site 918.

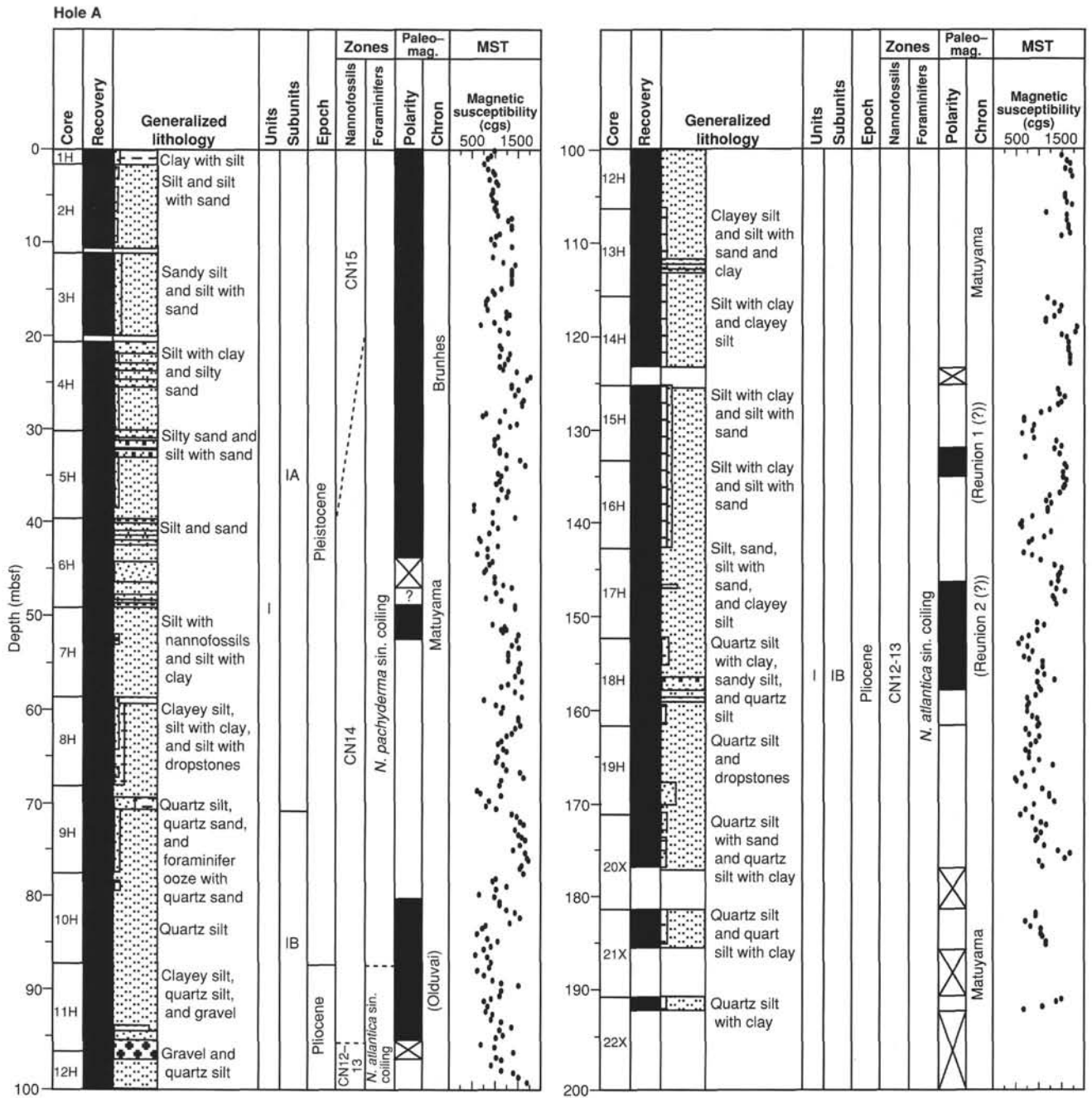


Figure 1. Site summary for Site 918.

Internally, Sequence 3 can be divided into two intervals of approximately equal thickness (300 m). They are separated by a seismic unconformity, where the reflectors in the lower interval show toplap or truncation and onto which the reflectors in the upper interval downlap. The lower interval is characterized by closely spaced, coherent reflectors having high amplitudes, in contrast to the upper interval, which is nearly transparent, except for a few marked reflectors in the lower part. The reflectors in the lower interval are subparallel or tend to converge in a basinward direction. In the lower part of the upper interval of Sequence 3, two coherent reflectors border a sheet that is internally transparent, except for a few reflectors forming shingled or mounded patterns. The thickness of the sheet at Site 918 is about 125 m (645–770 mbsf). The sheet thins slightly on either side of Site 918.

The internal reflectors in the lower part of Sequence 2 show downlap onto the basinward inclined top surface of Sequence 3 (Figs. 4 and 5). The top of Sequence 2 is defined by erosional truncation of internal reflectors (Fig. 5). The thickness of Sequence 2 at Site 918 is about 397 m (68–465 mbsf). Internally, Sequence 2 is composed of two subsequences (2A and 2B).

Subsequence 2B is bounded on its upper surface by an unconformity defined by apparent truncation of the internal reflectors. Subsequence 2B thins basinward, with thicknesses that decrease from about 200 m west of Site 918 to about 100 m east of the site. At Site 918, the thickness is approximately 160 m (305–465 mbsf). The lower part of Subsequence 2B is almost transparent, whereas high-amplitude, coherent, and parallel reflectors are seen near the top of

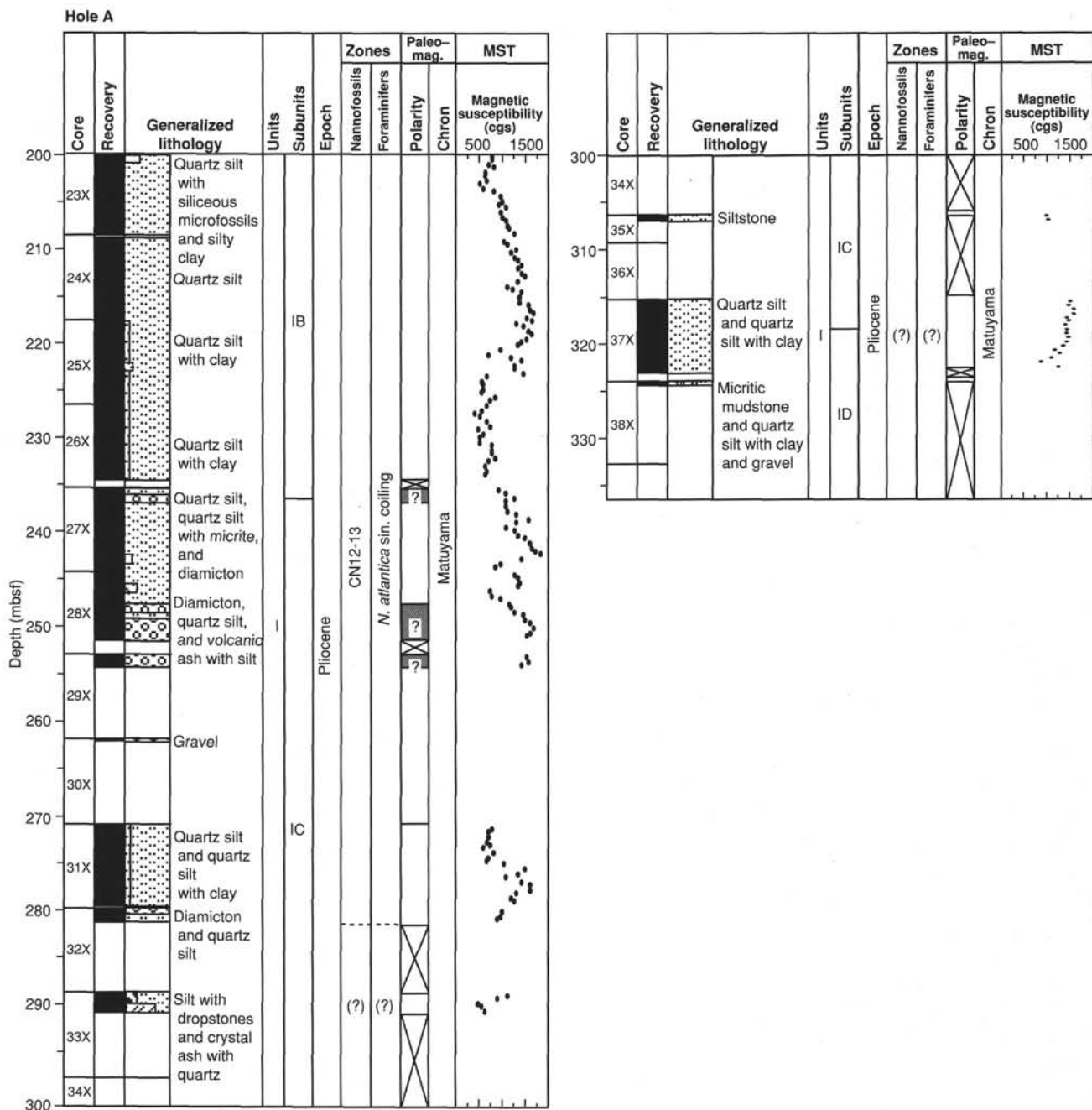


Figure 1 (continued).

the subsequence. The reflector spacing is approximately a constant 20 m at Site 918, decreasing somewhat in a basinward direction.

In Subsequence 2A, the lowermost reflectors onlap the basinward dipping basal unconformity. For purposes of description, Subsequence 2A has been divided into two intervals, with characteristic external shapes and internal reflector configurations. The lowest interval is a wedge thinning in a landward direction, which is about 58 m thick at Site 918 (247–305 mbsf). Internal reflectors are generally parallel or basinward diverging. Amplitudes are strong near Site 918, but generally decrease basinward. The wedge is overlain by a transparent sheet, which pinches out about 3 km southeast of Site 918.

The transparent sheet is covered by an interval with a mounded reflector configuration. In the lower part, the mounds are 0.5 to 1.0 km wide and 30 to 40 m high. Internal reflectors apparently have been

truncated at the flanks of the mounds. The reflectors above the mounds are concordant with the surface of the mounds. The mounded interval is capped by a reflector, which, in the vicinity of Site 918, has high amplitude and continuity. At Site 918, the thickness of the mounded interval is 66 m (159–225 mbsf).

The upper interval in Sequence 2A is characterized by parallel internal reflectors, which in the lower part, tend to be concordant with the surface of the mounded interval, but in the upper part, the reflectors are almost horizontal.

The erosional unconformity, which forms the base of Sequence 1, cuts deeply into Sequence 2 in the vicinity of Site 918. Site 918 is located in a local erosional channel, whose floor lies about 65 m below the present seafloor (Fig. 4). The seafloor forms the top surface of Sequence 1. In general, internal reflectors are concordant with the

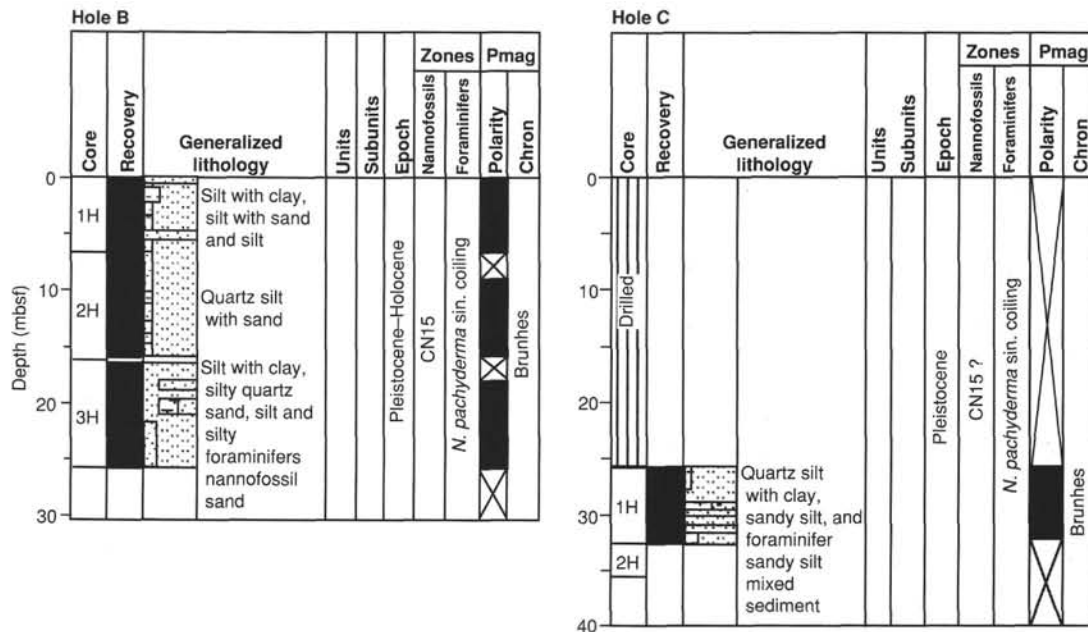


Figure 1 (continued).

seafloor, but local erosion in channel structures occurs, and local, very thin (10 m), post-Sequence 1 infill may be present in such places. A 1- to 2-km-wide depression in the seafloor is located about 2 km on the landward side of Site 918, below which Sequence 1 is only about 40 m thick (Fig. 4). However, the channel relief is not entirely erosional and, for a large part, is also constructional.

At Site 918, at least 55 m of material has been removed from Sequence 2 prior to deposition of Sequence 1, and even deeper erosion is indicated landward of Site 918 (Fig. 5). The internal reflectors in Sequence 1 are tightly spaced and have an extremely high continuity and short period length. The amplitudes are moderate, with a few pronounced exceptions in the vicinity of Site 918. Internal reflectors in Sequence 1 onlap the eroded flanks of the erosional depressions cut into Sequence 2. In the local depression at Site 918, internal reflections both onlap and downlap onto the basal unconformity and form a fill, up to about 25 m thick, that progrades in the landward direction. At this level, a minor, internal unconformity is seen. Above this unconformity, reflectors are largely concordant with the seafloor and dip gently toward the depression in the seafloor, suggesting a partly constructive origin of the seafloor topography. Local truncation (toplap) of internal Sequence 1 reflectors seems locally to occur below a recent, thin (10 m) layer at the sea bed.

**Summary of Site Objectives**

The main objectives at Site 918 can be summarized as follows:

1. Deep basement sampling to determine the composition of the SDRS and its possible variation with depth, the magnetic polarity of the SDRS in this position, and the age and emplacement environment of the SDRS.
2. Sampling of the top of the SDRS and overlying sediments to characterize the emplacement environment and the age of the youngest volcanism using combined biostratigraphy and magnetostratigraphy.
3. Sampling of the Paleogene sediments overlying the SDRS to determine the initial subsidence of the SDRS and to provide detailed correlation of important biostratigraphic and magnetostratigraphic events within the Eocene.
4. Sampling the Neogene sediments to study Northern Hemisphere cooling, in particular, introduction of North Atlantic Deep Water into the basin, cooling of the surface water, and onset and history of glaciation in southern Greenland.

Important and, in part, excellent results were obtained for all four objectives. In particular, the recovery of ice-rafted material and diamicton down to 543.6 m (upper Miocene) was a major discovery. However, the basement penetration obtained (121.6 m) was not sufficient to establish whether a systematic geochemical trend with depth is present within the SDRS, although the data obtained do not indicate such behavior. Likewise, the fairly thin Eocene section present at Site 918 is not as ideal as had been expected for general magnetostratigraphic and biostratigraphic correlations. In summary, Objectives 1 and 3 were met, with some deficiencies, and Objectives 2 and 4 were fully met.

**OPERATIONS**

**Hole 918A**

After a short 3.5-kHz seismic survey of the area, a beacon (Datasonics Model 354B, 15 kHz, 208 dB, s.n. 754) was dropped on location at 1100 hr on 26 October. The vessel came about and was lowering thrusters and hydrophones over location by 1130 hr. The advanced-piston core/extended-core barrel (APC/XCB) bottom-hole assembly (BHA) was made up with a nonmagnetic drill collar and a used RBI C-3, 11 7/16-in. bit. The BHA was run in the hole, and at 1615 hr, the first APC core was shot. We recovered 1.81 m of clayey silt and established the mud line at 1868.5 mbsf. The corrected precision depth recorder reading normalized to driller's datum was 1877.0 m.

APC-coring advanced through clay and silt, peppered with gravel and glacial dropstones, until a refusal depth of 171.3 mbsf (Core 152-918A-19H) was reached. Table 1 documents this and all coring activity at Site 918. From the APC-cored interval, we recovered 171.48 m (101.3% of the interval cored). The cores were oriented, starting with Core 152-918A-4H, and successful water sampling/temperature probe (WSTP) runs were conducted at 49.3, 96.8, 152.3, and 190.9 mbsf. Biogenic methane was present in concentrations as high as 85,000 ppm and was responsible for some core expansion. Ethane was detected at a level of 1 ppm.

The XCB was deployed, and XCB-coring advanced from 171.3 to 332.7 mbsf. The interval cored was 161.4 m long, with a recovery of 86.8 m (53.8%). The XCB-coring system was able to penetrate the soft formation readily, but the increasing numbers of glacial dropstones jammed liners, core-catchers, and cutting shoes. In addition, seven XCB cutting shoes were destroyed as a result of trying to core

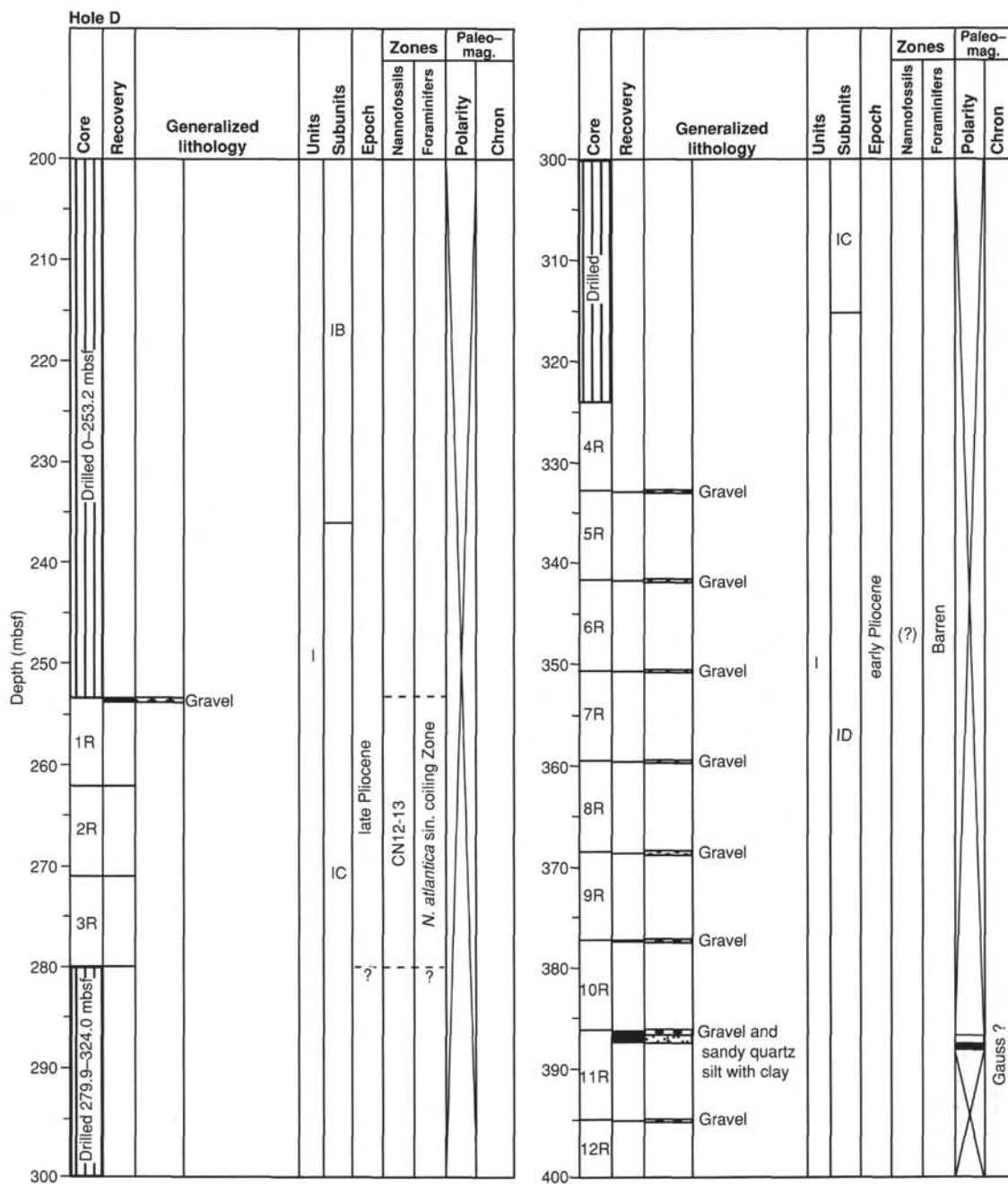


Figure 1 (continued).

the soft sediment littered with hard glacial cobbles. At a depth of 332.7 mbsf, we terminated XCB-coring as a result of the poor recovery and ineffectiveness of the XCB-coring system when recovering these sediments. At 0600 hr on 28 October, the drill pipe was pulled to the surface, with the bit clearing the mud line at 0715 hr. After the vessel was offset 10 m south, Hole 918B was initiated.

**Hole 918B**

From the first core barrel taken in Hole 918B, we recovered 6.85 m of sediment and established the mud line for Hole 918B at 1868.2 mbsl. A total of three piston cores were obtained from this hole. The second core barrel was bent by dropstones and we could just barely retract it into the outer barrel. The third core barrel became stuck and had to be worked for several minutes before it could be freed and

retrieved. At this point, the hole was terminated and the bit pulled to the surface. The bit cleared the seafloor at 1200 hr on 28 October.

**Jet-in Test**

The vessel was offset 10 m northeast, and a jet-in test was conducted. The bit was set on bottom with approximately 5 kips weight on bit (WOB) and the mud pump was set to 40 strokes per minute (spm). It took 1.5 hr to advance the bit to 39.3 mbsf.

**Hole 918C**

The vessel was not offset for the third APC hole. The bit was washed down to 25.8 mbsf, and the first core obtained. The second piston core fired, but did not advance, as indicated by the absence of pres-

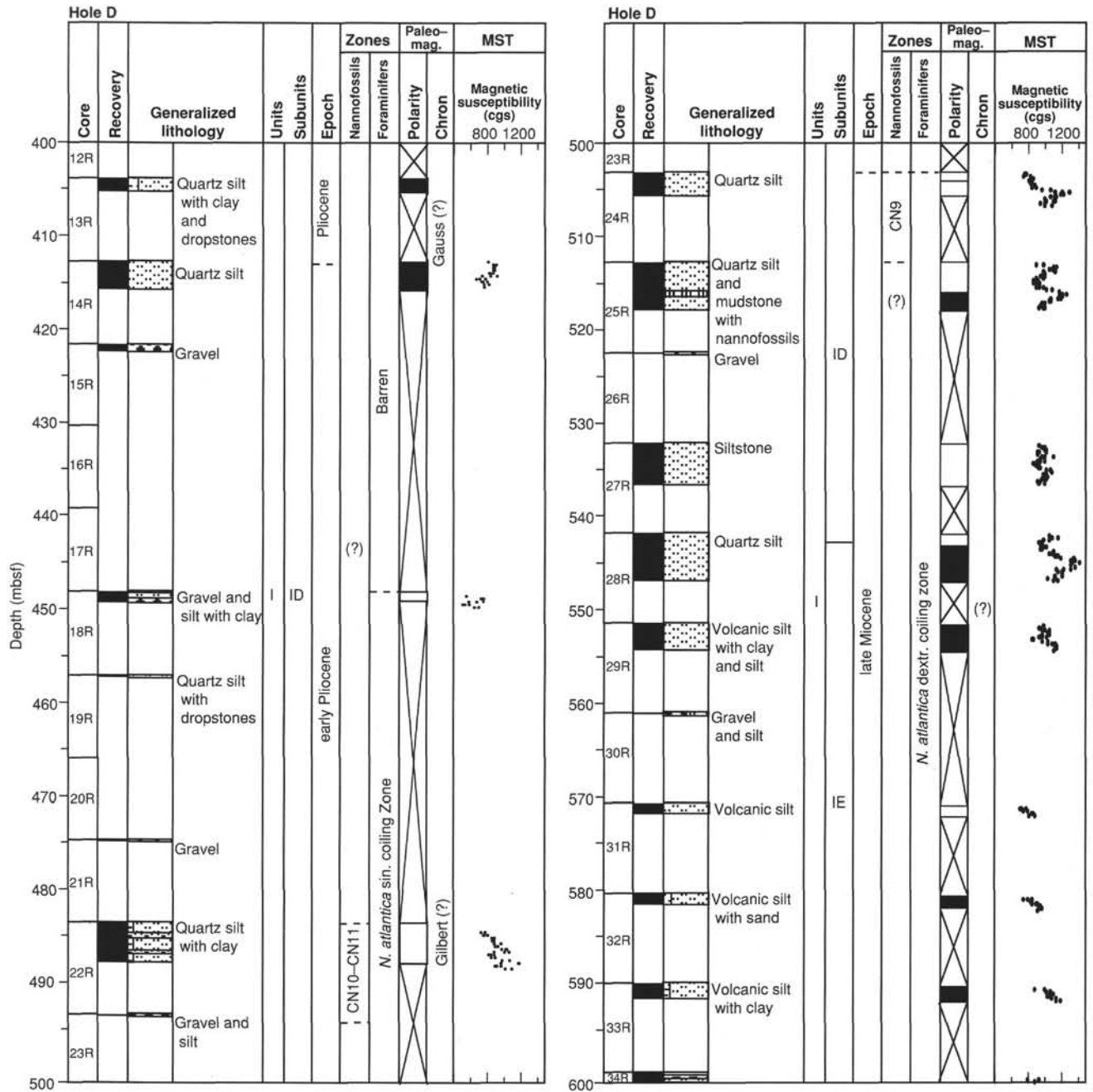


Figure 1 (continued).

sure bleeding down into the pipe. The core barrel was retrieved with a piece of rock jammed into the cutting shoe. With time dwindling for the unplanned APC hole, operations were terminated, and the bit was pulled to the surface. At 2130 hr on 28 October, the bit was on deck.

**Hole 918D**

Because more than the allotted time was spent in operations at Site 917, the RCB pilot hole was combined with the reentry hole. Our plan was to wash in a reentry cone with 33 m of 16-in. casing, unlatch the paddle running tool, and drill ahead to 253.2 mbsf, where RCB-coring would be resumed. Coring would then proceed into basement without setting the 11 3/4-in. casing. If an additional string of casing were required, then the hole would be opened with a 14 3/4-in. drill bit and the casing installed.

After a reentry cone was assembled and moved into the moon pool, the BHA with the paddle running tool (PRT) was made up with two joints of 16-in. casing and a Texas-patterned running shoe (33 m). The hanger was picked up and the PRT was then made up to the casing and cone.

At 0600 hr on 29 October, the reentry cone and 33 m of 16-in. casing were run to bottom. After a 2-hr jet-in procedure, the PRT shifting tool was run down by wireline; it released the PRT bushing from the BHA. The drilling assembly was then drilled ahead to 253 mbsf with a center bit. A 10-bbl high-viscosity mud pill was circulated after every third connection. At 2000 hr on 29 October, a core barrel was dropped and coring initiated. After coring from Cores 152-918D-1R to -3R (253.3–279.9 mbsf), and recovering only 0.60 m of glacial till, a center bit deplugger was dropped on the core barrel for Core 152-918D-4R, and the bit was drilled ahead another 41.1 m, where, again, coring resumed.

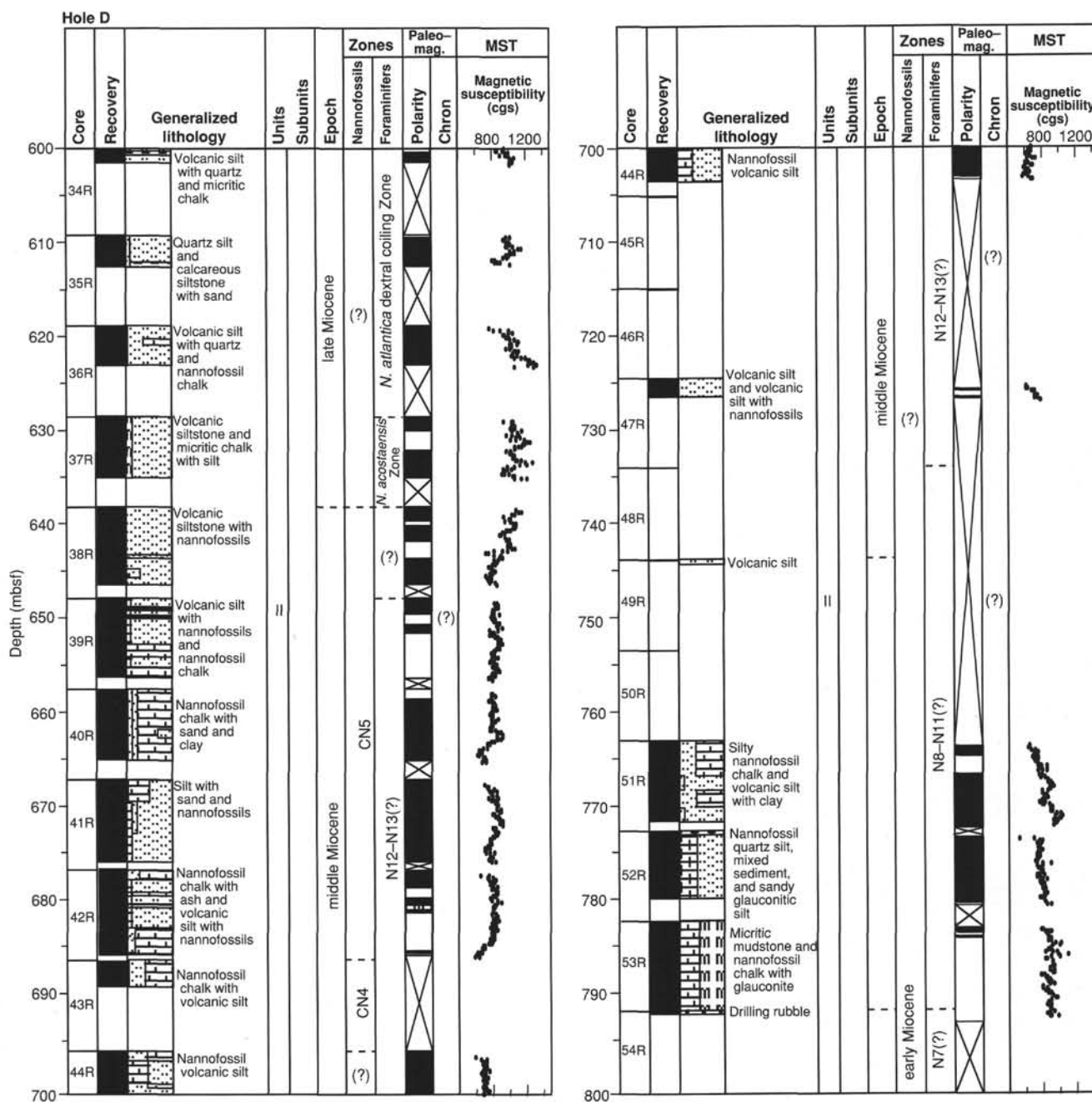


Figure 1 (continued).

RCB-coring then advanced from 324.0 to 696.1 mbsf with a 10-bbl high-viscosity mud pill circulated before every connection. At 0615 hr on 1 November, coring was interrupted for a wiper trip. The drill pipe was pulled in stands up to 288 mbsf, without experiencing overpull. The pipe was run down to 667 mbsf, where it encountered 30 m of fill. The top drive was picked up and the hole washed and reamed to bottom, after which a 15-bbl high-viscosity mud pill was circulated. One tight spot was observed at 628 mbsf during washing and reaming at which 40,000 lb of overpull was experienced.

**Reentry Number 5, Leg 152**

RCB-coring resumed at 1200 hr on 1 November, when we cored from 696.1 to 898.1 mbsf (Cores 152-918D-44R to -64R) until 2300

hr on 2 November. By this time, the bit had accumulated 34.4 hr in penetrating nearly 900 m of sediment laced with dropstones. The hole was flushed with a 20-bbl high-viscosity mud pill, and the top drive was set back in preparation for pulling out of the hole to change the bit. The drill pipe was pulled to the surface with no tight spots being encountered. The bit cleared the seafloor at 0055 hr and was on deck at 0500 hr on 3 November, where it was inspected and graded (5, 2, BT, N, CT, M, E, 1/16, HR).

The old bit, the PRT, and two head subs were laid down and a new RBI C-4 RCB bit and an additional outer core barrel (OCB) were added to the BHA. The BHA was run into the hole and by 0950 hr on 3 November, a small vibration isolated television (VIT) camera survey was conducted to find the cone. At 1020 hr, the bit entered the cone after passing over Hole 918C. The VIT was retrieved, and the bit was run into the hole to 857 mbsf, where the top drive was picked up. The

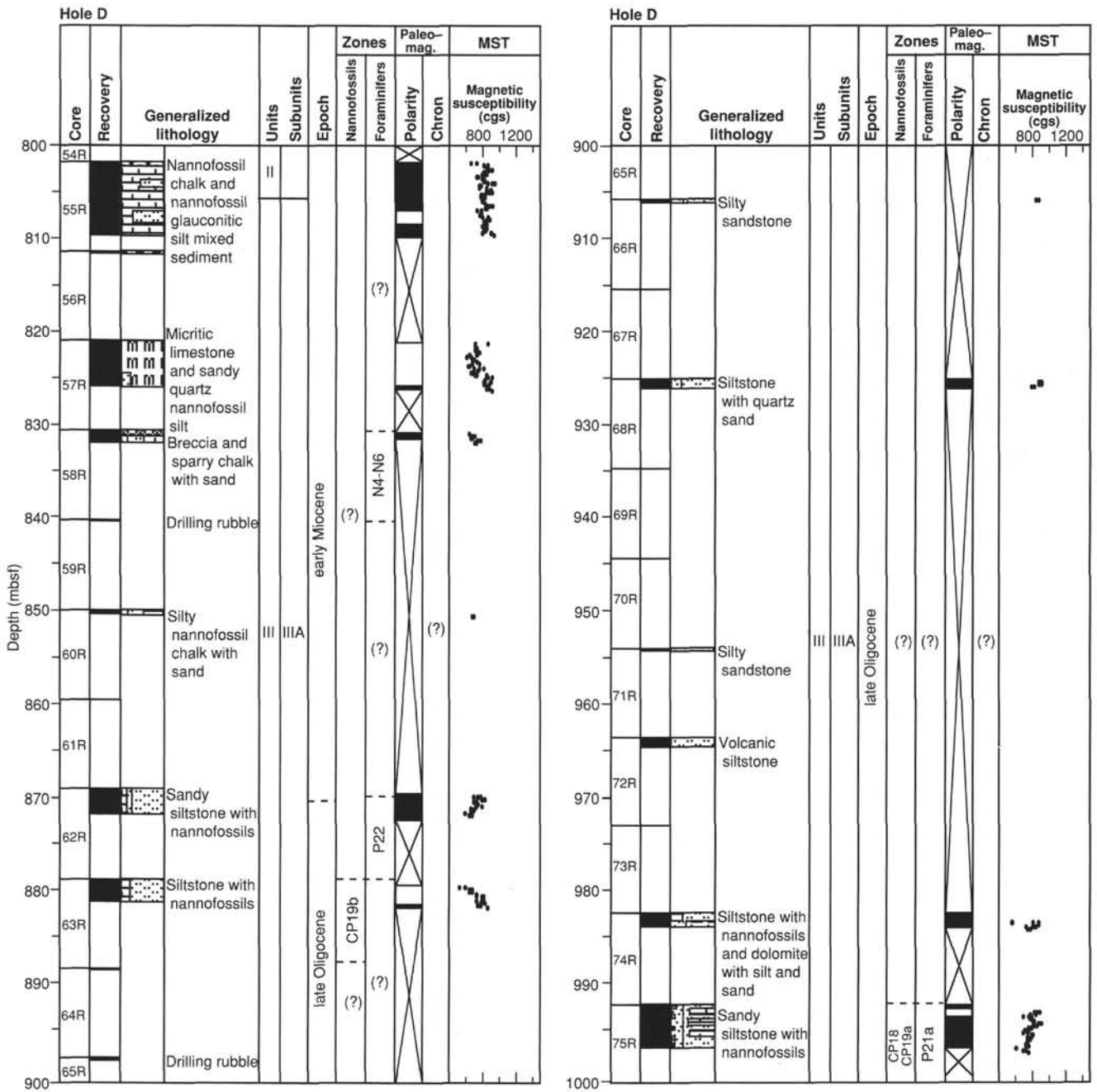


Figure 1 (continued).

center bit was dropped, and the hole was washed and reamed from 857 to 884 mbsf. Approximately 12 m of soft fill was washed away.

RCB-coring resumed at 1500 hr on 3 November. Rotary coring advanced from 898.1 to 1108.2 mbsf (Cores 152-918D-65R to -86R) through an interval characterized by turbidites having very rapid penetration rates (typically 5–10 min/core) and low recovery (202.5 m cored, 18.04 m recovered; 8.9%). The formation then firmed up as volcanic sandstone and siltstone were penetrated. The rate of penetration (ROP) gradually decreased from 23.0 to 11.5 m/hr in the interval from 1108.2 to 1165.8 mbsf (Cores 152-918D-87R to -92R). A drift survey was conducted at 1146.5 mbsf; the hole angle was measured to be a little less than 3°.

What was initially thought to be basaltic basement was penetrated in the interval from 1165.8 to 1180.4 mbsf (Cores 152-918D-93R and -94R). The basalt was fresh and very hard and required 150 min of

rotation to penetrate 5.0 m (ROP of 2.0 m/hr). As we thought basement had been reached, coring was interrupted to conduct a wiper trip, although later, we discovered it was only a thin basalt layer, presumably a sill.

The pipe was pulled up to 1127 mbsf with the top drive attached. The top drive was set back and the pipe was then pulled in stands to 259 mbsf. Between 40 and 50 kips of drag was observed when the bit was pulled from 1175 to 1089 mbsf. After the bit reached 259 mbsf, the wiper trip was stopped for 1 hr while 115 ft of drilling line was slipped and cut.

By 1400 hr on 5 November, the pipe was run into the hole and had contacted a hard bridge at 847 mbsf. The circulating head was made up and we tried to wash through this bridge. When this failed to move the bridge, the top drive was picked up and a center bit dropped. The hole was washed and reamed from 847 to 915 mbsf. The center bit

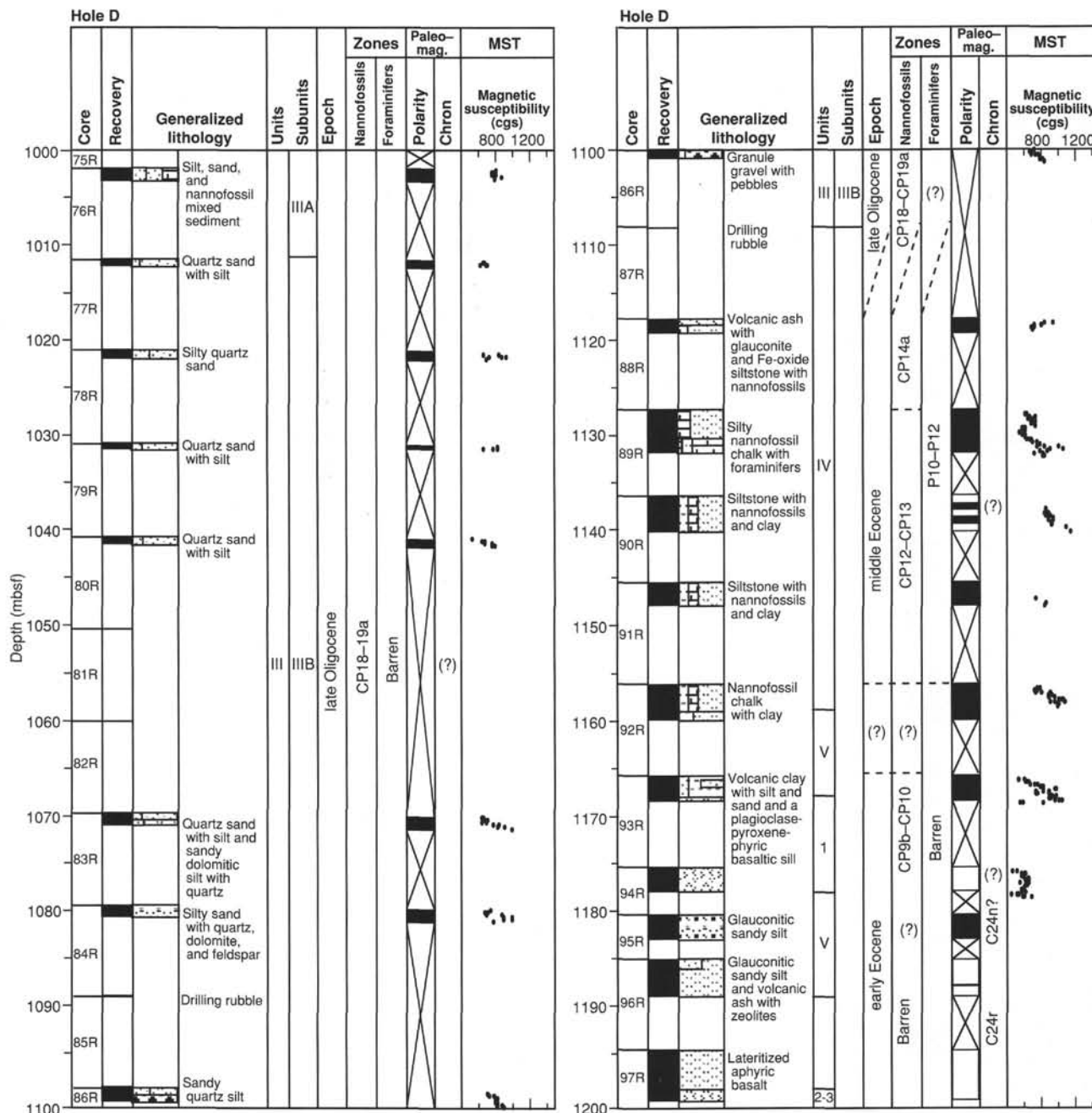


Figure 1 (continued).

was retrieved, the top drive set back, and the pipe was then advanced into the hole by adding a stand of pipe at a time. At 1069 mbsf, another bridge was contacted and, again, the top drive was picked up and a center bit dropped.

The hole was washed and reamed from 1069 to 1079 mbsf. During this operation, the hole was packed off and pump pressure rose to 1500 psi with only 40 spm. Two 20-bbl high-viscosity mud pills were circulated, and washing and reaming continued to the bottom of the hole, where 10 m of fill was found and cleared. When the wireline was run in to retrieve the center bit, the core barrel could not be unseated. A 20-bbl slug of 12 lb/gal mud was circulated, and we continued to try to release the core barrel.

After 2 hr of unsuccessful efforts at retrieving the barrel, we decided to pull out of the hole and to inspect the cause of the problem. The pipe was pulled up to 1145 mbsf, where the top drive was set

back. The pipe was pulled out of the hole, with the bit clearing the seafloor at 0530 hr on 6 November. The bit was on deck at 0845 hr.

We found that the core barrel had locked into the OCB by very fine sand. The sanded-in OCB with core barrel was laid down and a new OCB picked up. We also picked up a new, very hard formation bit (Smith F9CB), which was a more appropriate tool for penetrating the very hard basalt recovered in the last core.

### Reentry Number 6, Leg 152

The BHA was run in to 1805 mbsf, after which the VIT camera was deployed. The VIT camera and bit were lowered to 1874 m and a search conducted to find the reentry cone. During this time, a Force 10 storm was in progress. Although the storm did not seriously affect operations, it did extend the period before the bit was in position over

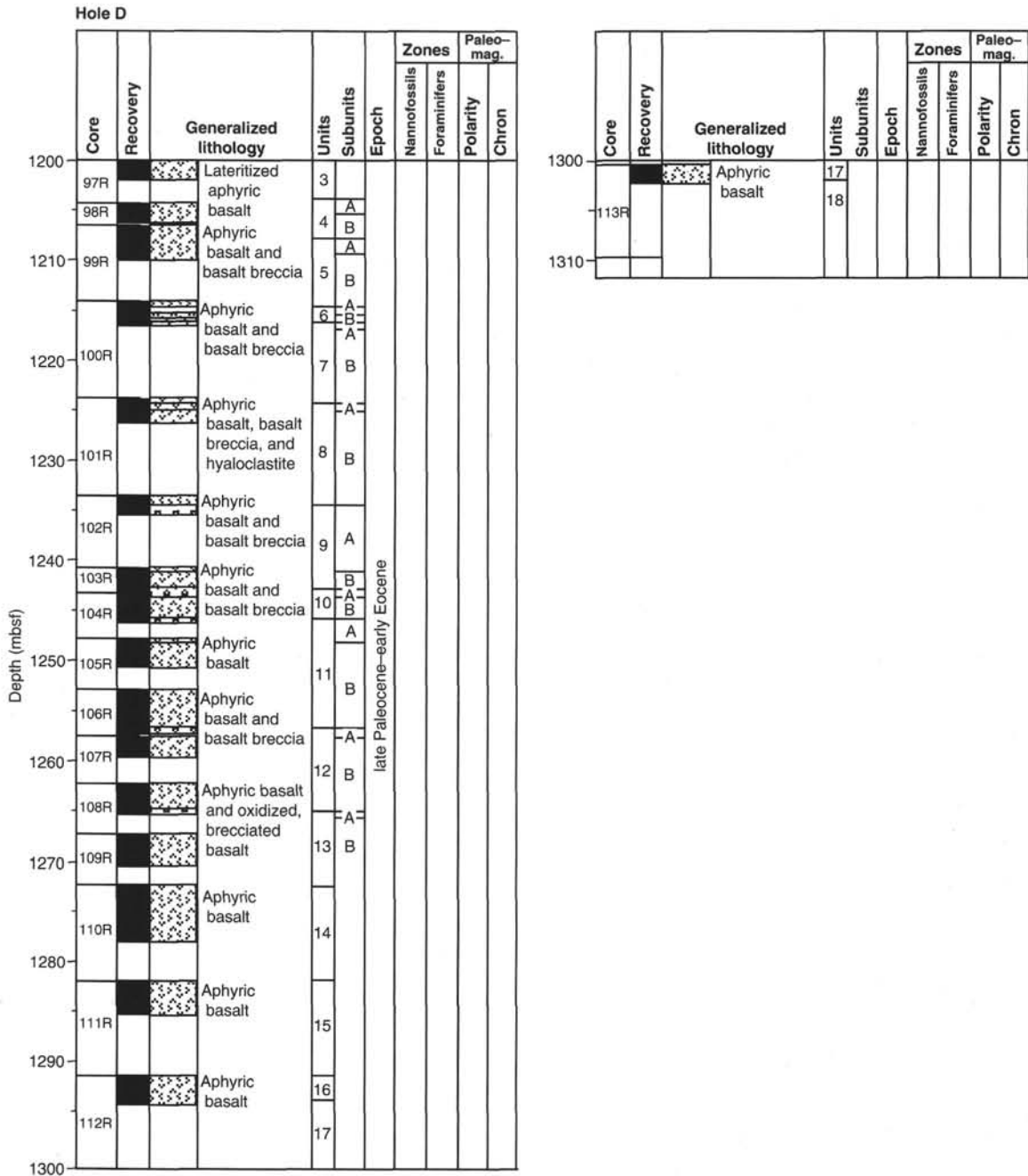


Figure 1 (continued).

the cone. After a 2.5-hr VIT survey, the bit reentered the cone at 2025 hr on 6 November.

The VIT was retrieved and the pipe was run to a depth of 1030 mbsf before the formation took weight and the top drive was required. The interval from 1030 to 1180 mbsf was washed and reamed, with a center bit being deployed, followed by the circulation of a 50-bbl high-viscosity mud flush. After 7 hr of washing and reaming, a core barrel was dropped and RCB-coring resumed at Hole 918D at 0700 hr on 7 November.

RCB-coring advanced from 1180.4 to 1271.9 mbsf into weathered, rubbly basalt with clay and altered volcanoclastic sediments. After a piece of basalt jammed in the core catcher during recovery of Core 152-918D-102R (1233.3–1240.5 mbsf) resulting in 2.01 m of recovery, we switched to retrieval of the core barrel for half cores. A 20-bbl

high-viscosity mud pill was circulated after every full-core interval. While cutting Core 152-918D-109R (1266.9–1271.9 mbsf), the torque was increased to 400 A and became erratic. The ROP slowed to 1.7 m/hr from a previous interval ROP of 3.8 m/hr. The bit had accumulated 36.2 hr of rotation by this time, and prudence indicated that we pull the BHA and inspect the condition of the bit. A 50-bbl high-viscosity mud pill was pumped to flush the hole and the drive was set back, after pulling the drill pipe to 1021 mbsf. The pipe then was pulled up in stands. The bit was on deck at 0030 hr on 10 November. An inspection of the bit indicated that it was in good condition, except that one of its four nozzles was missing. Rotation of the bit on the missing nozzle may have been responsible for the erratic torque.

A new RBI C-7 bit was made up with a nonmagnetic drill collar and run into the hole. We selected the C-7 bit because it has a slightly

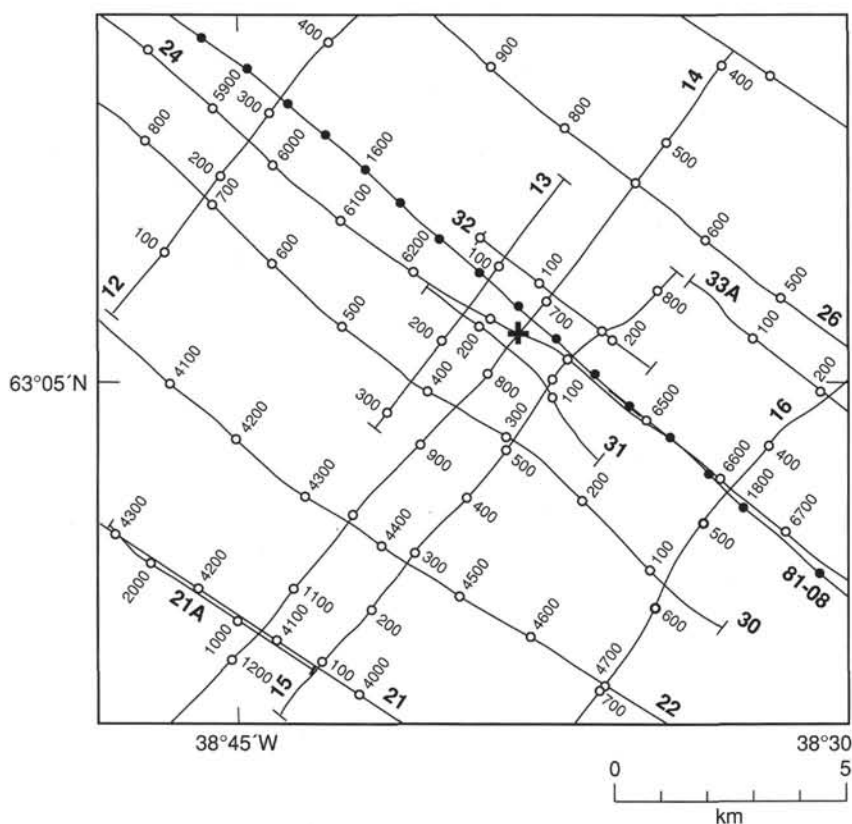


Figure 2. Location map of Site 918 (cross) and pre-cruise site-survey seismic data.

more aggressive cutting structure than that of the F9 and, consequently, is considered better able to penetrate rapidly through rubbly basalt. The drill pipe was run to 1826.8 mbsf, where we discontinued operations while waiting for an iceberg to pass.

At 1500 hr on 9 November, a large iceberg was observed north of our location. The iceberg had been detected on radar at 1630 hr, approximately 12 nmi north, drifting on an erratic southeasterly course at 0.8 kt. The iceberg was tracked through the night and early morning hours as it approached our location. As time passed, the iceberg grew smaller on the radar screen as it neared the vessel, and it was assumed that it was melting and breaking apart into smaller, bergy bits. Ironically, these could have been more dangerous as they are difficult to pick up on radar. Tracking of the ice was also made difficult by heavy seas. Suddenly, at 0400 hr on 10 November, about 4 nmi from the vessel, the iceberg disappeared from the radar. In view of the large initial size of the iceberg, we feared that several bergy bits of dangerous proportions might be bearing down on our location. We suspended reentry operations from 0400 to 0800 hr until a bergy bit was observed through the darkness directly east of the vessel at approximately 0.5 nmi.

### Reentry Number 7, Leg 152

The VIT camera was deployed, and the pipe lowered to 1874 m. The vessel was positioned over the cone, and the bit reentered the hole at 1015 hr after a 25-min search. Following retrieval of the VIT camera, the drill pipe was run into 847 mbsf, where the formation took weight. The top drive was picked up, and from noon until midnight on 10 November, the bit had to be washed and reamed to bottom. Some of the washing and reaming required using the center bit, and a 50-bbl high-viscosity mud pill was circulated at 1214 and 1270 mbsf. Coring of basalt resumed at midnight and advanced from 1271.9 to 1310.1 mbsf (Cores 152-918D-110R to -113R) by 1800 hr on 11 November.

At 1400 hr on 11 November, numerous icebergs began appearing north of the site; these were observed drifting southward toward our

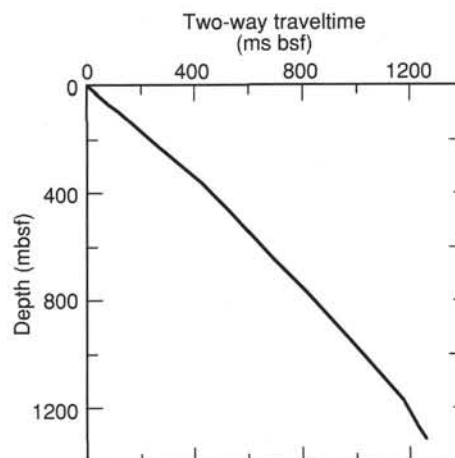


Figure 3. Preliminary two-way travelt ime vs. depth relationship at Site 918.

location. Many of these were bergy bits, which could not be detected by radar. By 1800 hr, the number of visible icebergs raised serious concern for the safety of the vessel. Coring operations were terminated, and the bit pulled out of the hole (POOH).

When the evening weather forecast from DMI arrived, it indicated that the winds had been predicted to diminish gradually over the next 72-hr period. We expected that as the winds abated, and the icebergs melted quickly in the warmer surface water ( $4^{\circ}$ – $6^{\circ}$ C) the threat from icebergs would diminish. During the evening, the deck crew used spotlights to observe the sea immediately in front of the vessel to detect any small chunks of ice. At midnight, a bergy bit (3 m high by 6 m long) was detected moving toward our location. As the bergy bit approached within one cable (0.1 nmi), the vessel was offset in dynamic positioning (DP) mode 200 m to starboard. After the bergy

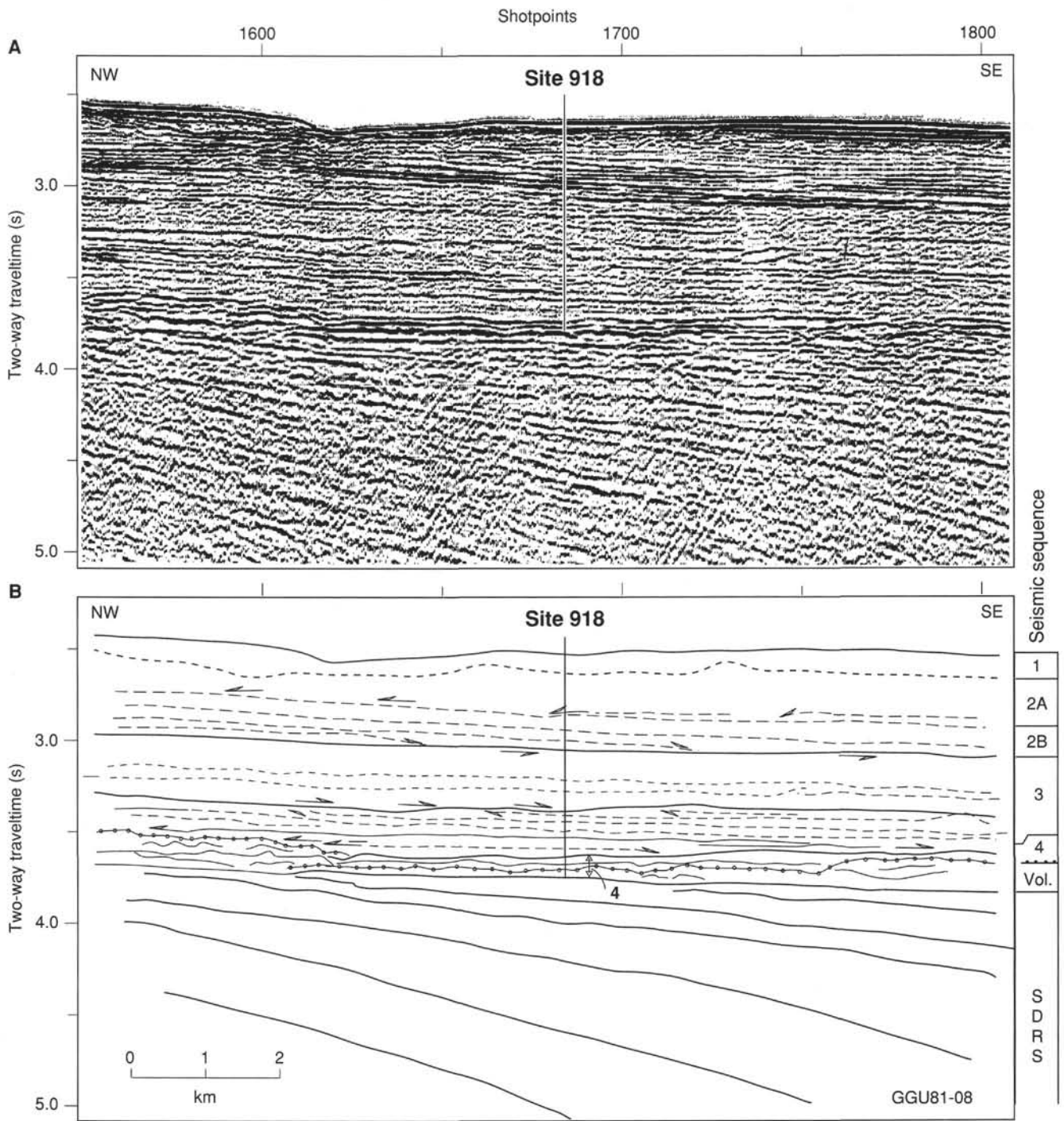


Figure 4. **A.** Seismic profile GGU81-08 in the vicinity of Site 918. **B.** Seismic stratigraphic interpretation is shown as line drawing. Seismic sequences are indicated in the column to the right. Vol. = the lower, partly volcanogenic part of seismic Sequence 4. SDRS = seaward-dipping reflector sequence. For location of the profile, see Figure 2.

bit passed directly over our location, the vessel was returned to the original coordinates.

The bit was pulled to the surface and was on deck at 2315 hr on 11 November. Although the bit was in nearly new condition after only 10.8 hr of rotation, a new C-7 bit was picked up to extend the coring period of what we assumed was to be the last bit used in this hole. A mechanical bit release (MBR) mechanism also was affixed to drop the bit outside the cone and to reenter it for logging. While the vessel was

standing by waiting for daylight and for the icebergs to clear the area, the new bit was lowered to 1852.8 mbsl.

### Reentry Number 8, Leg 152

At 0900 hr on 12 November, the VIT camera was deployed and at 1027 hr, the eighth reentry of Leg 152 was accomplished. The reentry operation was hampered by another Force 10 storm, which made the

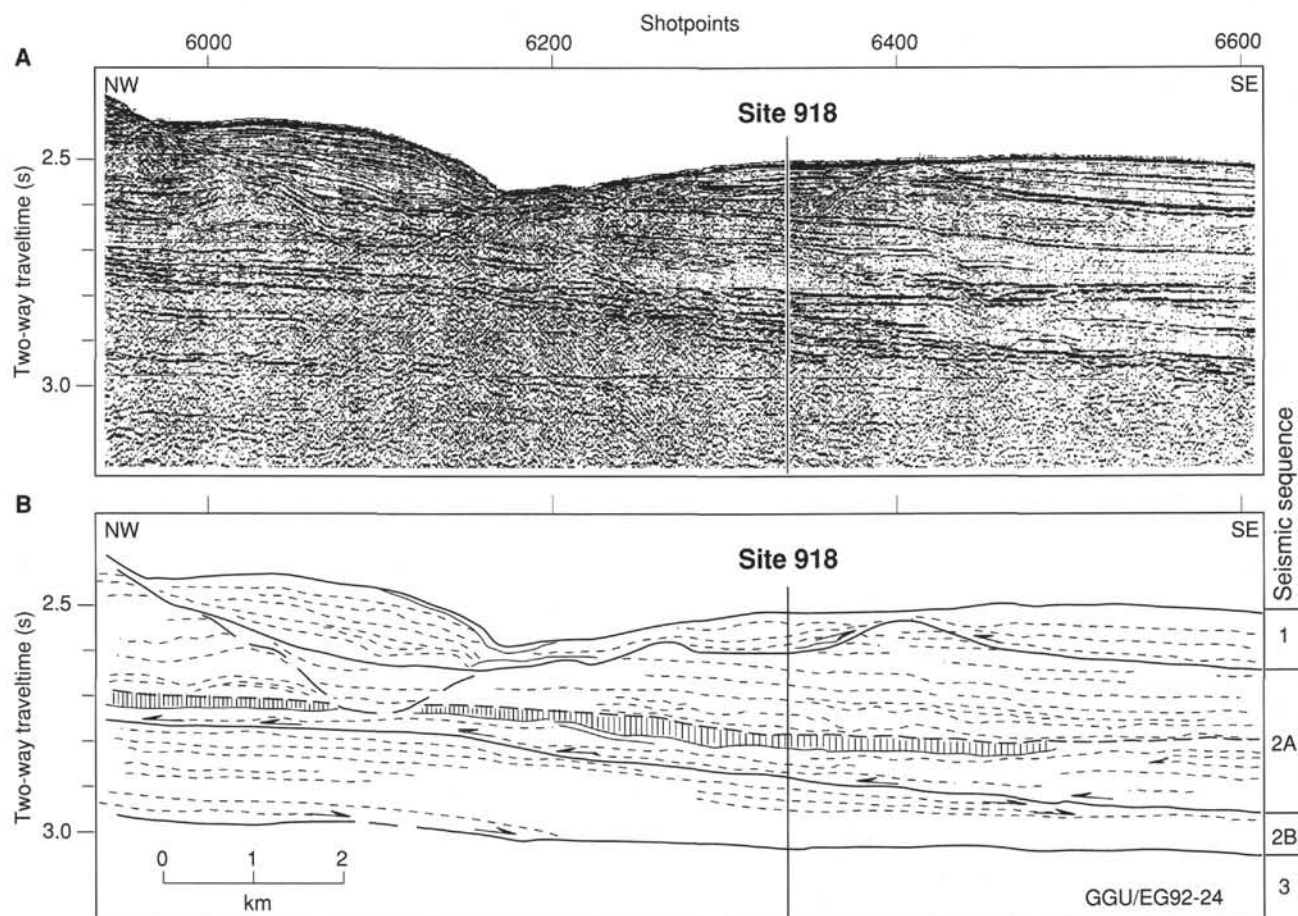


Figure 5. **A.** Seismic profile GGU/EG92-24 in the vicinity of Site 918. **B.** Seismic stratigraphic interpretation shown as line drawing. Sequences are indicated in the column to the right. For location of profile, see Figure 2.

vessel difficult to position over the hole. The reentry also was made more difficult by a sediment plume, which was located in the area that surrounded the reentry cone. This plume appeared to be emanating from the cone. The shipboard inorganic geochemist, Joris Gieskes, later viewed a video recording of the reentry and considered that the hole might have penetrated an underground aquifer.

The drill pipe was run in with stands until 240 mbsf, where the formation took weight. The pipe was pulled up to 232 mbsf and the VIT camera retrieved. At 1400 hr, we attempted to slack off the pipe to lower it to 240 mbsf, with no effect. When the pipe could not be lifted without exceeding the safe overpull limit, the top drive was picked up and circulation was established. The pipe could not be rotated and was firmly trapped by the hole.

For 1.5 hr, the pipe was worked with overpulls that ranged from 150 to 300 kips. Finally, the pipe came free at 1515 hr. The drill pipe was POOH using the top drive as far as 120 mbsf. After the top drive was set back, the pipe was POOH. The bit cleared the seafloor at 1650 hr. We decided that APC/XCB-coring at proposed Site EG63-3 would be more fruitful than our attempting to reclaim Hole 918D. Before securing operations at Site 918, the BHA was inspected and two drill collars were laid down. We discovered that one collar had a cracked pin and that the other had a zip-lift groove out of tolerance. Both beacons released upon command, but were lost in the darkness and heavy swells. At 0100 hr on 13 November, the ship's thrusters and hydrophones were secured, and the vessel was underway to proposed Site EG63-3.

Our operations in Hole 918D had obtained 113 cores (Table 1), while penetrating 1012.8 m of sediment and basement with 25.1% recovered (297.3 m was drilled). The main basaltic sequence was encountered at 1188.5 mbsf and was cored to a depth of 121.6 m, with

58.7 m (48.3%) recovered. A total of four bits were used (a fifth was deployed, but not used), with a total 93.9 hr of rotation. In retrospect, successful casing of this hole would have necessitated casing of the entire sediment section (nearly 1200 m) because the most unstable part was the lower 200 m. This depth interval was made up of poorly consolidated and unconsolidated turbidite sands and gravels.

## LITHOSTRATIGRAPHY

### Introduction

Site 918 is located on the upper continental rise, approximately 130 km off the East Greenland coast, in 1868.5 m of water. We divided the 1189.4-m-thick sediment section into six lithologic units that overlie a weathered basaltic basement (Table 2, Figs. 6 and 7). Some of the unit boundaries are not well defined because of gradational features and poor recovery over some intervals, especially in Hole 918D (Figs. 6 and 7).

Lithologic Unit I (Holocene-late Miocene) is dominantly a dark gray silt, with volcanogenic and nonvolcanic components, and forms the top 600.0 m of the section. It was divided into five subunits based on the presence of graded beds (Subunits IA and IB), the occurrence of a high concentration of ice-rafted debris (IRD) and dropstones (Subunit IC), a decrease in the concentration of dropstones (Subunit ID), and the absence of IRD and dropstones (Subunit IE).

Lithologic Unit II (early-late Miocene) is 206.5 m thick and comprises moderately to heavily burrowed nanofossil chalk and silt. Frequent micritic and glauconitic hardgrounds occur at the base and top of this unit. The silt beds contain a mixed suite of minerals derived from both volcanic and nonvolcanic source areas.

Table 1. Coring summary for Site 918.

Core	Date (1993)	Time (UTC)	Depth (mbsf)	Length cored (m)	Length recovered (m)	Recovery (%)	Core	Date (1993)	Time (UTC)	Depth (mbsf)	Length cored (m)	Length recovered (m)	Recovery (%)
152-918A-							32R	Oct 31	1900	580.3-590.0	9.7	1.47	15.1
1H	Oct 26	1725	0.0-1.8	1.8	1.81	100.0	33R	Oct 31	2015	590.0-599.6	9.6	1.59	16.5
2H	Oct 26	1810	1.8-11.3	9.5	9.14	96.2	34R	Oct 31	2115	599.6-609.2	9.6	2.09	21.8
3H	Oct 26	1845	11.3-20.8	9.5	8.93	94.0	35R	Oct 31	2230	609.2-618.9	9.7	3.26	33.6
4H	Oct 26	1945	20.8-30.3	9.5	9.76	103.0	36R	Oct 31	2340	618.9-628.6	9.7	4.27	44.0
5H	Oct 26	2030	30.3-39.8	9.5	9.76	103.0	37R	Nov 1	0100	628.6-638.2	9.6	6.42	66.9
6H	Oct 26	2130	39.8-49.3	9.5	10.01	105.3	38R	Nov 1	0200	638.2-647.9	9.7	8.24	84.9
7H	Oct 26	2300	49.3-58.8	9.5	9.95	105.0	39R	Nov 1	0300	647.9-657.5	9.6	8.59	89.5
8H	Oct 26	2345	58.8-68.3	9.5	9.66	101.0	40R	Nov 1	0400	657.5-667.2	9.7	7.70	79.4
9H	Oct 27	0030	68.3-77.8	9.5	9.94	104.0	41R	Nov 1	0450	667.2-676.8	9.6	8.71	90.7
10H	Oct 27	0100	77.8-87.3	9.5	10.08	106.1	42R	Nov 1	0550	676.8-686.4	9.6	9.07	94.5
11H	Oct 27	0145	87.3-96.8	9.5	9.88	104.0	43R	Nov 1	0700	686.4-696.1	9.7	2.96	30.5
12H	Oct 27	0400	96.8-106.3	9.5	9.52	100.0	44R	Nov 1	1350	696.1-705.3	9.2	7.51	81.6
13H	Oct 27	0445	106.3-115.8	9.5	9.94	104.0	45R	Nov 1	1505	705.3-715.0	9.7	0.04	0.4
14H	Oct 27	0515	115.8-125.3	9.5	7.98	79.8	46R	Nov 1	1610	715.0-724.6	9.6	0.10	1.0
15H	Oct 27	0605	125.3-133.3	8.0	8.07	101.0	47R	Nov 1	1725	724.6-734.2	9.6	2.10	21.9
16H	Oct 27	0715	133.3-142.8	9.5	9.90	104.0	48R	Nov 1	1830	734.2-743.9	9.7	0.00	0.0
17H	Oct 27	0940	142.8-152.3	9.5	9.81	103.0	49R	Nov 1	1945	743.9-753.6	9.7	0.05	0.5
18H	Oct 27	1030	152.3-161.8	9.5	9.88	104.0	50R	Nov 1	2130	753.6-763.2	9.6	0.00	0.0
19H	Oct 27	1110	161.8-171.3	9.5	9.85	103.0	51R	Nov 2	0000	763.2-772.9	9.7	8.66	89.3
20X	Oct 27	1255	171.3-181.5	10.2	5.92	58.0	52R	Nov 2	0200	772.9-782.5	9.6	7.31	76.1
21X	Oct 27	1340	181.5-190.9	9.4	4.26	45.3	53R	Nov 2	0400	782.5-792.1	9.6	9.75	101.0
22X	Oct 27	1610	190.9-199.8	8.9	1.40	15.7	54R	Nov 2	0650	792.1-801.8	9.7	0.28	2.9
23X	Oct 27	1725	199.8-208.7	8.9	8.76	98.4	55R	Nov 2	0840	801.8-811.4	9.6	7.98	83.1
24X	Oct 27	1805	208.7-217.6	8.9	9.41	106.0	56R	Nov 2	1040	811.4-821.0	9.6	0.17	1.8
25X	Oct 27	1845	217.6-226.5	8.9	9.68	109.0	57R	Nov 2	1300	821.0-830.7	9.7	5.16	53.2
26X	Oct 27	1930	226.5-235.2	8.7	7.92	91.0	58R	Nov 2	1410	830.7-840.4	9.7	1.10	11.3
27X	Oct 27	2010	235.2-244.1	8.9	8.90	100.0	59R	Nov 2	1550	840.4-850.0	9.6	0.10	1.0
28X	Oct 27	2050	244.1-252.8	8.7	7.33	84.2	60R	Nov 2	1750	850.0-859.6	9.6	0.35	3.6
29X	Oct 27	2140	252.8-261.7	8.9	1.33	14.9	61R	Nov 2	1830	859.6-869.3	9.7	0.00	0.0
30X	Oct 27	2230	261.7-270.6	8.9	0.23	2.6	62R	Nov 2	2000	869.3-878.9	9.6	2.43	25.3
31X	Oct 27	2300	270.6-279.5	8.9	8.77	98.5	63R	Nov 2	2200	878.9-888.5	9.6	2.50	26.0
32X	Oct 27	2335	279.5-288.4	8.9	1.54	17.3	64R	Nov 2	2345	888.5-898.1	9.6	0.03	0.3
33X	Oct 28	0015	288.4-297.3	8.9	2.30	25.8	65R	Nov 3	1720	898.1-905.7	7.6	0.19	2.5
34X	Oct 28	0100	297.3-306.2	8.9	0.00	0.0	66R	Nov 3	1840	905.7-915.3	9.6	0.27	2.8
35X	Oct 28	0230	306.2-309.1	2.9	0.64	22.0	67R	Nov 3	1930	915.3-925.0	9.7	0.07	0.7
36X	Oct 28	0330	309.1-315.1	6.0	0.00	0.0	68R	Nov 3	2030	925.0-934.7	9.7	1.09	11.2
37X	Oct 28	0445	315.1-323.9	8.8	7.92	90.0	69R	Nov 3	2115	934.7-944.4	9.7	0.00	0.0
38X	Oct 28	0630	323.9-332.7	8.8	0.49	5.6	70R	Nov 3	2215	944.4-954.0	9.6	0.00	0.0
Coring totals:				332.7	260.27	78.2	71R	Nov 3	2300	954.0-963.7	9.7	0.09	0.9
152-918B-							72R	Nov 4	0030	963.7-973.0	9.3	0.72	7.7
1H	Oct 28	0945	0.0-6.8	6.8	6.85	101.0	73R	Nov 4	0200	973.0-982.7	9.7	0.00	0.0
2H	Oct 28	1130	6.8-16.3	9.5	9.11	95.9	74R	Nov 4	0330	982.7-992.3	9.6	1.18	12.3
3H	Oct 28	1220	16.3-25.8	9.5	9.52	100.0	75R	Nov 4	0445	992.3-1002.0	9.7	4.69	48.3
Coring totals:				25.8	25.48	98.8	76R	Nov 4	0600	1002.0-1011.6	9.6	1.29	13.4
152-918C-							77R	Nov 4	0650	1011.6-1021.2	9.6	0.60	6.3
*** Washed from 0.0 to 25.8 mbsf ***							78R	Nov 4	0740	1021.2-1030.9	9.7	0.70	7.2
1H	Oct 28	1650	25.8-35.3	9.5	9.59	101.0	79R	Nov 4	0840	1030.9-1040.6	9.7	0.55	5.7
2H	Oct 28	1740	35.3-35.4	0.1	0.05	50.0	80R	Nov 4	1015	1040.6-1050.3	9.7	0.87	9.0
Coring totals:				9.6	9.64	100.0	81R	Nov 4	1115	1050.3-1060.0	9.7	0.00	0.0
152-918D-							82R	Nov 4	1250	1060.0-1069.6	9.6	0.00	0.0
*** Drilled from 0.0 to 253.2 mbsf ***							83R	Nov 4	1350	1069.6-1079.3	9.7	1.41	14.5
1R	Oct 29	2200	253.2-262.0	8.8	0.60	6.8	84R	Nov 4	1520	1079.3-1088.9	9.6	1.27	13.2
2R	Oct 29	2300	262.0-271.0	9.0	0.00	0.0	85R	Nov 4	1625	1088.9-1098.5	9.6	0.14	1.5
3R	Oct 30	0000	271.0-279.9	8.9	0.00	0.0	86R	Nov 4	1730	1098.5-1108.2	9.7	2.72	28.0
*** Drilled from 279.9 to 324.0 mbsf ***							87R	Nov 4	1915	1108.2-1117.8	9.6	0.19	2.0
4R	Oct 30	0345	324.0-332.8	8.8	0.14	1.6	88R	Nov 4	2030	1117.8-1127.4	9.6	1.23	12.8
5R	Oct 30	0530	332.8-341.7	8.9	0.18	2.0	89R	Nov 4	2215	1127.4-1137.1	9.7	4.80	49.5
6R	Oct 30	0630	341.7-350.6	8.9	0.08	0.9	90R	Nov 5	0030	1137.1-1146.5	9.4	3.21	34.1
7R	Oct 30	0740	350.6-359.5	8.9	0.13	1.5	91R	Nov 5	0215	1146.5-1156.2	9.7	1.50	15.4
8R	Oct 30	0925	359.5-368.4	8.9	0.17	1.9	92R	Nov 5	0415	1156.2-1165.8	9.6	2.20	22.9
9R	Oct 30	1125	368.4-377.2	8.8	0.24	2.7	93R	Nov 5	0740	1165.8-1175.4	9.6	2.62	27.3
10R	Oct 30	1315	377.2-386.1	8.9	0.23	2.6	94R	Nov 5	1120	1175.4-1180.4	5.0	2.61	52.2
11R	Oct 30	1450	386.1-395.0	8.9	1.27	14.2	95R	Nov 7	1130	1180.4-1185.1	4.7	3.44	73.2
12R	Oct 30	1650	395.0-403.9	8.9	0.05	0.6	96R	Nov 7	1405	1185.1-1194.7	9.6	3.94	41.0
13R	Oct 30	1730	403.9-412.8	8.9	1.48	16.6	97R	Nov 7	1700	1194.7-1204.4	9.7	7.34	75.7
14R	Oct 30	1830	412.8-421.7	8.9	2.71	30.4	98R	Nov 7	1930	1204.4-1206.5	2.1	1.96	93.3
15R	Oct 30	1930	421.7-430.4	8.7	0.50	5.8	99R	Nov 7	2310	1206.5-1214.0	7.5	3.58	47.7
16R	Oct 30	2030	430.4-439.3	8.9	0.00	0.0	100R	Nov 8	0300	1214.0-1223.7	9.7	2.37	24.4
17R	Oct 30	2200	439.3-448.2	8.9	0.00	0.0	101R	Nov 8	0825	1223.7-1233.3	9.6	2.50	26.0
18R	Oct 31	0215	448.2-457.1	8.9	1.16	13.0	102R	Nov 8	1605	1233.3-1240.5	7.2	2.04	28.3
19R	Oct 31	0315	457.1-466.1	9.0	0.21	2.3	103R	Nov 8	2145	1240.5-1243.0	2.5	2.65	106.0
20R	Oct 31	0420	466.1-474.9	8.8	0.00	0.0	104R	Nov 9	0045	1243.0-1247.6	4.6	3.00	65.2
21R	Oct 31	0520	474.9-483.8	8.9	0.20	2.3	105R	Nov 9	0445	1247.6-1252.6	5.0	2.95	59.0
22R	Oct 31	0630	483.8-493.6	9.8	4.21	42.9	106R	Nov 9	0825	1252.6-1257.2	4.6	4.55	98.9
23R	Oct 31	0800	493.6-503.2	9.6	1.29	2.0	107R	Nov 9	1130	1257.2-1262.2	5.0	2.13	42.6
24R	Oct 31	0920	503.2-512.8	9.6	3.67	38.2	108R	Nov 9	1350	1262.2-1266.9	4.7	3.01	64.0
25R	Oct 31	1050	512.8-522.5	9.7	5.11	52.7	109R	Nov 9	1750	1266.9-1271.9	5.0	3.27	65.4
26R	Oct 31	1220	522.5-532.1	9.6	0.03	0.3	110R	Nov 11	0445	1271.9-1281.5	9.6	5.83	60.7
27R	Oct 31	1340	532.1-541.8	9.7	4.39	45.2	111R	Nov 11	0830	1281.5-1290.9	9.4	3.17	33.7
28R	Oct 31	1450	541.8-551.4	9.6	5.10	53.1	112R						

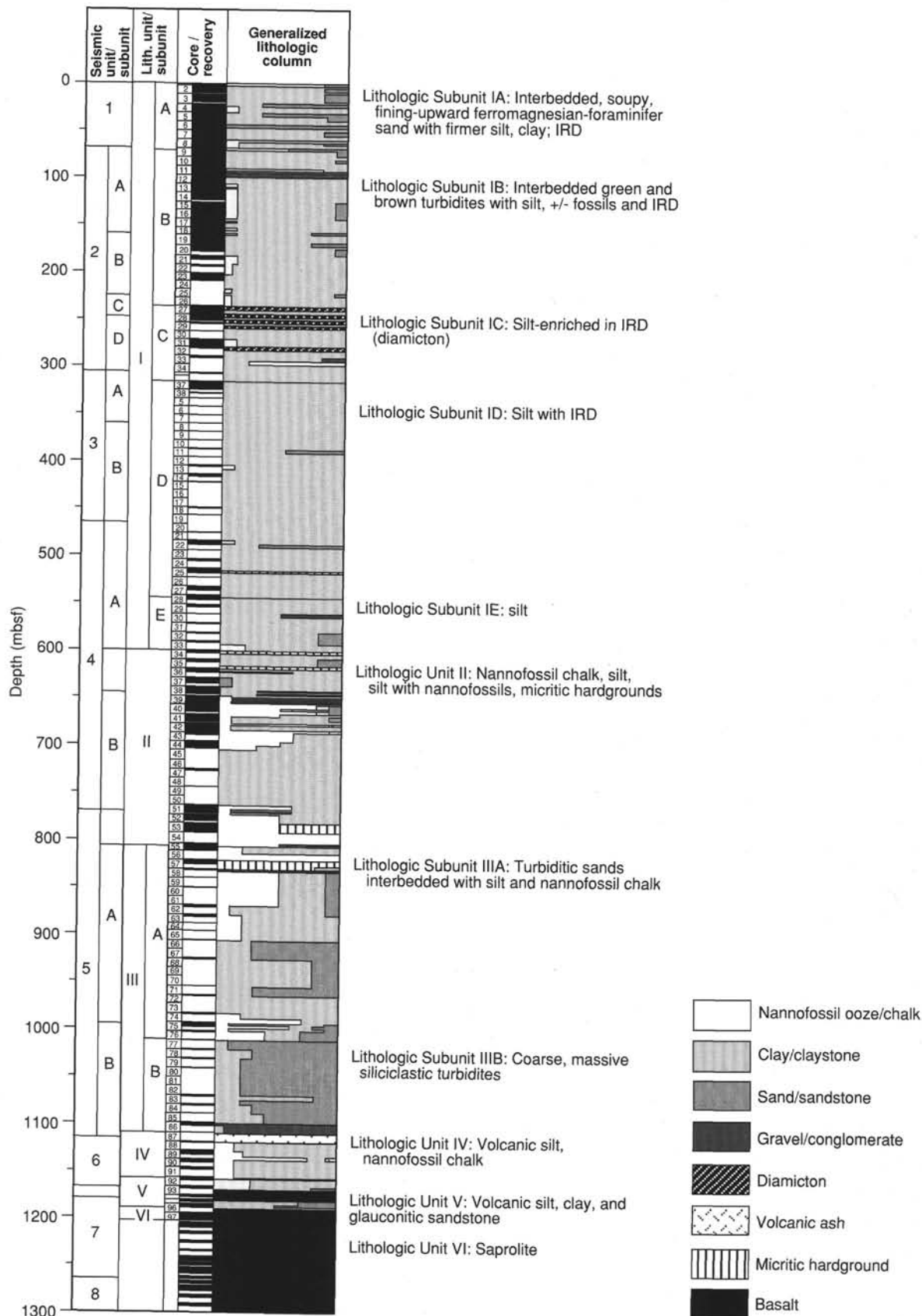


Figure 6. Composite stratigraphic column for Site 918, illustrating the lithologic units and subunits.

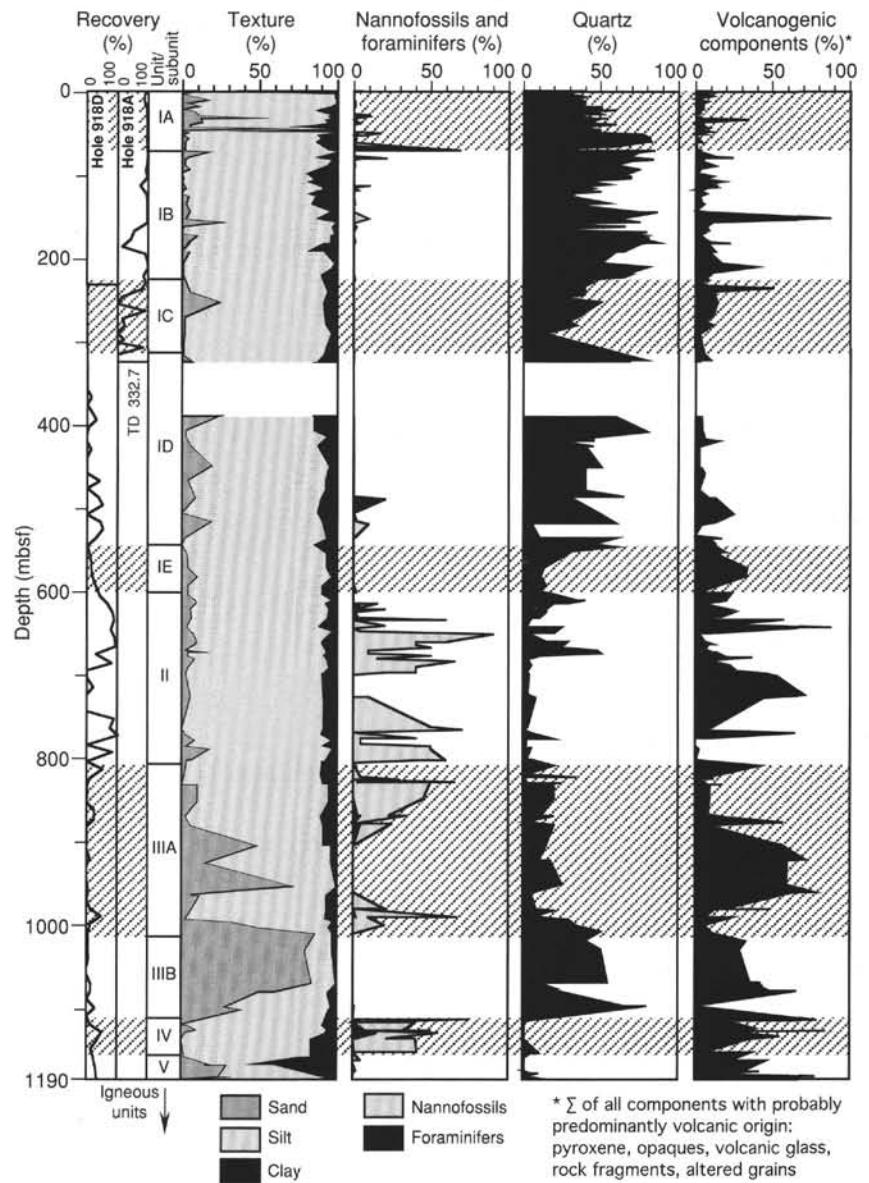


Figure 7. Composition of lithologic units, showing recovery, texture, and terrigenous and biogenic components.

Lithologic Unit III (early Miocene–late Oligocene) comprises sand, silt, and nannofossil chalk and was divided into two subunits. The upper Subunit IIIA includes interbeds of thin, massive, or laminated sand with frequent silt and nannofossil chalk beds. The lower Subunit IIIB has massive, quartz-rich turbiditic sands, which are intermittently heavily bioturbated. Dolomite and glauconite are common constituents in the lower subunit, with glauconite pellets increasing downcore. The base of this unit is a 1-m-thick (or greater), unconsolidated, poorly recovered gravel.

Lithologic Unit IV (middle Eocene) is 49.7 m thick and comprises interbeds of nannofossil chalk and volcanoclastic silt with nannofossils.

Lithologic Unit V (early Eocene) is 31.5 m thick and consists of a glauconitic sandy silt with interbedded calcareous sand. It is distinguished from Unit IV by the paucity of microfossils and the high abundance of glauconite pellets (up to 70%).

Lithologic Unit VI (age unknown, presumed late Paleocene to early Eocene) is the subaerially weathered top of the basalt pile. The upper 5.3 m was described by the sedimentologists, but the weathering extends 17 m into the basalt.

### Description of Lithologic Units

Lithologic Unit I: thin sand beds fining-upward into quartz- and volcanoclastic silt; dropstones; occasional enrichments in microfossils  
 Intervals: 152-918A-1H-1 to -37X; 152-918B-1H-1 to -3H-CC; 152-918C-1H-1 to -2H-CC; 152-918D-1R-1 to -34R-1, 40 cm  
 Depth: 0–600.0 mbsf  
 Thickness: 600.0 m  
 Age: late Miocene–Holocene

Lithologic Unit I, predominantly silt, is divided into five subunits based on the presence of fining-upward sand beds or laminae, and on the abundance of IRD as dropstones (Table 2, Fig. 6). Dropstones are common to the upper four subunits. A total of 208 in-situ gravel clasts, larger than 1 cm in diameter, were identified in lithologic Unit I (Figs. 8A and 8B). Basalt fragments comprise 33% of the suite, gneiss 18%, sedimentary rocks 16%, and granite 14% (Fig. 9). Smaller amounts are contributed by metasedimentary rocks, dolerite, and gabbro. We used 10 or more dropstones per section as an arbitrary limit for identifying diamictites, which correspond to zones of predominantly

Table 2. Summary of lithologic units, Site 918.

Lithologic unit	Lithology	Depth (mbsf)	Core, interval	Thickness (m)	Age
IA	Interbedded, soupy, fining-upward ferromagnesian-foraminifer sand with firmer silt, clay; IRD	0–71.1	152-918A-1H-1 to -9H-2, 130 cm	71.1	Holocene–Pleistocene
IB	Interbedded green and brown turbidites with silt, fossils and IRD	71.1–236.0	152-918A-9H-2, 130 cm, to -27X-1, 80 cm	164.9	Pleistocene–Pliocene
IC	Silt enriched in IRD (diamiction)	236.0–317.8	152-918A-27X-1, 80 cm, to -37X-2, 120 cm	81.5	Pliocene
ID	Silt with IRD	317.8–543.6	152-918A-37X-2, 120 cm, to -38X-CC, and 918D-11R-1 to -2H-CC	225.8	early Pliocene–late Miocene
IE	Silt	543.6–600.0	and 918D-11R-1, to -28R-2, 52 cm	56.4	late Miocene
II	Nannofossil chalk, silt, silt with nannofossils, micritic hardgrounds	600.0–806.5	152-918D-28R-2, 52 cm, to -34R-1, 40 cm	206.5	early Miocene–late Miocene
IIIA	Turbiditic sands interbedded with silt and nannofossil chalk	806.5–1011.6	152-918D-55R-5, 20 cm, to -76R-CC	205.1	early Miocene–late Oligocene
IIIB	Coarse, massive siliciclastic turbidites	1011.6–1108.2	152-918D-76R-CC to -86R-CC	96.6	late Oligocene
IV	Volcanic silt, nannofossil chalk	1108.2–1157.9	152-918D-87R-1 to -92R-2, 25 cm	49.7	middle Eocene
V	Volcanic silt, clay and glauconitic sandstone	1157.9–1189.4	152-918D-92R-2, 25 cm, to -96R-3, 128 cm	31.5	early Eocene
VI	Highly weathered lava flows	1189.4–1204.4	152-918D-96R-3, 128cm, to -97R-CC	5.3+	Unknown

glaciomarine deposition (Fig. 8B). At least 12 diamictites are present in lithologic Unit I, largely concentrated in Subunits IA and IC (Fig. 8A). The diamictites in these intervals consist of cobble- and granule-sized gravel floating in a silty matrix that is composed largely of rock and mineral fragments.

Lithologic Subunit IA: interbedded soupy, fining-upward sand and firmer silt; dropstones present throughout

Intervals: 152-918A-1H-1 to -9H-2, 130 cm; 152-918B-1H-1 to -3H-CC; 152-918C-1H-1 to -2H-CC

Depth: 0–71.1 mbsf

Thickness: 71.1 m

Age: Pleistocene–Holocene

Lithologic Subunit IA comprises a series of fine sand to silt, fining-upward sequences with occasional enrichments in clay or microfossils. The silt is laminated or massive, with the latter frequently bioturbated. Massive silt is generally underlain by laminated silt, which grades downward into laminated or massive sand (Fig. 10). We have interpreted these sequences as turbidites (similar to the type A package discussed below for Subunit IB). Quartz and feldspar are the two major mineral components of the sand, with green amphibole, garnet, zircon, and opaque minerals as accessories. Many of the sand laminae are black as a result of enrichment in ferromagnesian minerals, particularly amphibole. The silt matrix, determined by XRD analysis, is composed of “rock flour,” predominantly quartz, feldspar, and amphibole (Table 3). A weak smectite peak was observed in Cores 152-918A-3H and -4H. Dropstones and smaller IRD are scattered throughout the sequence with no preference for sand or silt intervals.

Although this subunit is similar to the type A turbidite package discussed below for Subunit IB, an erosional contact with a nonfossiliferous, laminated silt overlying a massive foraminifer ooze occurs at 71.1 mbsf. The sediment above this contact is richer in dropstones than the sediment immediately below. We suggest that these lithologic changes, together with the seismic reflection data (see “Background and Scientific Objectives” section, this chapter), justify the separation of Subunits IA and IB.

Lithologic Subunit IB: interbeds of two types of turbidites, all with dropstones/IRD: (1) brown sand-silt fining-upward sequences (type A) and (2) greenish-gray sand-silt fining-upward sequences (type B)

Intervals: 152-918A-9H-2, 130 cm, to -27X-1, 80 cm

Depth: 71.1–236.0 mbsf

Thickness: 164.9 m

Age: Pliocene–Pleistocene

Two sets of fining-upward sand-silt couplets in this subunit differ in color and bedding characteristics. We tentatively interpret both sets

as turbidites. One set is a distinct greenish-gray, while the other is brownish-gray. Based on core descriptions, smear-slide data, and carbonate contents (see “Organic Chemistry” section, this chapter), we divided the couplets in this subunit into nine intervals (Table 4). We informally refer to these as sediment “packages” to distinguish them from lithostratigraphic units and we classified them into two types of deposit, type A and type B.

Of the nine intervals, three were classified as distinct type A packages and two as type A\* packages denoting their less distinct character. The type A\* packages differ from the type A in being finer grained with less well-developed bedding. The type A and A\* packages have fining-upward beds, ranging in thickness from 5 cm to 1 m. The basal sections of some beds are poorly sorted sand that grades upward into medium- and fine-grained silt. A 2.8-m-thick polymict gravel at 94.9 to 97.7 mbsf (Cores 152-918A-11H to -12H) is the base of a type A package. Type A package sediment contains more microfossils (foraminifers *Neoglobobulimina pachyderma* and *N. Atlantica* sinistral coiling at 10%, diatoms to 5%, and nannofossils to 20%) than type B packages and, on average have higher CaCO<sub>3</sub> contents.

Four distinct type B packages are seen in this subunit (Fig. 11). Type B package sediment is lighter in color and has laminae of white quartz silt that range from 5 mm to 2 cm in thickness. The quartz content is very high, particularly in the thin quartz silt laminae, and the package generally contains fewer microfossils and lower CaCO<sub>3</sub> contents than the type A package sediment.

Lithologic Subunit IC: silt enriched in dropstones (diamiction)

Interval: 152-918A-27X-1, 80 cm, to 37X-2, 120 cm

Depth: 236.0–317.8 mbsf

Thickness: 81.5 m

Age: Pliocene

Lithologic Subunit IC comprises a massive, pebbly silt (diamiction) interbedded within massive silt. This subunit is poorly sorted, has little internal structure, and contains pebble- to cobble-sized clasts suspended in a very immature and poorly sorted sand and silt matrix (Figs. 12 and 13). These diamiction deposits are somewhat similar to the poorly sorted proximal deposits of a debris flow. Sixty-five gravel clasts (Fig. 8), larger than 1 cm in diameter, were observed in place in a silty matrix intermittently enriched in quartz or clay in Cores 152-918A-27X-1 through -33X-CC (235.2–297.4 mbsf). Quartz (50%–65%) and feldspar (5%–15%) are the dominant mineral components in the sediment matrix. Several accessory minerals are present, including amphibole, sphene, chlorite, garnet, and pyroxene. Foraminifers (sinistraly coiled *N. atlantica*) as well as diatoms and sponge spicules, occur in trace amounts, up to a few percent in fine silty horizons.

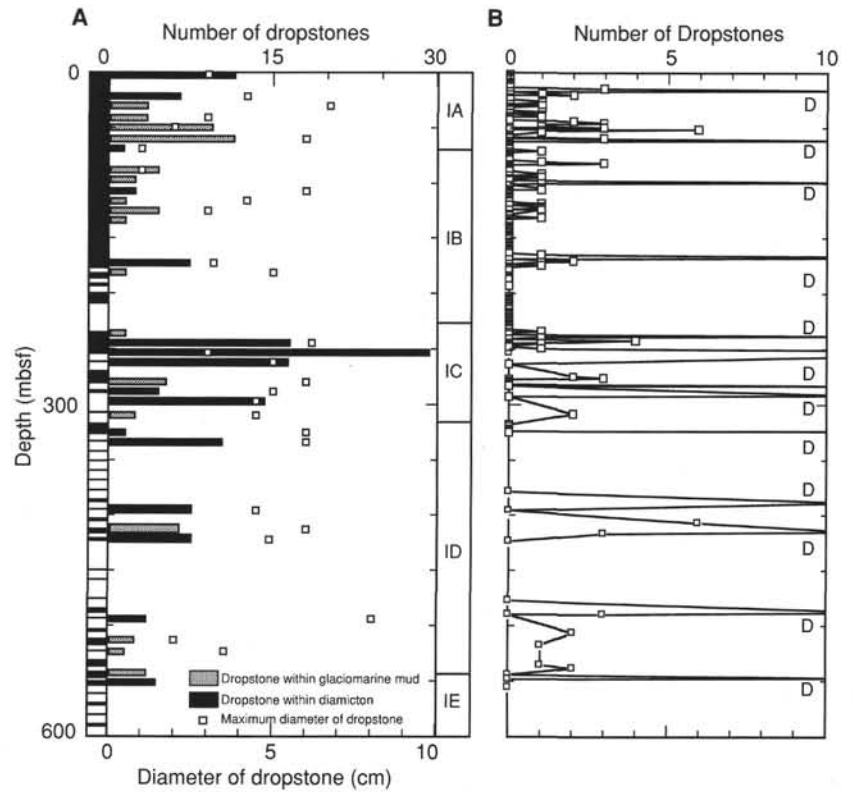


Figure 8. Abundance and maximum diameter of dropstones (>1 cm) in Unit I. **A.** Abundance of dropstones averaged over each core. **B.** Abundance of dropstones per section, with diamictites labeled (D).

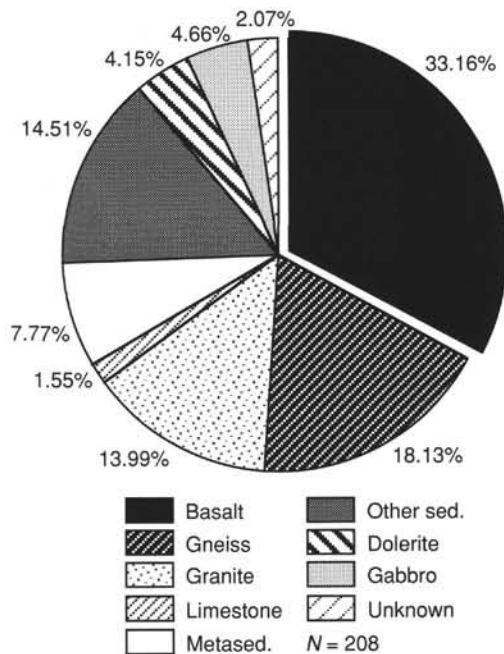


Figure 9. Dropstone composition in lithologic Unit I. We recorded 208 dropstones having a diameter greater than 1 cm.

Lithologic Subunit ID: silt with dropstones  
 Intervals: 152-918A-37X-2, 120 cm, to -38X-CC; 152-918D-1R-1 to -28R-2, 52 cm  
 Depth: 317.8–543.6 mbsf  
 Thickness: 225.8 m  
 Age: late Miocene–early Pliocene

Lithologic Subunit ID is distinguished from Subunit IC by an abrupt decrease in the occurrence of dropstones in Core 152-918A-37X (Fig. 8). The matrix material, however, is similar to the silt of Subunit IC and is composed of siliciclastic terrigenous debris and volcanoclastic components. Subunit ID was only poorly recovered in Cores 152-918D-4R through -28R. However, the residual occurrence of the quartz silt matrix, down to Core 152-918D-28R, and rare but in part large dropstones (several centimeters across, some even drilled through) in place suggest that this lithology persists to 543.6 mbsf. The last occurrence of unequivocal, in-situ dropstones was observed in Core 152-918D-28R at 543.6 mbsf (Fig. 14). A decrease in the accumulation rate of terrigenous material is indicated by an increase in burrows (*Planolites*, *Chondrites*, *Zoophycos*) in the lower part of this subunit.

Lithologic Subunit IE: quartzose and volcanoclastic silt  
 Intervals: 152-918D-28R-2, 52 cm, to 152-918D-34R-1, 40 cm  
 Depth: 543.6–600.0 mbsf  
 Thickness: 56.4 m  
 Age: late Miocene

Lithologic Subunit IE is lithologically identical to Subunit ID, except that no dropstones are present and slight bioturbation is pervasive. Another key difference is the occurrence of kaolinite in Core 152-918D-29R, also identified in the underlying lithologic Unit II (Table 3). Subunit IE is separated from the underlying lithologic Unit II at the first downhole occurrence of a micritic hardground.

Lithologic Unit II: silt with variable amounts of nannofossils and clay, and nannofossil chalk with silt  
 Intervals: 152-918D-34R-1, 40 cm, to -55R-5, 20 cm  
 Depth: 600.0–806.5 mbsf  
 Thickness: 206.5 m  
 Age: early Miocene–late Miocene

Lithologic Unit II comprises nannofossil chalk and very dark gray silt with nannofossils, moderately to heavily burrowed by predomi-

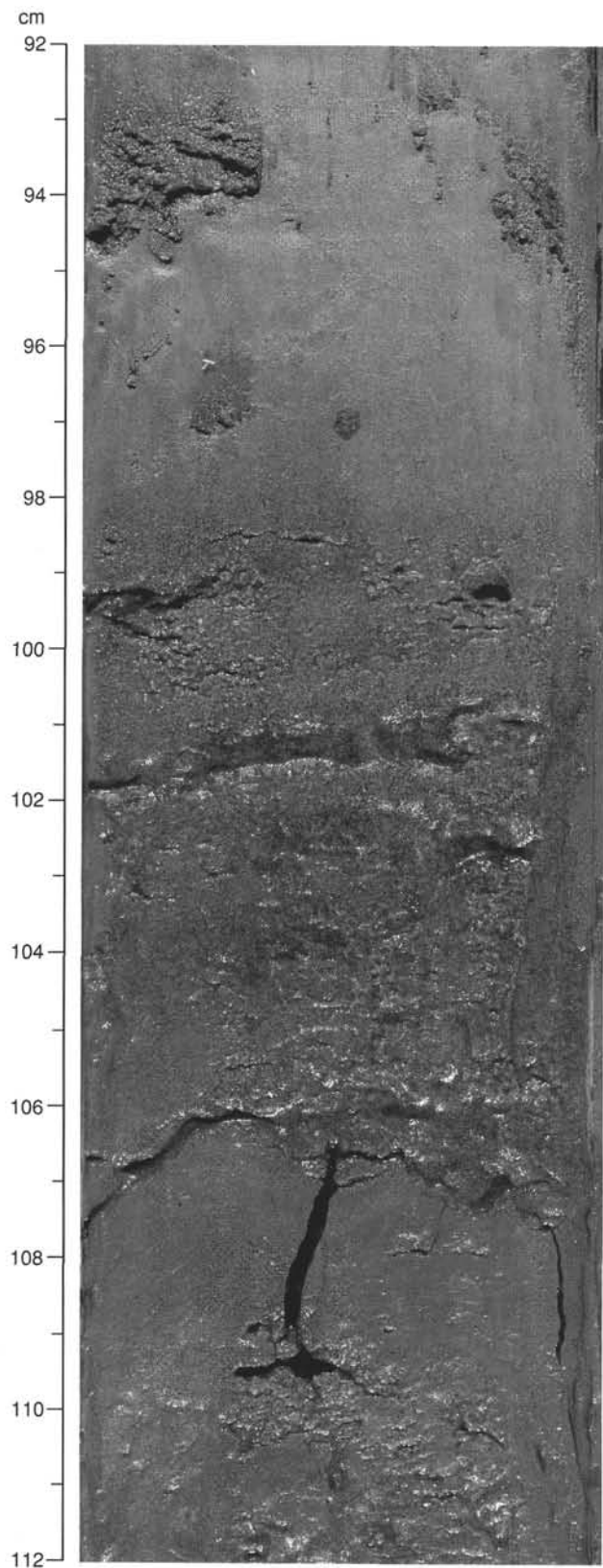


Figure 10. Lithologic Subunit IA (Interval 152-918A-4H-2, 92–112 cm), a type A turbidite with amphibole-enriched sand grading upward into massive silt. Note slight burrowing on left of core at 92 to 97 cm and granule-sized dropstone in center of core at 97 cm.

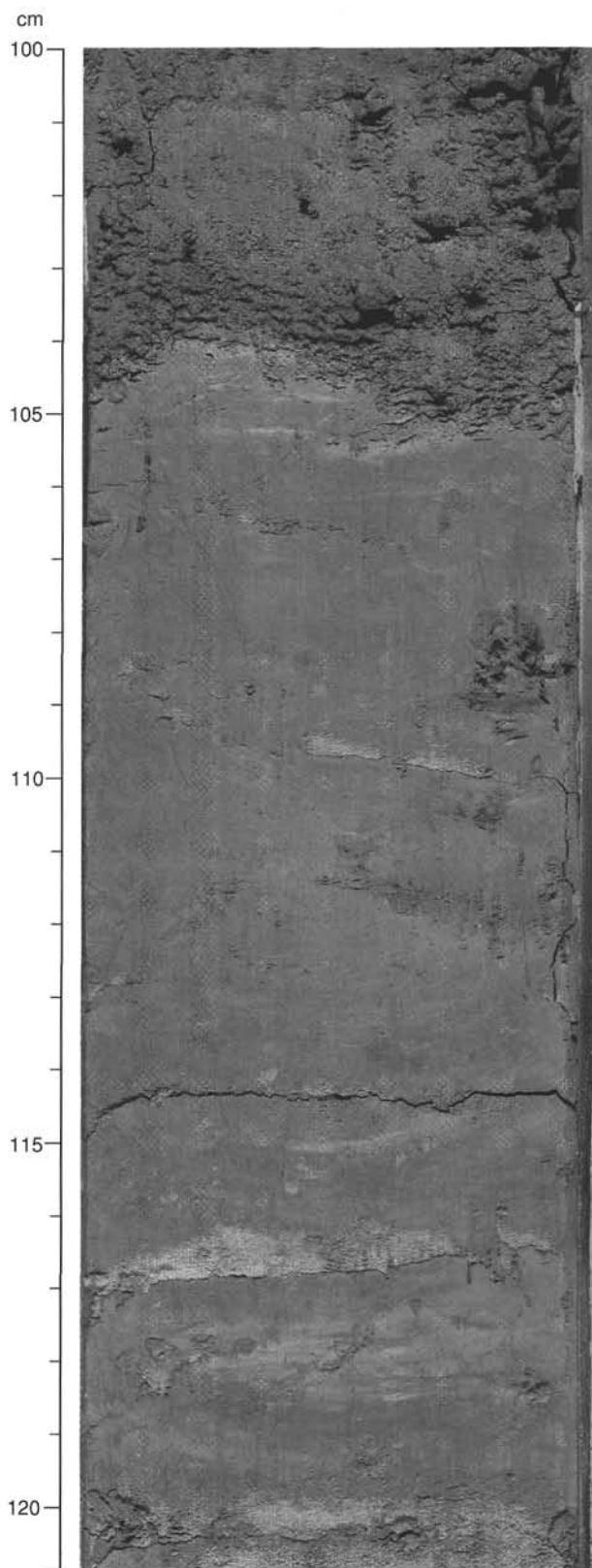


Figure 11. Lithologic Subunit IB (Interval 152-918A-17H-3, 100–121 cm). From 100 to 105 cm, one can see the base of a type A (grayish-brown) turbidite, showing its erosional contact with the underlying (105–121 cm) series of type B turbidites. Type A turbidites are thicker-bedded and are dominated by volcanogenic components. Type B turbidites are thinner sand-silt couplets, dominated by nonvolcanic (continental) components, and are devoid of microfossils.

**Table 3. Results of shipboard X-ray diffraction analysis of bulk samples, Site 918.**

Core, section, interval (cm)	Qtz.	Felds.	Amph.	Mica	Calc.	Dol.	Pyri.	Smc.	Ill.	Kao.	Zeo.	Glau.
<b>152-918A-</b>												
3H-3, 37-38	X	X	X	X				X				
3H-6, 131-132	X	X			X							
4H-2, 14-15	X	X	X	X				X				
4H-5, 70-71	X	X	X	X								
5H-2, 55-56	X	X	X	X								
13H-4, 69-70	X	X	X					X				
14H-2, 47-48	X	X	X									
15H-3, 73-73	X	X	X					X				
24X-5, 144-145	X	X		X				X		X		
26X-3, 87-88	X	X						X				
27X-1, 56-58	X	X						X				
27X-1, 92-93	X	X	X	X								
27X-1, 125-126	X	X						X				
27X-6, 104-105	X	X						X				
28X-4, 26-27	X	X	X					X				
28X-4, 117-118	X	X	X									
28X-5, 54-55	X	X	X	X								
<b>152-918D-</b>												
1R-1, 63-64	X	X	X									
29R-2, 30-31	X	X						X	X	X		
35R-2, 55-56	X	X						X	X	X		
37R-3, 74-75	X	X						X	X	X		
41R-5, 0-2	X	X			X			X	X	X		
44R-3, 132-133	X	X			X			X	X	X		
51R-6, 72-75	X	X					X	X	X			
57R-4, 7-8	X	X	X		X			X			X	
68R-1, 19-20	X	X						X				
68R-1, 61-62	X	X						X				
74R-CC, 8-9	X	X				X						
88R-1, 8-10								X				X

Notes: Qtz. = quartz; Felds. = feldspar; Amph. = amphibole; Calc. = calcite; Dol. = dolomite; Pyri. = pyrite; Smc. = smectite; Ill. = illite; Kao. = kaolinite; Zeo. = zeolite; Glau. = glauconite.

**Table 4. Characteristics of types A and B turbidites, lithologic Subunit IB, Site 918.**

Package	Interval (cm) Hole 918A	Depth (mbsf)	Thickness (m)	Characteristics	Fossils	CaCO <sub>3</sub>
1	9H-2, 127 to 10H-6, 12	71.07-85.42	14.35	Type B: Thin turbidite silts with white quartz laminae, light green.	Barren at top, common at base	Very low
2	10H-6, 12 to 12H-2, 37	85.42-98.67	13.25	Type A: Turbidite sand and silt beds 10 cm to 1 m thick.	Abundant at top, barren at base	Medium to low
3	12H-2, 37 to 13H-5, 5	98.67-112.35	13.67	Type B: Thin turbidite silts with white quartz laminae, light green.	Barren throughout package	Very low
4	13H-5, 5 to 14H-3, 70	112.35-119.50	7.15	Type A: Turbidite sand and silt beds 5 cm to 1 m thick.	Common to abundant	Medium
5	14H-3, 70 to 16H-2, 110	119.50-135.90	16.40	Type B: Thin turbidite silts with white quartz laminae, light green.	Small traces only	Low
6	16H-2, 110 to 19H-5, 70	135.90-168.50	32.60	Type A: Turbidite sands and silts with small Type B at 147.85-148.2 and at 156.5-156.75 mbsf.	Top is low and common silic. fossils near base	Low
7	19H-5, 70 to 19H-6, 60	168.50-169.90	1.40	Type B: Thin turbidite silts with white quartz laminae.	Barren to small traces of fossils	Low
8	19H-6, 60 to 22X-1, 105	169.90-191.50	22.05	Type A(-): Thick turbidite silt beds finer-grained than Type A.	Barren near top, high silic. base	Low to medium
9	22X-1, 105 to 25X-6, 130	191.50-226.4	34.9	Type A(-): Fine-grained distal turbidites; may be lumped in 8.	Silic. fossils near base	One high value, rest very low

nantly *Thalassinoides*, *Planolites*, *Chondrites*, and *Zoophycos* (Figs. 15 and 16). The very high content of nannofossils (up to 90% for the dominant lithology; a mean of about 30%-40%, Fig. 7) makes this unit the most carbonate-rich recovered at Site 918 (see "Inorganic Chemistry" section, this chapter). Complete or fragmented bivalves (Fig. 17), rare sponge spicules, and radiolarians also are present in the sediment. Phillipsite occurs in small amounts (2%-4%). The silt contains a volcanoclastic component of altered vitric grains (ash?) and rock fragments (up to 40%; Fig. 7). The presence of illite and kaolinite with some quartz suggests a continental source for the silt as well (Table 3).

The upper contact of the unit is placed at the first downhole occurrence of a micrite bed. The first actual chalk occurs in Core 152-918D-36R at 621.1 mbsf. We counted more than 30 cycles of silt-nannofossil chalk that culminate in a series of glaucony hardgrounds showing erosional features at their tops (Fig. 18). Above each of these contacts is a poorly sorted, sandy interval enriched in quartz, illite, rip-up clasts from the hardgrounds, and ripples constructed of glauconite pellets (Fig. 19). Poor sorting of the overlying sand and the erosive contact with the hardgrounds indicate likely transport and deposition of the sand by highly concentrated flows possibly related to the initiation of bottom water overflow from the Arctic Ocean into the Irminger Basin. It is noteworthy that above the last glaucony hardground/coarse sand

couplet in Section 152-918D-37R-1, only one thin, nannofossil chalk bed and two micritic horizons occur before the onset of noncalcareous silt deposition (lithologic Unit I), suggesting that cold bottom waters had raised the calcium-carbonate compensation depth (see "Biostratigraphy" section, this chapter).

Slow depositional rates and hiatuses are indicated by glauconitic hardgrounds, pellets, and matrix-replacing cement in the lower parts of this subunit, in Cores 152-918D-51R to -55R (Fig. 20). The hardgrounds are often burrowed by *Thalassinoides*-type organisms (Fig. 20). The lower part of the unit (725-811 mbsf) is also fractured by numerous normal faults coated with slickensides. Displacement along some of these is at least as great as the core width (6-7 cm), as different beds are commonly seen juxtaposed in the core.

Lithologic Unit III: quartz silt with enrichment in quartz sand or nannofossils and quartz sand turbidites  
 Interval: 152-918D-55R-5, 20 cm, to -86R-CC  
 Depth: 806.5-1108.2 mbsf  
 Thickness: 301.7 m  
 Age: early Miocene-late Oligocene

This unit is divided into an upper, silty, intermittently calcareous or sandy lithologic Subunit IIIA and a lower, coarse sand Subunit IIIB.

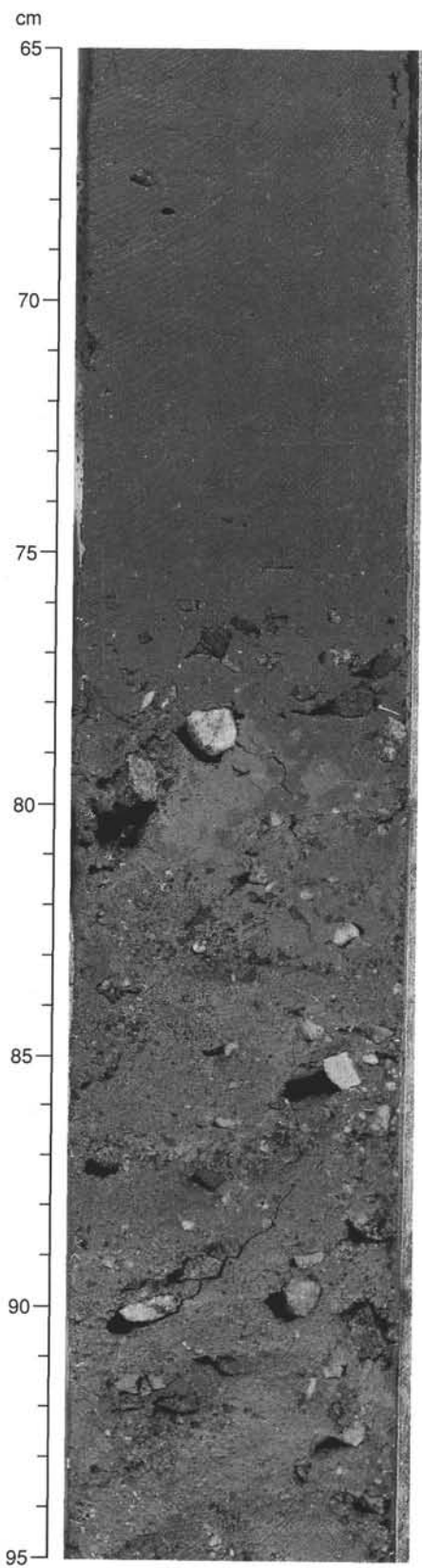


Figure 12. Lithologic Subunit IC, silt enriched with ice-rafted debris (Interval 152-918A-27X-1, 65-95 cm). Silt matrix of rock flour with abundant, angular pebbles interbedded with dark gray, massive silt.

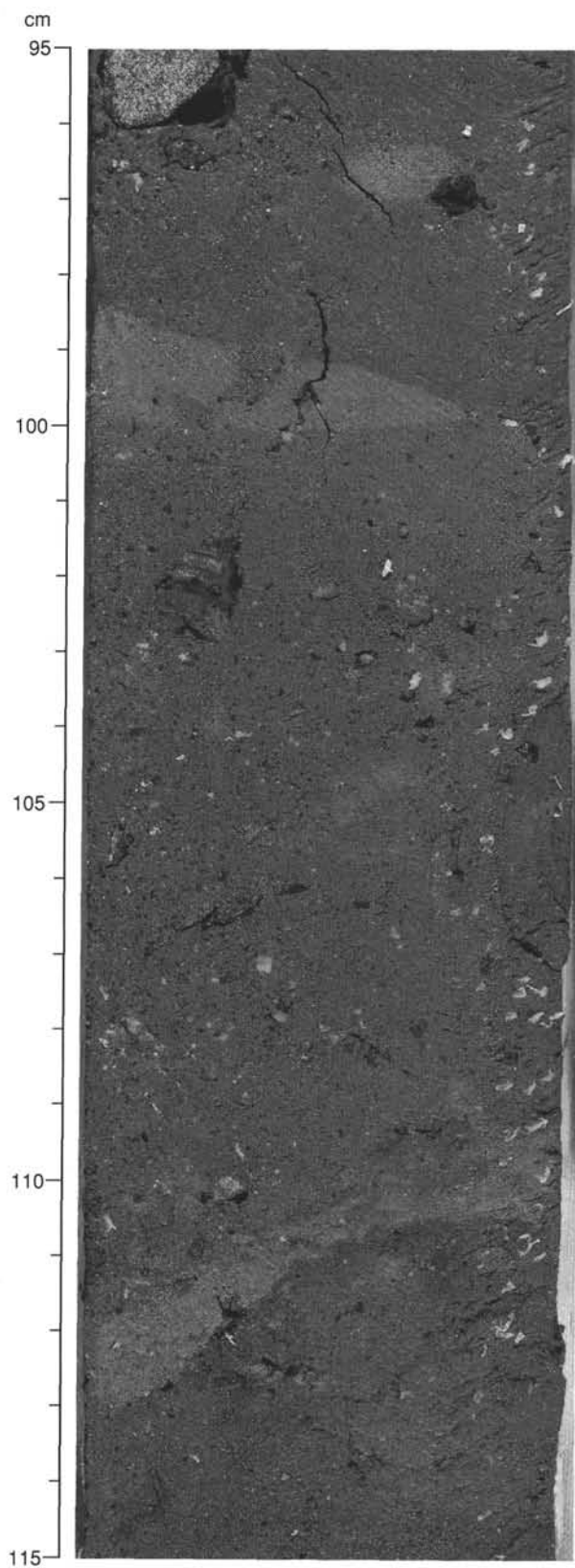


Figure 13. Lithologic Subunit IC (Interval 152-918A-28X-3, 95-115 cm). Massive, compact pebbly silt.

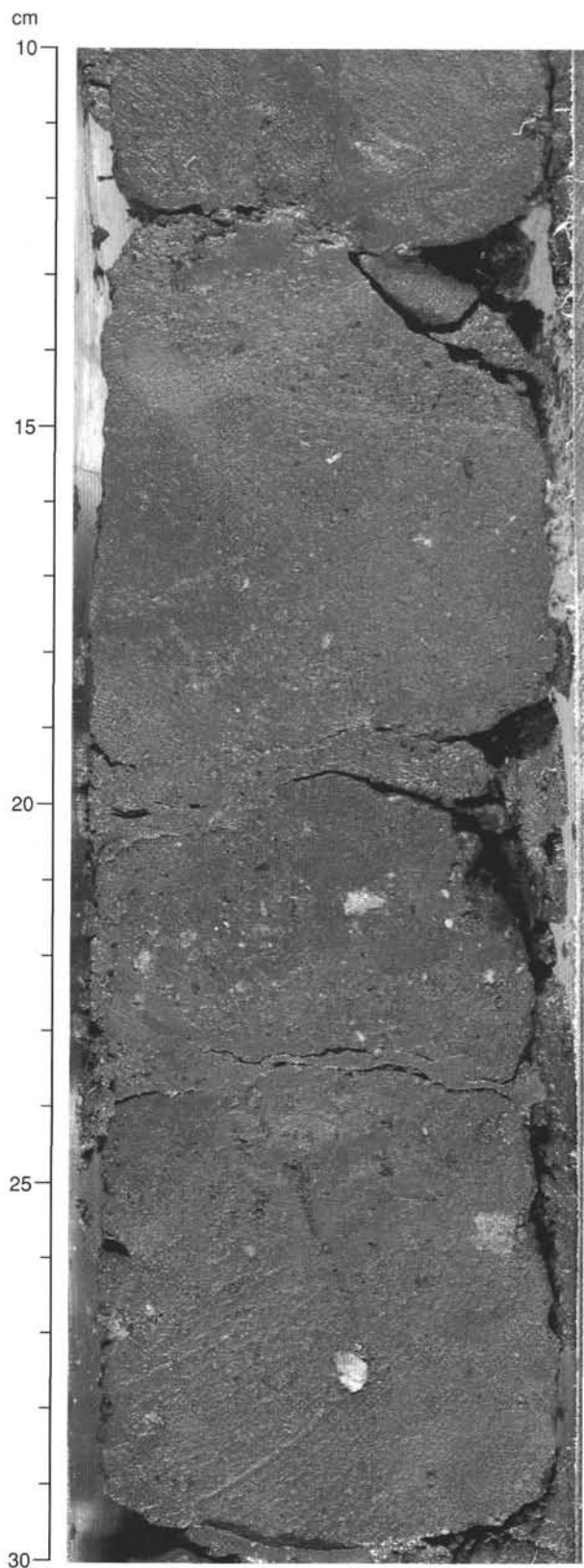


Figure 14. Last occurrence of dropstones observed in place in Section 152-918D-28R-2, 10–30 cm, lithologic Subunit ID. This interval has been dated by nannofossils, foraminifers, and sedimentation rates to about 7 Ma.

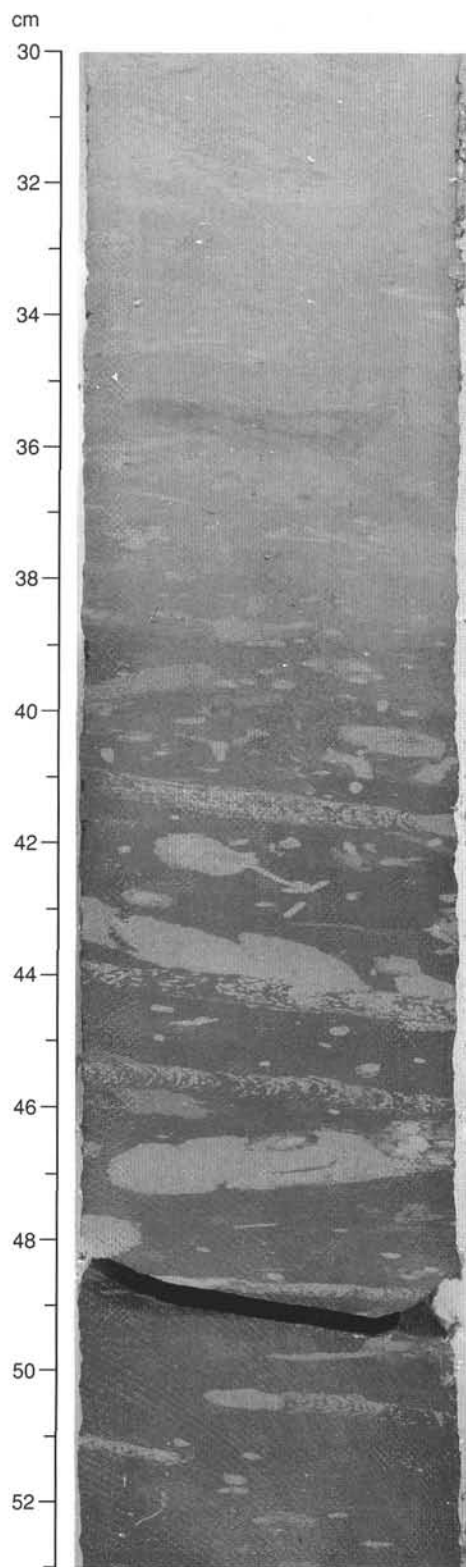


Figure 15. Lithologic Unit II (Interval 152-918D-51R-5, 30–53 cm). The dominant lithology is a massive, bioturbated chalk (30–38 cm) that is interbedded with dark gray silt, usually enriched in nannofossils (38–53 cm). Bioturbation is common in this unit. Several *Zoophycos*, *Planolites*, and *Chondrites* burrows are clearly outlined in the dark silt and faintly outlined in the chalk.

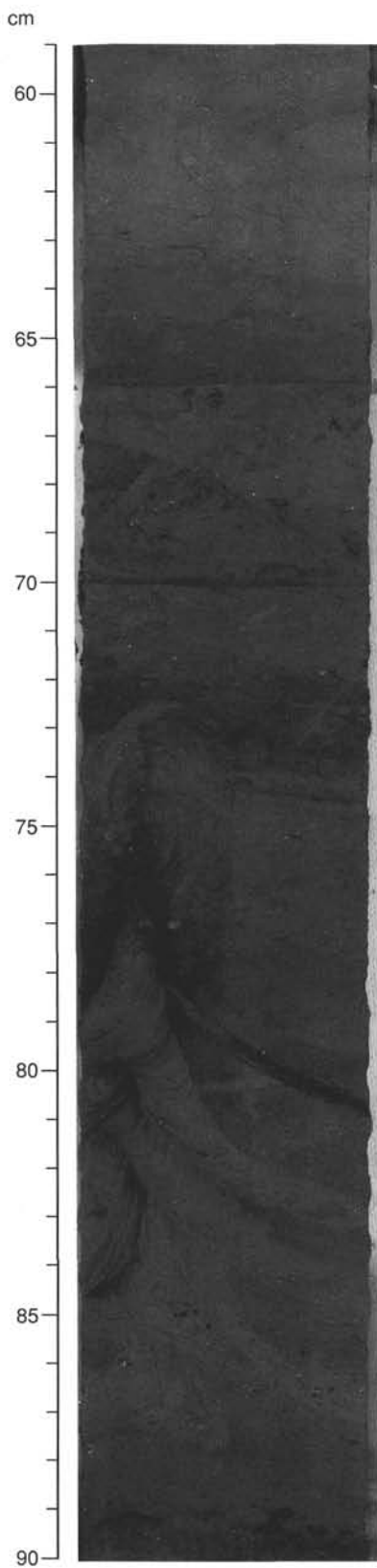


Figure 16. Lithologic Unit II (Interval 152-918D-41R-4, 59-90 cm). The *Zoophycos* organism has burrowed into sediment later enriched by glaucony (dark band, 72-74 cm).

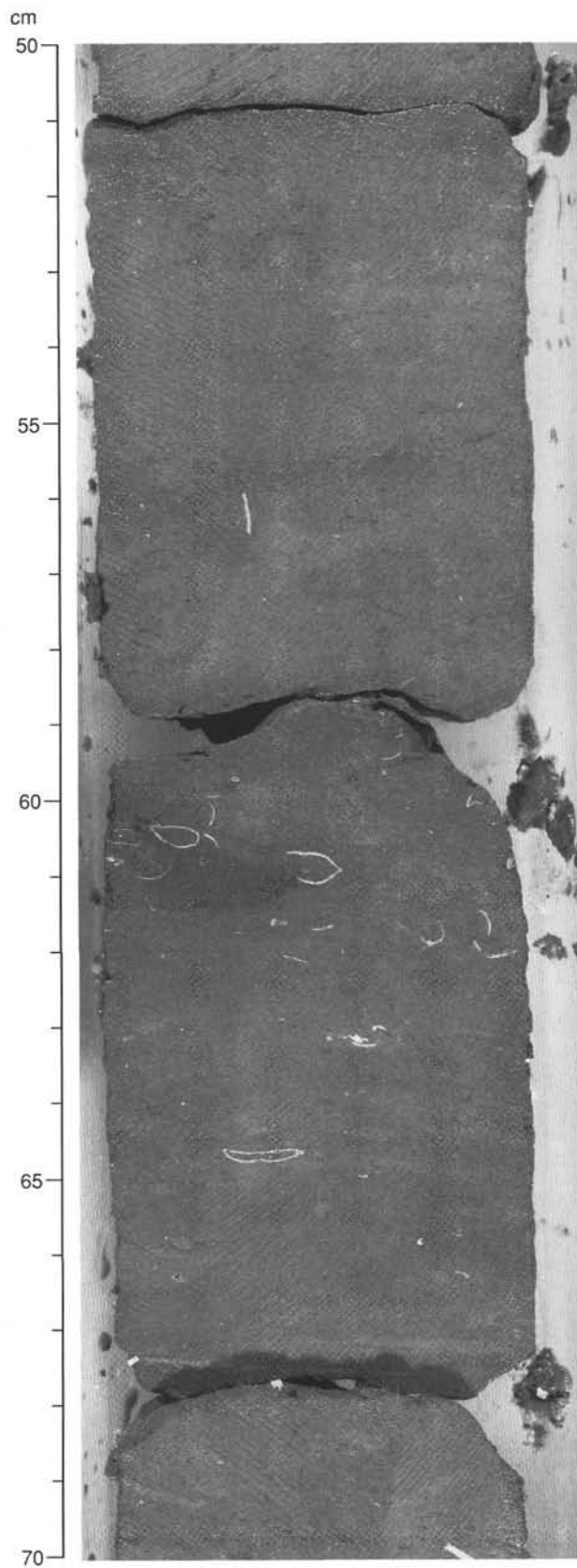


Figure 17. Lithologic Unit II (Interval 152-918D-40R-4, 50-70 cm). Complete and fragmented bivalves in the dark gray silt interbeds of nanfossil chalk.

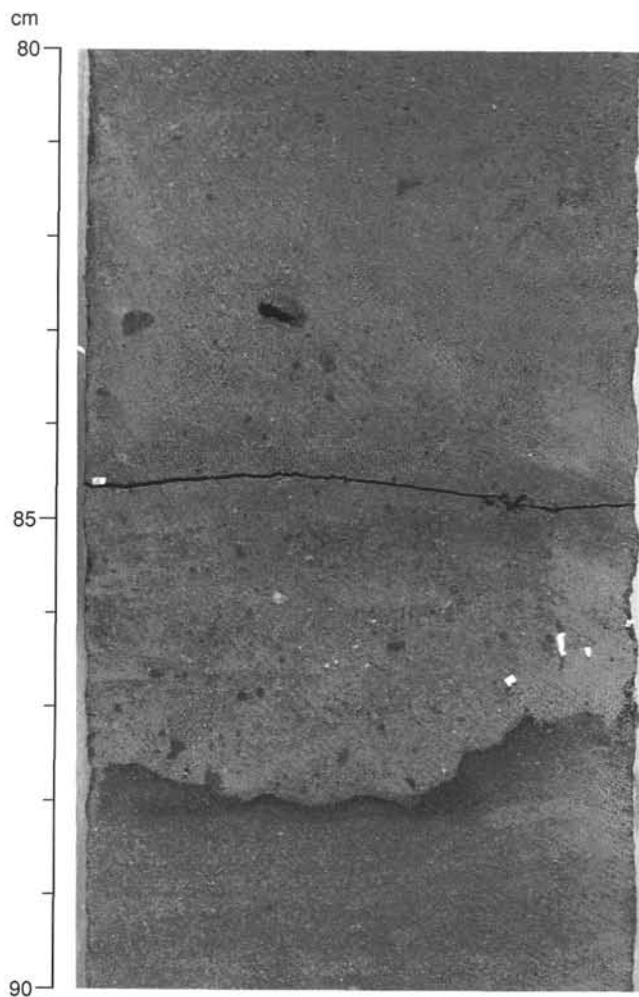


Figure 18. Upper lithologic Unit II (Interval 152-918D-37R-3, 80–90 cm); glauconitic hardground with erosive upper contact at 87–88 cm. Above the hardground, coarse sand, mollusk debris, and glaucony rip-up clasts float in a silt-clay matrix. Such hardground/coarse sand couplets are related to the initial overflow of NADW into the Irminger Basin. Calcareous deposition stops at this site within 10 m above the highest couplet.

Lithologic Subunit IIIA: quartz silt with enrichment in quartz sand or nannofossils  
 Interval: 152-918D-55R-5, 20 cm, to -76R-CC  
 Depth: 806.5–1011.6 mbsf  
 Thickness: 205.1 m  
 Age: early Miocene–late Oligocene

Lithologic Subunit IIIA comprises interbeds of nannofossil chalk similar to those of lithologic Unit II, and massive to faintly laminated silt and thin sand. Erosive contacts, cross-lamination (Fig. 21), and the massive nature of many of the sand beds (Fig. 22) indicate transport and deposition by turbidity currents. Burrows and glauconitic laminae and clasts are concentrated over intervals where sedimentation was not affected by turbidity currents (Fig. 22). Pyrite occurs as isolated nodules or disseminated grains. Wood is sometimes concentrated along sand bedding planes (Fig. 21). Nanofossils (up to 65%) remain the dominant component of the chalk (Fig. 7), complemented with some bivalve fragments and echinoid spines. The silt and sand beds are composed of quartz, feldspar, and volcanoclastic grains (Fig. 7). Smectite was the only clay mineral identified by XRD analysis (Table 3).

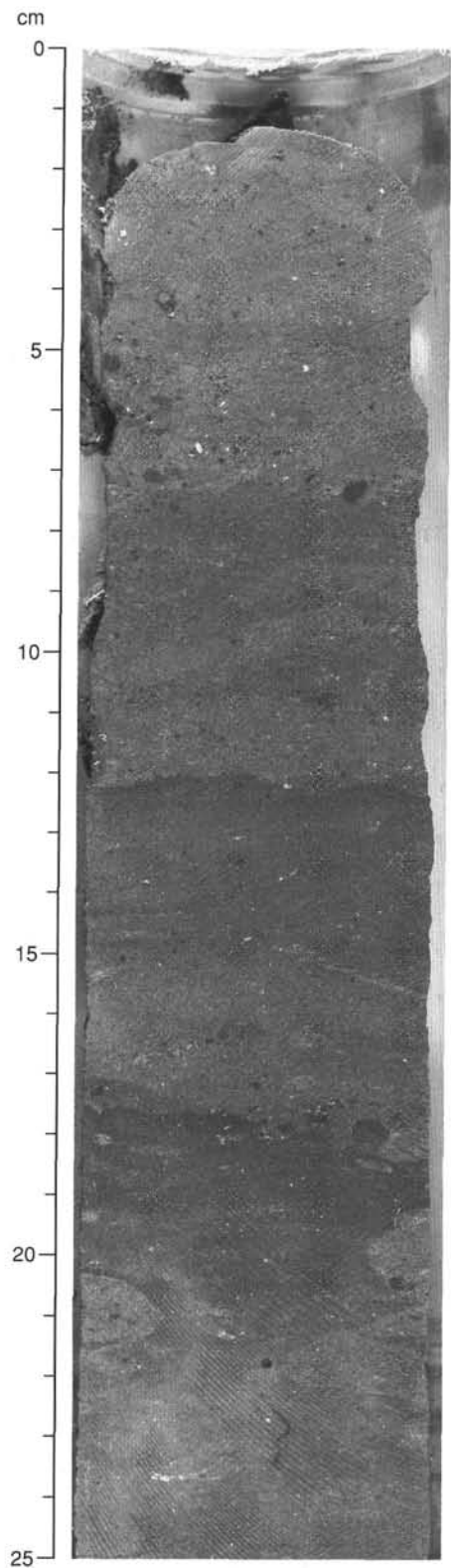


Figure 19. Upper lithologic Unit II (Interval 152-918D-38R-1, 0–25 cm); burrowed glaucony hardground (18–19 cm) and a fainter, less-developed hardground at 7 to 8 cm. The hardgrounds have eroded, as indicated by the dark, glaucony rip-up clasts immediately above and scattered in the coarse material above the hardgrounds. Glauconite pellets have been molded into ripples visible at 12 to 13 cm.

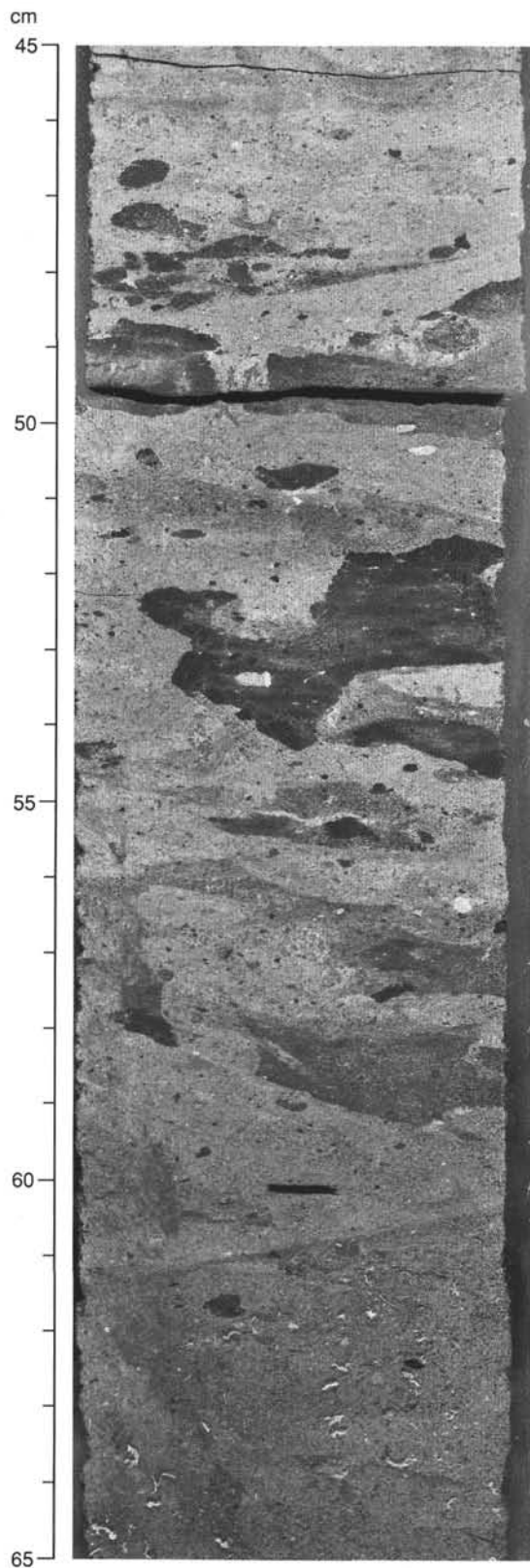


Figure 20. Lower lithologic Unit II (Interval 152-918D-57R-4, 45–65 cm); glauconitic cement replacing matrix (51–60 cm) and a glauconitic hardground with a *Thalassinoides*-type burrow (48–51 cm).

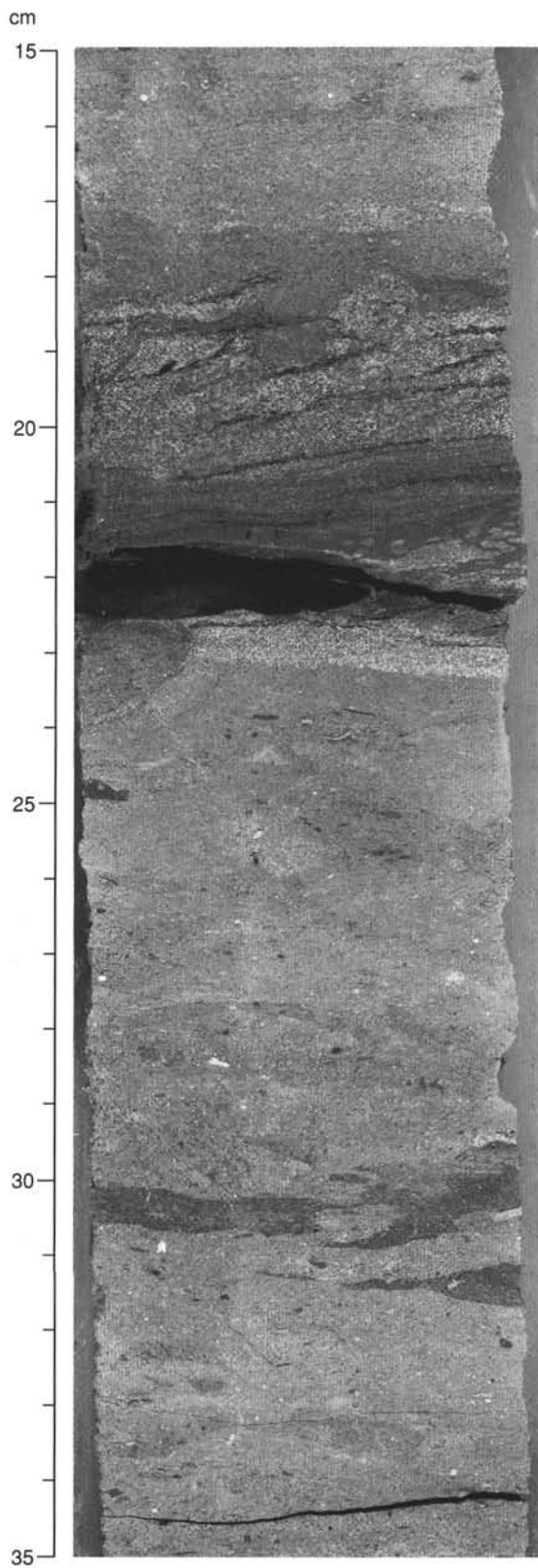


Figure 21. Lithologic Subunit IIIA (Interval 152-918D-57R-4, 15–35 cm); turbidite (Bouma  $T_c$ ) with cross-laminae (ripples) and concentrated wood fragments interbedded in highly bioturbated nanofossil chalk (24–35 cm). The top of the turbidite is bioturbated.

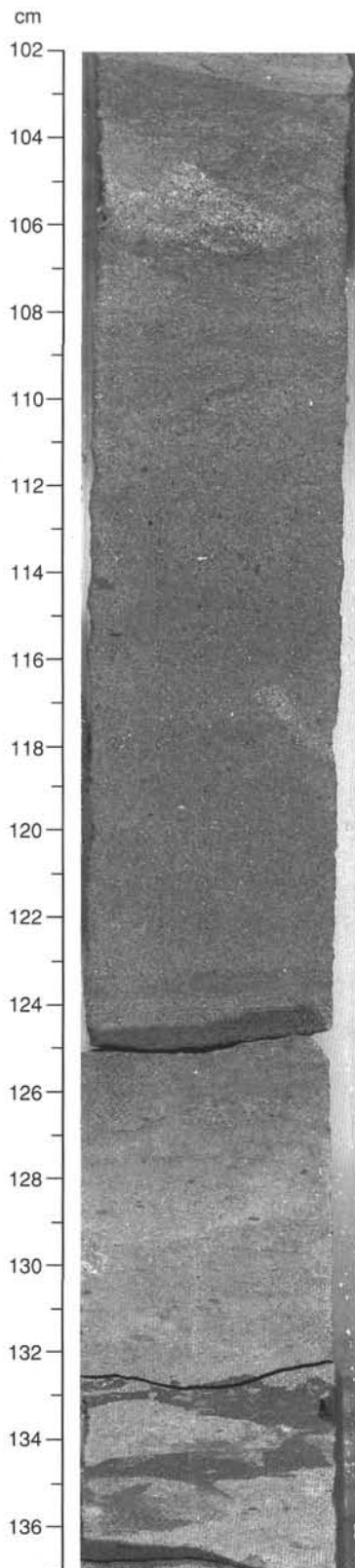


Figure 22. Lithologic Subunit IIIA (Interval 152-918D-57R-3, 102-137 cm); massive turbiditic sand (Bouma  $T_3$ ; 103-124 cm) interbedded in glauconitized nannofossil chalk and silt (124-137 cm).

Lithologic Subunit IIIB: massive quartz sand  
Interval: 152-918D-77R-1 to -86R-CC  
Depth: 1011.6-1108.2 mbsf  
Thickness: 96.6 m  
Age: late Oligocene

Lithologic Subunit IIIB is unique because of the coarse terrigenous sediment that was recovered and the high accumulation rates (see "Sedimentation Rates" section, this chapter), the result of deposition by turbidity currents. The sand occurs as massive (Fig. 23) or highly bioturbated (Fig. 24), dark greenish quartz sand beds. Quartz grains (up to 65% of total) are angular to rounded. Feldspar (up to 15%), dolomite (up to 15%), and a large amount of altered grains (up to 40%) are the major mineralogic components. Accessory minerals, such as amphibole, zoisite, epidote, pyroxene, and garnet, indicate a diverse array of continental sources. Brownish horizons (minor lithology), enriched by up to 35% dolomitic silt, occur within this subunit. Faint laminae composed of glauconite pellets, glauconitic hardgrounds, and small pieces of wood also are present. Nannofossils and other microfossils are almost absent (Fig. 7).

Core 152-918D-86R (1098.5-1108.2 mbsf) contains a 2 m-thick massive, granule-sized gravel (mean size, 2-4 mm), with pebbles consisting of mixed basalt, gabbro, granite, gneiss, sandstone, pyroxenite, quartz, and feldspar clasts (Fig. 25).

Lithologic Unit IV: nannofossil chalk and silt with nannofossils enriched in clay or altered volcanoclastic grains  
Interval: 152-918D-87R-1 to -92R-2, 25 cm  
Depth: 1108.2-1157.9 mbsf  
Thickness: 49.7 m  
Age: middle-early Eocene

Lithologic Unit IV comprises burrowed, silty nannofossil chalk and silt with nannofossils enriched in clay (Fig. 26). The upper contact of Unit IV with Unit III was not recovered, but the highest level recovered, Section 152-918D-88R-1, is marked by a thin, dark brown manganese hardground covered with a fine horizon (4 cm minimum thickness) of nannofossil chalk (Fig. 27). In addition to nannofossils (up to 50%), echinoid spines, benthic foraminifers, bivalves, and echinoderms are present, as are burrows of *Chondrites* and *Planolites*. The silt is dominated by volcanoclastic (altered glass, basalt clasts, Fig. 7) or volcanic derived products (smectite; Table 3). Glaucony occurs either as fine silty laminae or as individual pellets throughout the lithology. An enrichment in iron oxide grains gives the lithology a dark brown color.

Lithologic Unit V: glauconitic sandy silt  
Interval: 152-918D-92R-2, 25 cm, to -96R-3, 128 cm  
Depth: 1157.9-1189.4 mbsf  
Thickness: 31.5 m  
Age: early Eocene

This black green unit consists of black volcanoclastic silt, with up to 70% glauconite pellets, interbedded with extensively bioturbated green calcareous sand (Fig. 28). There are a few traces of nannofossils, foraminifers, and recrystallized radiolarians. This unit differs from the overlying unit by having no chalk (Fig. 7) and a much higher abundance of glauconite pellets. Fresh basalt (sill?) occurs within this unit in Core 152-918D-94R. The contact between the basalt and the enclosing sediment was missed because of drilling disturbance and lack of recovery, so no firm evidence exists for possible contact metamorphism. Below the basalt layer both glaucony and grain size increase in the sediment downcore to the sharp, uneven contact with the underlying, highly altered basalt saprolite (Fig. 29).

Lithologic Unit VI: highly weathered basaltic lava flows  
Interval: 152-918D-96R-3, 128 cm, to -97R-CC  
Depth: 1189.4-1204.4  
Thickness: >5.3 m  
Age: Unknown, presumed late Paleocene-early Eocene

The upper part of the basalt pile is extensively weathered and comprises lithologic Unit VI. Although only 5.3 m (Cores 152-918D-96R to -97R) were described by the sedimentologists, intense weathering extends at least 17 m into the basalt (igneous Unit 4, Core 152-918D-98R) where the color changes from red and yellowish brown to gray. Alteration extends even deeper. The lower boundary of Unit VI has somewhat arbitrarily been defined at 1204.4 mbsf.

The weathered basalt is dominantly a limonite-brown color and is entirely altered to clay and iron oxides, hydroxides, and oxy-hydroxides. Vesicles and veins are filled with iron oxides, hydroxides, and oxy-hydroxides. Vesicles and veins are filled with iron oxides and an unknown blue mineral. One drilling biscuit at 152-918D-96R-CC, 23–26 cm, was a bright, malachite green when the core was opened but darkened to brown while the core was being described. Relict flow structure becomes increasingly evident in Core 152-918D-97R, with three igneous flow units recognized (igneous Units 2, 3, and 4A).

### Summary and Discussion

An important discovery from Site 918 is the unquestionably in-situ dropstones in upper Miocene sediment (Fig. 14). Biostratigraphic control and sedimentation rates provide a minimum age of about 7 m.y. for the oldest dropstones (see "Sedimentation Rates" section, this chapter). These dropstones occur in the upper 600.0-m-thick lithologic Unit I, predominantly silt and enriched in dropstones over the upper 543.6 m. The upper 226.4 m of this section, Subunits IA and IB, is highly influenced by a submarine fan system that supplied coarse detritus to this area.

Lithologic Unit II is predominantly nannofossil chalk with interbedded silt, which records another important event: the initiation of cold bottom currents into the Irminger Basin. This is recorded by the glauconitic hardgrounds overlain by coarse, poorly sorted sand in Cores 152-918D-37R and -38R. The glauconitic hardgrounds suggest nondeposition of nannofossils as well as terrigenous silt, for some unknown period of time. That this influx represents nascent North Atlantic Deep Water (NADW) is substantiated by the appearance of NADW-affiliated benthic foraminifers within and above these hiatuses, but not below (see "Biostratigraphy" section, this chapter). The significance of the hiatus prior to each "overflow" event is a topic for shore-based studies. Nannofossil deposition, recovered as one thin chalk bed and two micritic beds in Cores 152-918D-34R to -36R, stops within 10 m above the youngest hardground (see also "Organic Geochemistry" section, this chapter). This suggests that the initiation of bottom water had a profound effect on the CCD level, calcareous plankton productivity, or both. Coccoliths and foraminifers before this event are indicative of warmer waters than occur in the basin today (see "Biostratigraphy" section, this chapter). In addition, benthic fauna change over this same interval from a rich *Zoophycos-Planolites-Chondrites* assemblage to a sparse *Chondrites* assemblage.

The occurrence of glauconitic hardgrounds, replacement cement, and abundant pellets downcore to the lower part of lithologic Unit II suggests that chalk deposition was cyclic from the outset (late Oligocene) and that there was no source for terrigenous silt to fill in the gaps, as occurred during deposition of the middle part of this unit.

The bioturbation in this interval is as striking as it is abundant (Figs. 15 and 16). In a broad sense, most of the sediment from lithologic Unit II can be assigned to the ichnofacies *Zoophycos* (Fig. 16) of Seilacher (1967). A decrease in the diversity of trace fossils from lithologic Units II through I suggests increasing hostility in the benthic environment associated either with high sedimentation rates (e.g., ice-rafting deposition, turbidity current) or with anoxic or low-oxygen bottom waters.

The influx of volcanogenic grains (altered glass, rock fragments), especially those showing vesicles (gas bubbles), observed in the upper part of Unit II (Fig. 10) during the middle and upper Miocene, may be related to an episode of explosive volcanism. Airborne transport followed by reworking in the deep-sea environment (bottom

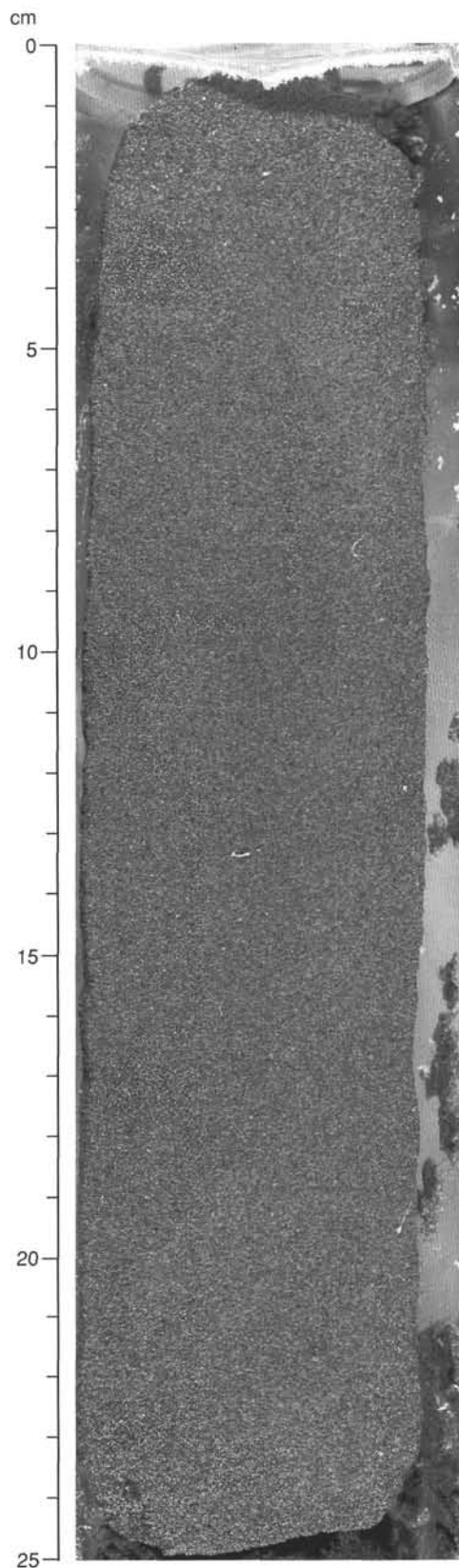


Figure 23. Lithologic Subunit IIIB (Interval 152-918D-77R-1, 0–25 cm): massive turbiditic sand (Bouma  $T_a$ ).

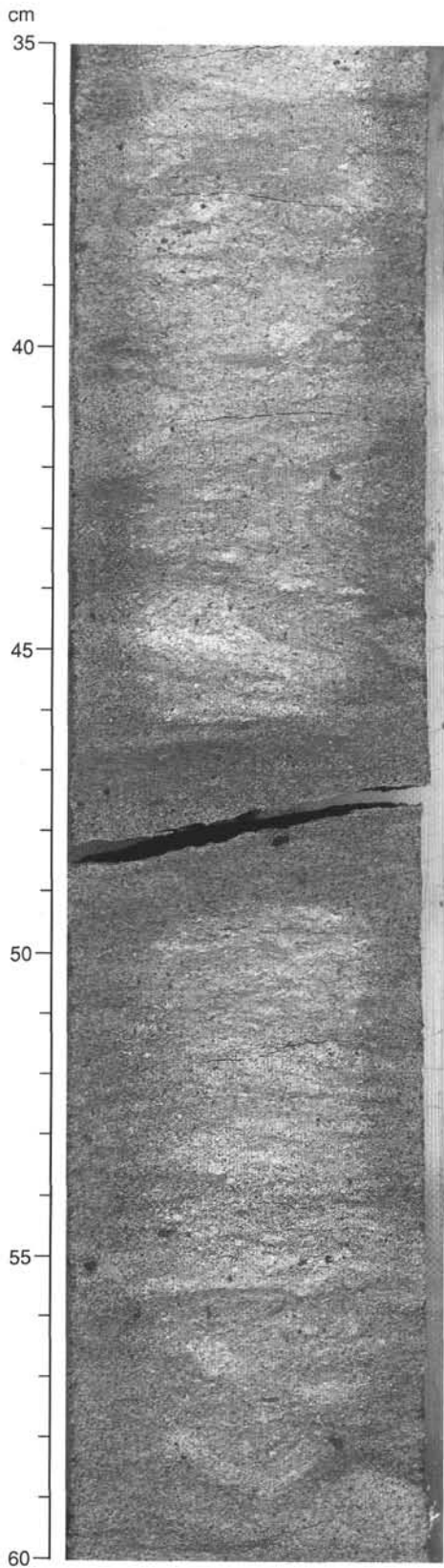


Figure 24. Lithologic Subunit IIIB (Interval 152-918D-76R-1, 35–60 cm); massive turbiditic sand (Bouma T<sub>a</sub>), enriched in glauconite pellets and extensively bioturbated.

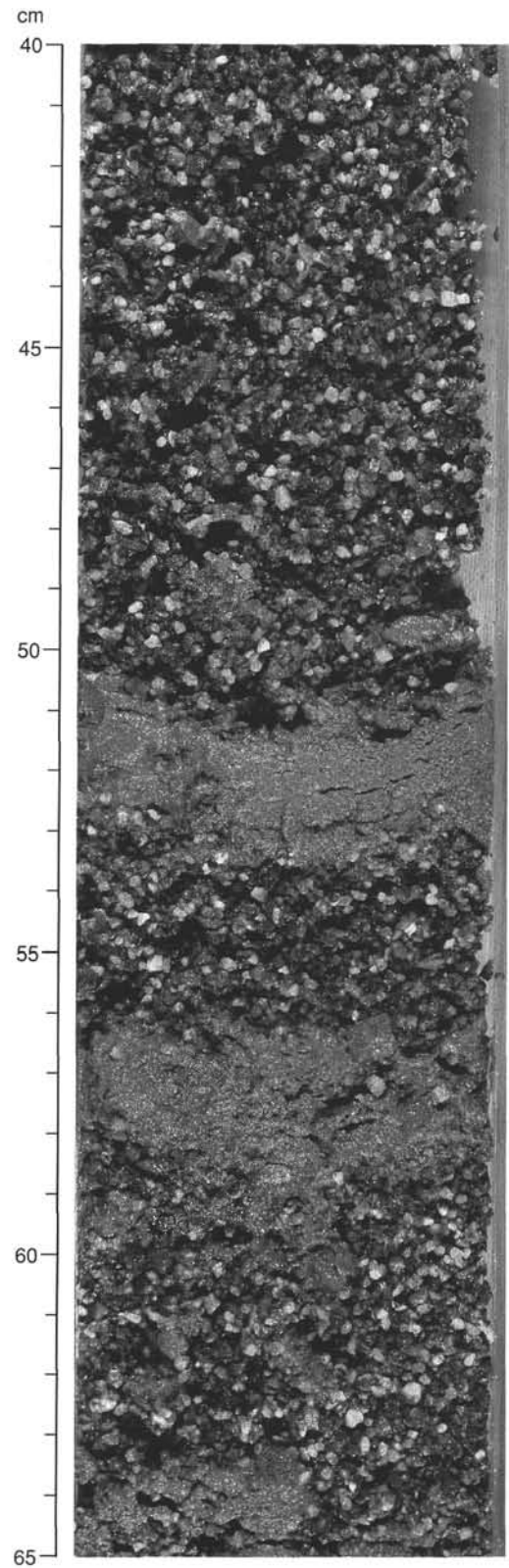


Figure 25. Lithologic Subunit IIIB (Interval 152-918D-86R-2, 40–65 cm); granule-sized gravel interbedded with silty sand. This sediment was recovered from near the base of the upper Oligocene turbidite sequence, and was deposited in a submarine fan channel.

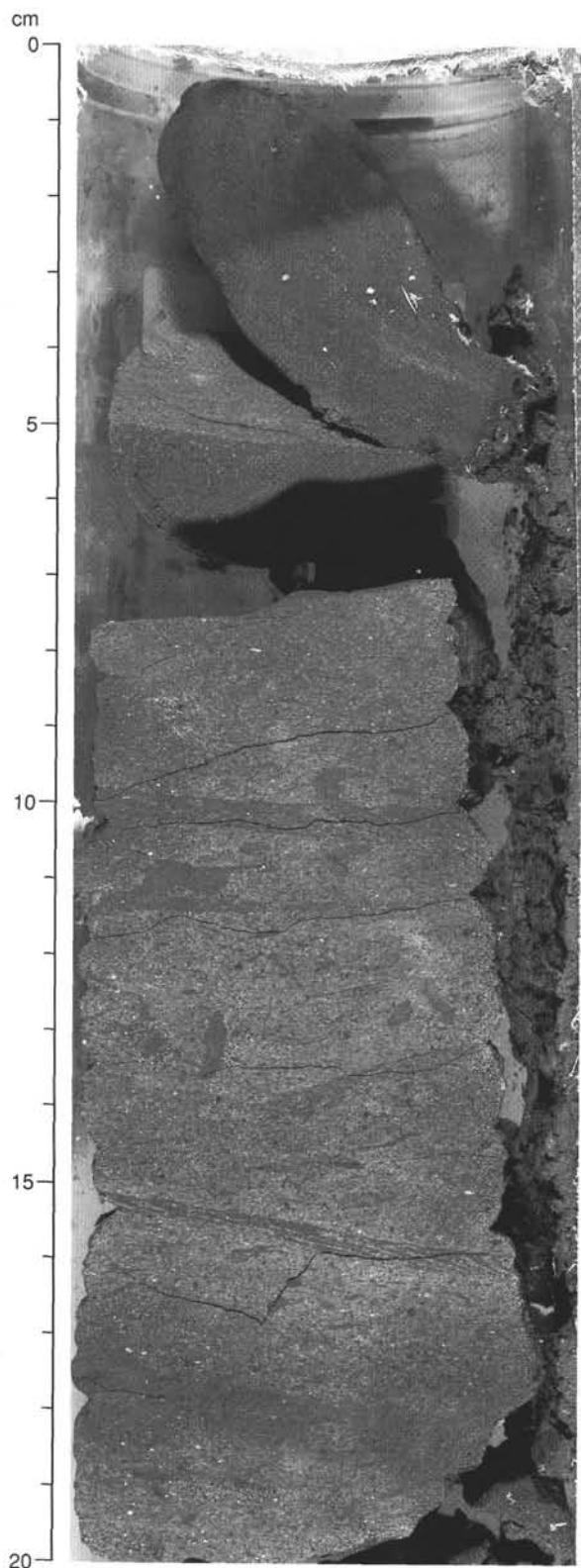


Figure 26. Lithologic Unit IV (Interval 152-918D-89R-1, 0-20 cm); silty nannofossil chalk interbedded with dark volcaniclastic silt. The chalk is extensively bioturbated by *Zoophycos*, *Chondrites*, and possible *Planolites*.

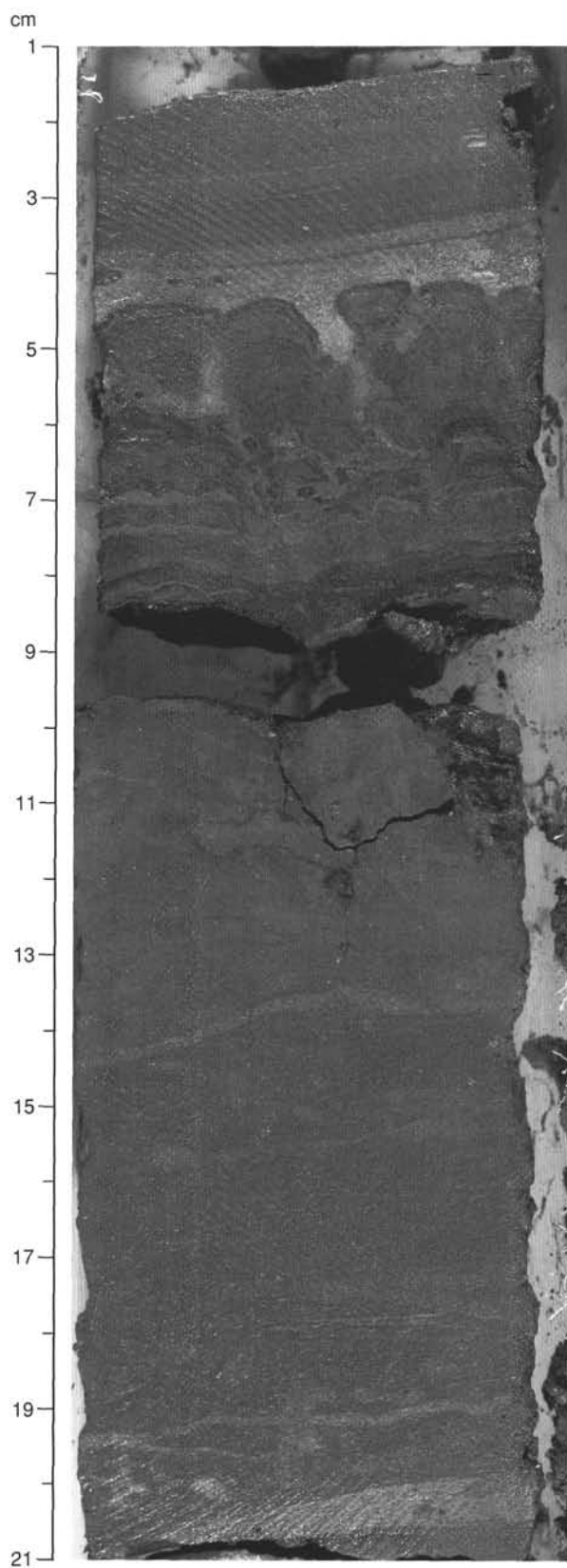


Figure 27. Top of lithologic Unit IV; manganese hardground in Section 152-918D-88R-1, 1-21 cm.

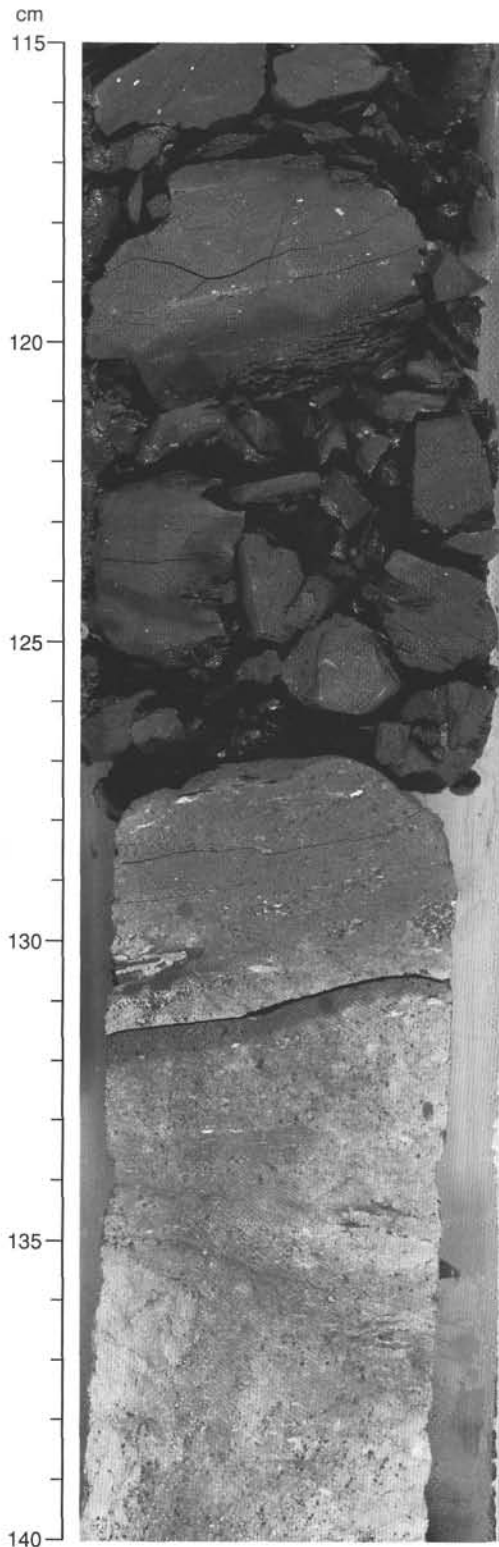


Figure 28. Lithologic Unit V (Interval 152-918D-93R-1, 115–140 cm); black volcanoclastic silt with intermittent calcite-cemented greensand beds. The sand is extensively bioturbated, while the silt contains only rare burrows of *Chondrites*. White specks in the black silt are recrystallized radiolarians.

current, gravity flows) might explain the long-distance transport of this ash debris to Site 918. Erosion during the late Oligocene–early Eocene of volcanic sequences outcropping in East Greenland may also be a source for the lithic volcanogenic material.

During the late Oligocene, a submarine fan system developed off the East Greenland coast and fed gravel and finer-grained sediment into the basin, (lithologic Unit III). The base of Subunit IIIB is marked by a gravelly channel fill, with interbedded fine sand and silt laminae, suggesting the “overbank” deposits of another channel. The sand is dominantly massive (Bouma  $T_a$ ), which also suggests proximity to the main feeder channel or channels. Some intervals of sand have been intensively bioturbated and are rich in glauconite pellets, indicating periodic hiatuses in deposition. This may have been caused by a change in the source area or by channel switching away from this site. The sand persists into the overlying Subunit IIIA, but depositional rates for the sand decline, allowing for the accumulation of nannofossil chalk in the interim. The large volume of sand indicates a steady supply through the late Oligocene and into the early Miocene. Large sand volumes might be generated by large-scale uplift or by intensive weathering and delta development in the source area. The abundance of wood fragments and paucity of feldspar suggest a delta-fed submarine fan system.

Prior to fan deposition, during the mid- to late Eocene, the sediment from Site 918 shows starved basin conditions, as indicated by the thin silt and nannofossil chalk deposits of lithologic Unit IV. The silt is largely volcanogenic and abundant glauconite pellets suggest steady, but slow, erosion of a volcanic terrain. Benthic foraminifer assemblages indicate the basin was probably 200 to 600 m deep (see “Biostratigraphy” section, this chapter). Just prior to fan development, sedimentation rates were low enough to develop the thin manganese crust at the top of Unit IV (Fig. 27). This marked change in sedimentation suggests that a major change in the basin geometry and/or climate took place between the late Eocene and the late Oligocene.

Lithologic Unit V also represents starved basin conditions, but the greater abundance of glaucony, the occurrence of massive, calcite-cemented sand beds, similar to those recovered at Sites 914 and 915 (see “Lithostratigraphy” section, “Site 914” and “Site 915” chapters and “Shelf Stratigraphy Summary” chapter, this volume), and interpreted as storm-deposited shallow marine sand, as well as the absence of chalk, all suggest a shallower environment of deposition than that of lithologic Unit IV. Benthic foraminifers confirm our observations, as mid- to outer-shelf assemblages were identified from this unit (see “Biostratigraphy” section, this chapter). At the base, the coarse greensand of Unit V immediately overlies lithologic Unit VI, a basalt saprolite. While highly altered to clays and iron oxides, the original structure of lava flows is still faintly visible in this limonite-brown horizon.

## BIOSTRATIGRAPHY

About 1200 m of sediments were cored at Site 918 on the East Greenland upper continental rise, at a water depth of 1850 m. In addition to the volcanic basement objective, this site was selected for studying the history of the East Greenland glaciations, the subsidence history of the Irminger Basin, and the early formation of the North Atlantic Deep Water (NADW).

Calcareous nannofossil and planktonic foraminifers provided the necessary time framework for shipboard studies of the sediments. Benthic foraminifer data allowed us to reconstruct a general subsidence history for the Irminger Basin from the early Eocene to the Holocene.

Preliminary examination of *Bolboforma* (algae *Chrysophyta*) in cores having rare or no planktonic foraminifers resulted in useful age information for the lower and middle Miocene sediments. Because the taxonomy and stratigraphic ranges of *Bolboforma* are less well known than those of the major planktonic fossil groups (e.g., Qvale and Spiegler, 1989), detailed shore-based studies will be needed to establish a reliable *Bolboforma* biostratigraphy.

### Calcareous Nannofossils

Most of the core-catcher samples from Hole 918A contain rare-to-few nannofossils. *Emiliania huxleyi* appears to be present from Samples 152-918A-1H-CC through -5H-CC (Fig. 30). However, the identification of this small species (about 3  $\mu\text{m}$  long) is problematic on board the ship because of constant vibration of the microscope, which makes it difficult to examine the specimens with a magnification of more than 1000 $\times$ . If the species occurs down to Core 152-918A-5H, it would mean a condensed lower Brunhes interval or the presence of unconformities. Detailed shore-based studies will clarify this problem.

The highest occurrence of *Pseudoemiliania lacunosa* was recorded in Sample 152-918A-7H-CC, near the lower boundary of the Brunhes interval (Fig. 30). This bioevent is known to occur in the middle of the Brunhes magnetic chron elsewhere. One possibility is that an interval stretching from the lower part of the Brunhes through the Jaramillo is missing (see above). Another possibility is that *P. lacunosa* is present in Samples 152-918A-5H-CC and -6H-CC, but was not seen because of the general low abundances of nannofossils in these two core-catcher samples. Shore-based study of additional samples from these intervals should help resolve this problem.

Samples 152-918A-8H-CC and -9H-CC contain only a few specimens of nannofossils. However, Sample 152-918A-10H-CC contains *Reticulofenestra asanoi*, *Gephyrocapsa* spp. (small), and *Calcidiscus leptoporus*. *Pseudoemiliania lacunosa* is scattered down to Sample 152-918A-31X-CC, whereas *Reticulofenestra gelida* is absent; the interval from Samples 152-918A-11H-CC through -31X-CC thus can be placed in the upper Pliocene (CN12–CN13). Core-catcher samples from Cores 152-918A-32X through -38X are barren of nannofossils.

All core-catcher samples from Holes 918B and 918C appear to contain *Emiliania huxleyi* (see above for discussion of the difficulty with identification of this species on board the ship), and both holes were assigned to the Pleistocene–Holocene (CN15) (Figs. 31 and 32).

No sediment was recovered from Cores 152-918D-1R through -3R. Based on depth correlation with Hole 918A, this interval should be upper Pliocene (CN12–CN13). Core-catcher samples, where available from Cores 152-918D-5R through -21R, either are barren of calcareous nannofossils or contain rare specimens of nannofossils that did not allow for zonal assignment. Samples 152-918D-22R-CC and -23R-CC contain common nannofossils with relatively diverse assemblages. The presence of *Reticulofenestra gelida* in these samples indicates an early Pliocene age (CN10–CN11).

Common nannofossils occur in Sample 152-918D-24R-CC. Among many species present is *Discoaster quinquerramus*, the last occurrence of which at middle latitudes is 5.3 Ma. As discoasters, which preferred warm waters, invariably disappeared earlier at higher latitudes, the last occurrence of *D. quinquerramus* at Site 918 must be older than 5.3 Ma (late Miocene). This age is highly significant because glaciomarine sediments, including dropstones, occur at least as far downhole as Core 152-918D-28R. These cores thus provide the first clear evidence for extensive glaciation in the Northern Hemisphere during the late Miocene.

The interval from Cores 152-918D-25R through -36R contain generally low-abundance and low-diversity nannofossil assemblages. Cores 152-918D-37R through -62R, however, contain mostly very abundant and diverse nannofossil assemblages. The large change around Core 152-918D-37R is interpreted as a large decrease in surface water temperature.

Samples 152-918D-60R-CC and -62R-CC contain a few specimens of Oligocene species (probably reworked) in otherwise Miocene assemblages. The first unambiguous Oligocene nannofossil assemblage was found in Sample 152-918D-63R-CC, which contains *Reticulofenestra bisecta*, and *R. daviesii*, among others. Core-catcher samples from Cores 152-918D-64R through -85R contain no nannofossils. Five samples from different lithologies and sedimentary clasts in Core 152-918D-86R yielded *Reticulofenestra bisecta*, *Cyclicar-*

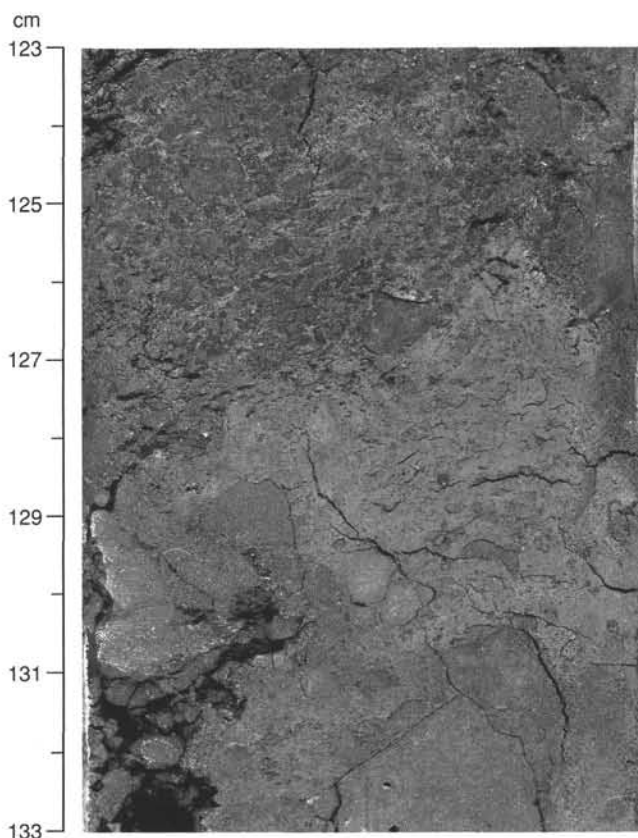


Figure 29. Contact of lithologic Unit V (Interval 152-918D-96R-3, 123–133 cm) with underlying, highly altered volcanic basement. Above the contact is a dark greensand, while the underlying material is yellowish-brown clay.

*golithus floridanus*, *C. abisectus*, but no *Reticulofenestra umbilica*, and can be assigned a late Oligocene age.

Sample 152-918D-88R-CC contains abundant nannofossils with *Chiasmolithus solitus*, with a few specimens of *Reticulofenestra umbilica* and has been placed in Zone CP14a (middle Eocene). A major unconformity thus can be inferred in Core 152-918D-87R, which had no core recovery.

Samples 152-918D-89R-CC through -91R-CC also contain abundant nannofossils. Common-to-abundant shallow-water forms (e.g., *Transversopontis pulcher*, *Zygrhablithus bijugatus*) were encountered. The presence of *Chiasmolithus solitus* in the absence of *Reticulofenestra umbilica* and *Toweius callosus* places these samples in Zones CP12–CP13. Sample 152-918D-92R-CC contains rare nannofossils and cannot be confidently placed in a nannofossil zone. A diverse nannofossil assemblage is present in Sample 152-918D-93R-CC, which can be assigned to Zones CP9b through CP10, based on the presence of *Tribracliatius orthostylus*.

No core-catcher sample was available from Core 152-918D-94R, from which only basalt was recovered. Sample 152-918D-95R-CC yielded a few specimens of nannofossils that do not allow us to determine a useful age. The presence of these fossils, however, indicates an open-marine environment for the deposition of the sediment. Core-catcher samples from Cores 152-918D-96R through -99R, an interval of mostly weathered basalt, do not contain nannofossils.

### Planktonic Foraminifers

Planktonic foraminifers are generally common and well preserved in sediments from Hole 918A. Their abundance, however, decreases

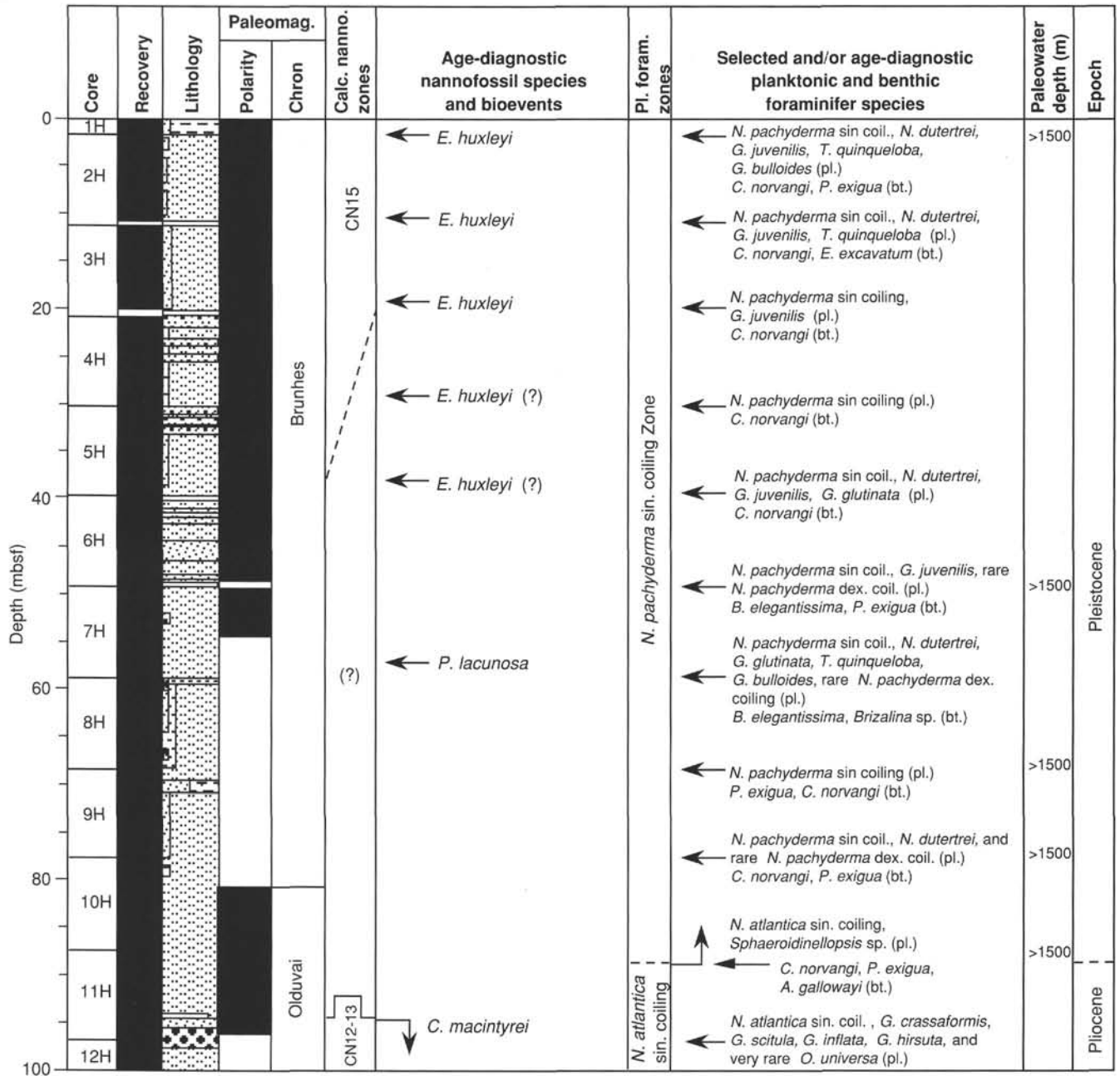


Figure 30. Biostratigraphic summary of Hole 918A. Paleowater depths inferred by benthic foraminiferal species also are shown. pl. = planktonic foraminifers, bt. = benthic foraminifers.

in the Pliocene. *Neogloboquadrina pachyderma* sinistral-coiling Zone, spanning the Pleistocene–Holocene interval, was identified from Samples 152-918A-1H-CC to -10H-CC. Planktonic foraminiferal assemblages generally show low species diversity throughout this zone. They contain common sinistraly coiled *N. pachyderma*, *T. quinqueloba*, *G. bulloides*, *G. glutinata*, along with rare *D. dutertrei* and dextrally coiled *N. pachyderma*. The first two late Pliocene zones, *N. pachyderma* dextral-coiling Zone and the upper *N. atlantica* dextral-coiling Zone, were not observed in the studied samples. Therefore, the Pleistocene–Pliocene transition has been placed between Sample 152-918A-10H-CC and -11H-1, 41–43 cm, where sinistraly coiled *N. atlantica* was first observed. The lower *N. atlantica* sinistral-coiling Zone was identified from Samples 152-918A-11H-1, 41–43 cm, to -31H-CC. Planktonic foraminiferal assemblages in this

zone consist of common sinistraly coiled *N. atlantica*, sinistraly and rare dextrally coiled *N. pachyderma*, and *N. humerosa*. Only Sample 152-918A-11H-CC contains a diverse assemblage that consists of sinistraly coiled *N. atlantica*, *G. juvenilis*, *G. glutinata*, *G. bulloides*, along with the warm-water species *G. inflata*, *G. scitula*, *G. crassaformis*, *G. hirsuta*, and a single specimen of *Orbulina universa* (Fig. 30). Samples 152-918A-32H-CC to -33H-CC are barren of planktonic foraminifers.

Four samples were analyzed from Hole 918B and a single sample from Hole 918C. The generally well-preserved and low-diversity planktonic foraminiferal assemblages are assigned to the *N. pachyderma* sinistral-coiling Zone. They consist of common sinistraly coiled *N. pachyderma*, *G. bulloides*, rarer *G. juvenilis* and *T. quinqueloba*, and very rare *N. dutertrei* (Figs. 31 and 32).

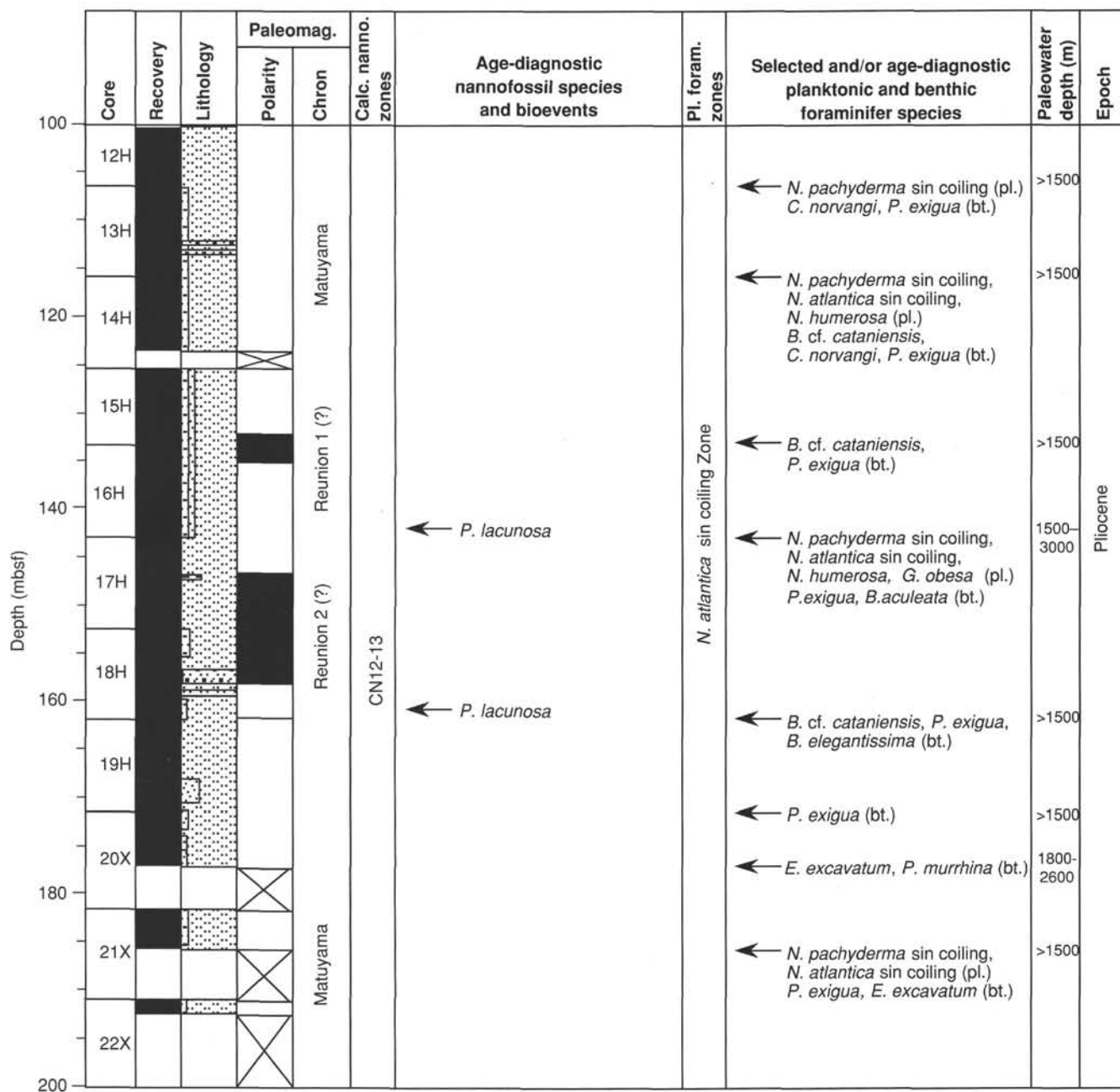


Figure 30 (continued).

The first 253 m of sediments were washed in Hole 918D. The first analyzed sample (152-918D-1R-CC), which contains rare and generally poorly preserved sinistrally coiled specimens of *N. atlantica* and *N. pachyderma*, has been attributed to the upper Pliocene *N. atlantica* sinistral-coiling Zone.

Although unrecovered intervals or sediments barren of microfossils were frequently encountered in the Pliocene interval, *Neogloboquadrina atlantica* dextral-coiling Zone was identified in Samples 152-918D-24R-CC to -36R-CC. Planktonic foraminiferal assemblages are generally moderately preserved and are dominated by cold-water faunas consisting of dextrally coiled specimens of *N. atlantica*, sinistrally coiled specimens of *N. pachyderma*, along with rare dextrally coiled specimens of *N. pachyderma*, *G. glutinata*, *G. juvenilis*, *T. quinqueloba*, and *G. bulloides*. Rarely, the assemblages contain a few specimens of "*G.*" *venezuelana*, *G. scitula*, *N. humerosa*, *Z. woodi*, *Sphaeroidinellopsis* sp., and small-sized specimens of *G. suterae*.

*Neogloboquadrina pseudopima* occurs only in Sample 152-918D-23R-CC, whereas a single specimen of *G. cf. menardii* was observed in Sample 152-918D-36R-CC. *Neogloboquadrina acostaensis* first occurs in Sample 152-918D-38R-CC. Because *N. atlantica* was not observed, this core was tentatively attributed to the *N. acostaensis* Zone.

Major difficulties were encountered in zonal assignment of middle Miocene assemblages because of rarity or absence of the zonal markers. Detailed shore-based studies will be needed to refine the biostratigraphy of this interval.

The Zone N12-N13? interval has been tentatively identified from Sample 152-918D-39R-CC to Sample 152-918D-47R-CC. Planktonic foraminiferal assemblages in this interval are generally moderately to well preserved and consist of common *G. bulloides*, *G. scitula*, *G. miozea*, *P. acrostoma*, and rarer warm-to-temperate water species, such as *G. trilobus*, *G. quadrilobatus*, *D. baroemoensis*, *G. dehiscens*, and "*G.*" *venezuelana*. Sample 152-918D-39R-CC

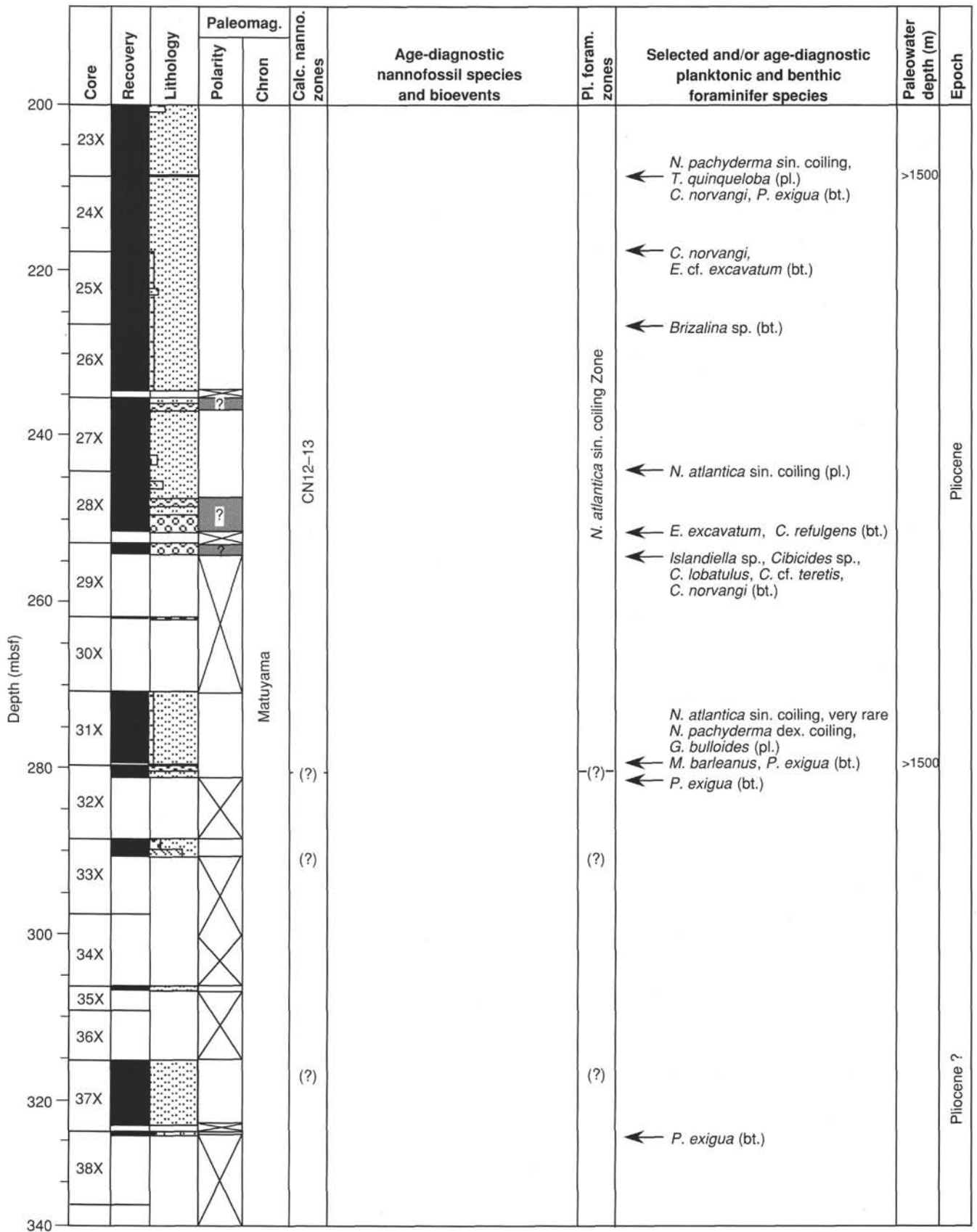


Figure 30 (continued).

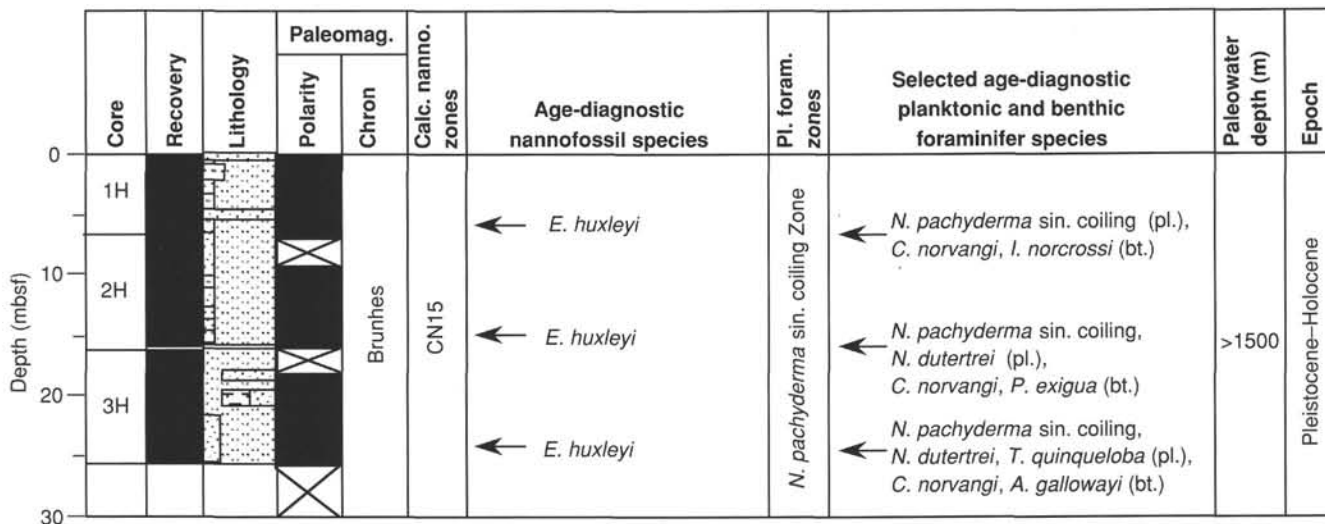


Figure 31. Biostratigraphic summary of Hole 918B. Paleowater depths inferred by benthic foraminiferal species also are shown. pl. = planktonic foraminifers, bt. = benthic foraminifers.

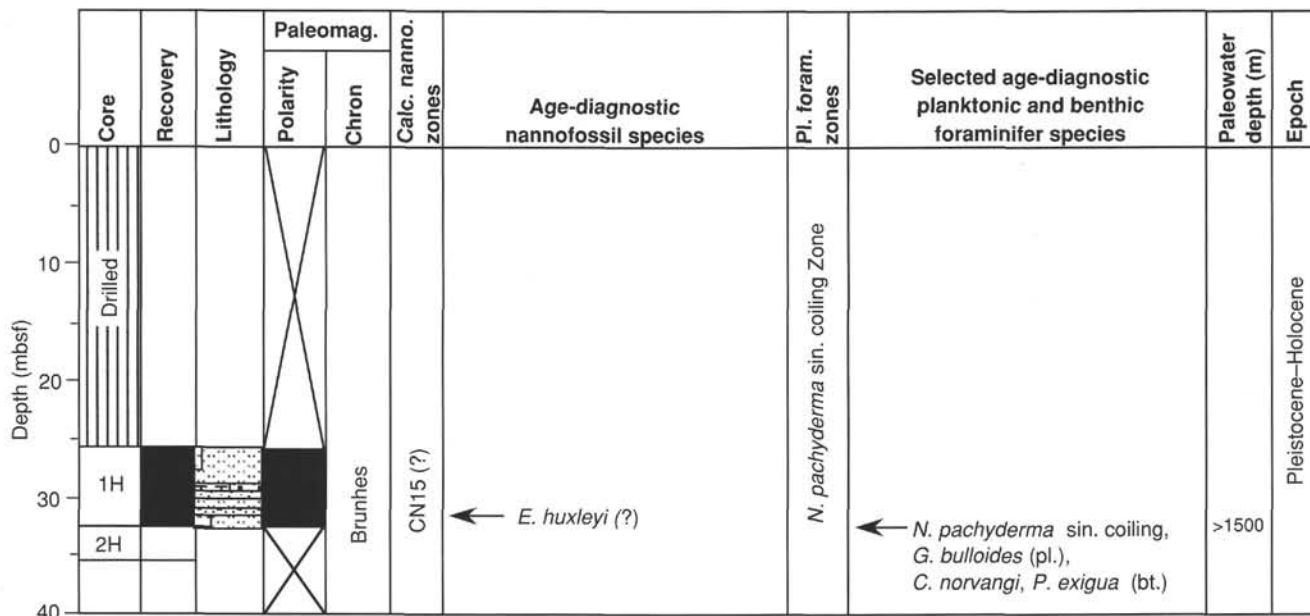


Figure 32. Biostratigraphic summary of Hole 918C. Paleowater depths inferred by benthic foraminiferal species also are shown. pl. = planktonic foraminifers, bt. = benthic foraminifers.

also contains rare specimens of *Globorotalia praemenardii*. *Globorotalia rom. suterae* is common to abundant from Samples 152-918D-47R-CC to -44-CC.

The Zone N8-N11(?) interval has been identified from Samples 152-918D-48R-CC to -53R-CC. Planktonic assemblages are generally moderately preserved and consist of rare to common *G. bulloides*, *G. miozea*, *G. dehiscens*, "*G.*" *venezuelana*, *G. zealandica*, and *Z. woodi*, along with the temperate water species *P. siakensis* and *P. acrostoma* and the warm-water species *G. trilobus*. Sample 152-918D-52R-CC also contains the warm-water species *Globigerinoides bisphericus* and *Praeorbulina transitoria*, along with ancestral specimens of *G. miozea*, and, therefore, may be tentatively attributed to Zone N8. Poore (1979) documented the presence of *G. cf. suterae* from Zones N12 to N14. This species, however, seems to have a longer stratigraphic range at Site 918.

Zone N7(?) has been tentatively identified based on the presence of *G. altiapertura* and the absence of *Catapsydrax* spp. in Sample 152-918D-54R-CC. The assemblage found in this sample consists of the poorly preserved warm water species *G. trilobus*, *G. quadrilobatus*, *D. altispira globosa*, and *G. praescitula*.

The Zone N4-N6 interval can be identified from Samples 152-918D-44R-4, 71-74 cm, to -58R-CC, based on the presence of poorly to moderately preserved specimens of *Catapsydrax unicavus*, *Catapsydrax* spp., *G. quadrilobatus*, *G. trilobus*, *Z. connecta*, *D. altispira globosa*, *Globorotaloides cf. stainforthi*, *G. variabilis*, and *P. incognita*.

Extremely rare and moderately preserved specimens of *P. pseudokugleri*, along with "*Globigerina*" *ciperoensis*, *P. semivera*, *C. dissimilis*, and *G. variabilis*, indicate the late Oligocene Zone P22 for Sample 152-918D-62R-CC. Subzone P21a (late Oligocene) was tentatively identified in Sample 152-918D-75R-CC, based on the pres-

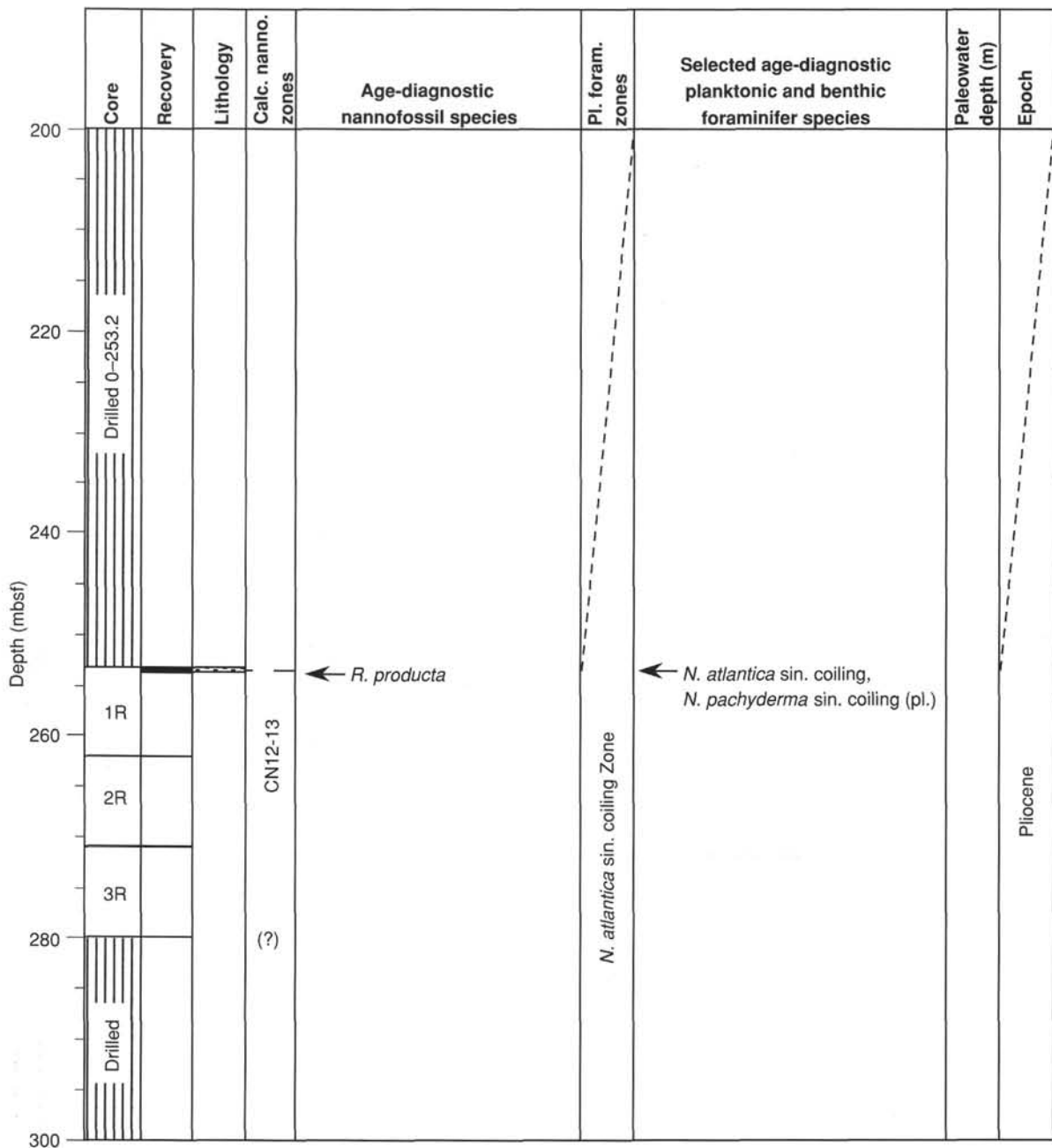


Figure 33. Biostratigraphic summary of Hole 918D. Paleowater depths inferred by benthic foraminiferal species also are shown. pl. = planktonic foraminifers, bt. = benthic foraminifers.

ence of rare and poorly preserved *Chiloguembelina cubensis* and on comparison with nannofossil data.

Sample 152-918D-88R-CC contains a well-preserved middle Eocene assemblage attributed to Zones P10–P12. This consists of *Pseudohastigerina wilcoxensis*, *P. danvillensis*, *Acarinina densa*, *A. pentacamerata*, *S. eocaena*, and *Turborotalia griffinae*. Samples 152-918D-89R-CC, -90R-CC, and -91R-CC contain less diversified and moderately preserved middle Eocene assemblages (Zones P10–P12), consisting of *P. wilcoxensis*, *P. danvillensis*; *A. pentacamerata*, *P. wilcoxensis*, and *T. griffinae*; *P. wilcoxensis* and *S. eocaena*, respectively (Fig. 33). Samples 152-918D-92R-CC through -99R-CC are barren of planktonic foraminifers.

Some preliminary paleoenvironmental inferences have been made here on the basis of planktonic foraminiferal data collected on board

the ship. Pliocene to Holocene planktonic foraminiferal assemblages recovered at Site 918 are characterized by common-to-abundant, sinistrally coiled specimens of *N. pachyderma* and *N. atlantica*, *G. bulloides*, and *T. quinqueloba*, along with rare *N. dutertrei*, *N. acostaensis*, and *N. humerosa*. These assemblages were interpreted to reflect cool-water and/or glacial environments (Aksu et al., 1989). A warmer, and probably interglacial, episode has been tentatively identified in the upper Pliocene Sample 152-918A-11R-CC, based on the presence of several temperate or warm-water species, such as *G. inflata*, *G. scitula*, *G. crassaformis*, *G. hirsuta*, and very rare *Orbulina universa*.

Planktonic foraminiferal assemblages consisting of relatively common *N. atlantica* dextral-coiling and *G. bulloides*, and very rare *N. acostaensis*, *N. humerosa*, *G. scitula*, and *G. suterae* suggest that cool

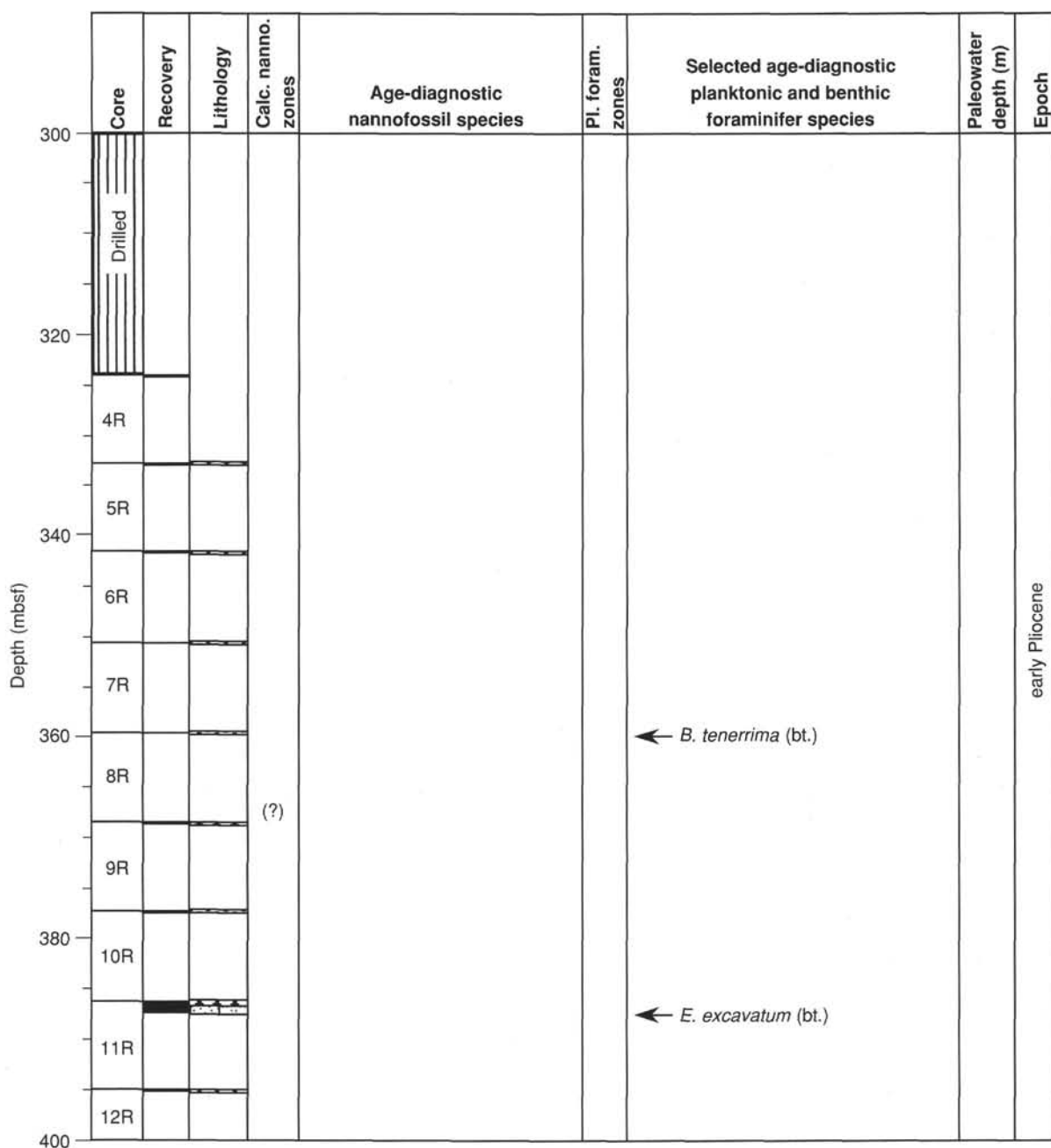


Figure 33 (continued).

surface-water conditions persisted throughout the middle-late Miocene. Apparently, slightly warmer conditions were registered during the earliest late Miocene, as indicated by the high abundance of *N. acostaensis* and the first occurrence of the *G. menardii* Group.

Relatively higher species diversity, increased abundance of planktonic faunas, and the occurrence of tropical forms (such as *Globigerinoides* spp.) in the middle Miocene indicate relative warm surface water during this period.

The early Miocene planktonic foraminiferal assemblages include warm-water species *G. trilobus*, *G. quadrilobatus*, *G. altiapertura*, and *Dentoglobigerina altispira globosa*.

### Benthic Foraminifers

All core-catcher samples plus some additional samples were examined from the cores taken from Holes 918A, 918B, 918C, and

918D. Benthic foraminifers are few in Eocene and Pliocene–Pleistocene samples and are generally rare in Oligocene to upper Miocene samples. Preservation of upper Miocene to Quaternary benthic foraminifers is moderate and that of lower Eocene to middle Miocene benthic foraminifers is poor.

The Pliocene–Quaternary benthic foraminiferal fauna identified from the interval above Sample 152-918A-24X-CC, as well as from all core-catcher samples from Holes 918B and 918C and Samples 152-918D-18R-CC and -19R-CC, are characterized by common or abundant *Cassidulina norvangi*. Most of these assemblages include *Cassidulina teretis*, *C. cf. teretis*, *Elphidium excavatum*, and *Pseudoparrella exigua*. *Cassidulina teretis* was abundant during the Pliocene–Pleistocene glacial interval (Murray, 1984). The presence of *Elphidium excavatum* has been related to a glacial marine unit (Mackensen et al., 1985). Thus, the fauna recognized in the above samples indicates glacial conditions, as is obvious from the sedimentary facies of diamictons

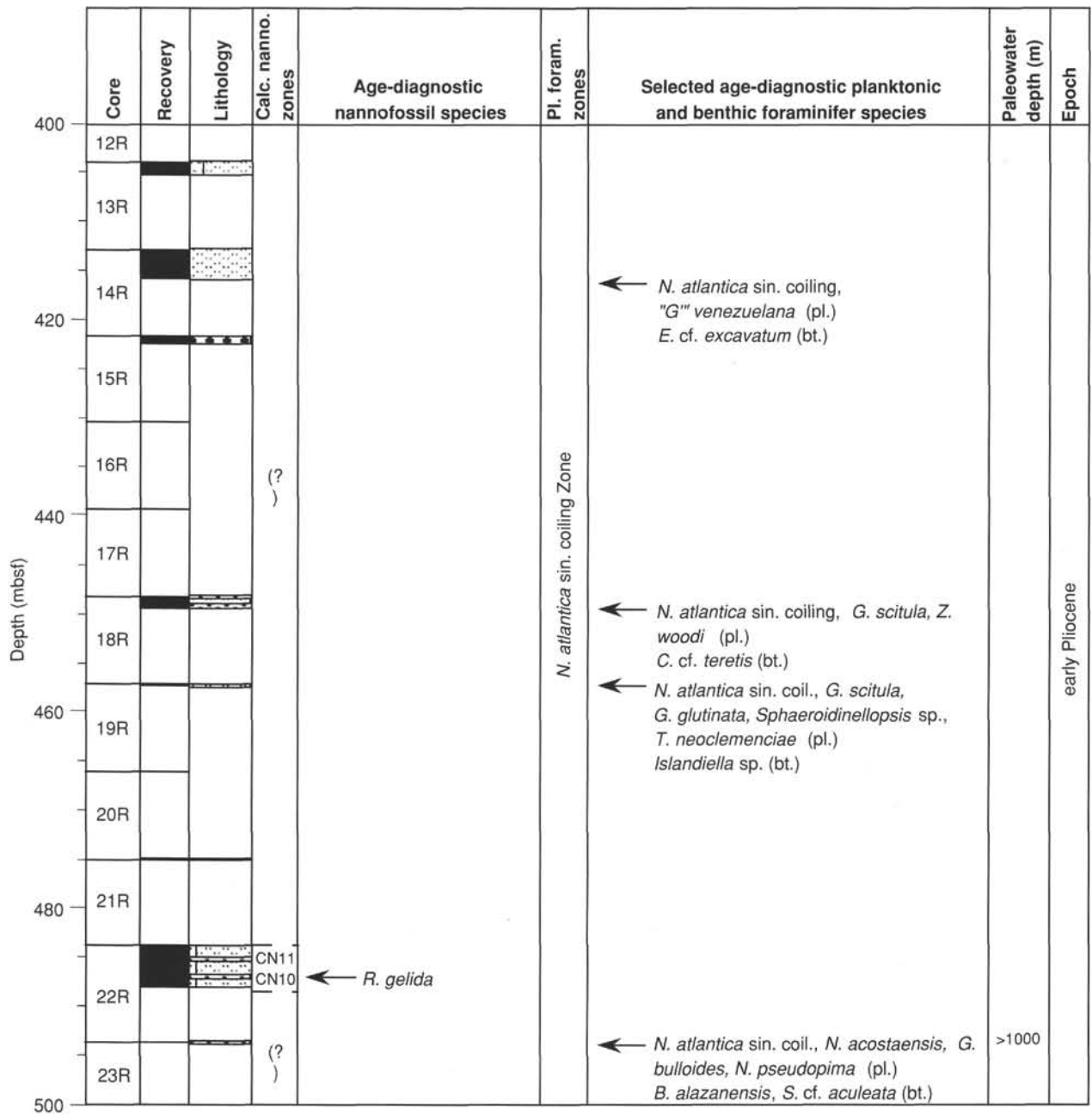


Figure 33 (continued).

and diamictites. A significant number of specimens of *Pseudoparrella exigua*, which lives in water deeper than 1500 m (Murray, 1984) in the modern northeastern Atlantic, were found in Samples 152-918A-9H-CC through -13H-CC, -18H-CC, -19H-CC, -21X-CC, -23X-CC, -31X-CC, and -918B-2H-CC. *Pyrgo murrhina*, which is abundant in modern water depths of 1800 to 2600 m (Schafer and Cole, 1982), occurs in Sample 152-918A-20X-CC. Sample 152-918A-16H-CC includes common *P. exigua* with few *Bulimina aculeata*, which lives in water depths of 1500 to 3000 m (Murray, 1984). The paleowater depths for Samples 152-918A-16H-CC and -20X-CC thus can be inferred as being at 1800 to 2600 m.

The assemblage in Samples 152-918A-28X-CC and -31X-CC contains few to common *E. excavatum* with few *P. exigua*; this indicates a glacial environment and paleowater depths greater than 1500 m.

Samples 152-918A-25X-CC, -29X-CC, -918D-8R-CC, -11R-CC, and -14R-CC contain very rare benthic foraminifers. Samples 152-

918A-14H-CC, -17H-CC, -22X-CC, -26X-CC, -27X-CC, -33X-CC, -35X-CC, -37X-CC, -918D-1R-CC, -9R-CC, and -13R-CC are barren of benthic foraminifers.

Upper Miocene fauna from the interval between Samples 152-918D-23R-CC and -37R-3, 58-60 cm, are characterized by the occurrence of *Pseudoparrella exigua* with *Bulimina alazanensis*, *Cibicides kullenbergi*, or *Laticarinina pauperata*. Schnitker (1974) showed that a fauna dominated by *Epistominella exigua* (= *P. exigua*) is closely associated with the Norwegian Sea Overflow Water. Therefore, it appears that the benthic foraminiferal fauna has been affected by NADW since this period. In the Holocene northeastern Atlantic, *E. exigua* (= *P. exigua*) is distributed in a water depth deeper than 1500 m (Murray, 1984). The assemblage found in Sample 152-918D-23R-CC includes *Bulimina alazanensis*. This species now occurs in water deeper than 1000 m (Murray, 1984). Therefore, the fauna suggests a paleowater depth deeper than 1500 m.

Depth (mbsf)	Core	Recovery	Lithology	Calc. nanno. zones	Age-diagnostic nannofossil species	Pl. foram. zones	Selected age-diagnostic planktonic and benthic foraminifer species	Occurrence of <i>Bolboforma</i>	Paleo water depth (m)	Epoch
500	23R			(?)						
	24R			CN9	← <i>D. quinqueringus</i>		← <i>N. atlantica</i> dex. coiling, <i>N. pachyderma</i> sin. coiling, <i>N. pachyderma</i> dex. coiling, <i>N. acostaensis</i> (pl.) <i>P. exigua</i> (bt.)	← <i>B. badenensis</i> , <i>B. metzmacheri</i>	>1500	
	25R									
520	26R									
	27R			(?)						
	28R									
	29R					<i>N. atlantica</i> dextral coiling Zone	← <i>Orthomorphina</i> ? sp. (bt.)			
560	30R						← <i>Orthomorphina</i> ? sp. (bt.)	← <i>B. laevis</i>		
	31R						← <i>Fissurina</i> sp. (bt.)	← <i>B. laevis</i>		
580	32R						← <i>N. atlantica</i> dex. coiling, <i>N. acostaensis</i> , <i>G. scitula</i> (pl.)	← <i>Bolboforma</i> sp.		
	33R						← <i>N. atlantica</i> dex. coiling, <i>N. acostaensis</i> , <i>G. scitula</i> , <i>G. glutinata</i> , <i>G. juvenilis</i> (pl.), <i>P. exigua</i> (bt.)	← <i>B. laevis</i>	>1500	late Miocene
600										

Figure 33 (continued).

Sample 152-918D-38R-CC contains very rare benthic foraminifers. The lower to middle Miocene fauna from Samples 152-918D-39R-CC through -54R-CC are characterized by common occurrences of *Melonis barleanus*, with few *Pullenia bulloides*. This combination was described as the *Melonis zaandami* (*M. barleanus*) Species Assemblage by Mackensen et al. (1985), who suggested that this assemblage has an association with fine-grained substrata. Large amounts of *M. zaandami* (= *M. barleanus*) may also reflect higher productivity (Lutze et al., 1979), as indicated by abundant nannofossils in this interval. Samples 152-918D-39R-CC, -41R-CC, -43R-CC, and -54R-CC include common *Cibicidoides kullenbergi* or *Oridorsalis umbonatus* and indicate paleowater depths greater than 1500 m (Murray, 1984). Samples 152-918D-42R-CC, -44R-CC, -49R-CC, and -51R-CC contain very rare benthic foraminifers.

Sample 152-918D-62R-CC from the Oligocene contains *Globocassidulina subglobosa* and *Oridorsalis umbonatus* and suggests a

paleowater depth of 700 to 4000 m (Murray, 1984). Core-catcher samples from the interval between Samples 152-918D-84R-CC and -63R-CC are barren, or nearly barren, of benthic foraminifers.

Eocene fauna from the interval between Samples 152-918D-88R-CC and -93R-CC show stratigraphic succession. *Globocassidulina subglobosa* and *Oridorsalis ecuadorensis* are commonly found in Sample 152-918D-88R-CC. The co-occurrence of these species indicates a paleowater depth of 700 to 4000 m (Murray, 1984). The assemblage in Sample 152-918D-90R-CC resembles that in Sample 38-338-34-CC from the outer Vøring Plateau, Norwegian Sea (Hulsbos et al., 1989), because it contains abundant *Lenticulina* spp. with few *Cibicidoides* spp., *Nuttallides truempyi*, *Stilostomella* spp., and *Oridorsalis* sp. Hulsbos et al. (1989) interpreted this assemblage as being indicative of an upper bathyal depth (200-600 m). Sample 152-918D-89R-CC contains common *Lenticulina* spp. with a small numbers of *Cibicidoides sinistralis* and *Cibicidoides* spp. Sample

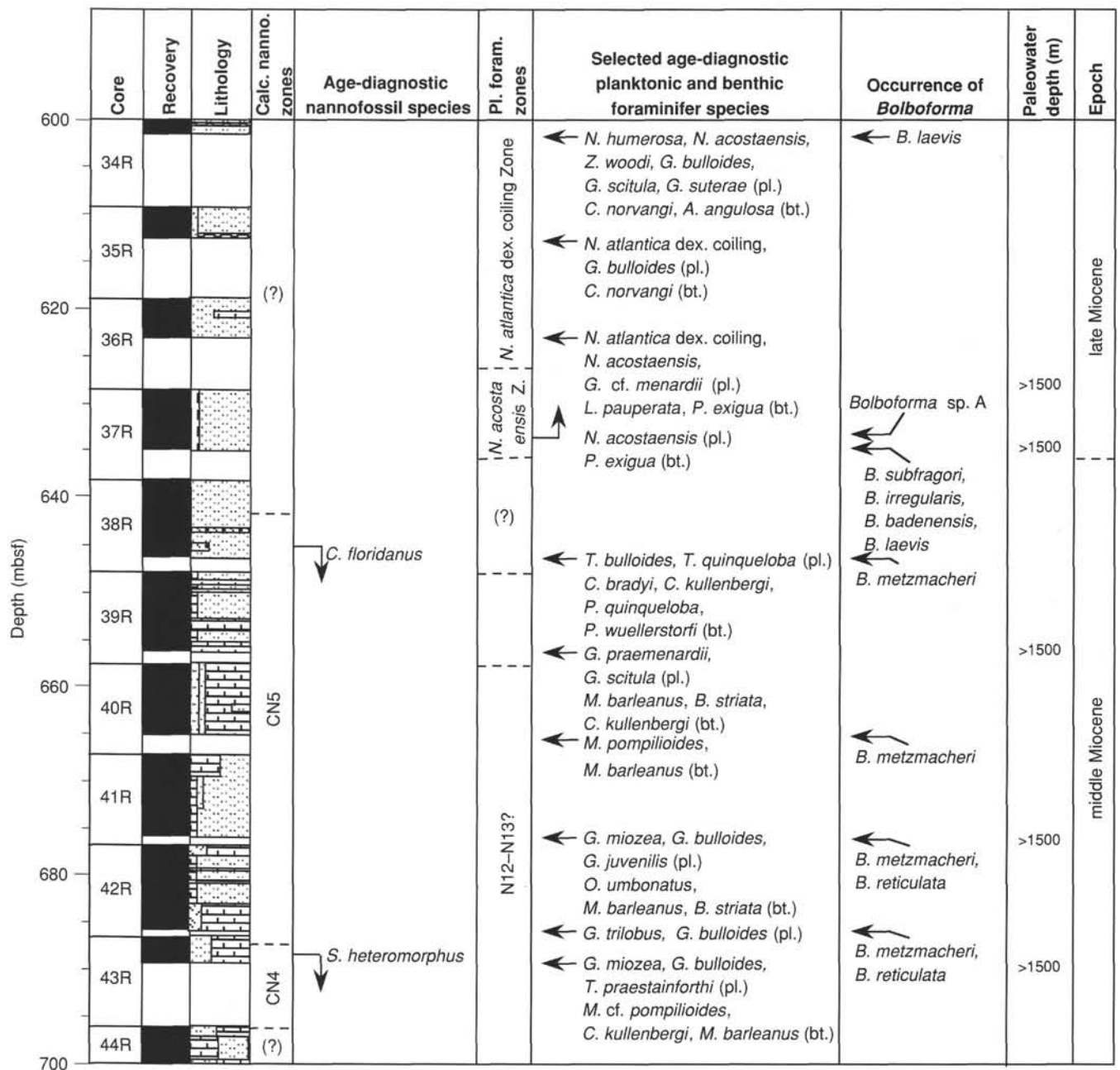


Figure 33 (continued).

152-918D-91R-CC contains abundant *Lenticulina* spp. with common *C. sinistralis*. Similar assemblages have been recorded at DSDP Sites 403 and 404 on the Rockall Plateau, North Atlantic (Murray, 1979). These assemblages have been interpreted as indicating normal marine, inner shelf (shallower than 75 m), to epibathyal (shallower than 600 m; Murray, 1979). A paleowater depth of less than 600 m thus can be estimated for Samples 152-918D-89R-CC and -91R-CC. Sample 152-918D-92R-CC contains common *Anomalinoidea* cf. *howelli* and *Lenticulina* spp., a mid- to outer-shelf assemblage (paleowater depth of 75–200 m; Murray, 1984). The assemblage in Sample 152-918D-93R-CC is dominated by *A. cf. howelli*. This may suggest a mid-shelf environment (paleowater depth of 75–150 m; Murray, 1984). Samples 152-918D-95R-CC through -97R-CC and -99R-CC are barren of benthic foraminifers (Fig. 33).

### *Bolboforma*

Generally, common and well-preserved specimens of *Bolboforma* (algae Chrysophyta) are scattered in the Miocene interval in Hole 918D (Fig. 33). The zonation proposed by Qvale and Spiegler (1989) could not be applied aboard the ship because *Bolboforma* were scattered and the marker species were rare or absent.

Upper Miocene *Bolboforma* assemblages were found in Samples 152-918A-24R-CC to -38R-CC. Sample 152-918A-24R-CC contains a few specimens of *Bolboforma badenensis* and *Bolboforma metzmacheri*, along with a species that resembles *Bolboforma* sp. B, recorded in the Labrador Sea by Pallant and Kaminski (1989). *Bolboforma laevis* occurs consistently from Samples 152-918A-30R-CC to -34R-CC. The *Bolboforma* assemblage in Sample 152-918A-37R-

Depth (mbsf)	Core	Recovery	Lithology	Calc. nanno. zones	Age-diagnostic nannofossil species	Pl. foram. zones	Selected age-diagnostic planktonic and benthic foraminifer species	Occurrence of <i>Bolboforma</i>	Paleowater depth (m)	Epoch
700	44R						<i>G. quadrilobatus</i> , <i>G. trilobus</i> , <i>D. baroemoenensis</i> , <i>G. glutinata</i> , <i>G. cf. suterae</i> (pl.)	<i>B. reticulata</i> <i>B. laevis</i> , <i>B. metzmacheri</i>		
	45R					(?)	<i>G. miozea</i> , <i>P. acrostoma</i> , <i>G. scitula</i> , and common <i>G. cf. suterae</i> (pl.)	<i>B. metzmacheri</i>		
720	46R									
	47R					N13?	<i>G. miozea</i> , <i>P. acrostoma</i> , <i>G. scitula</i> , and common <i>G. cf. suterae</i> (pl.) <i>B. striata</i> (bt.)			Middle Miocene
740	48R									
	49R				(?)		<i>B. striata</i> , <i>Melonis</i> sp., <i>Gyroidinoides</i> sp. (bt.)			
760	50R					N8-n11?				
	51R						<i>Lagena</i> sp., <i>B. striata</i> (bt.)			(?)
780	52R						<i>G. miozea</i> , <i>G. dehiscens</i> , <i>G. cf. suterae</i> , <i>G. venezuelana</i> (pl.) <i>M. barleanus</i> (bt.)			
	53R						<i>P. acrostoma</i> , <i>Z. woodi</i> , <i>P. siakensis</i> , <i>G. trilobus</i> (pl.) <i>M. barleanus</i> (bt.)			
800	54R					N7?	<i>G. altiapertura</i> , <i>G. quadrilobatus</i> , <i>D. altispira globosa</i> , <i>G. trilobus</i> , <i>G. praescitula</i> (pl.) <i>O. umbonatus</i> (bt.)		>1500	e. Mio.

Figure 33 (continued).

CC has the highest diversity among those examined. It consists of *Bolboforma clodiusi*, *Bolboforma subfragori*, *Bolboforma irregularis*, *B. metzmacheri*, *B. badenensis*, *B. laevis*, and *Bolboforma* sp. A of Pallant and Kaminski (1989).

Middle Miocene assemblages are less diverse and only *B. metzmacheri*, *B. laevis*, and *Bolboforma reticulata* occur sporadically between Samples 152-918A-39R-CC and -52R-CC. A few specimens of *B. laevis* were found only in Sample 152-918A-52R-CC (lower Miocene) and in Sample 152-918A-61R-CC (upper Oligocene).

### PALEOMAGNETISM

Paleomagnetic studies were conducted on material from each of the four holes drilled at Site 918. Drilling at Holes 918A, 918B, and

918C recovered late Pliocene age and younger sediments. Coring in Hole 918D began at 253.2 mbsf, where late Miocene through early Eocene age sediments were recovered. Volcanic basement was encountered at 1189.4 mbsf. Coring continued down to 1310.1 mbsf. The initial natural remanent magnetization (NRM) of each sedimentary archive-half core section was measured using the WCC. Each core section was alternating field (AF) demagnetized at 15 and 25 mT.

Paleomagnetic studies of the igneous rocks (including material from a sill) in Hole 918D were performed with discrete samples (8 cm<sup>3</sup>) and were concerned with magnetostratigraphy and an elementary evaluation of their magnetic properties. Measurements of the NRM, anhysteretic remanent magnetization (ARM), and bulk susceptibility were undertaken to establish stratigraphic relationships and to compare with observations provided by the igneous petrology studies (see "Igneous Petrology" section, this chapter).

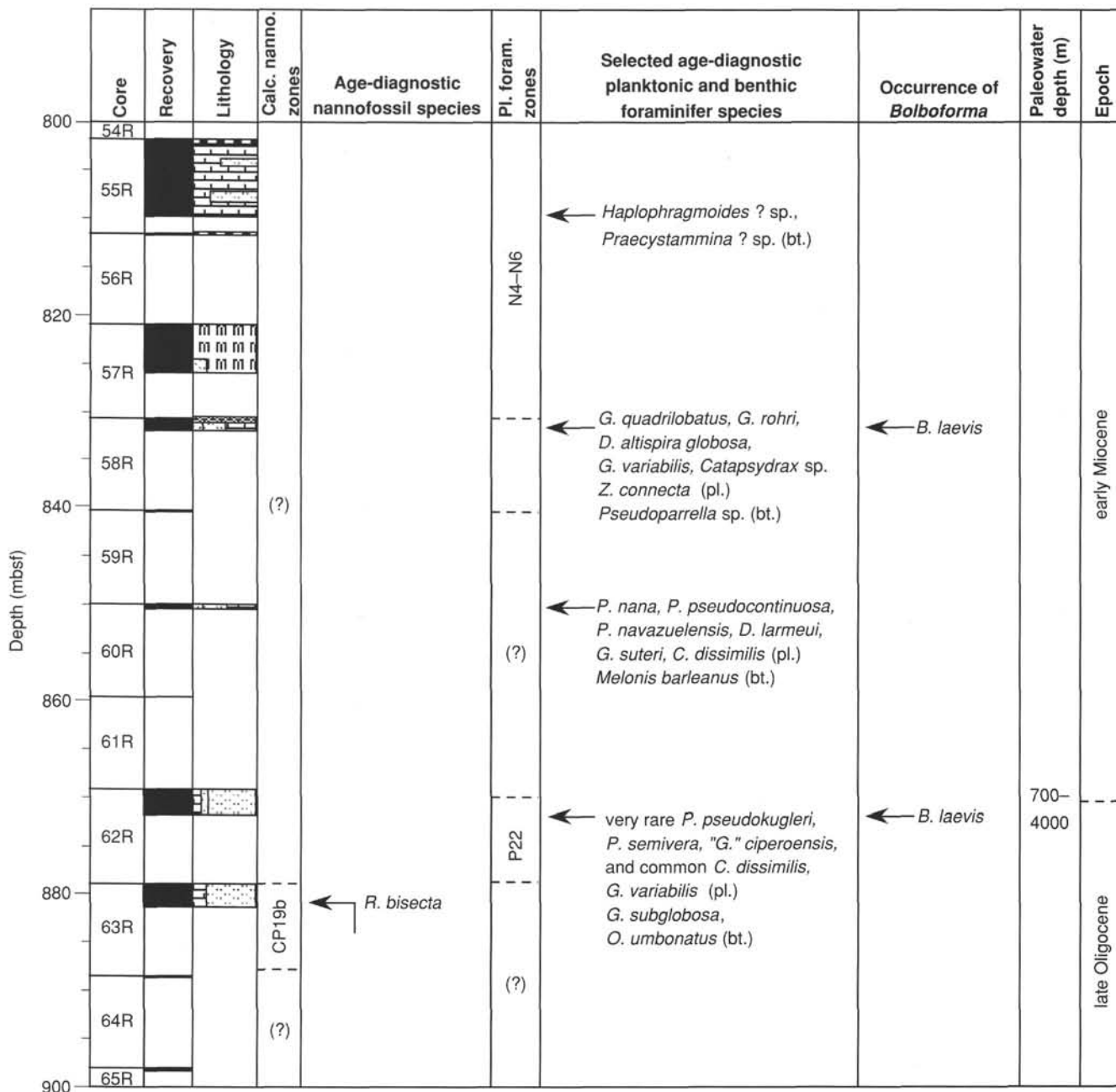


Figure 33 (continued).

**Hole 918A**

Hole 918A penetrated 330 m of Pliocene–Pleistocene sediments. Advanced piston coring (APC) in the upper one-half of the hole (down to Core 152-918A-19H) averaged a recovery of 101.3%. The Tensor tool (see “Paleomagnetism” section, “Explanatory Notes” chapter, this volume) was used to orient the declination of 10 of these APC cores (152-918A-4H to -6H, -12H to -17H, and -19H). Extended-core barrel (XCB) coring continued until Core 152-918A-38X, with recovery averaging 53.8%.

Initial NRM intensities typically were 200 to more than 1000 mA/m (in many cases, the initial magnetization was too strong for the WCC to measure). Generally, the NRM direction was steeply dipping (70°–90°) and downward. The 25-mT AF step reduced the intensities

to typically 5% to 15% of the NRM value, and inclinations were typically between 50° and 80° (positive or negative). Data from cores oriented by the Tensor tool record declinations ( $\pm 30^\circ$  from the north-south azimuth), consistent with the polarity deduced from the magnetic inclinations. This information suggests that demagnetization to 25 mT successfully isolated the primary remanence direction and that polarity determinations for these cores are wholly reliable. Importantly, it justifies the small amount of time taken for obtaining this information and vindicates ODP’s continued efforts to obtain oriented core material. The magnetostratigraphy of Hole 918A is summarized in Figure 34. Records of normal polarity were identified in the following intervals: 152-918A-1H, 0 cm, to -6H-6, 20 cm (0–47.5 mbsf); 152-918A-6H-7, 20 cm, to -7H-3, 60 cm (49.0–52.9 mbsf); 152-918A-10H-3, 30 cm, to -11H-6, 90 cm (81.1–95.7 mbsf); 152-

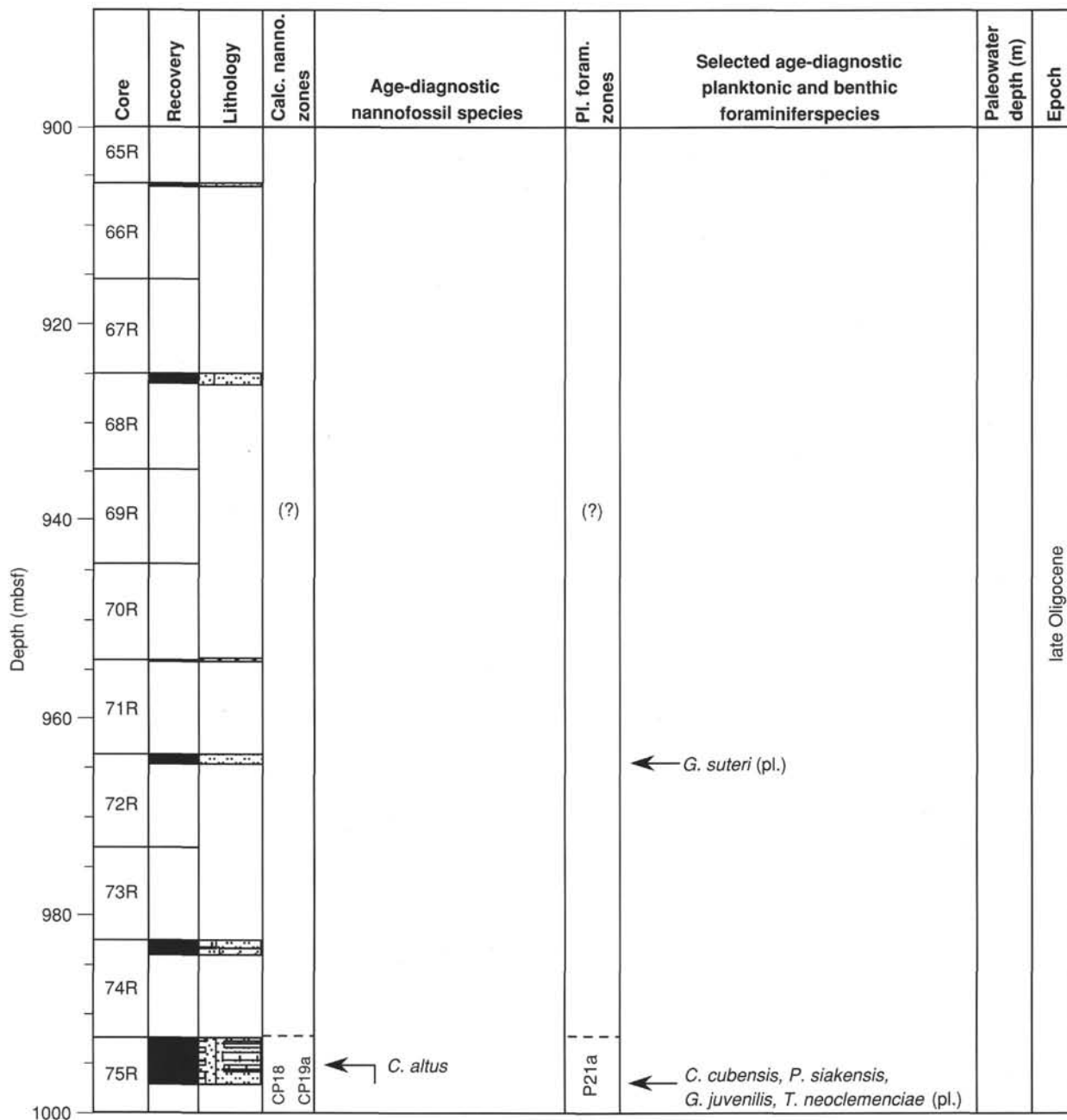


Figure 33 (continued).

918A-16H-1, 0 cm, to -16H-2, 70 cm (133.3–135.5 mbsf); 152-918A-17H-3, 100 cm, to -18H-4, 150 cm (146.8–158.3). The remainder of the succession has reverse polarity.

Nannofossil and foraminiferal biostratigraphy (see “Biostratigraphy” section, this chapter) has been used to calibrate the polarity record with the geomagnetic polarity time scale. Nannofossil Zone CN15 is identified in the upper part of the Hole in Cores 152-918A-1H to -3H (and possibly as far down as -5H). Foraminiferal data indicate that the Pliocene/Pleistocene boundary is positioned immediately below Core 152-918A-10H, at about 88 mbsf. An additional constraint in interpreting the magnetostratigraphic record of Hole 918A is provided by the site survey seismic studies (see “Background and Scientific Objectives” section, this chapter). An erosional surface is identified at 68 mbsf, and approximately 60 m of stratigraphy (estimated from the seismics) is locally missing from the succession.

The normal polarity sediments identified over the intervals 152-918A-1H, 0 cm, to -6H-6, 20 cm, and 152-918A-6H-7, 20 cm, to -7H-3, 60 cm, are correlated with the Brunhes Chron. The dominantly reversely magnetized interval beneath this level (152-918A-7H-3, 60 cm, to -37X) is correlated with the Matuyama Chron. The normal polarity interval identified in the interval 152-918A-10H-3, 30 cm, to -11H-6, 90 cm, is thought to represent the Olduvai Chron. Therefore, the hiatus at 68 mbsf falls within the latter part of the Matuyama, and post-dates the start of Olduvai event. Normal polarity sediments identified in Intervals 152-918A-16H-1, 0 cm, to -16H-2, 70 cm, and 152-918A-17H-3, 100 cm, to -18H-4, 150 cm, are thought to be records associated with the Réunion Event(s). The Jaramillo Event probably is not recorded in Hole 918A because of the local hiatus. We interpret the total absence of normal polarity sediments in the lower part of Hole 918A as indicating that the maximum age of the sedi-

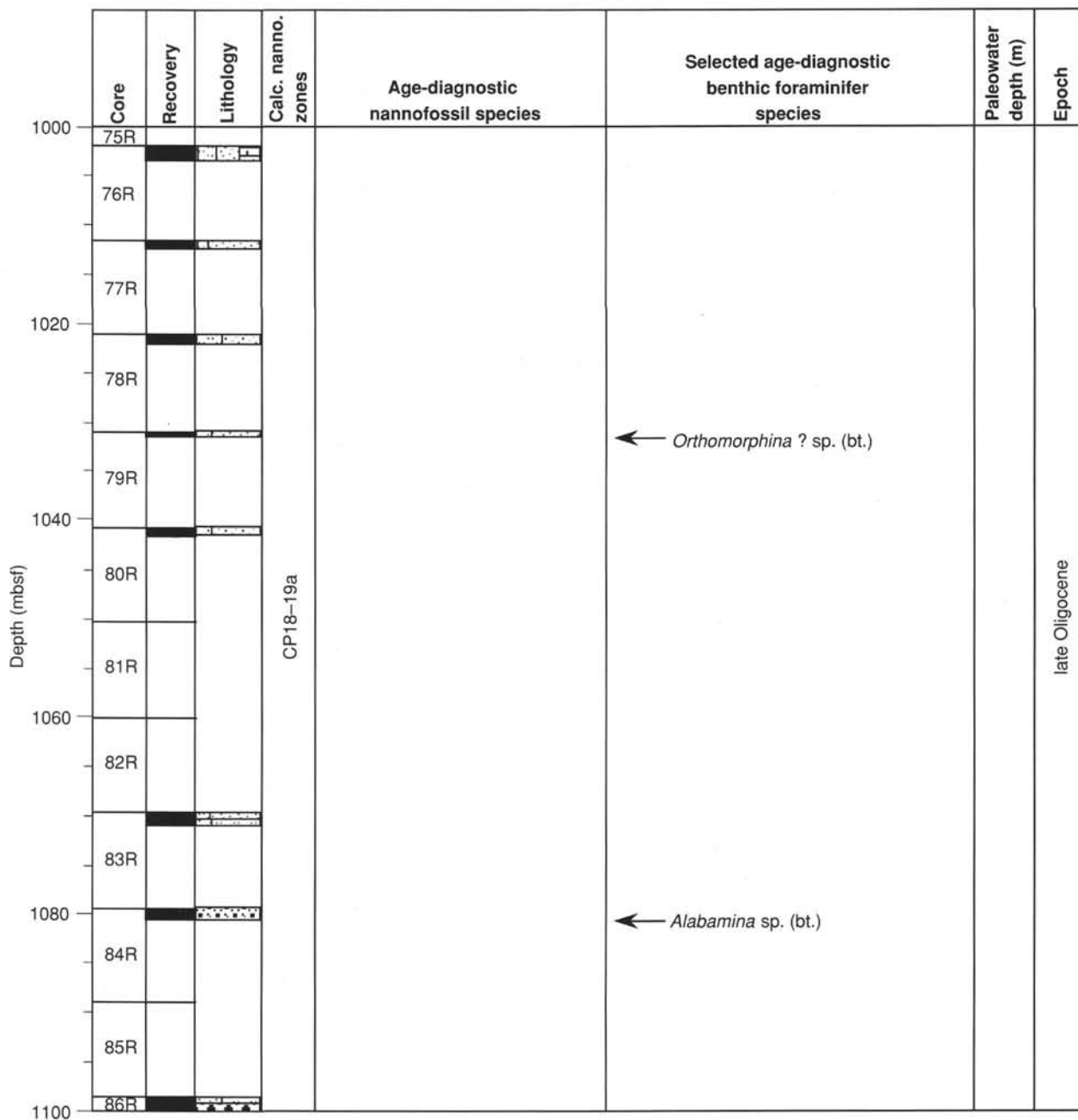


Figure 33 (continued).

ments in this hole is younger than the normal polarity Gauss Chron (i.e., less than 2.6 Ma).

Post-cruise studies will concentrate on the transitions between each of the normal and reversed intervals identified in Hole 918A. It is possible that the high sedimentation rates throughout this hole may have preserved a detailed pattern of geomagnetic field behavior. Comparisons will be made with similar records obtained elsewhere.

### Holes 918B and 918C

Three cores (152-918B-1H to -3H), drilled in Hole 918B, (0–25.8 mbsf) are normally magnetized and are correlated with the Brunhes Chron. Two cores were recovered in Hole 918C. Paleomagnetic data

were obtained from Core 152-918C-1R (25.8–35.3 mbsf). The sediments are normally magnetized and correlate with the Brunhes Chron.

### Hole 918D

#### Sediments

Initial NRM intensities from the sediments recovered in Hole 918D were typically 20 to more than 1000 mA/m (in many cases, the initial magnetization was too strong for the whole-core magnetometer to measure). As with Hole 918A, the initial NRM direction dips steeply (70°–90°) and directed downward. The 25-mT AF demagnetization reduced the intensities to typically 5% to 30% of the NRM value, and inclinations were typically between 50° and 80° (positive

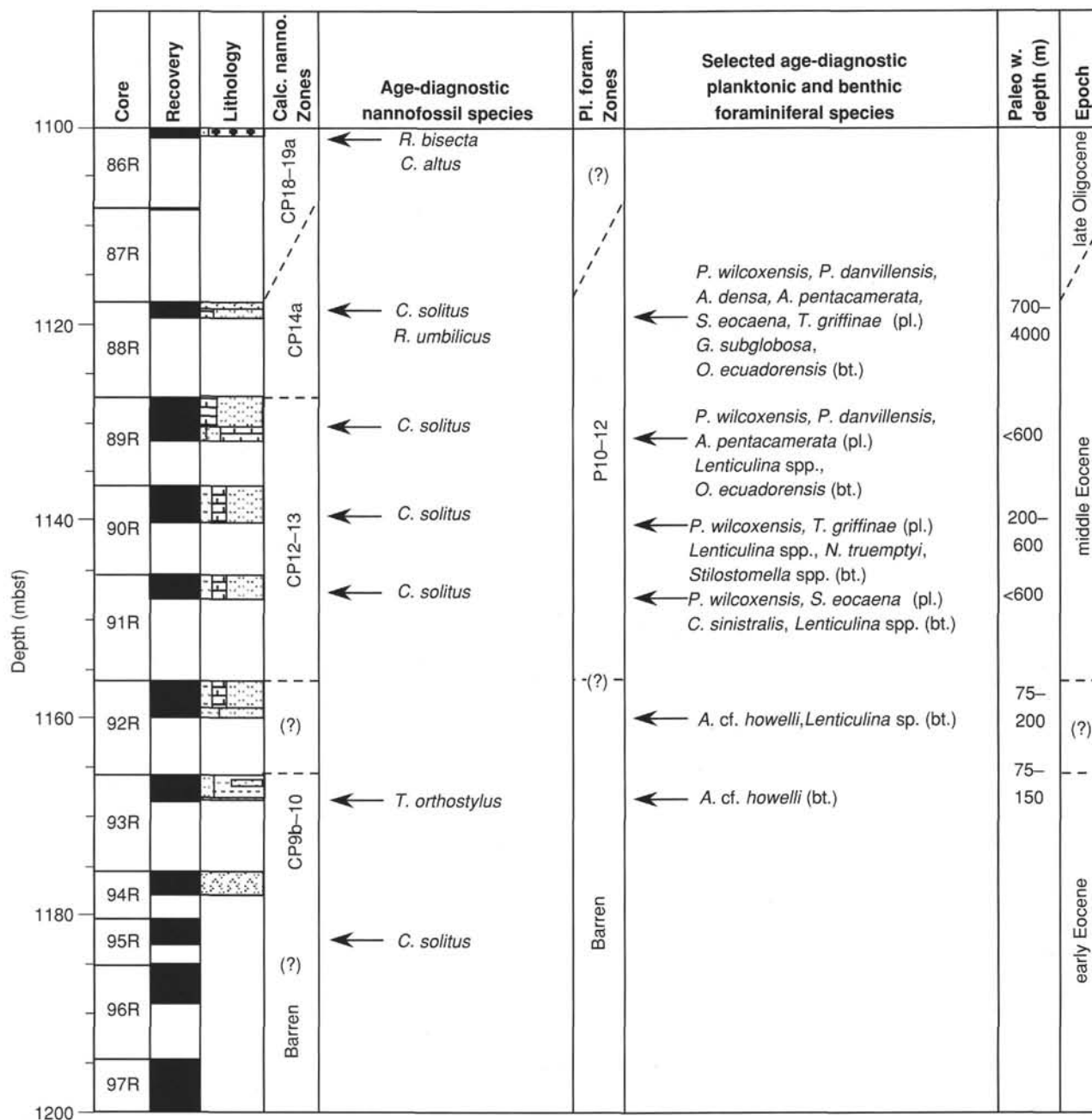


Figure 33 (continued).

or negative). Magnetostratigraphic data were obtained from all of the undisturbed core sections. The magnetostratigraphy of the sediments in Hole 918D is summarized in Figure 35.

At present, biostratigraphic data from Hole 918D are of limited use for calibrating the polarity record of Hole 918D to the geomagnetic polarity time scale. The problem of correlation is compounded by low recovery across many intervals. As yet, it is not possible to correlate any of the normal and reversed polarity magnetozones with the geomagnetic polarity time scale. It is anticipated that shore-based biostratigraphic studies will facilitate some correlations at a later date. The most pertinent observation of the magnetostratigraphy of sediments in Hole 918D concerns the reversely magnetized interval (Sections 152-918D-96R-2 and -96R-3) immediately above basement. The sediments are of early Eocene age (see "Biostratigraphy" section,

this chapter), and it is conceivable that the reversed polarity is a record of the latter part of Chron C24r. We anticipate that data from shore-based biostratigraphic studies (in particular, dinoflagellates) will confirm, or disprove, this speculative correlation.

#### Basaltic Igneous Unit 1

Two samples were analyzed from basaltic igneous Unit 1, possibly a sill, within the Eocene sediments in Cores 152-918D-93R and -94R, between 1168 and 1178 mbsf. The remanence of igneous Unit 1 is dominated by a low-coercivity (removed at about 10 mT) component having a steep positive inclination. Between 10 and 30 mT, a reversed-polarity component of magnetization was identified, but no clear direction could be isolated. Beyond 30 mT, the magnetic intensity

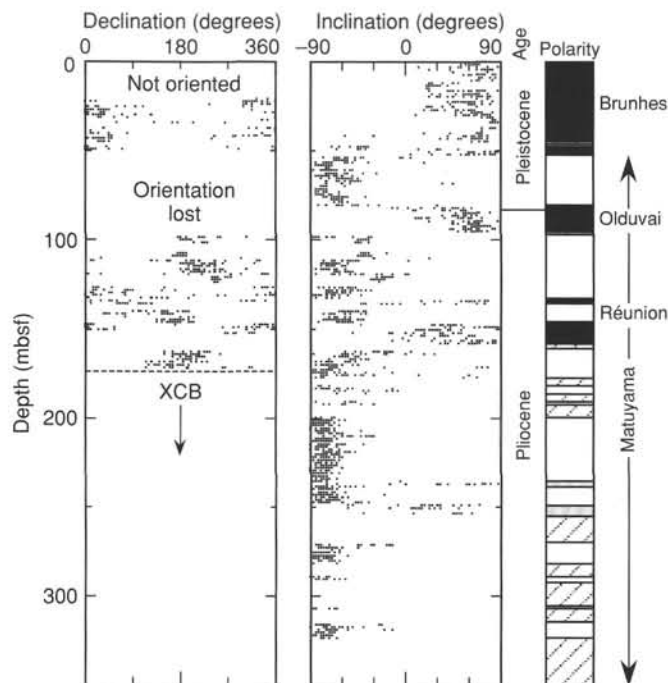


Figure 34. Summary of the magnetostratigraphy of Hole 918A, based on the directions obtained from the archive-half core sections following the 25-mT demagnetization. Shown are downhole plots of declination (corrected with the Tensor tool data) and inclination after 25-mT demagnetization. In the "Polarity" column, black = normal, white = reversed, stippled = undetermined, and hatched = no data. An important biostratigraphic datum is the Pliocene/Pleistocene boundary, positioned at about 88 mbsf (base of Core 152-918A-10H).

decays to <1% of the initial NRM, and it is not possible to define a stable magnetization direction. However, it is likely that the primary magnetization of basaltic Unit 1 is reversed.

The magnetic parameters measured for the two samples from igneous Unit 1 are different from the measurements in the basement flow units. NRM and ARM intensities, as well as bulk susceptibility values, are high (respectively, 9.96, 13.14, and  $4.35 \text{ A/m} \times 10^{-2} \text{ SI}$ , on average), and the median destructive field (MDF) of the ARM is low (1.8 mT). This information suggests that the remanence of the basaltic unit has been dominated by multidomain (large) titanomagnetite or titanomaghemite grains. Shore-based measurements should permit detailed analyses of the magnetic mineralogy.

#### Basement Rocks

Ten samples from the unweathered basement rocks recovered in Cores 152-918D-99R to -112R were studied. They have initial NRM intensities in the range of 0.9 to 6.0 A/m (Table 5). The initial NRM is dominated by a subvertical downward-dipping component, which probably was drilling induced. The low-coercivity component is isolated typically by the 20-mT demagnetization step, revealing a reversed-polarity remanence. Based on regional comparisons and the age of the magnetic anomaly at this site, the reversed-polarity magnetization correlates with Chron C24r. Characteristic inclination directions range between  $-30.7^\circ$  and  $-69.6^\circ$  (Fig. 36). The large dispersion of the reverse-polarity inclination directions has been attributed to secular variation and suggests that these lavas must have erupted over a significant period ( $>10^4 \text{ yr}$ ).

Several magnetic parameters were measured to evaluate the magnetic properties of the volcanic rocks in Hole 918D. The same instruments and procedures were used as for the samples from Hole 917A (see "Paleomagnetism" section, "Site 917" chapter, this volume). The

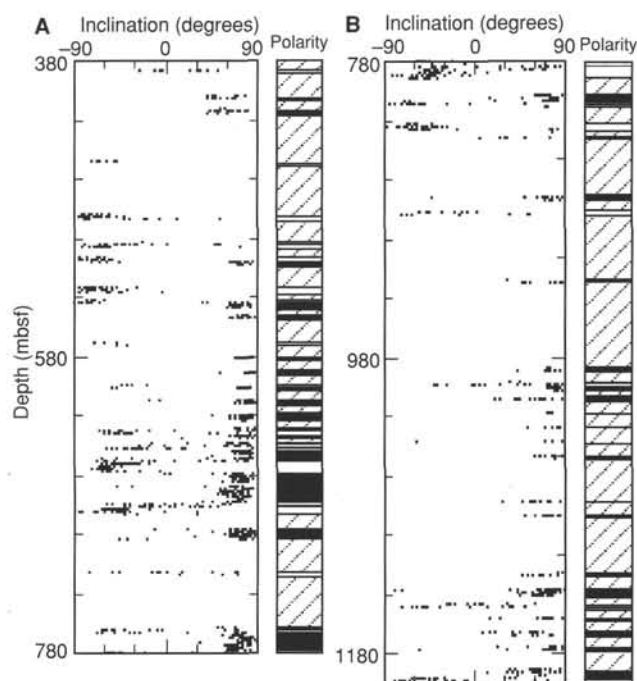


Figure 35. **A.** Summary of the magnetostratigraphy of Hole 918D (380–780 mbsf), based on the directions obtained from the archive-half core sections following 25-mT demagnetization. In the "Polarity" column, black = normal, white = reversed, and hatched = no data. **B.** Summary of the magnetostratigraphy of Hole 918D (780–1190 mbsf) based on the directions obtained from the archive-half core sections following 25-mT demagnetization. In the "Polarity" column, black = normal, white = reversed, and hatched = no data.

contribution of the low-coercivity component to the NRM is so large that the parameters using the initial value of NRM (median destructive field of NRM, Koenigsberger ratio, and NRM/ARM ratio) provide no useful paleomagnetic information. The data are presented in Table 5. These are of little use for elucidating the geological history of the lava succession and thus are not discussed further.

The mean value of the bulk magnetic susceptibility in the volcanic sequence is  $2.11 \times 10^{-2} \text{ SI}$  (see Table 5). These values are comparable with typical oceanic basalts (i.e.,  $2.7 \times 10^{-2} \text{ SI}$ ; Pariso and Johnson, 1991), but contrast with the values obtained from the Hole 917A basement rocks (mean value =  $1.63 \times 10^{-2} \text{ SI}$ ). No evolution with depth was observed.

Initial ARM values are similar to those obtained from the basalts in Hole 917A (Fig. 37), but MDFs of the ARM (mean value = 13.4 mT) are consistently lower than those of Hole 917A (mean value in Hole 917A = 21.9 mT). The MDF of the ARM for the bulk of the Hole 918D lavas is low (about 8 mT; Fig. 37). However, samples from igneous Units 12 through 14 (1260–1280 mbsf) have noticeably higher values, typically in the range of 20 to 30 mT (the values are comparable to those obtained from the Hole 917A lavas).

As at Hole 917A, complementary shore-based experiments of the igneous basement will be undertaken to determine precisely the magnetic mineralogy of individual flows and to identify possible stratigraphic variations.

#### SEDIMENTATION RATES AND SUBSIDENCE HISTORY

A number of age-control points are available for constructing a diagram of age vs. depth for the sedimentary column at Site 918 (Fig. 38). Most of these data points were based on biostratigraphic analyses of core-catcher samples. The age-vs.-depth curve should be refined

Table 5. Paleomagnetic data obtained from igneous rocks drilled in Hole 918D.

Core, section, interval (cm)	Piece	Depth (mbsf)	NRM (A/m)	MDF-NRM (mT)	St. inc. (°)	Suscept. (SI)	Q ratio	ARM (A/m)	MDF-ARM (mT)	NRM/ARM	Unit
152-918D-											
94R-1, 97-99	4E	1176.37	11.23*	3.0*	ND	3.58E-02	7.30*	15.0	2.2	0.75*	1
94R-2, 47-49	2	1177.20	8.68*	1.9*	ND	5.12E-02	3.94*	11.3	1.5	0.77*	1
99R-4, 27-30	2	1209.87	6.02*	13.7*	57.0	1.66E-02	8.45*	4.85	8.6	1.24*	5
100R-3, 24-26	1C	1215.68	2.08	21.6	56.0	2.63E-02	1.84	4.72	8.3	0.44	6
101R-4, 68-70	9	1226.37	1.94	25.5*	45.9	2.45E-02	1.84	7.11	8.5	0.27*	8
105R-3, 37-39	6	1250.79	0.88*	34.4*	55.8	2.97E-02	0.69*	7.16	8.8	0.12*	11
108R-1, 59-62	2C	1262.80	3.78	30.6*	30.7	1.65E-02	5.33	3.79	18.8	1.00	12
109R-1, 70-72	2E	1267.60	2.75	32.4	42.7	2.39E-02	2.67	5.77	32.7	0.48	13
110R-1, 121-123	11G	1273.11	3.26*	29.9*	62.5	2.28E-02	3.32*	4.65	21.1	0.70*	14
112R-1, 76-78	11A	1291.66	0.20	25.7*	48.4	1.29E-02	0.36*	2.56	6.3	0.08*	16
112R-3, 18-20	2B	1293.95	0.90*	28.5*	57.1	1.72E-02	1.22*	5.45	7.2	0.17*	17
14R-3, 97-101	7	113.62	1.29	31.3	50.7	0.66E-02	4.54	1.33	13.5	0.97	18

Notes: Samples 152-918D-94R-1, 97-99 cm, and -94R-1, 47-49 cm, are from a sill intruding early Eocene sediments. The remaining samples are from "fresh" volcanic basement. NRM = natural remanent magnetization; MDF-NRM = median destructive field of the NRM; St. inc. = stable inclination; Suscept. = bulk volume susceptibility; Q ratio = Koenigsberger ratio; ARM = anhysteretic remanent magnetization; MDF-ARM = median destructive field of the ARM; Unit = identified petrological unit (see "Igneous Petrology" section, this chapter); ND = not determined; \* = samples have a significant secondary magnetization.

when detailed examination of these core-catcher samples and a large number of additional samples is completed in shore-based studies. Sedimentation rates for different segments of the age-vs.-depth curve were calculated and are shown in Figure 38. These sedimentation rates were not corrected for compaction, and hiatuses too small to be identified by current biostratigraphies were not taken into account. Nevertheless, the age-vs.-depth curve and the sedimentation rate values shown in Figure 38 provide a useful, broad picture for characterizing the sediment accumulation pattern through time at Site 918. The age-vs.-depth curve also allows us to assign ages for two important stratigraphic levels: (1) about 7 Ma for the initiation of extensive Greenland glaciation, as recorded by the lowest occurrence of dropstones at 543.6 mbsf; (2) about 11 Ma for the initiation of modern NADW, as indicated by the sedimentary evidence for hiatus and scouring and major changes in planktonic and benthic microfossils at about 660 mbsf (see "Lithostratigraphy" and "Biostratigraphy" sections, this chapter).

Nannofossil biostratigraphy suggests that sediments deposited during the early part of the Brunhes through Jaramillo magnetic chrons (a total of about 0.8 m.y.) probably are missing at about 50 mbsf (see "Biostratigraphy" section, this chapter). An unconformity is also suggested by seismic data, but at a lower level (about 70 mbsf). Detailed shore-based biostratigraphic and magnetostratigraphic studies should resolve this discrepancy. Here, we tentatively assume that an interval representing about 0.8 m.y. of sedimentation has been eroded in the Pleistocene section. This will result in a sedimentation rate of about 8 cm/k.y. for the Pleistocene. This sedimentation rate is similar to that calculated for the same interval at Site 914 on the continental shelf (>9.2 cm/k.y.). The interval between data points 2 and 3 (Fig. 38) has a high sedimentation rate (19.9 cm/k.y.) and clearly shows the significant contribution of ice-rafted material during the Pliocene. Upper Oligocene turbidites (bracketed by data points 11 and 13) accumulated at high rates (6.3 cm/k.y.) also. The Oligocene turbidite sequence extends down to a major unconformity just below data point 15 (Fig. 38). As data point 15 coincides with an unconformity, only a minimum sedimentation rate (2.1 cm/yr) could be calculated between data points 13 and 15.

A low sedimentation rate (0.4 cm/k.y.) characterizes the middle and lower Eocene interval (between data points 16 and 17). Marine biological productivity was probably low in the basin during the Eocene as a result of the generally warm climate and extensive vegetation on the surrounding, probably low relief, land which, probably led to a similarly low supply of terrestrial material into the basin.

The depth (m below sea level) of the top of the basalt sequence at Site 918 has been reconstructed through time back to the early Eocene in Figure 39. The data used are estimates of paleowater depths based on benthic foraminifers and age-vs.-depth data shown in Figure 38. Because the ranges of these estimates of paleowater depth are large,

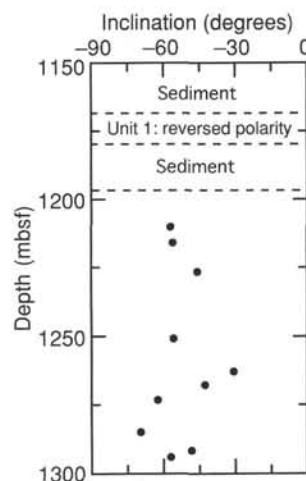


Figure 36. Plot of stable magnetic inclination vs. depth in the volcanic sequence of Hole 918D.

particularly for the Oligocene and younger intervals, the subsidence curve is not well constrained. The two dashed lines in Figure 39 are intended to aid a first-order comparison of the subsidence rate of the Eocene and that of the Oligocene through Holocene. The subsidence rate for the Eocene (Fig. 38) is about 40 m/m.y., and that for the Oligocene through Holocene interval is about 70 m/m.y. The higher average subsidence rate for the younger interval compared to the Eocene interval opposes predictions by cooling models (Parsons and Sclater, 1977), but may, at least partly, be explained by an increased rate of sedimentation.

## IGNEOUS PETROLOGY

### Lithological Units

Hole 918D reached basaltic rock at 1168.2 mbsf. The first igneous unit is probably a sill that intruded into the lowest part of the sedimentary sequence (see below, this section). A total of 2.8 m was recovered in two cores (152-918D-93R and -94R), but the unit might be as much as 12 m thick (1168.2-1180.4 mbsf). It was not possible to determine the precise thickness of the unit from rate-of-penetration data.

Unequivocal lava flows underlie lithologic Unit V at 1188.5 mbsf, and 18 flow units were recorded to the base of the hole at 1310.1 mbsf (Fig. 40). Core recovery for these units was 45.2%. Deep subaerial weathering has affected the top three flow units, and the first rock preserving any original igneous mineralogy was encountered in igne-

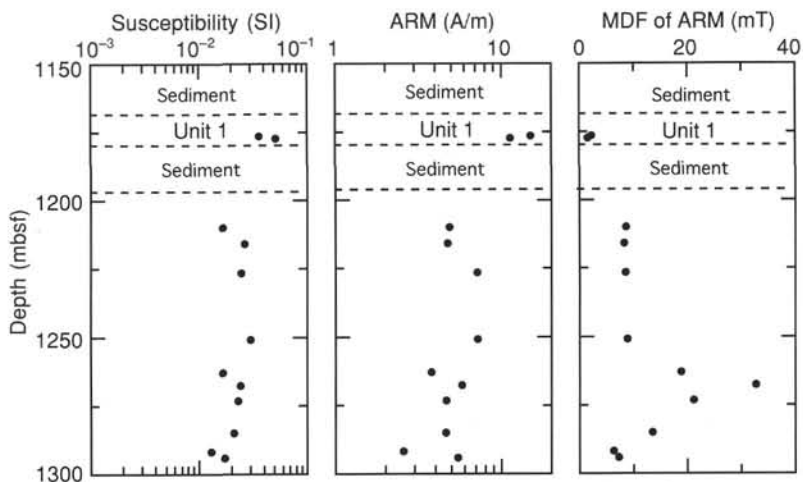


Figure 37. Plot of bulk magnetic susceptibility, ARM, and MDF of ARM vs. depth in the volcanic sequence of Hole 918D.

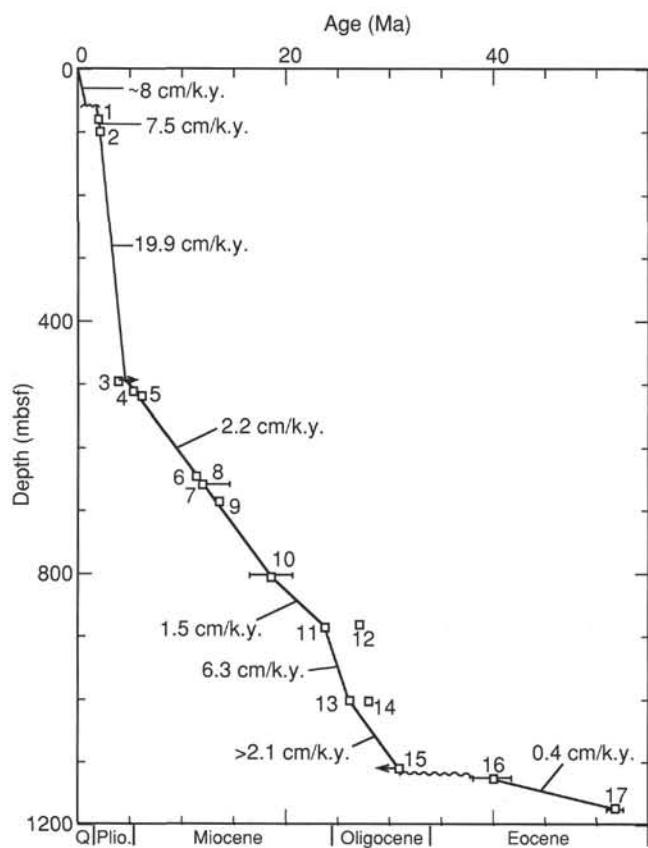


Figure 38. Diagram of age vs. depth for Site 918. Sedimentation rates for different stratigraphic intervals are shown. Data Point 1 = top of Olduvai Chron; 2 = base of Olduvai Chron; 3 = last occurrence (LO) of *Reticulofenestra gelida*; 4 = LO of *Discoaster quinquerramus*; 5 = coiling change from dominantly dextral to dominantly sinistrally coiled morphotypes of *Neoglobobadrina atlantica*; 6 = first occurrence (FO) of *Neoglobobadrina acostanensis*; 7 = LO of *Cyclicargolithus floridanus*; 8 = stratigraphic range of *Globorotalia praemenardii*; 9 = LO of *Sphenolithus heteromorphus*; 10 = stratigraphic range of *Globigerinoides altiaperturus*; 11 = LO of *Reticulofenestra bisecta*; 12 = FO of *Paragloborotalia pseudokugleri*; 13 = LO of *Chiasmolithus altus*; 14 = LO of *Chiloguembelina cubensis*; 15 = LO of *Reticulofenestra umbilicus*; 16 = the stratigraphic range of *Tribrachiatus orthostylus*; and 17 = Subzone CP14a.

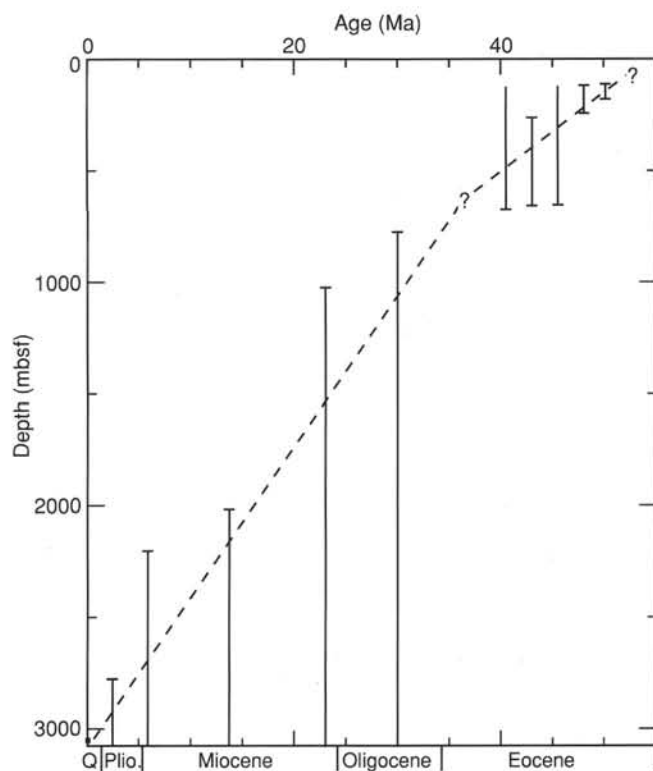


Figure 39. Inferred subsidence history of the top of the basalt sequence at Site 918 (dashed lines).

ous Unit 4 at 1206.0 mbsf (Core 152-918D-98R-2, 65 cm). Units 4 through 13 are separated by highly altered basalt breccia. Each breccia and underlying massive lava flow have been regarded here as a single lithologic unit, divided into A (breccia) and B (massive) subunits. This division serves only as a convenient means of defining units and does not imply that each A subunit was formed solely as part of the underlying B subunit. It is sometimes clear that an A subunit constitutes the base of the overlying and top of the underlying flow (see below, this section). Locations of the tops and bottoms of lithologic units are listed in Table 6.

The massive parts of each flow unit are remarkably constant in appearance. All are composed of aphanitic to fine-grained aphyric basalt with, in some cases, sparse microphenocrysts of altered olivine

**Table 6. Location of tops and bases of igneous units in Hole 918D.**

Unit	Top of core (Hole 918D) (cm)	Base of core (Hole 918D) (cm)
1	93R-2, 90	94R-3, 48
2	96R-3, 130	97R-2, 81
3	97R-2, 81	97R-5, 149
4A	97R-5, 149	98R-2, 65
4B	98R-2, 65	99R-1, 32
5A	99R-1, 32	99R-2, 133
5B	99R-3, 0	100R-1, 30
6A	100R-1, 30	100R-2, 67
6B	100R-3, 0	100R-3, 70
7A	100R-3, 70	100R-3, 109
7B	100R-3, 109	101R-1, 26
8A	101R-2, 0	101R-3, 94
8B	101R-4, 0	102R-1, 128
9A	102R-2, 0	103R-1, 8
9B	103R-1, 8	103R-2, 63
10A	103R-2, 63	104R-1, 47
10B	104R-1, 47	104R-3, 31
11A	104R-3, 31	105R-1, 110
11B	105R-1, 110	106R-4, 50
12A	106R-4, 50	106R-4, 110
12B	107R-1, 0	108R-3, 21
13A	108R-3, 21	108R-3, 65
13B	109R-1, 0	109R-3, 70
14	110R-1, 0	110R-5, 78
15	111R-1, 0	111R-3, 119
16	112R-1, 0	112R-2, 38
17	112R-2, 38	113R-1, 35
18	113R-1, 35	113R-2, 52
19	113R-2, 52	113R-2, 113

and fresh plagioclase. Unit 1 (the probable sill) is coarser grained and contains microphenocrysts of plagioclase and clinopyroxene.

### Flow Morphology and Lithology

A total of 19 igneous units was drilled in Hole 918D. The uppermost unit may be a sill or a lava, whereas the other 18 units are lava flows. The "sill" is between 3 and 12 m thick and is separated from the lavas by between 8 and 16 m of sediments. The drilled lava sequence is 120.7 m thick. With the exception of Unit 19, of which only the upper part was penetrated, the lavas (Units 2 through 18) range in thickness from 1.4 m (Unit 18) to 10.7 m (Unit 11), with an average thickness of 7.1 m.

The "sill" (Unit 1) was emplaced into/onto shallow-marine sediments (see "Lithostratigraphy" section, this chapter). Clearly, it is different from the underlying lava sequence with respect to degree of alteration, lithology, and composition (see later, this section). It does not belong to the main seaward-dipping reflector sequence, and it is most probably related to a later, small, off-axis volcano, which is seen in the seismic profiles on top of the seaward-dipping reflectors just 3.5 km west of Site 918 (see "Background and Scientific Objectives" section, this chapter). The recovered rock is fresh, homogeneous, and vesicle-free, and no contacts with the surrounding sediments have been preserved. We were unable to decide whether the unit is a lava or a sill. Even if it is a sill, it may be related to the nearby volcano. Seismic profiles indicate that the volcano and the lowest sediments are contemporary. There are no lithological differences between the sediments above and below the sill (see "Lithostratigraphy" section, this chapter).

The shallow-marine sediments below the sill rest on deeply weathered lavas of the seaward-dipping reflector sequence. The uppermost of these lavas (Units 2–4A, 1189.4–1206.1 mbsf) have been thoroughly altered and oxidized to red saprolite. This weathered zone is 17.6 m thick, but the igneous structures have been well preserved and are undisturbed, which suggests that the weathered zone corresponds to only the C Horizon of a soil profile. Thus, the original soil profile must have been even thicker.

Below the weathered zone lies a sequence of alternating zones of gray, massive basalt and red, oxidized, altered basalt having a fragmental structure. The red zones have been heavily disturbed by drill-

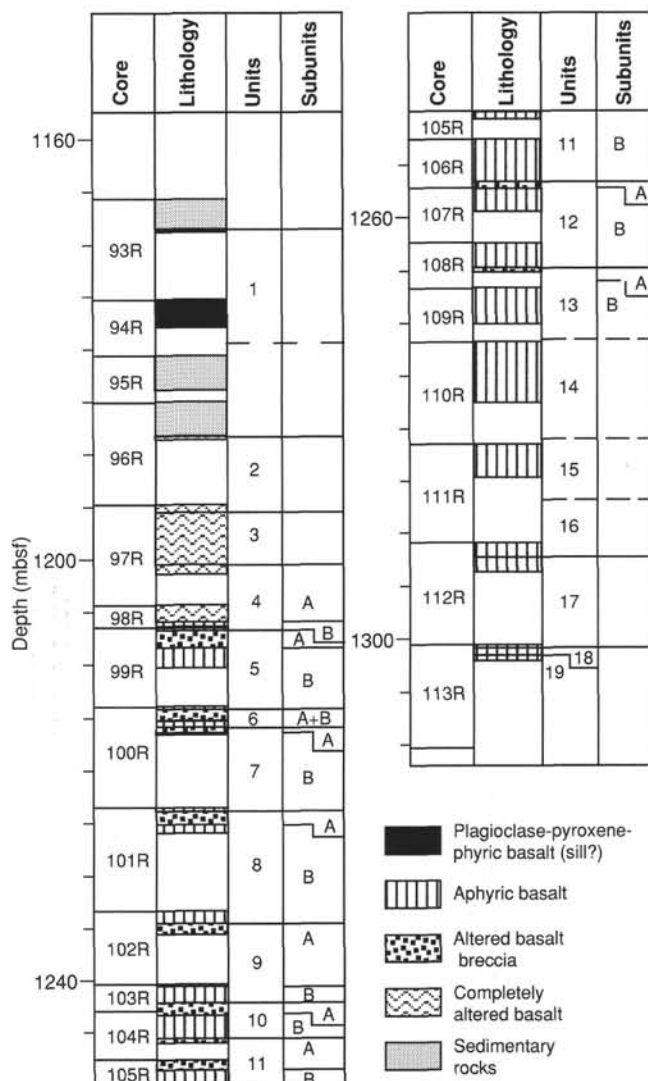


Figure 40. Stratigraphic log showing the volcanic succession cored at Site 918.

ing and have usually disintegrated into gravel in a loose matrix of clay; contacts have not been preserved. The red zones were considered to be highly altered, brecciated flow tops, and Units 4 through 13 each consist of A (red, brecciated) and B (gray, massive) subunits. Units 14 through 19 have better-preserved, reddened, but nonbrecciated, tops and bases. Reddened flow tops are often, but not always, characterized by peaks in the magnetic susceptibility in the MST logs (see "Physical Properties" section, this chapter). Inspection of the MST logs, in some cases, showed such susceptibility peaks within the red zones, indicating that they partly consist of brecciated flow bases (Units 5A, 7A, 8A, 9A). Other red units seem to consist solely of flow tops (Units 10A, 12A). Some red zones, however, showed no MST signal (Units 6A, 11A, 13A), and we decided to maintain all the red zones as "A" subunits, even though some of them probably include the base of the overlying flow. Because of the poor state of preservation of the red zones, it was usually not possible to distinguish between subaerial and subaqueous brecciation. Only Unit 8A includes remains of indisputable small (1–2 cm) pillow structures in the flow top. However, the strong oxidation indicates that subaerial conditions were dominant and the presence of water temporary.

Units 3 to 8 and 12 are aa lavas having flow-banded central portions and brecciated tops and bases. Units 10 and 13 through 19 are pahoehoe lavas with finely vesicular tops and bases, disseminated vesicles, and in some flow units, segregation patches. Units 9 and 11

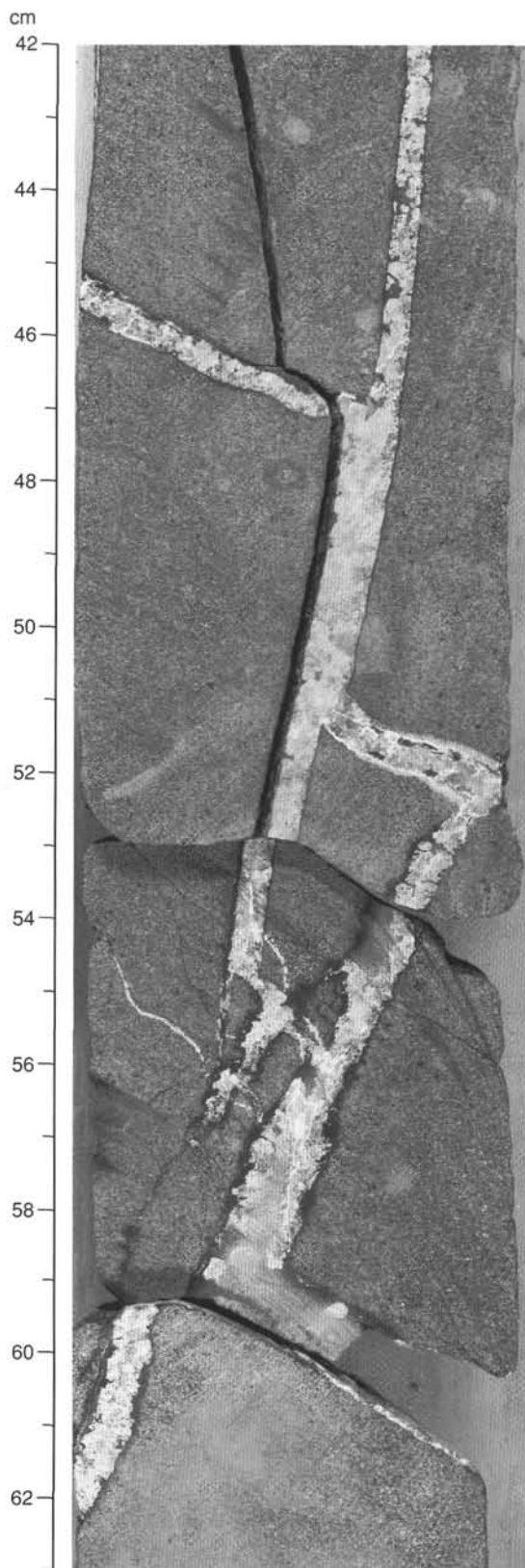


Figure 41. Photograph of calcite-filled fractures in Unit 1 (Interval 152-918D-94R-1, 42–63 cm).

show mixed features. Thus, a transition from pahoehoe lavas to aa lavas occurs with time in the succession.

The volcanic succession in Hole 918D can be interpreted as the most distal, landward portion of the volcanic rocks that erupted from the central SDRS-producing rift system when the system was situated some distance to the southeast of Site 918 (see "Introduction" chapter, this volume). Lavas would have only occasionally flowed so far west from the main eruption center, and the supply would diminish with time and eventually stop as the rift axis migrated seaward relative to the Site 918 position. Successively longer time spans between the lavas would lead to increased weathering upward in the sequence, and the clay in the disturbed red A subunits could represent disrupted interbasaltic soil horizons. The switch from pahoehoe to aa flow type with time may also have led to increased weathering. The presence of about 20 m of thoroughly weathered basalt on top of the succession indicates that the original top of the offlapping basalt sequence has been preserved with a minimum of erosion. Only the top of the soil profile could have been removed by the marine transgression.

### Structure

The only structure that can be used to estimate any tilting of the lava pile is the parallel flow-banding in the aa lavas. This shows variable dips from 0° to 20°; thus, the data are not conclusive. The seismic profiles (see "Background and Scientific Objectives" section, this chapter) indicate that the uppermost lavas of the SDRS are very close to horizontal.

The drilled lavas are unfaulted and, in general, not fractured. Fractures with slickensides can be found in the thoroughly weathered Units 4A and 5A and may be the result of local compaction. In contrast, the fresh sill, Unit 1, contains calcite-filled fractures up to 1 cm wide, apparently produced under tension (Fig. 41).

### Petrography

The volcanic succession comprises 18 lava flows (Units 2–19) and one unit (Unit 1) that has been interpreted as a sill. Units 2, 3, and most of 4 have been completely altered and oxidized. Eight thin sections of the basaltic units were studied, and two main petrographic types were defined.

#### *Plagioclase-pyroxene-phyric Basalt (Unit 1)*

This lithology contains about 5% glomeroporphyritic clusters of plagioclase (0.5–1 mm) and clinopyroxene. Fresh subhedral olivine microphenocrysts (0.5%) are present and have been slightly altered to greenish clays along the fractures. The groundmass is a fine-grained intergranular mixture of plagioclase, clinopyroxene, and minor olivine (0.2–0.3 mm). An opaque oxide mineral (6.5%) is a late-crystallizing phase. Brown devitrified glass constitutes about 6.6% of the rock and includes quenched plagioclase and clinopyroxene microlites and opaque grains.

#### *Aphyric Basalt (Units 4–19)*

These rocks are very fine-grained tholeiites. Olivine, when originally present, forms rare (<1%) microphenocrysts up to 0.5 mm in diameter and is always altered to clays. Rounded margins on the olivine microphenocrysts suggest disequilibrium between the olivine and the magma. Units 11 and 12 contain sparse (<1%) tabular plagioclase microphenocrysts up to 1 mm long. The aphyric basalts have an intersertal to intergranular matrix of plagioclase (45%–50%), clinopyroxene (34%–37%), and opaque oxide (3.5%–7%). Some elongate and slightly altered clinopyroxenes may be pigeonite. The alternating intersertal and intergranular textures define a broad flow-banding or ovoid patches visible in hand specimen. The darker color of the glassy intersertal domains (8%–12%) is caused by the presence of clays that replace the glass. These flow-bands and ovoid patches represent more

differentiated melts that segregated during cooling of the flow, and this is also supported by the greater abundance of opaque oxide minerals in the bands.

### Alteration

Except for the highly weathered Units 2 to 4 and the brecciated horizons separating Units 4 through 13, lavas from Site 918 are well preserved with only olivine and glass having been altered to clays. The major difference in alteration between the volcanic sequences of Sites 917 and 918 is the absence of zeolite from the latter. Calcite is also less abundant, except in the upper part of the sequence (Units 1 and 4–7), reflecting the fact that the Site 918 volcanic rocks are less fractured than those at Site 917. Some unusual, white to yellowish brown, concentric calcite vesicle fillings up to 40 mm across were observed in Units 4 and 5 (Fig. 42). Vesicles in the other aphyric basalt units are mainly lined with a thin layer of dark green clay and filled with pale green clays, or, rarely, with calcite or a mixed calcite-clay assemblage. Blebs of native copper are prominent in all the upper units (4–14). These are mainly associated with the dark green clay that lines the vesicles or the veins; some specks also are seen, in both thin section and hand specimen, dispersed in the groundmass.

### Compositional Variation

Of the 19 igneous units identified in the volcanic succession at Site 918, eight were analyzed on board the *JOIDES Resolution* by X-ray fluorescence (XRF) methods. Results for major elements are reported in Table 7 and those for trace elements in Table 8. Procedures for sample preparation, run conditions for the spectrometer, and results of analyses of standards and duplicates are described in the "Igneous Petrology" section of the "Explanatory Notes" chapter (this volume).

The lavas (Units 2–19) encountered at Site 918 are relatively uniform in major- and trace-element composition and closely resemble the basalts from Site 915. Unit 1 has been interpreted as a sill and has a markedly different composition from the lavas. Figure 43 shows the variation of CaO with MgO in the igneous units of Sites 918, 917, and 915. In the basalts of Site 918 (and 915), MgO is restricted to between 7 and 9 wt%, indicating that all of the magmas were subjected to a uniform degree of fractional crystallization. The Site 918 basalts lie at the maximum in the CaO-MgO trend defined by the Site 917 lavas. Liquids move along the trend to lower MgO and higher CaO values as they crystallize olivine and then decrease from the maximum as olivine and plagioclase and later clinopyroxene crystallize. This is consistent with the petrography of the lavas, which are aphyric and have sparse microphenocrysts of olivine with or without plagioclase. These observations contrast sharply with the wide range of lava compositions and crystallization histories found in the Site 917 volcanic succession.

Incompatible element contents and ratios in the Site 918 lavas overlap the less enriched end of the ranges observed in the Site 917 lavas. For example, Ba/Zr is approximately 0.5 for all the Site 918 lavas, and ranges from 0.25 to 8 in the Site 917 lavas. This suggests that the Site 918 magmas did not interact with the continental lithosphere. Site 918 probably lies seaward of the continent/ocean transition (see "Background and Scientific Objectives" section, this chapter).

The sill (Unit 1) is more differentiated than the lavas, as shown by its lower MgO content. In addition, higher Zr/Y values, lower Zr/Nb values, and higher contents of all incompatible elements in this unit may indicate derivation of the parental magma by a smaller degree of melting.

### Conclusions

1. The succession consists of 19 igneous units that make up 18 subaerial lava flows and one unit inferred to be a sill. This "sill" is probably associated with a nearby post-SDRS volcano.

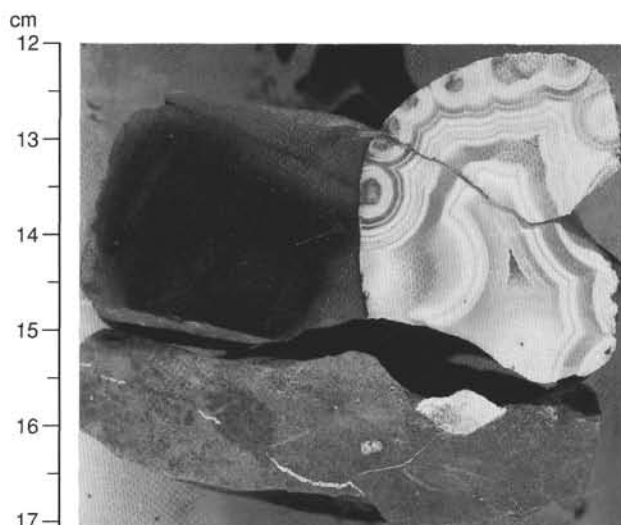


Figure 42. Photograph of banded calcite filling a vesicle in Unit 4B (Interval 152-918D-98R-3, 12–17 cm).

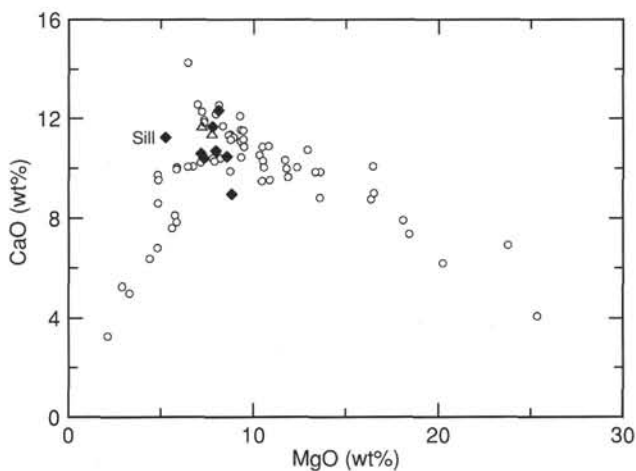


Figure 43. CaO vs. MgO for igneous units from Sites 917, 915, and 918. Open circles = Site 917, open triangles = Site 915, and closed diamonds = Site 918.

2. The upper three lava flows (Units 2–4) are deeply weathered and oxidized. Units 4 through 13 are separated by altered basalt breccia. These altered horizons increase in thickness toward the top of the section, indicating successively longer time intervals between lava flows.

3. All of the lava flows consist of aphyric basalt, some with sparse microphenocrysts of olivine and occasionally plagioclase.

4. The lava flows show little variation in composition, with MgO varying only between 7 and 9 wt%. The sill is more evolved (5.23 wt% MgO).

5. Low incompatible-element abundances and Ba/Zr values and high Zr/Nb values in the lava flows are comparable to values typical of N-MORB. This indicates derivation of the magmas from a depleted mantle source, with no observable contamination from the continental lithosphere.

### ORGANIC GEOCHEMISTRY

The organic geochemistry analyses performed at Site 918 included measurements of total carbon, inorganic carbon, total nitro-

Table 7. Shipboard X-ray fluorescence major-element analyses of Site 918 igneous rocks.

Unit	Core, section, interval (cm)	Depth (mbsf)	SiO <sub>2</sub>	TiO <sub>2</sub>	Al <sub>2</sub> O <sub>3</sub>	Fe <sub>2</sub> O <sub>3</sub>	MnO	MgO	CaO	Na <sub>2</sub> O	K <sub>2</sub> O	P <sub>2</sub> O <sub>5</sub>	Total	LOI
1	152-918D-94R-2, 54–57 (Piece 2)	1177.27	49.26	3.02	13.38	14.31	0.19	5.23	11.24	2.67	0.57	0.35	100.20	0.39
5B	152-918D-99R-4, 27–30 (Piece 2)	1209.87	50.48	1.23	15.55	11.61	0.23	8.54	10.47	2.41	0.07	0.05	100.62	1.63
8B	152-918D-101R-4, 52–55 (Piece 7)	1226.21	51.06	1.30	13.65	14.94	0.29	7.29	10.41	2.17	0.05	0.07	101.22	0.38
11B	152-918D-105R-3, 30–35 (Piece 5)	1250.71	51.26	1.29	14.00	13.86	0.26	7.14	10.59	2.06	0.07	0.07	100.58	0.77
12B	152-928D-108R-1, 59–62 (Piece 2C)	1262.79	50.18	0.99	13.57	13.51	0.23	8.11	12.34	1.66	0.05	0.04	100.67	0.74
13B	152-918D-109R-1, 60–64 (Piece 2D)	1267.50	50.61	1.27	15.36	12.85	0.12	8.82	8.96	2.23	0.14	0.04	100.38	2.31
14	152-928D-110R-4, 107–111 (Piece 10)	1277.32	50.66	1.18	13.97	13.54	0.18	7.77	11.68	2.13	0.09	0.06	101.25	0.53
15	152-918D-111R-3, 108–111 (Piece 12)	1285.43	50.51	1.44	14.11	14.41	0.30	7.94	10.71	2.20	0.08	0.08	101.76	0.74

Notes: Values are in weight percent. LOI = loss on ignition. Analysts were Don Sims and Mary Ann Cusimano.

Table 8. Shipboard X-ray fluorescence trace-element analyses of Site 918 igneous rocks.

Igneous unit	Core, section, interval (cm)	Depth (mbsf)	V	Cr	Ni	Cu	Zn	Rb	Sr	Y	Zr	Nb	Ba	Ce
1	152-918D-94R-2, 54–57 (Piece 2)	1177.27	—	82	66	266	114	9.3	227.5	34.3	194.2	30.0	206	56
5B	152-918D-99R-4, 27–30 (Piece 2)	1209.87	447	112	82	223	99	4.4	87.9	26.5	52.2	1.7	25	1
8B	152-918D-101R-4, 52–55 (Piece 7)	1226.21	487	58	60	268	113	3.6	78.9	28.2	59.3	3.1	29	3
11B	152-918D-105R-3, 30–35 (Piece 5)	1250.71	466	79	57	204	108	4.1	77.7	28.7	58.4	2.6	25	3
12B	152-928D-108R-1, 59–62 (Piece 2C)	1262.79	352	152	83	158	90	4.1	66.7	26.4	41.1	2.3	16	0
13B	152-918D-109R-1, 60–64 (Piece 2D)	1267.50	440	127	84	83	98	4.3	93.5	27.0	56.0	3.1	22	5
14	152-928D-110R-4, 107–111 (Piece 10)	1277.32	421	108	81	164	92	4.5	80.9	29.4	53.2	3.4	25	1
15	152-918D-111R-3, 108–111 (Piece 12)	1285.43	469	100	69	108	102	3.8	81.3	30.2	66.8	4.0	28	7

Notes: Values are in parts per million. Analysts were Don Sims and Mary Ann Cusimano.

gen, total sulfur, and Rock-Eval pyrolysis (for methods see “Explanatory Notes” chapter, this volume).

### Elemental Analyses

During drilling of Site 918, 295 sediment samples were collected for elemental analyses. The results are summarized in Table 9 and presented in Figures 44 to 47.

Carbonate contents vary between 0 and 47 wt% and depend strongly on lithology (Fig. 44). In the siliciclastic-dominated glaciomarine sediments of Unit I (see “Lithostratigraphy” section, this chapter), carbonate values are low and range mainly between 0 and 5 wt%. Some single layers show contents of up to 12 wt%. According to the smear slide descriptions of the Pliocene to Pleistocene siltstones and sandstones, planktonic foraminifers dominate the carbonate content in the upper 600 m. The change from lithologic Unit I to Unit II at 600 mbsf is marked by a dramatic increase in carbonate content up to values of 45 wt%. These high values are consistent down to Unit IV and result from the occurrence of nannofossil-bearing chalks and siltstones. Short-term changes in lithology from chalky to sandy and silty intervals are reflected by the high amplitude variation of the carbonate record. In lithologic Unit V, which contains glauconitic sandstones between 1157.9 and 1189.4 mbsf (see “Lithostratigraphy” section, this chapter), no carbonate could be detected.

Total organic carbon values for the sediments of Site 918 are low throughout the entire column and range from 0 to 0.5 wt%. However, single spikes of up to 1.65 wt% were observed (Fig. 45). Small-scale increases from about 0.2 to 0.5 wt%, as recorded at the transition from lithologic Unit I to Unit II (about 610 mbsf, Fig. 45), may reflect enhanced nannoplankton sedimentation that resulted from increased surface-water productivity (see “Biostratigraphy” section, this chapter).

Total nitrogen values at Site 918 vary between 0 and 0.11 wt%. Total sulfur contents range from 0 to about 3 wt% (Table 9). Highest sulfur values were observed in the early Eocene sediments (1135–1168 mbsf; Cores 152-918D-90R to -93R). The main portion of sulfur occurs as authigenic pyrite, which forms large nodules and frustules within the siltstones (see “Lithostratigraphy” section, this chapter).

### Composition of Organic Matter

To characterize the type of organic matter in the sediments of Site 918, total organic carbon/total nitrogen ratios, and hydrogen index values from Rock-Eval pyrolysis are used (see “Organic Geochemistry” section, “Site 916” chapter, this volume). Most of the TOC/TN values are below 12, indicating a marine predominance in the organic matter (Fig. 46; Bordovskiy, 1965; Emerson and Hedges, 1988). Samples having higher total organic carbon contents correlate with elevated TOC/TN values (Fig. 47). This is corroborated by the results of the Rock-Eval pyrolysis performed on samples having TOC contents higher than 0.5 wt% (Fig. 48, Table 10; e.g., Espitalié et al., 1977; Peters, 1986). When plotting hydrogen index and oxygen index values of these samples into a “van Krevelen”-type diagram, a clear dominance of terrigenous organic (kerogen III; Espitalié et al., 1977) matter is indicated.

According to the provenance of the organic matter, two different mechanisms for the accumulation of organic carbon at Site 918 can be recognized. The background productivity of marine plankton leads to the preservation of about 0.3 wt% marine organic carbon in the sediment. In addition, episodic terrigenous organic matter supply by turbidity currents results in high TOC spikes. Estimates about the amounts of marine and terrestrial organic carbon still have to be confirmed by shore-based elemental and microscope analyses.

### Volatile Hydrocarbons

Concentrations of methane (C<sub>1</sub>), ethane (C<sub>2</sub>), and propane (C<sub>3</sub>) were routinely monitored for each core according to shipboard safety and pollution prevention considerations. The results are displayed in Figure 49 and Table 11. Between 1200 and 550 mbsf, methane concentrations are close to the detection limit of the Hach-Carle gas chromatograph (see “Explanatory Notes” chapter, this volume). At about 550 mbsf, methane increases dramatically to values of between 3,500 and 85,000 ppm (Fig. 49) and decreases again to near zero at 80 mbsf. Low concentrations then are constant from this level up to the top of the sediment column.

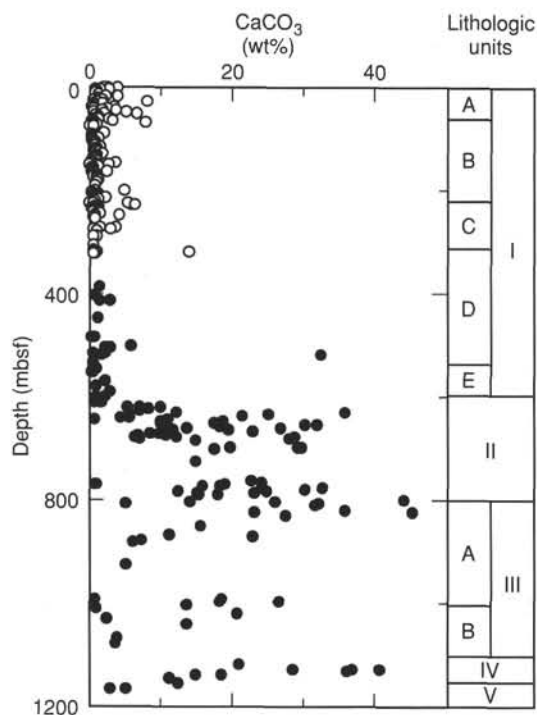


Figure 44. Results of calcium carbonate ( $\text{CaCO}_3$ ) vs. depth in Holes 918A (open circles) and 918D (solid circles). Lithologic column according to sediment description (see "Lithostratigraphy" section, this chapter).

Two principal gas sources are possible. The first is migration of methane into the turbiditic siltstones and sandstones of Unit I from underlying rocks, where methane may have been produced thermogenically. Evidence for diffusive migration of gas from deeper sources was found in Leg 151. However, at Site 918, no significant amounts of higher hydrocarbons (such as ethane or propane) were detected. Thermal generation of gases is not expected because of a geothermal gradient of about  $55^\circ\text{C}/\text{km}$ , which suggests a formation temperature of about  $60^\circ\text{C}$  at the bottom of the sediment column (see "Heat Flow" section, this chapter).

The source for methane at Site 918 is most likely in-situ bacterial methanogenesis resulting from fermentation and deamination of organic matter in the sediments. When sulfate becomes depleted in the pore waters, no decomposition of organic matter during sulfate reduction is possible, and microbial methane production follows (e.g., Claypool and Kvenvolden, 1983; Gieskes, 1983). This leads to the inverse relationship between methane concentration and sulfate content of interstitial waters (Fig. 49, see "Inorganic Geochemistry" section, this chapter). The concentration profile of methane shows a characteristic pattern, similar to profiles found in sediments of the Nankai Trough (Leg 131; Taira, Hill, Firth, et al., 1991) and off Portugal (Leg 149; Sawyer, Whitmarsh, Klaus, et al., 1994). In lithologic Unit I, large amounts of organic carbon were rapidly buried during deposition under very high sedimentation rates (about  $19\text{ m/m.y.}$ , Fig. 49; see "Sedimentation Rates" section, this chapter). The sulfur is rapidly exhausted at 80 mbsf, and methane production occurs below this depth. The decrease in methane at 550 mbsf correlates with the increase in pore-water sulfate, indicating a deep reservoir of sulfate in the Miocene and Oligocene sediments of lithologic Units II and III, which was preserved by the relatively slow sedimentation rates (see "Inorganic Geochemistry" section, this chapter).

## INORGANIC GEOCHEMISTRY

At Site 918, a detailed interstitial water sampling program was undertaken, with special, dense sampling in the upper parts of the

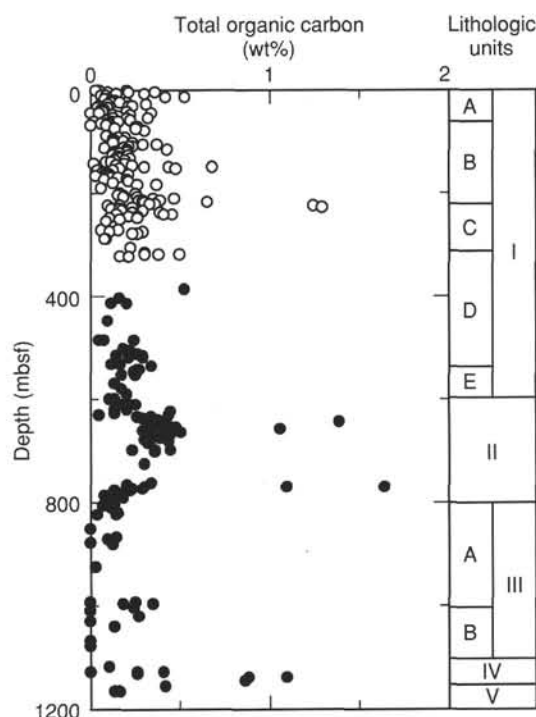


Figure 45. Results of total organic carbon (TOC) vs. depth in Holes 918A (open circles) and 918D (solid circles). Lithologic column according to sediment description (see "Lithostratigraphy" section, this chapter).

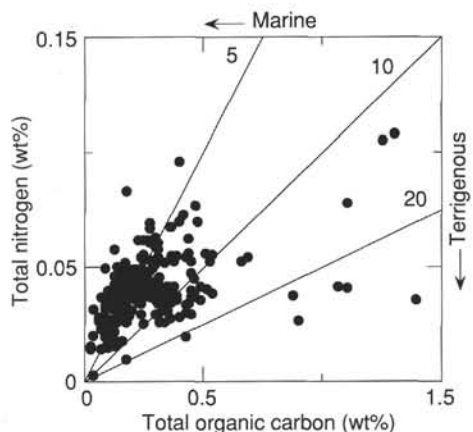


Figure 46. Total organic carbon (TOC) vs. total nitrogen in sediments of Holes 918A and 918D. TOC/TN values of  $<10$  suggest major proportions of marine organic matter, TOC/TN values  $>10$  suggest major proportions of terrigenous organic matter.

sediment column, in Holes 918A, 918B, and 918C. The reason for this more detailed sampling program was that early diagenetic reactions involving the bacterial decomposition of organic matter are particularly pronounced in the upper sections of the sediment column.

The data obtained are presented in Tables 12 and 13. Data on salinity, pH, and alkalinity were obtained only from those horizons where sufficient sample sizes were available for analysis. In almost all horizons, care was taken to preserve samples in glass ampoules for future work on stable isotopes of the interstitial waters.

In the following section, the shipboard results of the interstitial water program are discussed in a tentative manner. Further work on stable isotopes of oxygen, deuterium, strontium, lithium, and boron will be necessary to provide closer constraints on the interpretation of the interstitial water chemistry in terms of reactions occurring in the sediment column.

Table 9. Summary of organic chemistry analyses at Site 918.

Core, section, interval (cm)	Depth (mbsf)	TC (wt%)	IC (wt%)	TOC (wt%)	CaCO <sub>3</sub> (wt%)	TN (wt%)	TS (wt%)	TOC/TN (ratio)	Core, section, interval (cm)	Depth (mbsf)	TC (wt%)	IC (wt%)	TOC (wt%)	CaCO <sub>3</sub> (wt%)	TN (wt%)	TS (wt%)	TOC/TN (ratio)
152-918A-									17H-1, 115-116	143.95	0.25	0.05	0.20	0.42	0.05	0.00	4.3
1H-1, 33-34	0.33	0.52	0.47	0.05	3.92	0.03	0.00	1.9	17H-2, 114-115	145.44	0.31	0.07	0.24	0.58	0.05	0.00	4.5
1H-1, 62-63	0.62	0.51	0.30	0.21	2.50	0.04	0.09	5.7	17H-3, 73-74	146.53	0.59	0.44	0.15	3.67	0.02	0.00	7.9
1H-2, 28-29	1.78	0.27	0.24	0.03	2.00	0.02	0.05	1.5	17H-4, 127-128	148.57	0.45	0.01	0.44	0.08	0.05	0.00	8.3
2H-1, 73-74	2.53	0.55	0.33	0.22	2.75	0.04	0.00	5.8	17H-5, 74-75	149.54	0.43	0.13	0.30	1.08	0.04	0.00	7.3
2H-2, 58-59	3.88	0.54	0.18	0.36	1.50	0.06	0.10	6.5	17H-6, 122-123	151.52	1.00	0.32	0.68	2.67	0.05	0.00	12.3
2H-3, 33-34	5.13	0.21	0.11	0.10	0.92	0.03	0.06	3.6	18H-1, 119-120	153.49	0.62	0.14	0.48	1.17	0.04	0.00	13.3
2H-4, 65-66	6.95	0.42	0.12	0.30	1.00	0.04	0.07	6.9	18H-2, 28-29	154.08	0.33	0.16	0.17	1.33	0.03	0.00	6.5
2H-5, 21-22	8.01	0.29	0.14	0.15	1.17	0.03	0.00	4.4	18H-3, 128-129	156.58	0.19	0.06	0.13	0.50	0.03	0.00	5.0
2H-6, 51-52	9.81	0.19	0.13	0.06	1.08	0.01	0.06	4.1	18H-4, 82-83	157.62	0.08	0.04	0.04	0.33	0.00	0.00	
3H-1, 36-37	11.66	0.18	0.09	0.09	0.75	0.02	0.00	4.8	18H-5, 23-24	158.53	0.17	0.08	0.09	0.67	0.00	0.00	1.53
3H-2, 73-74	13.53	0.57	0.15	0.42	1.25	0.05	0.00	7.7	18H-6, 43-44	160.23	0.13	0.06	0.07	0.50	0.00	0.00	0.23
3H-3, 30-31	14.60	0.69	0.16	0.53	1.33	0.06	0.00	9.4	18H-7, 48-49	161.78	0.16	0.07	0.09	0.58	0.02	0.09	4.8
3H-4, 27-28	16.07	0.37	0.27	0.10	2.25	0.03	0.00	3.7	19H-1, 23-24	162.03	0.27	0.05	0.22	0.42	0.04	0.06	5.5
3H-6, 27-28	19.07	0.56	0.48	0.08	4.00	0.03	0.00	2.4	19H-2, 35-36	163.65	0.19	0.08	0.11	0.67	0.02	0.05	5.0
3H-7, 38-39	20.68	0.27	0.13	0.14	1.08	0.04	0.00	3.8	19H-3, 34-35	165.14	0.40	0.30	0.10	2.50	0.02	0.04	4.4
4H-1, 76-77	21.56	0.28	0.16	0.12	1.33	0.03	0.00	3.8	19H-4, 34-35	166.64	0.22	0.11	0.11	0.92	0.04	1.36	2.6
4H-2, 125-126	23.55	0.33	0.21	0.12	1.75	0.02	0.07	6.3	19H-5, 35-36	168.15	0.12	0.09	0.03	0.75	0.03	0.02	1.0
4H-3, 32-33	24.12	0.31	0.10	0.21	0.83	0.04	0.00	5.1	19H-6, 34-35	169.64	0.18	0.06	0.12	0.50	0.04	0.01	3.0
4H-4, 36-37	25.66	0.25	0.08	0.17	0.67	0.04	0.00	4.7	19H-7, 35-36	171.15	0.18	0.06	0.12	0.50	0.04	0.13	2.8
4H-5, 63-64	27.43	0.45	0.14	0.31	1.17	0.05	0.00	6.8	20X-1, 37-38	171.67	0.22	0.06	0.16	0.50	0.05	0.16	3.2
4H-6, 31-32	28.61	1.06	0.96	0.10	8.00	0.04	0.00	2.7	20X-2, 27-28	173.07	0.28	0.07	0.21	0.58	0.05	0.12	4.6
4H-7, 13-14	29.93	0.29	0.07	0.22	0.58	0.05	0.00	4.7	20X-3, 27-28	174.57	0.20	0.12	0.08	1.00	0.02	0.11	4.2
5H-1, 126-127	31.56	0.46	0.22	0.24	1.83	0.05	0.00	5.2	20X-4, 26-27	176.06	0.34	0.12	0.22	1.00	0.04	0.49	6.2
5H-2, 80-81	32.60	0.13	0.08	0.05	0.67	0.03	0.00	1.8	21X-1, 35-36	181.85	0.30	0.17	0.13	1.42	0.03	0.12	3.7
5H-3, 128-129	34.58	0.10	0.06	0.04	0.50	0.00	0.00		21X-2, 34-35	183.34	0.41	0.14	0.27	1.17	0.05	0.06	5.6
5H-4, 126-127	36.06	0.18	0.08	0.10	0.67	0.03	0.00	3.9	21X-3, 20-21	184.70	0.50	0.13	0.37	1.08	0.04	0.24	8.9
5H-5, 133-134	37.63	0.49	0.43	0.06	3.58	0.00	0.00		22X-1, 26-27	191.16	0.16	0.10	0.06	0.83	0.02	0.10	2.5
5H-6, 132-133	39.12	0.12	0.04	0.08	0.33	0.05	0.00	1.6	23X-1, 26-27	200.06	0.28	0.11	0.17	0.92	0.05	0.15	3.8
5H-7, 27-28	39.57	0.27	0.06	0.21	0.50	0.04	0.00	4.8	23X-2, 26-27	201.56	0.85	0.59	0.26	4.91	0.06	0.22	4.1
6H-2, 40-41	41.70	0.38	0.31	0.07	2.58	0.00	0.00		23X-3, 26-27	203.06	0.23	0.04	0.19	0.33	0.05	0.16	3.9
6H-3, 41-42	43.21	0.80	0.46	0.34	3.83	0.03	0.00	10.5	23X-4, 27-28	204.57	0.20	0.04	0.16	0.33	0.05	0.06	3.1
6H-4, 40-41	44.70	0.20	0.21	0.00	1.75	0.00	0.00		23X-5, 32-33	206.12	0.35	0.16	0.19	1.33	0.04	0.31	4.3
6H-5, 40-41	46.20	0.26	0.21	0.05	1.75	0.00	0.00		23X-6, 32-33	207.62	0.35	0.08	0.27	0.67	0.07	0.25	3.9
6H-6, 33-34	47.63	0.74	0.61	0.13	5.08	0.05	0.00	2.6	24X-1, 106-107	209.76	0.46	0.11	0.35	0.92	0.07	0.43	5.1
6H-7, 41-42	49.21	0.31	0.08	0.23	0.67	0.05	0.00	4.2	24X-2, 109-110	211.29	0.60	0.13	0.47	1.08	0.07	0.35	6.7
7H-1, 122-123	50.52	0.95	0.79	0.16	6.58	0.00	0.00		24X-3, 108-109	212.78	0.39	0.11	0.28	0.92	0.05	0.06	5.6
7H-2, 30-31	51.10	0.40	0.24	0.16	2.00	0.04	0.00	4.0	24X-4, 109-110	214.29	0.51	0.22	0.29	1.83	0.06	0.08	4.9
7H-3, 123-124	53.53	0.25	0.12	0.13	1.00	0.04	0.00	3.7	24X-5, 107-108	215.77	0.65	0.26	0.39	2.17	0.07	0.06	5.6
7H-4, 112-113	54.92	0.30	0.09	0.21	0.75	0.04	0.00	5.1	24X-6, 94-95	217.14	0.41	0.11	0.30	0.92	0.06	0.05	4.9
7H-5, 111-112	56.41	0.42	0.10	0.32	0.83	0.04	0.08	9.1	25X-1, 107-108	218.67	0.82	0.17	0.65	1.42	0.05	0.08	12.2
7H-6, 94-95	57.74	0.38	0.15	0.23	1.25	0.03	0.12	7.9	25X-2, 108-109	220.18	0.45	0.09	0.36	0.75	0.07	0.05	5.3
8H-1, 139-140	60.19	0.46	0.34	0.12	2.83	0.02	0.14	5.2	25X-3, 107-108	221.67	0.42	0.09	0.33	0.75	0.05	0.05	6.3
8H-2, 34-35	60.64	0.09	0.07	0.02	0.58	0.01	0.08	1.6	25X-4, 107-108	223.17	1.91	0.66	1.25	5.50	0.11	0.28	11.8
8H-3, 34-35	62.14	0.33	0.17	0.16	1.42	0.03	0.00	4.7	25X-5, 107-108	224.67	0.18	0.01	0.17	0.08	0.03	0.12	6.4
8H-4, 23-24	63.53	0.51	0.40	0.11	3.33	0.03	0.03	4.2	25X-6, 108-109	226.18	0.18	0.08	0.10	0.67	0.04	0.12	2.9
8H-5, 125-126	66.05	0.14	0.04	0.10	0.33	0.02	0.06	4.5	26X-1, 21-22	226.71	2.06	0.76	1.30	6.33	0.11	0.39	11.9
8H-6, 35-36	66.65	0.13	0.07	0.06	0.58	0.03	0.13	2.4	26X-2, 21-22	228.21	0.94	0.70	0.24	5.83	0.05	0.16	5.0
8H-7, 33-34	68.13	0.15	0.06	0.09	0.50	0.02	0.13	5.0	26X-3, 21-22	229.71	0.32	0.16	0.16	1.33	0.05	0.08	3.5
9H-1, 127-128	69.57	0.95	0.95	0.00	7.91	0.03	0.00		26X-4, 21-22	231.21	0.25	0.13	0.12	1.08	0.06	0.07	2.1
9H-2, 113-114	70.93	0.39	0.13	0.26	1.08	0.05	0.00	5.7	26X-5, 21-22	232.71	0.26	0.09	0.17	0.75	0.05	0.57	3.6
9H-3, 114-115	72.44	0.33	0.06	0.27	0.50	0.04	0.00	6.3	26X-6, 25-26	234.25	0.23	0.05	0.18	0.42	0.05	0.09	3.6
9H-5, 113-114	75.43	0.16	0.02	0.14	0.17	0.03	0.12	4.2	27X-1, 44-45	235.64	0.38	0.09	0.29	0.75	0.05	0.07	5.4
9H-7, 37-38	77.67	0.36	0.06	0.30	0.50	0.04	0.05	6.8	27X-2, 42-43	237.12	0.30	0.06	0.24	0.50	0.06	0.07	4.2
9H-6, 112-113	76.92	0.34	0.08	0.26	0.67	0.04	0.03	6.4	27X-3, 44-45	238.64	0.52	0.13	0.39	1.08	0.10	0.05	4.0
11H-1, 122-123	88.52	0.34	0.25	0.09	2.08	0.02	0.17	4.2	27X-4, 42-43	240.12	0.57	0.11	0.46	0.92	0.08	0.55	5.9
11H-3, 110-111	91.40	0.24	0.04	0.20	0.33	0.04	0.15	5.0	27X-5, 41-42	241.61	0.52	0.11	0.41	0.92	0.07	0.09	5.6
11H-4, 104-105	92.84	0.21	0.05	0.16	0.42	0.04	0.03	3.8	27X-6, 41-42	243.11	0.23	0.08	0.15	0.67	0.04	0.11	3.7
11H-5, 105-106	94.35	0.17	0.04	0.13	0.33	0.04	0.07	3.1	28X-1, 24-25	244.34	0.39	0.12	0.27	1.00	0.05	0.08	5.0
12H-1, 109-110	97.89	0.36	0.17	0.19	1.42	0.05	0.18	3.9	28X-2, 32-33	245.92	0.40	0.18	0.22	1.50	0.06	0.05	3.5
12H-2, 113-114	99.43	0.18	0.05	0.13	0.42	0.03	0.07	3.8	28X-3, 36-37	247.46	0.79	0.52	0.27	4.33	0.07	0.19	4.0
12H-3, 113-114	100.93	0.32	0.08	0.24	0.67	0.04	0.03	6.5	28X-4, 55-56	249.15	0.22	0.11	0.11	0.92	0.03	0.11	3.5
12H-4, 108-109	102.38	0.18	0.05	0.13	0.42	0.03	0.05	4.1	28X-5, 35-36	250.45	0.24	0.07	0.17	0.58	0.03	0.09	5.6
12H-6, 70-71	105.00	0.37	0.08	0.29	0.67	0.04	0.04	7.6	29X-1, 82-83	253.62	0.19	0.10	0.09	0.83	0.03	0.06	3.2
13H-1, 101-102	107.31	0.46	0.09	0.37	0.75	0.05	0.15	7.0	31X-1, 80-81	271.40	0.24	0.18	0.06	1.50	0.04	1.73	1.6
13H-2, 99-100	108.79	0.34	0.10	0.24	0.83	0.05	0.05	5.4									

Table 9 (continued).

Core, section, interval (cm)	Depth (mbsf)	TC (wt%)	IC (wt%)	TOC (wt%)	CaCO <sub>3</sub> (wt%)	TN (wt%)	TS (wt%)	TOC/TN (ratio)	Core, section, interval (cm)	Depth (mbsf)	TC (wt%)	IC (wt%)	TOC (wt%)	CaCO <sub>3</sub> (wt%)	TN (wt%)	TS (wt%)	TOC/TN (ratio)
22R-1, 24-26	484.04	0.19	0.11	0.08	0.92	0.03	0.07	2.4	42R-5, 28-29	683.08	3.80	3.36	0.44	27.99	0.04	0.66	10.9
22R-2, 22-23	485.52	0.10	0.05	0.05	0.42	0.03	0.03	1.8	42R-6, 40-41	684.70	2.12	1.80	0.32	14.99	0.03	0.34	10.0
22R-3, 33-35	487.13	0.31	0.06	0.25	0.50	0.04	0.06	6.5	44R-1, 131-132	697.41	3.95	3.50	0.45	29.16	0.04	0.32	11.4
24R-1, 40-41	503.60	0.91	0.72	0.19	6.00	0.03	0.22	6.1	44R-2, 70-71	698.30	3.92	3.56	0.36	29.65	0.04	0.28	10.3
24R-2, 39-40	505.09	0.49	0.26	0.23	2.17	0.03	0.17	6.6	44R-3, 54-55	699.64	2.62	2.38	0.24	19.83	0.03	0.24	9.3
24R-3, 47-48	506.67	0.56	0.35	0.21	2.92	0.04	0.19	5.9	44R-5, 79-81	702.89	2.46	2.10	0.36	17.49	0.04	0.27	10.1
25R-1, 40-42	513.20	0.55	0.28	0.27	2.33	0.04	0.26	6.2	47R-2, 55-57	726.65	2.09	1.79	0.30	14.91	0.03	1.22	10.0
25R-2, 50-51	514.80	0.55	0.26	0.29	2.17	0.04	0.25	6.7	51R-1, 75-77	763.95	3.05	2.71	0.34	22.57	0.04	0.47	8.2
25R-3, 100-102	516.80	0.23	0.08	0.15	0.67	0.03	0.14	4.6	51R-2, 49-50	765.19	3.12	2.91	0.21	24.24	0.04	0.50	5.0
25R-4, 58-60	517.88	4.17	3.88	0.29	32.32	0.05	0.07	5.7	51R-3, 79-81	766.99	1.02	0.50	0.52	4.17	0.05	0.44	9.9
25R-5, 49-50	519.29	0.45	0.23	0.22	1.92	0.04	0.08	6.1	51R-4, 140-143	769.10	2.59	2.29	0.30	19.08	0.05	0.34	6.5
27R-1, 81-82	532.91	0.18	0.06	0.12	0.50	0.03	0.08	3.7	51R-5, 78-80	769.98	1.75	0.10	1.65	0.83	0.11	3.00	15.5
27R-2, 37-38	533.97	0.24	0.07	0.17	0.58	0.03	0.05	5.1	51R-6, 77-80	771.47	1.22	0.12	1.10	1.00	0.08	2.84	14.0
27R-3, 71-72	535.81	0.40	0.06	0.34	0.50	0.04	0.08	8.6	52R-1, 63-64	773.53	2.16	1.92	0.24	15.99	0.04	0.38	6.2
28R-1, 97-98	542.77	0.34	0.07	0.27	0.58	0.04	0.08	6.8	52R-2, 24-25	774.64	2.49	2.20	0.29	18.33	0.04	0.27	8.0
28R-2, 112-113	544.42	0.34	0.06	0.28	0.50	0.04	0.09	6.6	52R-3, 63-64	776.53	3.12	2.89	0.23	24.07	0.04	0.29	5.4
28R-3, 73-74	545.53	0.39	0.12	0.27	1.00	0.04	0.15	6.2	52R-4, 128-129	778.68	4.05	3.91	0.14	32.57	0.03	0.53	5.0
28R-4, 42-43	546.72	0.31	0.06	0.25	0.50	0.04	0.05	6.4	52R-5, 59-60	779.49	3.77	3.62	0.15	30.15	0.03	0.24	5.6
29R-1, 56-57	551.96	0.25	0.07	0.18	0.58	0.03	0.08	6.2	52R-6, 19-20	782.69	3.17	2.98	0.19	24.82	0.05	0.28	4.0
29R-2, 29-30	553.19	0.30	0.04	0.26	0.33	0.04	0.17	6.1	53R-2, 74-75	784.74	1.68	1.50	0.18	12.50	0.03	0.30	6.4
31R-1, 77-78	571.47	0.40	0.26	0.14	2.17	0.04	0.11	3.7	53R-3, 53-54	786.03	2.88	2.77	0.11	23.07	0.03	0.18	4.0
32R-1, 90-92	581.20	0.31	0.13	0.18	1.08	0.04	0.13	4.7	53R-4, 125-126	788.25	1.90	1.82	0.08	15.16	0.03	0.03	2.8
33R-1, 32-33	590.32	0.58	0.37	0.21	3.08	0.04	0.16	4.9	53R-5, 100-101	789.50	2.29	2.16	0.13	17.99	0.03	0.00	4.0
34R-1, 90-91	600.50	0.27	0.13	0.14	1.08	0.04	0.00	3.6	53R-6, 48-50	790.48	2.05	1.86	0.19	15.49	0.04	0.12	5.0
34R-2, 43-45	601.53	0.37	0.26	0.11	2.17	0.04	0.02	3.0	55R-1, 31-32	802.11	5.39	5.29	0.10	44.07	0.00	0.03	
35R-1, 14-15	609.34	0.43	0.20	0.23	1.67	0.04	0.15	5.3	55R-2, 21-22	803.51	1.80	1.69	0.11	14.08	0.00	0.05	
35R-2, 73-74	611.43	0.30	0.11	0.19	0.92	0.04	0.08	5.1	55R-3, 18-19	804.98	3.26	3.12	0.14	25.99	0.00	2.08	
35R-CC, 3-4	612.23	0.48	0.22	0.26	1.83	0.04	0.21	6.9	55R-4, 65-66	806.95	3.98	3.86	0.12	32.15	0.02	0.00	7.8
36R-1, 117-118	620.07	0.99	0.85	0.14	7.08	0.03	0.07	4.3	55R-5, 56-57	808.36	0.70	0.63	0.07	5.25	0.00	0.05	
36R-2, 119-120	621.59	0.87	0.66	0.21	5.50	0.04	0.12	5.7	55R-6, 37-38	809.67	3.92	3.80	0.12	31.65	0.02	0.00	6.5
36R-3, 53-54	622.43	1.41	1.20	0.21	10.00	0.04	0.07	5.1	57R-1, 138-139	822.38	4.47	4.31	0.16	35.90	0.00	0.29	
36R-CC, 5-6	623.45	1.45	1.00	0.45	8.33	0.05	0.06	9.8	57R-2, 137-138	823.87	5.57	5.42	0.15	45.15	0.00	0.05	
37R-1, 37-38	628.97	1.00	0.86	0.14	7.16	0.03	0.13	4.7	57R-3, 146-147	825.46	2.83	2.79	0.04	23.24	0.00	0.00	
37R-2, 18-19	630.28	1.91	1.47	0.44	12.25	0.05	0.05	9.2	58R-1, 28-30	830.98	3.40	3.30	0.10	27.49	0.00	0.00	
37R-3, 37-38	631.97	4.36	4.31	0.05	35.90	0.00	0.00		60R-1, 23-25	850.23	1.89	1.89	0.00	15.74	0.00	0.00	
37R-4, 25-26	633.35	1.02	0.68	0.34	5.66	0.03	0.06	10.3	62R-1, 23-24	869.53	1.51	1.36	0.15	11.33	0.00	0.21	
37R-5, 26-27	634.86	3.28	3.01	0.27	25.07	0.04	0.23	7.3	62R-2, 20-22	871.00	2.85	2.75	0.10	22.91	0.00	0.00	
38R-1, 88-90	639.08	2.87	2.58	0.29	21.49	0.04	0.00	8.0	63R-1, 108-110	879.98	0.87	0.89	0.00	7.41	0.00	0.00	
38R-2, 25-26	639.95	1.05	0.67	0.38	5.58	0.04	0.15	10.6	63R-2, 88-90	881.28	0.87	0.74	0.13	6.16	0.00	0.00	
38R-3, 118-120	642.38	0.84	0.53	0.31	4.41	0.03	0.23	11.8	68R-1, 86-87	925.86	0.64	0.61	0.03	5.08	0.00	0.04	
38R-4, 105-106	643.75	1.49	0.10	1.39	0.83	0.04	0.11	38.4	75R-1, 75-76	993.05	0.02	0.11	0.00	0.92	0.00	0.00	
38R-5, 76-78	644.96	1.65	1.31	0.34	10.91	0.04	0.47	9.5	75R-2, 130-132	995.10	2.48	2.22	0.26	18.49	0.00	0.00	
39R-1, 25-26	648.15	1.64	1.21	0.43	10.08	0.06	0.24	6.8	75R-3, 59-61	995.89	3.53	3.18	0.35	26.49	0.00	0.00	
39R-2, 31-32	649.71	2.62	2.26	0.36	18.83	0.04	0.27	9.4	75R-4, 31-33	997.11	2.39	2.20	0.19	18.33	0.00	0.00	
39R-3, 18-19	651.08	2.48	2.10	0.38	17.49	0.04	0.66	10.0	76R-1, 108-110	1003.08	1.89	1.64	0.25	13.66	0.00	0.00	
39R-4, 20-22	652.60	1.53	1.20	0.33	10.00	0.03	0.27	9.4	77R-1, 54-55	1012.14	0.03	0.13	0.00	1.08	0.00	0.00	
39R-5, 35-37	654.25	4.15	3.83	0.32	31.90	0.04	0.00	8.0	78R-1, 50-51	1021.70	2.78	2.50	0.28	20.83	0.00	0.00	
39R-6, 80-82	656.20	4.11	3.63	0.48	30.24	0.04	0.00	11.6	79R-1, 40-41	1031.30	0.23	0.31	0.00	2.58	0.00	0.00	
40R-1, 44-45	657.94	3.26	2.20	1.06	18.33	0.04	0.20	25.2	80R-1, 17-18	1040.77	1.78	1.64	0.14	13.66	0.00	0.00	
40R-2, 128-129	660.28	3.53	3.22	0.31	26.82	0.04	0.51	7.4	83R-1, 56-57	1070.16	0.21	0.48	0.00	4.00	0.00	0.00	
40R-3, 113-114	661.63	1.64	1.35	0.29	11.25	0.03	0.24	9.6	84R-1, 40-41	1079.70	0.35	0.44	0.00	3.67	0.00	0.00	
40R-4, 118-120	663.18	2.09	1.64	0.45	13.66	0.04	0.59	11.5	88R-1, 47-49	1118.27	2.62	2.51	0.11	20.91	0.00	0.00	
40R-5, 71-72	664.21	1.83	1.40	0.43	11.66	0.03	0.31	12.4	89R-2, 135-137	1130.25	4.82	4.88	0.00	40.65	0.00	0.00	
40R-6, 28-30	665.28	2.86	2.35	0.51	19.58	0.04	0.24	12.5	89R-3, 11-12	1130.51	4.83	4.42	0.41	36.82	0.00	0.00	
41R-1, 78-79	667.98	3.21	2.76	0.45	22.99	0.04	0.64	12.1	89R-3, 54-56	1130.94	3.70	3.43	0.27	28.57	0.00	0.00	
41R-2, 119-120	669.89	1.68	1.26	0.42	10.50	0.03	0.54	12.5	89R-4, 50-51	1132.40	4.60	4.33	0.27	36.07	0.00	0.00	
41R-3, 34-35	670.54	1.61	1.17	0.44	9.75	0.04	0.24	11.8	90R-2, 25-26	1138.85	3.12	2.23	0.89	18.58	0.03	1.36	33.4
41R-4, 108-109	672.78	1.39	1.04	0.35	8.66	0.03	0.47	12.6	90R-3, 24-25	1140.34	2.89	1.79	1.10	14.91	0.04	1.70	26.4
41R-5, 71-72	673.91	1.22	0.83	0.39	6.91	0.03	0.54	13.6	91R-1, 26-27	1146.76	2.21	1.34	0.87	11.16	0.04	2.24	22.8
41R-6, 27-28	674.97	1.72	1.30	0.42	10.83	0.03	0.34	13.8	92R-1, 97-98	1157.17	1.91	1.49	0.42	12.41	0.02	2.32	21.7
42R-1, 28-29	677.08	3.80	3.46	0.34	28.82	0.03	0.39	11.0	93R-1, 131-132	1167.11	0.51	0.37	0.14	3.08	0.02	1.55	8.0
42R-2, 14-15	678.44	1.78	1.48	0.30	12.33	0.03	0.41	8.8	93R-2, 20-21	1167.50	0.80	0.63	0.17	5.25	0.01	0.56	17.4
42R-3, 53-54	680.33	1.10	0.77	0.33	6.41	0.03	0.65	12.9									
42R-4, 67-68	681.97	1.30	0.86	0.44	7.16	0.03	0.57	15.0									

Notes: TC = total carbon, IC = inorganic carbon, TOC = total organic carbon, CaCO<sub>3</sub> = calcium carbonate, TN = total nitrogen, TS = total sulfur, TOC/TN = total organic carbon/total nitrogen ratios, HI = hydrogen index, OI = oxygen index.

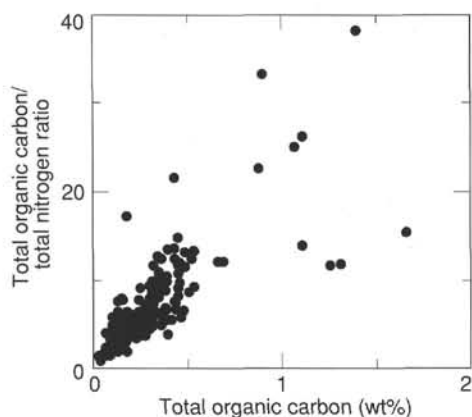


Table 10. Summary of the Rock-Eval pyrolysis results, Site 918.

Core, section, interval (cm)	Depth (mbsf)	S <sub>1</sub> (mgHC/gRock)	S <sub>2</sub> (mgHC/gRock)	S <sub>3</sub> (mgHC/gRock)	TOC (wt%)	HI (mgHC/gC)	OI (mgCO <sub>2</sub> /gC)	T <sub>max</sub> (°C)
152-918A-								
3H-3, 30-31	14.60	0.06	0.59	0.47	0.53	111	89	515
17H-6, 122-123	151.52	0.05	0.51	1.08	0.68	75	160	438
25H-1, 107-108	218.67	0.04	0.23	1.09	0.65	36	169	517
25H-4, 107-108	223.17	0.17	1.01	2.96	1.25	81	238	430
26H-1, 21-22	226.71	0.07	1.07	3.72	1.30	83	287	424
37H-2, 124-125	317.84	0.07	0.11	2.54	0.50	22	512	395
152-918D-								
11R-1, 101-102	387.11	0.05	0.29	0.29	0.53	55	55	442
38R-4, 105-106	643.75	0.12	0.07	1.45	1.39	5	105	417
40R-1, 44-45	657.94	0.08	0.22	1.69	1.06	21	160	413
40R-6, 28-30	665.28	0.09	0.16	1.40	0.51	31	274	414
51R-5, 78-80	769.98	0.26	1.08	1.41	1.65	65	85	409
51R-6, 77-80	771.47	0.32	0.54	0.87	1.10	49	79	422
90R-2, 25-26	1138.85	0.09	0.49	1.45	0.89	55	163	435
90R-3, 24-25	1140.34	0.09	0.59	1.50	1.10	54	137	430
91R-1, 26-27	1146.76	0.58	0.50	1.40	0.87	58	162	432

Note: HI = hydrogen index; OI = oxygen index.

Table 11. Results of the headspace gas analysis using the Hach-Carle gas chromatograph, Site 918.

Core, section, interval (cm)	Depth (mbsf)	C <sub>1</sub>	C <sub>2</sub>	C <sub>2=</sub>	Core, section, interval (cm)	Depth (mbsf)	C <sub>1</sub>	C <sub>2</sub>	C <sub>2=</sub>
152-918A-									
1H-2, 55-60	2.08	2			25R-3, 0-5	515.83	13	1	
2H-5, 0-5	7.83	5			27R-2, 0-5	533.63	8		
3H-6, 0-5	18.83	3			28R-4, 0-5	546.33	3		
4H-6, 0-5	28.33	3			29R-2, 0-5	552.93	6		
5H-6, 0-5	37.83	3			30R-CC, 14-15	561.14	9	1	
6H-6, 0-5	47.33	2			31R-CC, 8-9	571.78	3	1	1
7H-6, 0-5	56.83	3			32R-1, 0-5	580.33	4		
8H-6, 0-5	66.33	2			33R-1, 0-5	590.03	3		
9H-6, 0-5	75.83	3			34R-1, 0-5	599.63	3		
10H-6, 0-5	85.33	2,810			35R-1, 0-5	609.23	3		
11H-6, 0-5	94.83	4,245			36R-1, 0-5	618.93	3		
12H-4, 0-5	101.33	7,549			37R-1, 0-5	625.63	2		
13H-5, 0-5	112.33	6,558			38R-2, 0-5	639.73	3		
14H-5, 0-5	121.83	10,550			39R-2, 0-5	649.43	3		
15H-5, 0-5	131.33	49,716	2		40R-1, 0-5	657.53	4	1	
16H-5, 0-5	139.33	34,723	1		41R-2, 0-5	668.73	2		
17H-5, 145-150	150.28	17,737	1		42R-2, 0-5	678.33	3		
18H-4, 0-5	156.83	15,530			43R-2, 0-5	687.93	2		
19H-5, 0-5	167.83	20,177	1		44R-3, 0-5	699.13	3		
20X-3, 0-5	174.33	86,104	1		47R-2, 0-5	726.13	4		
22X-1, 135-140	192.28	10,501	1	1	51R-1, 0-5	763.23	3		
23X-5, 0-5	205.83	19,852	1		52R-2, 0-5	774.43	3		
24X-5, 145-150	216.18	49,635	1	1	53R-2, 0-5	784.03	3		
25X-5, 0-5	223.63	8,775			55R-4, 110-112	807.41	2		
26X-5, 0-5	232.53	15,035	1	1	57R-1, 145-150	822.48	3		
27X-5, 0-5	241.23	20,790	1	1	58R-1, 108-110	831.79	2		
28X-4, 0-5	248.63	18,308	2	1	60R-1, 5-7	850.06	2		
29X-1, 0-5	252.83	7,761			62R-2, 93-95	871.74	0		
30X-CC, 0-5	260.23	6,953			63R-1, 148-150	880.39	0		
31X-5, 0-5	276.63	25,120	1	1	68R-1, 0-5	925.03	2		
32X-1, 0-5	279.53	25,717	1		72R-1, 0-5	963.73	3		
33X-2, 0-5	289.93	11,899	1	1	74R-1, 0-3	982.72	2		
34X-1, 0-5	297.33	6,354	1		75R-2, 0-5	993.83	3		
37X-5, 85-90	321.98	8,513	1		76R-1, 0-5	1,002.03	4		
38X-CC, 0-5	322.43	2,908			77R-1, 0-5	1,011.63	4		
152-918B-									
1H-4, 0-5	4.50	6			78R-1, 0-5	1,021.23	3		
2H-5, 0-5	12.80	6			79R-1, 50-52	1,031.41	3		
3H-6, 0-5	23.80	6			80R-1, 0-3	1,040.62	2		
152-918C-									
1H-5, 0-5	31.80	4			83R-1, 136-139	1,070.98	1		
152-918D-									
13R-1, 4-5	403.95	3,210	1	1	84R-1, 0-5	1,079.33	1		
14R-1, 0-5	412.83	3,886	1	1	88R-1, 10-15	1,117.93	4		
22R-3, 0-5	486.83	9			89R-1, 0-5	1,127.43	4		
24R-2, 0-5	504.73	5			91R-1, 0-5	1,146.53	2		
					92R-2, 0-5	1,157.73	6		
					93R-2, 0-5	1,167.33	3		
					95R-2, 135-140	1,183.28	9		
					96R-3, 0-5	1,188.13	7		

Note: Methane (C<sub>1</sub>), ethane (C<sub>2</sub>), and iso-ethane (C<sub>2=</sub>) concentrations are given in ppm.

### Biogenic Components

Data for alkalinity, sulfate, and ammonium (HCO<sub>3</sub><sup>-</sup>, SO<sub>4</sub><sup>2-</sup>, NH<sub>4</sub><sup>+</sup>) are presented in Figure 50. Alkalinity (HCO<sub>3</sub><sup>-</sup>) production results from the bacterial decomposition of organic matter, both in the zone of sulfate reduction (upper 80 mbsf) and in the zone of methanogenesis

(80-500 mbsf). This typically leads to a maximum in alkalinity of 15 mM at 170 mbsf and is also accompanied by a maximum in ammonium concentration (~4 mM). The almost linear profile for dissolved sulfate, toward the methane boundary at 80 mbsf, suggests that sulfate reduction occurs mostly at this boundary and involves the oxidation of methane by sulfate-reducing bacteria.

Table 12. Chemical composition of interstitial water at Site 918.

Core, section, interval (cm)	Depth (mbsf)	pH	Alkalinity (mM)	Salinity (g/kg)	SO <sub>4</sub> (mM)	NH <sub>4</sub> (μM)	Cl <sup>-</sup> (mM)	B (mM)	H <sub>4</sub> SiO <sub>4</sub> (μM)
Bottom water	0	8	2.35	35	29	0	559	0.42	50
152-918A-									
2H-4, 150-155	7.8	7.17	7.38	34	25.6	560	560	0.68	473
4H-4, 145-150	26.8	7.92	5.26	33.8	18.8	575	562.5	0.72	461
7H-1, 0-20	49.3	7.69	5.55	33			562	0.4	
7H-4, 145-150	55.3	7.84	7.87	32	7.7	1180	561	0.62	548
10H-4, 145-150	83.8	7.9	11.44	31.5	0	1670	560	0.7	717
12H-1, 0-20	96.8	7.44	2.36	30					
13H-4, 145-150	112.3	7.84	12.6	31.5	0.1	2540	560	0.44	747
16H-4, 140-150	139.3	7.82	14.16	32	0.1	3950	561	0.5	827
17H-1, 0-20	142.8	7.92	13.18	32.5	0	2930	561		573
19H-4, 140-150	167.8	7.8	14.8	32	0	4440	561	0.46	830
22X-1, 0-20	191.1	7.74	13.65	32	0.25	3400	558	0.51	670
23X-40, 140-150	206	7.72	13.1	32	0	3670	560	0.43	666
26X-4, 140-150	232	7.95	11.4	32	0.6	3800	561	0.35	8.6
31X-1, 0-20	276	7.97	6.69	32	0.8	3640	559	0.33	859
37X-6, 90-100	322	8.08	3.39	31.5	0.1	2750	560	0.31	861
152-918B-									
1H-3, 145-150	4.5	7.86	6.34	34.5	26.5	240	558	0.47	382
2H-4, 145-150	12.8	7.93	8.47	34.2	22.1	660	559	0.46	611
3H-5, 145-150	23.8	8.15	6.15	34	17.1	1210	563	0.44	285
152-918C-									
1H-4, 145-150	30	7.93	5.44	34	16.6	620	564	0.43	406
152-918D-									
13R-1, 0-5	405	8.35	1.4	32.5	3.18	1200	571	0.29	448
22R-2, 140-150	485	8.75	1.02	32.5	4.05	640	570	0.29	200
25R-2, 140-150	515	8.85	0.98	33	4.65	480	573	0.28	172
28R-3, 140-150	545	8.93	1.29	33.8	6.5	450	571	0.305	164
31R-CC	575	8.91	1.12	33.8	7.9		569	0.333	128
34R-1, 2-10	602	9.02	0.89	33.8	8.9	390	572	0.25	38
37R-1, 140-150	632	8.43	1.14	33.8	10	375	564	0.215	42
40R-1, 140-150	660	8.32	1.04	33.8	10.3	375	562	0.2	210
44R-2, 139-150	700	8.36	0.68	34.5	13.2	380	562	0.22	142
47R-1, 50-60	728	8.38	1.13	34	13.6	345	559	0.2	171
51R-2, 140-150	765	8.33	0.9	33.8	14.7	302	558	0.3	103
55R-4, 112-122	803			34.5	15.7		557	0.19	
62R-1, 121-129	875				13.8		532	0.428	
68R-1, 91-100	930	8.16	1.55	34	12.5	250	552	0.225	56
74R-1, 3-14	985				12.9	210	538	0.24	46
80R-1, 0-11	1045			34	14.1	240	546	0.19	26
83R-1, 136-141	1070			33.5	15.7		555	0.18	
88R-1, 93-100	1125				17.1	190	545	0.15	
91R-1, 119-129	1150	7.83	1.52	34.5	21.4	170	548		37
95R-2, 140-150	1183					170	573		

In the upper section of the sediments (i.e., in the upper 30 mbsf), small maxima in alkalinity and ammonium were observed. These maxima occur in the sediment section above the first unconformity, dated as 1 Ma at 70 mbsf (see "Sedimentation Rates" section, this chapter). Thus, in the relatively young sediments above this unconformity, biogenic reactions have occurred at fast enough rates to have formed an overprint on the general trends in alkalinity, sulfate, and ammonium. However, below 50 mbsf, diffusive transport seems to characterize the concentration depth profiles of alkalinity, sulfate, and ammonium.

### Alkaline Earth Elements

Several major processes affect the concentration-depth profiles of calcium, magnesium, and strontium (Ca<sup>2+</sup>, Mg<sup>2+</sup>, Sr<sup>2+</sup>). The data are presented in Figure 50.

Calcium concentrations indicate a broad minimum at about 100 mbsf, which is also mirrored by minima in magnesium and strontium. The decrease in magnesium is larger than the decrease in calcium. We suggest that dolomitization characterizes these sediments and, therefore, is the cause of the above observations. This possibility will need further enquiry, principally by measuring oxygen and strontium isotopes. At other sites having similar characteristics (e.g., Site 808 in Nankai Trough [You et al., 1993; Gieskes et al., 1993; Kastner et al., 1993]), the decreases in magnesium and strontium were interpreted

in terms of alteration of volcanic matter, precisely based on isotopic studies. There is little doubt, however, that the decreases in calcium are related to carbonate precipitation reactions, which thus may explain the less-than-expected increases in bicarbonate alkalinity.

Below 250 mbsf, sharp increases in calcium and equally sharp decreases in magnesium characterize the pore fluids, with extremes reached in the depth range of 550 to 650 mbsf (i.e., in the zone marked by the presence of volcanogenic sediments, lithologic Unit IE, see "Lithostratigraphy" section, this chapter). As discussed below, a maximum in dissolved chloride also occurs in this interval. Below 650 mbsf, diffusive transport processes characterize the concentration gradients of calcium and magnesium, at least to a depth of 850 mbsf. Thus, the extremes in calcium and magnesium concentrations can be understood in terms of processes involving the alteration of volcanic material, dominating the processes that determine the distribution of these constituents in the sediment column.

Dissolved strontium shows a more erratic profile, with minima at about 100 and 500 mbsf. These minima may be related to the uptake in alteration products of volcanic materials, but this can best be confirmed by future studies of the strontium isotope geochemistry. A maximum in dissolved strontium occurs in upper parts of the sandy horizons, at about 925 mbsf (lithologic Unit III, see "Lithostratigraphy" section, this chapter). These sedimentary units are also characterized by much diminished gradients in calcium and magnesium. Phenomena characterizing the sediments below 825 mbsf are discussed in greater detail in a later section.

Table 13. Composition of interstitial waters at Site 918.

Core, section, interval (cm)	Depth (mbsf)	Li <sup>+</sup> (μM)	Na <sup>+</sup> (mM)	K <sup>+</sup> (mM)	Ca <sup>2+</sup> (mM)	Mg <sup>2+</sup> (mM)	Sr <sup>2+</sup> (μM)
Bottom water	0	27	480	10.4	10.54	54	87
152-918A-							
2H-4, 150-155	7.8	15	489	11	11.4	47.6	88
4H-4, 145-150	26.8	13	489	10.2	8.9	44	80
7H-1, 0-20	49.3	24	481	8.9	7.4	43.9	61
7H-4, 145-150	55.3	14.5	479	9.7	6.3	41.4	72
10H-4, 145-150	83.8	12	481	9.2	4	36.8	61.5
12H-1, 0-20	96.8						
13H-4, 145-150	112.3	12.5	478	7.9	5.1	38.3	66
16H-4, 140-150	139.3	13	481	7.9	5.45	37.9	67.5
17H-1, 0-20	142.8	17	473	7.3	5.82	41	67
19H-4, 140-150	167.8	18	477	7.5	5.65	39.9	
22X-1, 0-20	191.1	19	473	6.9	6.25	40.1	77
23X-40, 140-150	206	20	472	6.8	6.95	40.4	76
26X-4, 140-150	232	23	477	7.4	7.65	36.9	95.5
31X-1, 0-20	276	27	470	8.2	11.4	33.2	106
37X-6, 90-100	322	29	467	6.2	17.7	27.5	110
152-918B-							
1H-3, 145-150	4.5	15.5	484	11.4	11	50.1	86
2H-4, 145-150	12.8	14.5	480	10.8	10.65	50	85
3H-5, 145-150	23.8	15	481	11	9.15	46.6	76
152-918C-							
1H-4, 145-150	30	13	488	10.8	8.8	43.2	78
152-918D-							
13R-1, 0-5	405	38	455	1.1	43.7	17.5	83
22R-2, 140-150	485	51	443	2	59.3	7.7	90
25R-2, 140-150	515	57	442	2	63.8	5.95	79
28R-3, 140-150	545	55	438	1.4	67.7	5.4	103
31R-CC	575	59	436	2.1	67.6	6.3	104
34R-1, 2-10	602	67	444	2.3	65.5	6.5	109
37R-1, 140-150	632	94	440	2.7	62.8	8.6	152
40R-1, 140-150	660	116	441	3.4	57.5	12	170
44R-2, 139-150	700	110	446	4	52.9	16.5	174
47R-1, 50-60	728	126	442	3.3	55.6	15.4	153
51R-2, 140-150	765	163	444	3.5	47.9	22.5	190
55R-4, 112-122	803		441	3.7	42.2	22.5	
62R-1, 121-129	875	93	410	3.2	44	23	
68R-1, 91-100	930	96	435	3.6	46.9	23.1	288
74R-1, 3-14	985	84	429	2.7	41.1	25.6	255
80R-1, 0-11	1045	79	443	3.5	39.7	24.7	234
83R-1, 136-141	1070		450	3.6	42.1	27.4	224
88R-1, 93-100	1125	88	446	2.4	37.7	28.6	193
91R-1, 119-129	1150	91	449	3.6	37.5	32.4	170
95R-2, 140-150	1183				55.4	21.3	

### Alkali Metals

The concentration-depth profiles of the dissolved alkalis (Li<sup>+</sup>, K<sup>+</sup>, Na<sup>+</sup>) show very distinct patterns (Fig. 50). Dissolved lithium shows a slight decrease with depth in the upper sediments, to a minimum of 11 μM at 100 mbsf, followed by a gradual increase to 160 μM at 750 mbsf. A sharp decrease in Li<sup>+</sup> occurs in the sandy horizons below 750 mbsf.

Dissolved potassium shows a minimum at 200 mbsf and a second minimum at ~500 mbsf (accuracies are about ±1 mM). These minima probably result from uptake into clay minerals.

Sodium concentrations decrease rapidly with depth, particularly below 200 mbsf. A minimum occurs between 500 and 600 mbsf, and very low values occur in the sandy horizons below 825 mbsf. Causes for the observed decreases in sodium are discussed below.

### Chloride and the Na-Cl Ratio

The profile of chloride concentration vs. depth indicates considerable complexity (Fig. 51A). A small maximum occurs between 30 and 40 mbsf, which will be discussed later. The broad maximum at 500 to 600 mbsf indicates an increase of about 13 mM above the concentration of present-day seawater. This maximum also coincides with the extremes in calcium and magnesium concentrations, discussed above. These chloride increases appear to be the result of hydration of clay minerals during the in-situ alteration of volcanic material.

Below 850 mbsf, pronounced minima occur in the chloride concentration, with decreases of as much as 5% below present-day sea-

water values. These low chlorides are reminiscent of the observed low chloride concentrations in the lower parts of Sites 915 and 916. There, these low chloride concentrations were interpreted in terms of potential diffusive communication with low-chloride reservoirs in basement. In the present case, it seems likely that a core of fresher fluids has been advected (probably seaward) along the sandy horizons, which may act as aquifers. This was observed in Site 672 on the Barbados accretionary complex (Gieskes et al., 1990), as well as in the sandy horizon at the base of DSDP Site 438 of Leg 57, on the inner part of the Japan Trench (Moore and Gieskes, 1980). The nature of both the chloride and the sulfate profiles indicates that the concentration profiles are of a nonsteady-state nature. This implies that the concentration anomalies are of recent origin, probably as recent as the Holocene. We postulate that the origin of the fresher waters is located in the subaerial basalt flows, which may have trapped fresh water. Where the influx of fresh fluid is located remains to be determined.

The variations in dissolved chloride led to an investigation of the Na/Cl values, which would normalize any dilution effects caused by the influx or loss of fresh water. The results of this normalization indicate a clear minimum in Na/Cl in the volcanic zone around 550 mbsf. Thus, uptake of sodium was important in this zone, probably as a result of the formation of Na-zeolite.

### Volcanic Reaction Zone

As indicated above, reactions involving volcanic matter occurring in the sediment horizons from 530 to 650 mbsf (lithologic Subunit IE) appear chiefly responsible for the observed maximum and minimum

in calcium and magnesium. A plot of calcium vs. magnesium concentrations (Fig. 51B) indicates that diffusive mixing above and below these extremes has led to linear mixing trends, especially from depths of 550 to 300 mbsf and from 650 to 850 mbsf. Similarly, the Na/Cl values show a good correlation with Ca concentration (Fig. 51B), again implying that the main removal process involving sodium ions occurs in the volcanic-rich zone.

Similar observations have been made in other areas, particularly in the volcanic sediments of Sites 832 and 833 in the Aoba Basin, drilled during ODP Leg 134 (Collot et al., 1992). There, concentration extremes were much more pronounced, but concentration trends were similar (Martin, 1993). Interestingly, for Site 918 these reactions clearly are similar in nature, but may involve much more dispersed volcanic matter within an otherwise inert background matrix. Further studies of pore fluid oxygen and strontium isotopes may prove helpful (e.g., Lawrence and Gieskes, 1981).

### Dissolved Boron and Silica

Dissolved boron concentrations (Fig. 52A) show a general decreasing trend with depth. Detailed studies of the boron isotope ratios will help to discover the reasons for this profile, which may be related to the absorption of boron by clays.

Dissolved silica shows relatively high values in the upper 300 mbsf of the sediment column, with much lower values below 400 mbsf. The presence of diatoms was noted in the upper sediments, as well as some glacial flour. If the latter is mainly quartz, then opal solubility can lead to the higher dissolved silica concentrations.

### Chloride Maximum in the Upper 80 mbsf

Data for the chloride concentrations of Holes 918A, 918B, and 918C are presented in Figure 52B. Though increases in dissolved chloride in the upper 50 mbsf are small (<0.8%), the increases do suggest a maximum at about 30 to 40 mbsf. McDuff (1985) noticed similar maxima in cores drilled in red clays during DSDP Leg 86 in the North Pacific Ocean. He interpreted this maximum in terms of chloride increases in the ocean during the last Holocene glaciation period. This maximum would not as yet have been dissipated as a result of diffusive exchange processes (McDuff, 1985). These observations will be checked against future determination of the oxygen and hydrogen isotopic compositions of the interstitial waters, which, if not affected by other important reactions, should reflect this maximum.

### Summary and Conclusions

The interstitial water program conducted at Site 918 has led to several important observations:

1. In the upper sediments, a small, but distinct, maximum can be observed in dissolved chloride concentrations (at a depth between 30 and 40 mbsf). This increase may be related to a remnant of the Holocene salinity increase during the last glacial period.
2. Concentration gradients of dissolved sulfate suggest a sharp boundary with the zone of methane formation, presumably as a result of bacterial sulfate reduction involving methane production.
3. Concentration profiles of dissolved calcium and magnesium indicate a dominant influence on these profiles by the alteration of volcanic material in the depth range of 550 to 650 mbsf. These extremes of concentrations also are mirrored by the slight, but distinct, maximum in dissolved chloride in the same depth range.
4. Changes in sodium concentrations as well as in the Na/Cl values indicate that the zone of reactive volcanics is the sink for sodium, presumably as a result of Na-zeolite formation.
5. In the sandy sediments below 850 mbsf, low chloride concentrations were noted, while a minimum occurs in dissolved sulfate, and a sudden decrease is apparent in dissolved lithium. These obser-

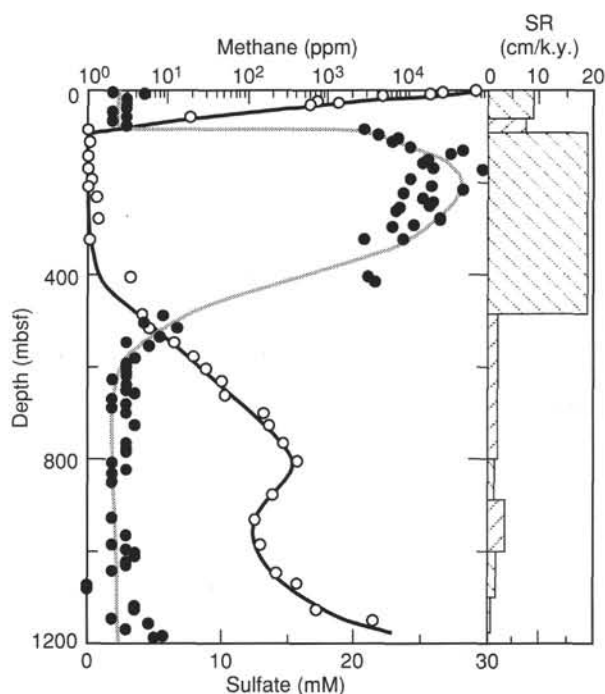


Figure 49. Results of methane measurements (solid circles) using the head-space technique vs. depth. Sulfur content (open circles) of pore waters from "Inorganic Geochemistry" section (this chapter). Sedimentation rates are given in centimeters per 1000 yr (see "Sedimentation Rates" section, this chapter).

Observations indicate that an advective flow of less-saline fluids occurs through these layers, presumably as a result of the release of meteoric fluids trapped in the basement. The source for these fluids is probably located in the direction of the Greenland mainland.

## PHYSICAL PROPERTIES

### Introduction

Cores were taken at Site 918 using a combination of APC, XCB, and RCB techniques. The quality and downcore frequency of the physical properties data reflect these techniques, with the highest quality data deriving from the continuous APC cores. Four holes (918A–918D) were cored at this site. Because of limited penetration and low recovery at Holes 918B and 918C, the discussion of the physical properties from Site 918 has been largely restricted to data from Holes 918A and 918D. Based principally on the MST and index property data, a series of 12 mechanical units (M1–M12) can be defined for Site 918. A detailed description of the physical properties of the basement rocks is not included in this discussion, as few samples were taken and little MST data obtained, owing to the discontinuous recovery and the often fragmented nature of the basalt.

### Multisensor Track (MST)

Only the more continuous sections were measured with the MST. Sections where stratigraphic continuity was absent, such as where the recovery consisted only of cobbles, isolated cored intervals through glacial boulders, or drilling rubble, were not measured. Continuous MST *P*-wave velocity measurements were restricted to the APC cores. GRAPE wet bulk density, magnetic susceptibility, and natural gamma data were collected for all MST runs. GRAPE wet bulk density data from XCB and RCB cores were not corrected for coring disturbance (reduced diameter), as recovery was often limited and the diameter of the recovered material was highly variable. Therefore, although the GRAPE data give an excellent indication of downcore trends, the use

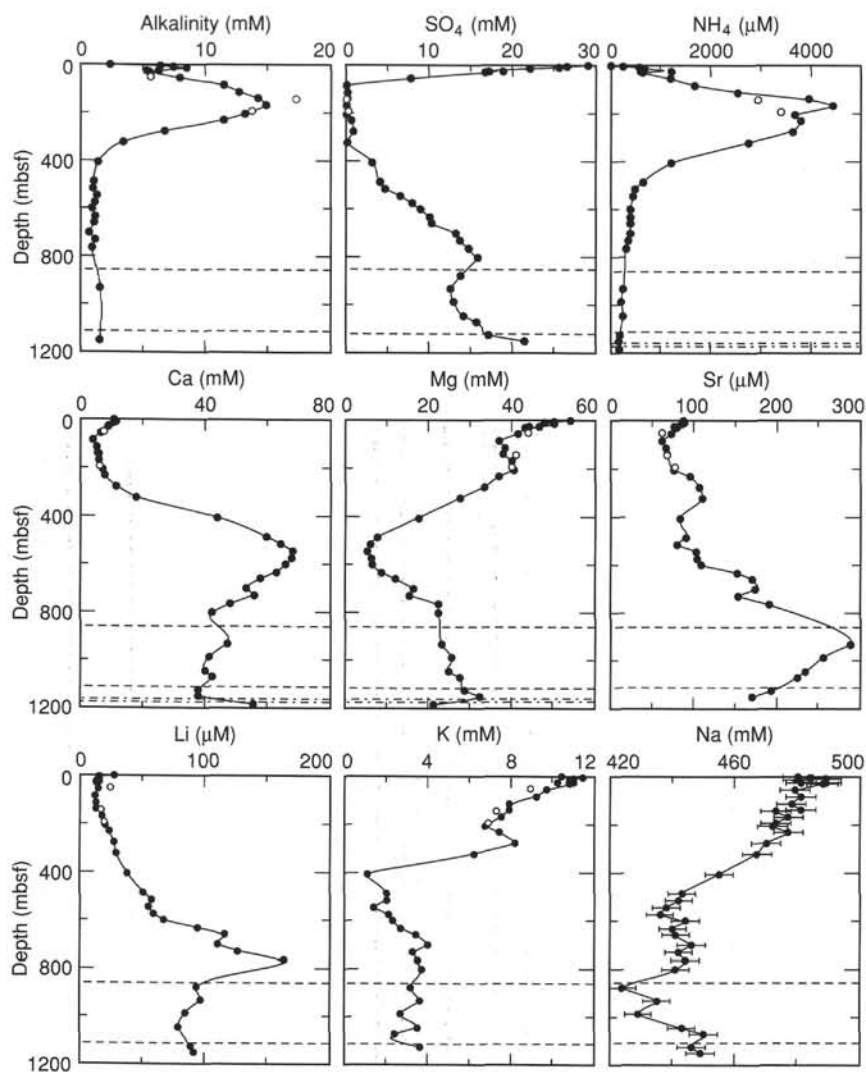


Figure 50. Distribution of biogenic elements (Alkalinity,  $\text{SO}_4$ ,  $\text{NH}_4$ ), alkaline earth elements (Ca, Mg, Sr), and alkali metals (Li, K, Na) in interstitial waters at Site 918. Dashed lines delineate sandy horizons; dash-dot lines indicate sill horizon. Open circles are data from WSTP samples.

of GRAPE bulk density values in quantitative analysis should be treated with caution. The MST data are presented in Figure 53.

The MST signal is characterized by many smaller-scale changes that reflect the complexity of the sediment packages referred to in the Site 918 "Lithostratigraphy" section (this chapter). Turbiditic sequences, fining-upward units, diamictons, carbonate-rich horizons, and glauconitic hardgrounds are revealed in great detail on a section-by-section scale, particularly in terms of the magnetic susceptibility, natural gamma, and GRAPE bulk density data. These changes are superimposed on a number of significant boundaries, which are defined either by changes in the magnitude or character of the MST signal, as discussed below.

Mechanical Unit M1 comprises the uppermost (0–34 mbsf; Sections 152-918A-1H-1 to -5H-3) sediments. The surficial sediments (0–4 mbsf) are characterized by a steady increase in GRAPE bulk density, which is attributed to compaction-driven dewatering. Averaged over Unit M1, GRAPE bulk density is about  $1.90 \text{ g/cm}^3$  and  $P$ -wave velocity is about  $1.6 \text{ km/s}$ . Magnetic susceptibility and natural gamma vary between 400 and 950 cgs and 600 and 1100 TC, respectively.

The boundary between mechanical Units M1 and M2 is most apparent in the  $P$ -wave velocity and GRAPE bulk density signal. This is an important observation as these differences probably create a sufficient contrast in acoustic impedance to produce the prominent seismic reflector at a depth of about 38 mbsf (see "Background and

Scientific Objectives" section, this chapter). Mechanical Unit M2 comprises sediments between 34 and 68 mbsf (Sections 152-918A-5H-3 to -8H-7). For Unit M2, the  $P$ -wave velocity and GRAPE bulk density average  $\approx 1.7 \text{ km/s}$  and  $2.10 \text{ g/cm}^3$ , respectively. The magnetic susceptibility and natural gamma signals are similar to those for mechanical Unit M1.

Mechanical Unit M3 is relatively thin (68–71 mbsf; Sections 152-918A-8H-1 to -9H-2). However, the acoustic impedance contrast at the boundary between Units M3 and M2 is sufficient for the generation of a seismic reflector. A major erosional unconformity is apparent on the seismic section, at a depth of about 68 mbsf (see "Background and Scientific Objectives" section, this chapter), and almost certainly correlates with this mechanical boundary. Unit M3 is characterized by a low ( $<2.00 \text{ g/cm}^3$ ) GRAPE bulk density and by a rapid downcore increase in  $P$ -wave velocity (from  $<1400 \text{ m/s}$  at 68.5 mbsf to  $>2000 \text{ m/s}$  at 70.5 mbsf). The base of Unit M3 correlates with the boundary between lithologic Subunits IA and IB, (see "Lithostratigraphy" section, this chapter).

Mechanical Unit M4 (71–78 mbsf; Cores 152-918A-9H to -10H) is characterized by a relatively homogeneous MST signature, particularly in terms of the GRAPE bulk density ( $\approx 2.0 \text{ g/cm}^3$ ), which contrasts strongly with the sharp swings in the MST data seen in the sediments above and below. This unit may correlate with Subunit M1b at Site 919 (see "Index Properties" below, and "Physical Properties" section, "Site 919" chapter, this volume).

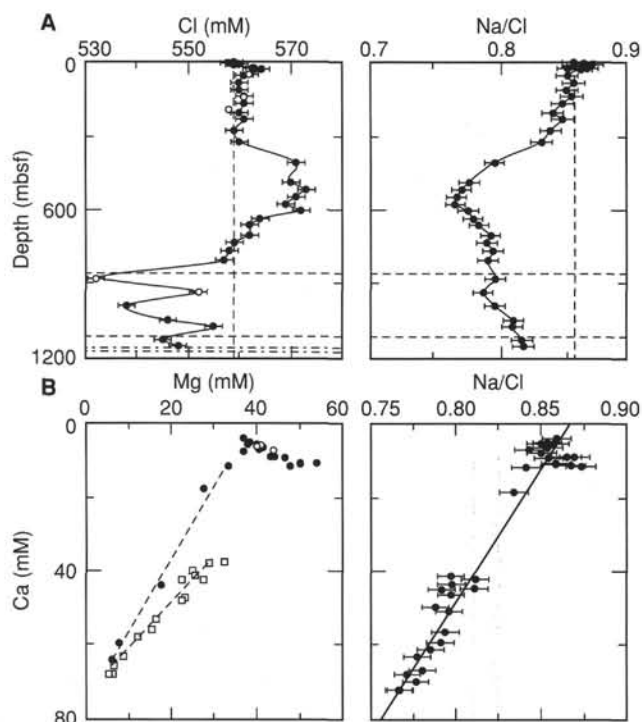


Figure 51. **A.** Chloride concentration and Na/Cl values in interstitial waters at Site 918. Horizontal lines as indicated in Figure 50. Vertical lines indicate values of present-day seawater. **B.** Correlations between dissolved calcium and magnesium and dissolved calcium with Na/Cl values at Site 918. Open circles are data from WSTP samples. Open squares are data from below the Ca maximum.

Mechanical Unit M5 (78–226 mbsf; Sections 152-918A-10H-2, to -26X-1) encompasses virtually the whole of lithologic Subunit IB and is defined principally according to the character of the MST signal. The unit comprises a diverse assemblage of sedimentary facies and appears to be cyclical in nature. This cyclicity is probably related to the turbiditic character of the sediment packages described in the “Lithostratigraphy” section (this chapter) and is defined particularly well by the natural gamma and magnetic susceptibility data. These data show a strong negative relationship, with peaks in natural gamma rays coinciding with magnetic susceptibility troughs. A particularly good example is seen between 120 and 140 mbsf (Cores 152-918A-14H to -16H). This relationship is likely related to grain size, with heavy magnetic minerals occurring in the sands and silts, and potassium-rich clays occurring in the finer-grained units. Refusal of the APC occurred at 171 mbsf, when coring was switched to the XCB. *P*-wave measurements were abandoned at this point.

The MST data for mechanical Units M6 (226–246 mbsf; Sections 152-918A-26X-1 to -29X-5) and M7 (246 to deeper than 292 mbsf; Section 152-918A-29X-5 to unknown) are similar to those data from Unit M5, and the distinction between the two units was largely made on the basis of index property measurements (see later section). The lower boundary of mechanical Unit M7 is uncertain because of the poor recovery between 292 and 400 mbsf.

The upper boundary of mechanical Unit M8 is similarly unclear, but its lower boundary is defined by a decrease in GRAPE bulk density and a local minimum in the natural gamma signal at 560 mbsf (Section 152-918D-28R-6). Unit M8 is characterized by an erratic natural gamma signal and a mean magnetic susceptibility of around 800 cgs. The natural gamma and magnetic susceptibility data are negatively related in Unit M8, as described for mechanical Unit M5.

The magnetic susceptibility in mechanical Unit M9 (560–640 mbsf; Sections 152-918D-28R-6 to -37R-1) averages about 500 cgs, and the natural gamma signal is similar to the signal for Unit M8. A

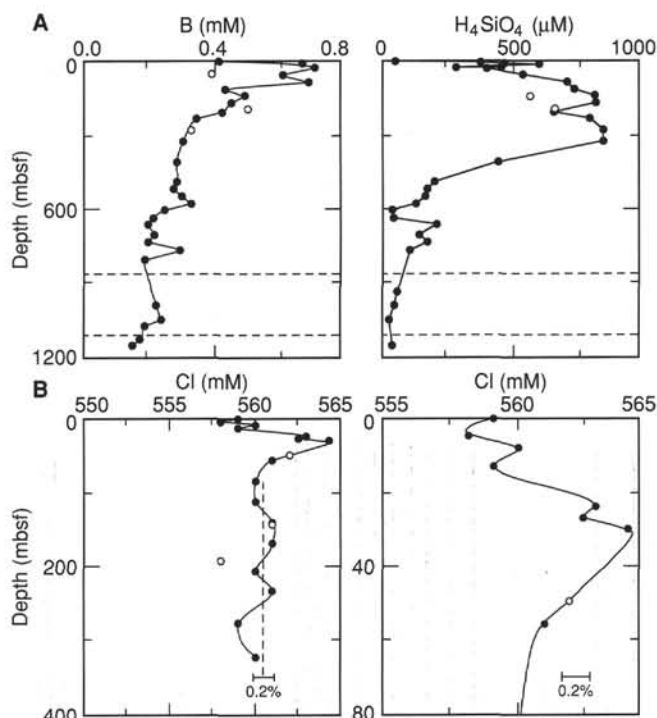


Figure 52. **A.** Distribution of boron and silica in interstitial waters at Site 918. Horizontal lines as indicated in Figure 50. **B.** Chloride concentrations in Holes 918A, 918B, and 918C. Figure at right is enlargement of the profile at left. Vertical dashed lines indicate present-day seawater chloride concentration. Open circles are data from WSTP samples.

significant difference exists between Units M8 and M9 with natural gamma and magnetic susceptibility signals positively related within Unit M9.

Mechanical Unit M10 (640–800 mbsf; Sections 152-918D-37R-1 to -53R-5) differs significantly from the units described above. GRAPE bulk density, magnetic susceptibility, and natural gamma signals fall off sharply from 640 to 660 mbsf. Natural gamma data, for example, falls sharply from  $\approx 1200$  TC at the base of Unit M9 to  $\approx 800$  TC at the top of Unit M10 (640–680 mbsf). This change is associated with an increase in the carbonate content and the consequent dilution of the MST signal (see “Inorganic Chemistry” and “Lithostratigraphy” sections, this chapter). Toward the base of this unit, the GRAPE bulk density, natural gamma, and magnetic susceptibility increase with depth. The point at which this increase stops is taken as the lower boundary of Unit M10.

The relatively poor recovery below 800 mbsf resulted in a highly discontinuous MST signal, and unit boundaries (for mechanical Units M11 and M12) have been largely defined in terms of their discrete index properties (see below).

## Index Properties

Wet bulk density, grain density, dry density, water content, porosity, and void ratio (see “Physical Properties” section, “Explanatory Notes” chapter, this volume) were determined for 487 discrete samples. These data are tabulated in Table 14 and illustrated in Figure 53. The mechanical units described above are also characterized by index properties.

Mechanical Units M1 and M2 are characterized by highly variable discrete bulk density (1.5–2.2 g/cm<sup>3</sup>), dry density (1.0–1.7 g/cm<sup>3</sup>), and porosity (40%–75%) values. Below about 50 mbsf, the index properties become more uniform. The index properties do not appear to reflect the division between mechanical Units M1 and M2.

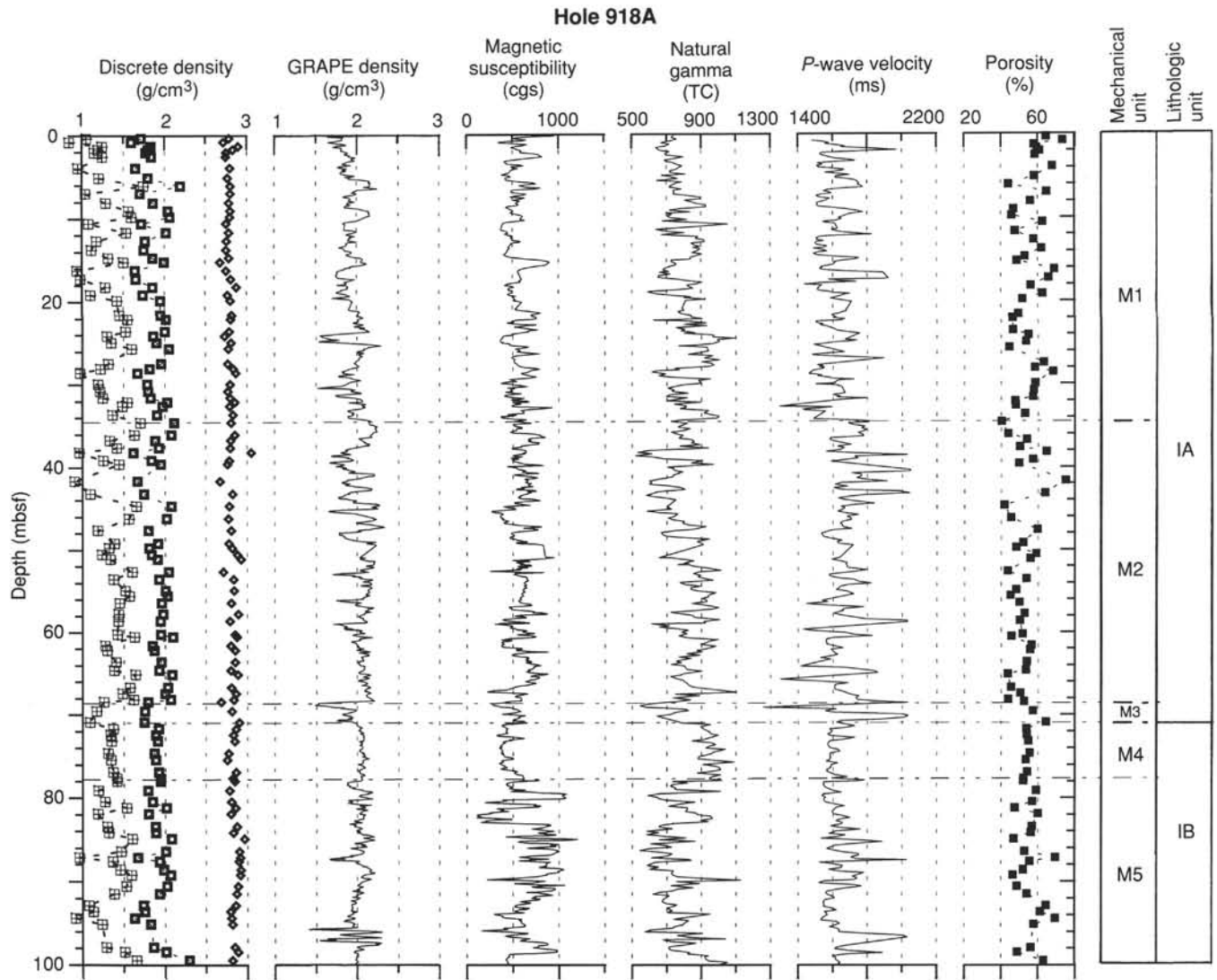


Figure 53. Composite plot of MST and discrete index property data for sediments recovered at Site 918. MST data comprise: GRAPE wet bulk density, magnetic susceptibility, and natural gamma rays. Discrete measurements include wet bulk density (open squares), grain density (open diamonds), dry density (hatched squares), and porosity (filled squares). GRAPE data are not corrected for drilling disturbance.

Mechanical Unit M3 is characterized by a downcore decrease in discrete bulk density (from about 2.10 g/cm<sup>3</sup> at the top of the unit to 1.70 g/cm<sup>3</sup> at the base) and a parallel increase in porosity (from about 55% to 65%).

Mechanical Unit M4 (71.0–78.0 mbsf) is characterized by constant porosity, grain density, and discrete bulk density. These parameters, together with the MST data, suggest that this unit correlates with mechanical Subunit M1b at Site 919.

With the exception of grain density, which remains relatively constant throughout Unit M5, all index properties in the upper portion of Unit M5 are highly variable, as seen in the upper parts of Units M1 and M2. This variability gradually lessens downcore, and the data are relatively uniform over the interval from 110 to 140 mbsf (Table 14). The regularity of the index property data clearly relates to the amplitude and frequency of variations in the MST magnetic susceptibility and natural gamma MST data. This is particularly apparent above and below 140 mbsf with the lower data showing the greater variability.

Mechanical Unit M6, which was not well defined by the MST data, is characterized by a reduced discrete bulk density and a slightly elevated porosity. Note that there is a slight downcore reduction in grain density.

The transition to mechanical Unit M7 is especially abrupt in terms of porosity. Porosity declines sharply from >60% at 248 mbsf (Section 152-918A-28X-3) to about 30% at 251 mbsf (Section 152-918A-28X-6). This is mirrored by an increase in discrete bulk density (1.7–2.3 g/cm<sup>3</sup>) over the same interval. Below 251 mbsf, the porosity increases from 50% to 60%, and the bulk density decreases to about 2.0 g/cm<sup>3</sup>.

The division between mechanical Units M8 and M9 is more apparent in the MST data than in terms of the index properties. Porosity remains constant at ≈40% over the interval from 400 to 640 mbsf. Grain density (≈2.8 g/cm<sup>3</sup>) and discrete bulk density (≈2.2 g/cm<sup>3</sup>) also are constant through these units.

The carbonate-rich Unit M10 is separated from adjacent sediments (M9 and M11) by a rapidly decreasing discrete bulk density (2.2–1.8 g/cm<sup>3</sup>) and increasing porosity (42%–60%) at the top of the unit, and similar magnitude reversed shifts at the base. The average grain density of Unit M10 is slightly less than for Units M9 and M11 whereas the average porosity is higher at ≈60%.

Mechanical Unit M11 (800–1100 mbsf; Sections 152-918A-53R-6 to -85R-1) is characterized by an index properties signature that is similar to that from Unit M8, albeit more variable. Within Unit M11,

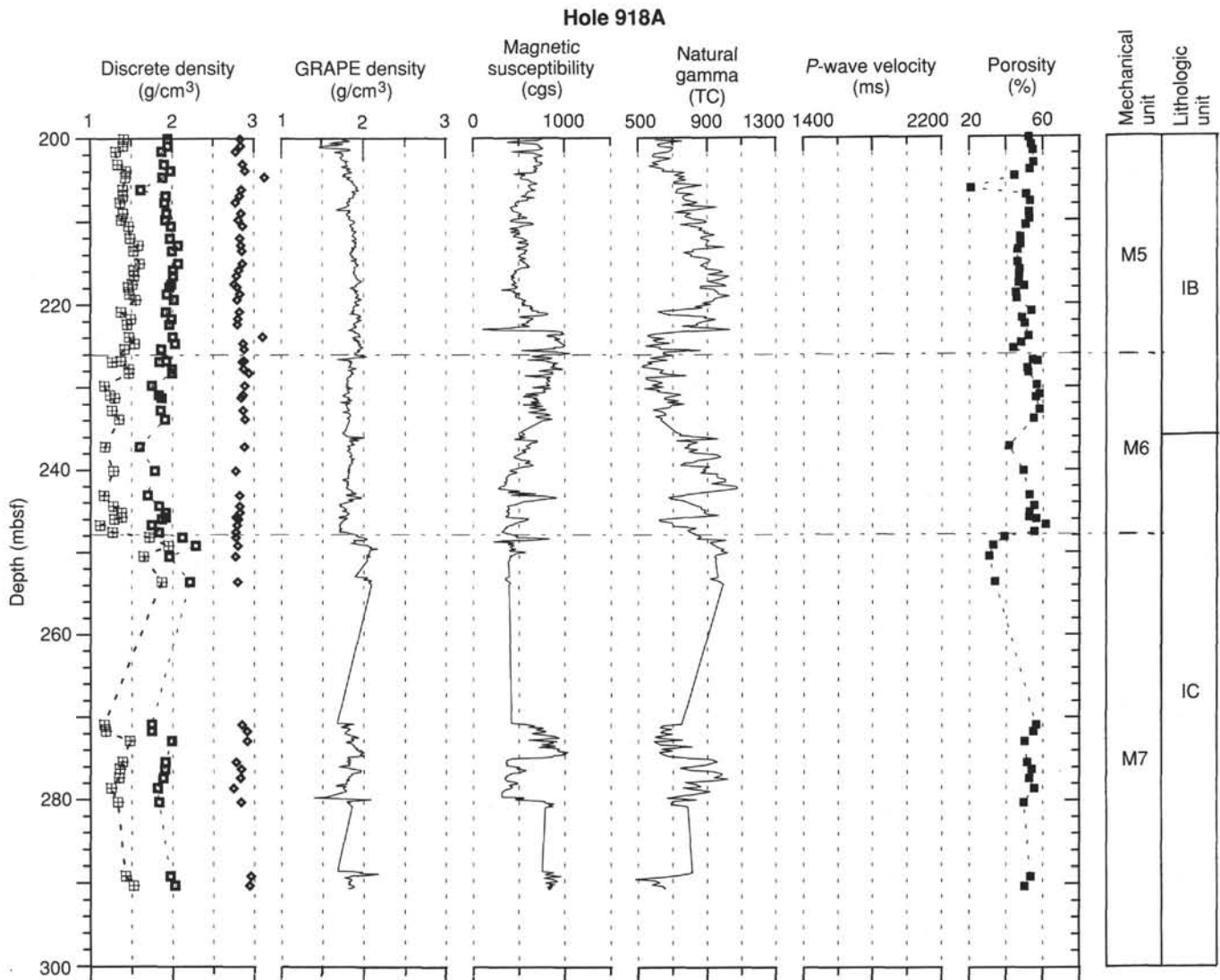


Figure 53 (continued).

(≈940 to 1000 mbsf), the character of the index properties changes, with discrete bulk density increasing both in magnitude (≈2.2–2.4 g/cm<sup>3</sup>) and variability. The porosity data also show a similar increase in variability over the same interval.

Mechanical Unit M12 (1100–1200 mbsf; Sections 152-918A-85R-1 to -96R-4) is characterized by a slight increase in grain density and a highly variable index property signature: porosity ranges between 35% and 80%, grain density between 1.6 and 2.3 g/cm<sup>3</sup>, and dry density between 1.0 and 1.9 g/cm<sup>3</sup>.

### Velocimetry

*P*-wave velocities were measured in Hole 918A (Cores 152-918A-1H to -7H), Hole 918B (Cores 152-918B-1H to -3H), and Hole 918C (Core 152-918C-1H) with the DSV. The Hamilton Frame was used for velocity measurements in Hole 918A (Cores 152-918A-27X to -28X and -37X) and in Hole 918D (Cores 152-918D-14R to 112R). The velocimetry results for Site 918 are listed in Table 15 and illustrated in Figures 54A and 54C.

In soft sediments, DSV velocities were measured parallel to the core axis ( $V_z$ ) and at right angles to the core axis, ( $V_x$ ). For indurated sediments, three velocity components were measured with the Hamilton Frame, namely, one parallel to the core axis ( $V_z$ ) and two ( $V_x$  and

$V_y$ ) at right angles to the core axis (see “Physical Properties” section, “Explanatory Notes” chapter, this volume).

Spacing of the acoustic velocity measurements is highly variable at Site 918. The average spacing to a depth of 50 mbsf is about 0.45 m. Below this, only seven measurements represent the interval from 51 to 484 mbsf. Two reasons exist for this low coverage. First, in Cores 152-918A-8H to -19H and 152-918A-20X to -26X, velocity measurements were impossible because of severe cracking created by the insertion of the DSV transducer probes into the cores. Furthermore, cutting of cubes with a sufficiently well-defined geometry for Hamilton Frame measurement was not possible. As a consequence, acoustic velocity is difficult to measure for sediments that are too stiff to evaluate with the DSV, but not sufficiently indurated to cube. Second, the core recovery in the interval from 320 to 484 mbsf (Hole 918D) was low. The random depth spacing of the velocity measurements at deeper levels largely reflects variability in core recovery in Hole 918D.

In the soft sediments, (≈0–50 mbsf)  $V_z$  and  $V_x$  scatter between 1500 and 1700 m/s and between 1600 and 1800 m/s, respectively (Fig. 54A). From the relation  $V_x/V_z$ , it is apparent that acoustic anisotropy increases with depth (Fig. 54B), over the same interval.

In the interval from 413 to 790 mbsf, acoustic velocities are mainly between 2000 and 2400 m/s. A few values exceeding 4000 m/s were measured on calcified sandstones (Fig. 54C and Table 15; 600.08 and

Table 14. Index property data for Site 918.

Core, section, interval (cm)	Depth (mbsf)	Water content $W_r$ (%)	Bulk density (g/cm <sup>3</sup> ) MB	Grain density (g/cm <sup>3</sup> ) MC	Dry density (g/cm <sup>3</sup> ) MB	Porosity (%) MC	Void ratio MC	Core, section, interval (cm)	Depth (mbsf)	Water content $W_r$ (%)	Bulk density (g/cm <sup>3</sup> ) MB	Grain density (g/cm <sup>3</sup> ) MC	Dry density (g/cm <sup>3</sup> ) MB	Porosity (%) MC	Void ratio MC
152-918A-								10H-1, 128-130	79.08	51.1	1.79	2.79	1.19	59.2	1.39
1H-1, 34-36	0.34	63.1	1.71	2.79	1.05	64.7	1.72	10H-2, 112-114	80.42	46.1	1.85	2.81	1.27	57.1	1.27
1H-1, 80-82	0.80	89.6	1.60	2.72	0.84	73.7	2.38	10H-3, 36-38	81.16	31.7	2.02	2.86	1.53	47.6	0.89
1H-2, 30-32	1.30	48.0	1.83	2.90	1.24	58.1	1.36	10H-3, 109-111	81.89	52.0	1.80	2.81	1.18	60.1	1.43
1H-CC, 10-12	1.70	51.4	1.80	2.83	1.19	59.6	1.42	10H-4, 112-114	83.42	44.9	1.88	2.88	1.30	56.9	1.26
2H-1, 25-27	2.05	54.9	1.77	2.76	1.14	61.2	1.48	10H-5, 36-38	84.16	43.9	1.89	2.83	1.31	56.2	1.21
2H-1, 75-77	2.55	48.4	1.84	2.75	1.24	58.6	1.30	10H-5, 112-114	84.92	30.0	2.08	2.96	1.60	46.9	0.87
2H-2, 60-62	3.90	73.5	1.65	2.80	0.95	68.1	2.01	10H-6, 111-113	86.41	36.8	2.01	2.90	1.47	52.7	1.04
2H-3, 30-32	5.10	49.7	1.80	2.77	1.20	58.4	1.34	10H-7, 36-38	87.16	74.4	1.67	2.91	0.96	69.6	2.12
2H-3, 125-127	6.05	26.0	2.19	2.80	1.74	44.1	0.71	11H-1, 33-35	87.63	41.7	1.93	2.90	1.36	55.5	1.18
2H-4, 70-72	6.95	64.2	1.70	2.81	1.04	65.0	1.76	11H-1, 125-127	88.55	36.6	1.98	2.92	1.45	52.0	1.05
2H-5, 24-26	8.04	44.8	1.86	2.79	1.28	56.1	1.22	11H-2, 38-40	89.18	29.8	2.07	2.92	1.59	46.4	0.85
2H-5, 125-127	9.05	30.8	2.04	2.81	1.56	47.0	0.84	11H-3, 25-27	90.55	32.7	2.02	2.89	1.53	48.6	0.92
2H-6, 49-51	9.79	29.4	2.07	2.80	1.60	45.8	0.80	11H-3, 112-114	91.42	40.0	1.93	2.87	1.38	54.0	1.12
2H-7, 27-29	10.57	59.6	1.72	2.75	1.08	62.8	1.60	11H-4, 106-108	92.86	61.5	1.73	2.86	1.07	64.5	1.72
3H-1, 32-34	11.62	31.9	2.02	2.79	1.53	47.6	0.87	11H-5, 30-32	93.60	55.8	1.76	2.80	1.13	61.4	1.52
3H-2, 70-72	12.65	50.3	1.77	2.76	1.17	57.7	1.36	11H-5, 107-109	94.37	77.8	1.63	2.81	0.92	69.5	2.14
3H-3, 25-27	13.70	57.3	1.75	2.75	1.11	62.1	1.54	11H-6, 33-35	95.13	48.1	1.83	2.82	1.23	57.9	1.32
3H-3, 124-126	14.69	41.3	1.86	2.79	1.31	53.0	1.12	12H-1, 111-113	97.91	44.8	1.86	2.85	1.29	56.3	1.25
3H-4, 25-27	15.20	33.2	2.00	2.68	1.50	48.7	0.87	12H-2, 15-17	98.45	33.2	2.02	2.89	1.51	49.1	0.94
3H-4, 126-128	16.21	75.7	1.64	2.76	0.93	69.1	2.04	12H-2, 116-118	99.46	39.2	2.30	2.82	1.65	63.2	1.08
3H-5, 73-75	17.18	69.3	1.65	2.81	0.98	66.1	1.90	12H-3, 34-36	100.14	40.8	1.89	2.81	1.34	53.5	1.12
3H-6, 24-26	18.19	45.1	1.86	2.88	1.28	56.4	1.27	12H-4, 27-29	101.57	39.2	1.92	2.85	1.38	52.7	1.09
3H-6, 119-121	19.14	58.4	1.74	2.77	1.10	62.6	1.58	12H-4, 110-112	102.40	37.9	1.93	2.81	1.40	51.8	1.04
3H-7, 34-36	19.79	37.4	1.95	2.80	1.42	51.8	1.02	12H-5, 109-111	103.89	376.4	1.98	0.83	0.42	152.9	3.05
4H-1, 74-76	21.54	35.0	1.95	2.82	1.45	49.4	0.96	12H-6, 27-29	104.57	37.3	1.92	2.77	1.40	51.0	1.01
4H-1, 125-127	22.05	30.7	2.02	2.81	1.54	46.2	0.84	12H-6, 90-92	105.20	36.5	1.84	2.80	1.35	48.0	1.00
4H-2, 122-124	23.52	31.3	2.00	2.79	1.52	46.5	0.85	12H-7, 37-39	105.67	36.6	1.74	2.81	1.28	45.7	1.00
4H-3, 30-32	24.10	43.2	1.86	2.73	1.30	54.8	1.15	13H-1, 101-103	107.31	41.0	1.87	2.79	1.33	53.0	1.12
4H-3, 107-109	24.87	40.7	1.90	2.81	1.35	53.6	1.12	13H-2, 98-100	108.78	41.9	1.88	2.82	1.32	54.1	1.16
4H-4, 34-36	25.64	28.5	2.05	2.78	1.60	44.5	0.77	13H-3, 102-104	110.32	43.1	1.85	2.82	1.29	54.3	1.19
4H-5, 61-63	27.41	49.1	1.96	2.77	1.31	63.0	1.33	13H-4, 98-100	111.78	39.9	1.89	2.79	1.35	52.7	1.09
4H-5, 124-126	28.04	49.1	1.81	2.83	1.22	58.3	1.36	13H-5, 32-34	112.62	48.3	1.84	2.84	1.24	58.7	1.34
4H-6, 29-31	28.59	72.3	1.67	2.87	0.97	68.3	2.03	13H-5, 120-122	113.50	40.0	1.94	2.83	1.39	54.2	1.11
4H-7, 10-12	29.90	50.5	1.79	2.80	1.19	58.7	1.38	13H-6, 30-32	114.10	38.2	1.92	2.83	1.39	52.0	1.06
5H-1, 49-51	30.79	48.9	1.80	2.77	1.21	57.8	1.32	13H-6, 119-121	114.99	37.1	1.93	2.80	1.41	51.0	1.02
5H-1, 123-125	31.53	47.2	1.83	2.80	1.24	57.3	1.29	13H-7, 36-38	115.66	38.3	1.93	2.80	1.39	52.1	1.05
5H-2, 24-26	32.04	31.6	2.03	2.86	1.54	47.7	0.88	14H-1, 31-33	116.11	39.9	1.89	2.80	1.35	52.6	1.09
5H-2, 77-79	32.57	33.2	1.97	2.79	1.48	48.0	0.90	14H-1, 112-114	116.92	33.5	1.95	2.74	1.46	47.8	0.90
5H-3, 29-31	33.59	39.9	1.90	2.83	1.36	53.0	1.10	14H-2, 73-75	118.03	37.2	1.93	2.82	1.41	51.1	1.02
5H-3, 125-127	34.55	24.1	2.12	2.81	1.71	40.2	0.66	14H-3, 30-32	119.10	31.8	1.97	2.74	1.49	46.3	0.85
5H-4, 123-125	36.03	27.5	2.08	2.86	1.63	43.8	0.77	14H-3, 118-120	119.98	37.9	1.93	2.82	1.40	51.8	1.04
5H-5, 36-38	36.66	41.7	1.88	2.80	1.33	54.0	1.14	14H-4, 84-86	121.14	41.6	1.87	2.81	1.32	53.7	1.14
5H-5, 131-133	37.61	36.4	1.93	2.80	1.41	50.2	0.99	14H-5, 53-55	122.33	40.3	1.90	2.85	1.36	53.4	1.12
5H-6, 35-37	38.15	69.3	1.62	3.05	0.95	64.6	2.07	15H-1, 118-120	126.48	35.2	1.97	2.84	1.46	50.0	0.97
5H-6, 131-133	39.11	46.9	1.84	2.79	1.25	57.4	1.28	15H-2, 28-30	127.08	34.7	1.96	2.84	1.46	49.3	0.96
5H-7, 29-31	39.59	35.2	1.95	2.77	1.44	49.6	0.95	15H-2, 118-120	127.98	24.0	1.96	2.83	1.58	37.0	0.66
6H-2, 37-39	41.67	85.1	1.67	2.67	0.90	75.0	2.22	15H-3, 27-29	128.57	30.5	1.88	2.90	1.44	42.8	0.86
6H-3, 37-39	43.17	59.9	1.75	2.83	1.09	63.9	1.65	15H-3, 118-120	129.48	36.2	1.98	2.92	1.45	51.4	1.03
6H-4, 37-39	44.67	26.0	2.08	2.78	1.65	41.9	0.71	15H-4, 27-29	130.07	36.0	1.97	2.88	1.45	50.9	1.01
6H-5, 37-39	46.17	29.8	2.03	2.78	1.56	45.5	0.81	15H-4, 118-120	130.98	32.7	2.01	2.88	1.51	48.4	0.92
6H-6, 30-32	47.60	51.6	1.80	2.81	1.19	59.8	1.42	15H-5, 27-29	131.57	29.6	2.02	2.81	1.56	45.1	0.81
6H-7, 38-40	49.18	38.3	1.92	2.78	1.39	51.9	1.04	15H-5, 133-135	132.63	37.0	1.93	2.80	1.41	50.9	1.01
7H-1, 40-42	49.70	37.3	1.81	2.82	1.32	48.1	1.03	16H-1, 35-37	133.65	40.6	1.89	2.79	1.34	53.3	1.11
7H-1, 120-122	50.50	48.9	1.84	2.88	1.24	59.0	1.38	16H-1, 111-113	134.41	34.3	1.97	2.82	1.47	49.2	0.95
7H-2, 28-30	51.08	43.1	1.91	2.93	1.34	56.2	1.23	16H-2, 80-82	135.60	37.6	1.93	2.79	1.40	51.5	1.02
7H-3, 30-32	52.60	27.9	2.05	2.71	1.60	43.7	0.74	16H-3, 30-32	136.60	34.1	1.98	2.87	1.48	49.3	0.96
7H-3, 120-122	53.50	39.9	1.93	2.84	1.38	53.7	1.11	16H-3, 112-114	137.42	25.8	2.10	2.82	1.67	42.0	0.71
7H-4, 109-111	54.89	32.5	2.01	2.84	1.52	48.2	0.90	16H-4, 74-76	138.54	27.3	2.08	2.80	1.64	43.6	0.75
7H-5, 25-27	55.55	29.6	2.03	2.84	1.57	45.3	0.87	16H-5, 31-33	139.61	35.3	1.94	2.86	1.44	49.5	0.99
7H-5, 109-111	56.39	35.3	1.96	2.81	1.45	50.0	0.97	16H-5, 112-114	140.42	34.7	2.02	2.94	1.50	50.7	1.00
7H-6, 92-94	57.72	37.5	1.98	2.89	1.44	52.8	1.06	16H-6, 80-82	141.60	19.1	2.27	2.88	1.90	35.5	0.54
7H-7, 31-33	58.61	36.0	1.95	2.79	1.43	50.3	0.98	17H-1, 112-114	143.92	44.5	1.88	2.86	1.30	56.5	1.24
8H-1, 141-143	60.21	37.3	1.95	2.85	1.42	51.8	1.04	17H-2, 26-28	144.56	40.0	1.91	2.83	1.36	53.1	1.10
8H-2, 22-24	60.52	28.7	2.10	2.88	1.63	45.6	0.81	17H-2, 111-113	145.41	38.5	1.70	2.84	1.23	46.2	1.07
8H-2, 129-131	61.59	45.5	1.85	2.80	1.27	56.5	1.24	17H-3, 75-77	146.55	38.0	1.94	2.77	1.40	52.1	1.03
8H-3, 34-36	62.14	44.1	1.87	2.85	1.30	55.9	1.23	17H-4, 27-29	147.57	33.6	1.96	2.76	1.47	48.2	0.91
8H-4, 25-27	63.55	39.4	1.95	2.86	1.40	53.9	1.10	17H-4, 129-131	148.59	33.9	1.99	2.86	1.49	49.3	0.95
8H-4, 127-129	64.57	39.6	1.93	2.81	1.38	53.4	1.08	17H-5, 72-74	149.52	26.8	2.05	2.77	1.62	42.4	0.73
8H-5, 30-32	65.10	27.2	2.08	2.89	1.64	43.5	0.77	17H-6, 43-45	150.73	29.1	2.11	2.93	1.64	46.5	0.83
8H-6, 36-38	66.66	29.6	2.04	2.81	1.57	45.4	0.81	17H-6, 124-126	151.54	27.0	2.09	2.85	1.65	43.5	0.75
8H-6, 113-115	67.43	34.8	2.00	2.86	1.48	50.5	0.97	18H-1, 24-26	152.54						

Table 14 (continued).

Core, section, interval (cm)	Depth (mbsf)	Water content W <sub>i</sub> (%)	Bulk density (g/cm <sup>3</sup> ) MB	Grain density (g/cm <sup>3</sup> ) MC	Dry density (g/cm <sup>3</sup> ) MB	Porosity (%) MC	Void ratio MC	Core, section, interval (cm)	Depth (mbsf)	Water content W <sub>i</sub> (%)	Bulk density (g/cm <sup>3</sup> ) MB	Grain density (g/cm <sup>3</sup> ) MC	Dry density (g/cm <sup>3</sup> ) MB	Porosity (%) MC	Void ratio MC
19H-3, 35-37	165.15	30.1	2.07	2.90	1.59	46.7	0.85	37X-3, 36-38	318.46	32.9	1.97	2.77	1.48	47.6	0.89
19H-3, 109-111	165.89	42.9	1.89	2.83	1.32	55.4	1.19	37X-4, 43-45	320.03	32.0	2.01	2.85	1.52	47.5	0.89
19H-4, 35-37	166.65	35.1	2.01	2.94	1.49	51.0	1.01	37X-6, 24-26	322.34	36.3	1.98	2.89	1.45	51.4	1.02
19H-5, 36-38	168.16	36.1	2.02	2.92	1.48	52.2	1.03								
19H-5, 124-126	169.04	27.6	2.10	2.85	1.64	44.3	0.77	152-918B-							
19H-6, 35-37	169.65	28.3	2.06	2.84	1.60	44.3	0.78	1H-1, 28-30	0.28	57.5	1.73	2.78	1.10	61.6	1.56
19H-7, 36-38	171.16	47.3	1.93	2.89	1.31	60.5	1.34	1H-1, 119-121	1.19	53.8	1.78	2.87	1.16	60.9	1.51
20H-1, 36-38	171.66	38.0	1.95	2.86	1.41	52.6	1.06	1H-2, 20-22	1.70	61.4	1.74	2.83	1.08	64.6	1.70
20H-1, 112-114	172.42	41.1	1.91	2.83	1.35	54.2	1.13	1H-3, 24-26	3.24	46.6	1.84	2.82	1.25	57.0	1.28
20H-2, 24-26	173.04	41.1	1.89	2.83	1.34	53.9	1.13	1H-3, 125-127	4.25	32.2	2.02	2.85	1.53	48.1	0.90
20H-3, 25-27	174.55	24.0	2.13	2.82	1.72	40.3	0.66	1H-4, 24-26	4.74	12.8	1.95	2.78	1.73	21.6	0.35
20H-3, 111-113	175.41	31.8	2.00	2.79	1.52	47.2	0.87	1H-5, 30-32	6.30	68.4	1.66	2.80	0.98	65.7	1.87
20H-4, 24-26	176.04	28.1	2.05	2.80	1.60	43.9	0.77	2H-1, 110-112	7.90	56.3	1.77	3.12	1.13	62.1	1.71
21H-1, 36-38	181.86	27.8	2.07	2.83	1.62	44.0	0.77	2H-2, 25-27	8.55	56.0	2.05	2.29	1.32	72.0	1.25
21H-1, 120-122	182.70	40.7	1.91	2.86	1.36	54.1	1.14	2H-2, 125-127	9.55	35.6	1.98	2.82	1.46	50.7	0.98
21H-2, 36-38	183.36	38.0	1.95	2.83	1.41	52.4	1.05	2H-3, 32-34	10.12	49.9	1.80	2.84	1.20	58.5	1.38
21H-3, 29-31	184.79	40.2	2.04	2.58	1.45	57.1	1.01	2H-4, 25-27	11.55	32.5	2.03	2.82	1.53	48.7	0.90
21H-3, 98-100	185.48	28.2	2.01	2.82	1.57	43.2	0.78	2H-4, 76-78	12.06	33.0	1.98	2.78	1.49	47.9	0.90
22X-1, 20-22	191.10	39.4	1.90	2.78	1.37	52.5	1.07	2H-5, 29-31	13.09	25.3	2.11	2.97	1.68	41.5	0.73
22X-1, 125-127	192.15	48.9	1.83	2.85	1.23	58.8	1.36	2H-5, 126-128	14.06	56.8	1.69	2.81	1.08	59.8	1.56
23X-1, 29-31	200.09	38.2	1.95	2.84	1.41	52.5	1.06	2H-6, 35-37	14.65	43.9	1.87	2.80	1.30	55.7	1.20
23X-1, 109-111	200.89	39.4	1.95	2.84	1.40	53.7	1.09	3H-1, 113-115	17.43	60.5	1.73	2.81	1.08	63.8	1.66
23X-2, 29-31	201.59	42.9	1.87	2.78	1.31	54.9	1.16	3H-2, 58-60	18.38	48.8	1.83	2.80	1.23	58.7	1.34
23X-3, 29-31	203.09	42.3	1.90	2.87	1.33	55.1	1.19	3H-2, 125-127	19.05	50.0	1.75	2.75	1.16	56.8	1.34
23X-3, 111-113	203.91	37.9	1.98	2.89	1.43	53.0	1.07	3H-3, 18-20	19.48	62.1	1.72	2.80	1.06	64.5	1.70
23X-4, 40-42	204.70	32.0	1.88	3.13	1.43	44.6	0.98	3H-3, 110-112	20.40	43.5	2.08	2.81	1.45	61.7	1.19
23X-5, 36-38	206.16	15.4	1.62	2.86	1.40	21.0	0.43	3H-4, 58-60	21.38	61.1	1.69	2.90	1.05	62.7	1.73
23X-5, 110-112	206.90	37.6	1.92	2.83	1.40	51.2	1.04	3H-5, 23-25	22.53	28.9	2.00	2.85	1.55	43.8	0.80
23X-6, 36-38	207.66	40.0	1.91	2.78	1.37	53.3	1.09	3H-5, 125-127	23.55	44.7	2.96	2.81	2.04	89.3	1.23
24X-1, 28-30	208.98	38.5	1.93	2.85	1.40	52.5	1.07	3H-6, 84-86	24.64	26.0	2.09	2.80	1.66	42.1	0.71
24X-1, 109-111	209.79	39.3	1.91	2.82	1.38	52.7	1.08	3H-7, 23-25	25.53	43.7	1.83	2.79	1.27	54.3	1.19
24X-2, 29-31	210.49	35.5	1.99	2.87	1.47	50.8	0.99								
24X-3, 28-30	211.98	32.9	1.97	2.83	1.49	47.8	0.91	152-918C-							
24X-3, 111-113	212.81	30.9	2.07	2.84	1.58	47.6	0.86	1H-1, 44-46	26.24	40.9	1.89	2.83	1.34	53.6	1.13
24X-4, 28-30	213.48	31.1	2.00	2.86	1.53	46.4	0.87	1H-1, 132-134	27.12	38.0	1.88	2.82	1.36	50.4	1.04
24X-5, 29-31	214.99	29.8	2.08	2.86	1.60	46.5	0.83	1H-2, 23-25	27.53	45.4	1.79	2.81	1.23	54.6	1.25
24X-5, 110-112	215.80	31.8	2.01	2.82	1.53	47.4	0.88	1H-3, 20-22	29.00	57.8	1.75	2.81	1.11	62.4	1.59
24X-6, 29-31	216.49	31.5	2.01	2.79	1.53	47.2	0.86	1H-3, 122-124	30.02	50.3	1.74	2.86	1.16	56.9	1.41
24X-7, 27-29	217.47	31.8	1.99	2.76	1.51	46.9	0.86	1H-4, 80-82	31.10	88.0	1.59	2.84	0.85	72.8	2.44
25X-1, 24-26	217.84	34.9	1.97	2.80	1.46	49.8	0.95	1H-5, 24-26	32.04	25.8	2.10	2.77	1.67	42.0	0.70
25X-1, 109-111	218.69	31.6	1.93	2.83	1.47	45.4	0.87	1H-5, 123-125	33.03	39.8	1.90	2.74	1.36	52.9	1.07
25X-2, 24-26	219.34	30.2	2.02	2.80	1.55	45.7	0.82	1H-6, 34-36	33.64	24.4	2.15	2.84	1.73	41.1	0.68
25X-3, 24-26	220.84	40.3	1.92	2.83	1.37	53.8	1.11	1H-7, 22-24	35.02	43.7	1.90	2.78	1.32	56.3	1.19
25X-3, 109-111	221.69	33.3	1.99	2.81	1.50	48.7	0.91								
25X-4, 26-28	222.36	35.5	1.97	2.80	1.45	50.3	0.97	152-918D-							
25X-5, 26-28	223.86	36.3	2.01	3.11	1.47	52.3	1.10	11R-1, 35-37	386.45	16.9	2.26	2.73	1.94	32.0	0.45
25X-5, 109-111	224.69	32.0	2.03	2.87	1.54	48.2	0.90	11R-1, 98-100	387.08	19.0	2.22	2.78	1.87	34.7	0.52
25X-6, 26-28	225.36	31.7	1.87	2.88	1.42	43.9	0.89	13R-1, 24-26	404.14	23.7	2.15	2.76	1.74	40.2	0.64
25X-7, 26-28	226.86	46.5	1.84	2.86	1.26	57.2	1.30	13R-1, 118-120	405.08	23.3	2.17	2.80	1.76	40.0	0.64
26X-1, 24-26	226.74	40.8	1.93	2.88	1.37	54.6	1.15	14R-1, 12-14	412.92	30.5	2.05	2.82	1.57	46.8	0.84
26X-1, 121-123	227.71	36.0	2.00	2.88	1.47	51.5	1.01	14R-1, 120-122	414.00	35.5	1.99	2.84	1.47	51.0	0.98
26X-2, 24-26	228.24	36.3	2.00	2.94	1.47	51.9	1.04	14R-2, 56-58	414.86	13.8	2.06	3.31	1.81	24.3	0.45
26X-3, 24-26	229.74	49.7	1.76	2.90	1.17	56.9	1.40	18R-1, 42-44	448.62	24.1	2.14	2.79	1.72	40.5	0.66
26X-3, 137-139	230.87	48.1	1.84	2.87	1.24	58.2	1.35	22R-1, 22-24	484.02	24.5	2.19	2.90	1.76	42.2	0.69
26X-4, 23-25	231.23	44.4	1.87	2.85	1.30	56.2	1.24	22R-1, 69-71	484.49	26.9	2.10	2.83	1.65	43.4	0.74
26X-5, 23-25	232.73	47.3	1.86	2.87	1.26	58.4	1.33	22R-2, 20-22	485.50	17.1	2.05	2.81	1.75	29.1	0.47
26X-6, 28-30	233.78	41.8	1.91	2.90	1.35	55.0	1.18	22R-3, 30-32	487.10	25.2	2.17	2.82	1.73	42.6	0.69
27X-2, 41-43	237.11	36.2	1.60	2.89	1.18	41.6	1.02	24R-1, 38-40	503.58	22.5	2.22	2.85	1.81	39.7	0.63
27X-4, 40-42	240.10	39.7	1.79	2.78	1.28	49.5	1.08	24R-1, 72-74	503.92	22.1	2.21	2.87	1.81	39.0	0.62
27X-6, 37-39	243.07	46.5	1.70	2.83	1.16	52.6	1.28	24R-2, 40-42	505.10	24.3	2.14	2.82	1.72	40.9	0.67
28X-1, 27-29	244.37	44.5	1.84	2.83	1.27	55.3	1.23	24R-3, 44-46	506.45	24.0	2.16	2.81	1.74	40.8	0.66
28X-1, 105-107	245.15	39.3	1.92	2.83	1.38	52.8	1.09	25R-1, 37-39	513.17	24.0	2.12	2.76	1.71	40.1	0.65
28X-2, 14-16	245.74	39.1	1.93	2.79	1.38	52.8	1.06	25R-2, 48-50	514.28	43.3	2.46	2.84	1.72	72.7	1.20
28X-2, 35-37	245.95	44.8	1.87	2.81	1.29	56.5	1.23	25R-3, 98-100	515.35	22.2	2.20	2.83	1.80	39.0	0.61
28X-2, 110-112	246.70	56.5	1.75	2.80	1.12	61.6	1.55	25R-4, 54-56	516.48	22.7	2.20	2.84	1.79	39.7	0.63
28X-3, 39-41	247.49	44.9	1.84	2.78	1.27	55.6	1.22	27R-1, 79-81	532.89	22.7	2.18	2.80	1.77	39.4	0.62
28X-3, 106-108	248.16	23.3	2.12	2.78	1.72	39.1	0.63	27R-2, 35-37	533.95	24.9	2.15	2.83	1.73	41.9	0.69
28X-4, 58-60	249.18	17.3	2.29	2.80	1.95	33.0	0.48	27R-3, 69-71	535.79	22.7	2.17	2.78	1.77	39.3	0.62
28X-5, 38-40	250.48	19.0	1.96	2.77	1.65	30.6	0.52	28R-1, 98-100	542.78	31.8	2.01	2.75	1.52	47.4	0.85
29X-1, 80-82	253.60	18.6	2.22	2.80	1.87	33.9	0.51	28R-2, 55-57	543.85	29.5	2.03	2.79	1.57	45.2	0.80
31X-1, 29-31	270.89	49.7	1.75	2.85	1.17	56.6	1.39	28R-2, 113-115	544.43	28.2	2.09	2.81	1.63	44.9	0.77
31X-1, 111-113	271.71	47.6	1.75	2.92	1.18	55.0	1.36	28R-3, 71-73	545.51	28.4	2.09	2.83	1.63	45.2	0.79
31X-2, 78-80	272.88	34.8	1.99	2.92											

Table 14 (continued).

Core, section, interval (cm)	Depth (mbsf)	Water content W <sub>i</sub> (%)	Bulk density (g/cm <sup>3</sup> ) MB	Grain density (g/cm <sup>3</sup> ) MC	Dry density (g/cm <sup>3</sup> ) MB	Porosity (%) MC	Void ratio MC	Core, section, interval (cm)	Depth (mbsf)	Water content W <sub>i</sub> (%)	Bulk density (g/cm <sup>3</sup> ) MB	Grain density (g/cm <sup>3</sup> ) MC	Dry density (g/cm <sup>3</sup> ) MB	Porosity (%) MC	Void ratio MC
35R-1, 16-18	609.36	33.3	2.21	2.89	1.66	53.8	0.94	53R-4, 69-71	787.69	22.5	2.21	2.70	1.80	39.7	0.59
35R-2, 75-77	611.45	34.7	2.22	2.67	1.65	55.7	0.90	53R-4, 123-125	788.23	40.7	2.06	2.50	1.46	58.1	0.99
35R-CC, 6-8	612.38	5.7	2.57	2.72	2.43	13.5	0.15	53R-5, 104-106	789.54	36.0	2.11	2.55	1.55	54.4	0.89
36R-1, 114-116	620.04	25.4	2.10	2.75	1.67	41.4	0.68	53R-6, 45-47	790.45	28.0	2.11	2.68	1.65	45.0	0.73
36R-2, 120-122	621.60	25.3	2.12	2.80	1.69	41.8	0.69	53R-7, 4-6	791.54	34.7	2.03	2.73	1.51	51.1	0.93
36R-3, 54-56	622.44	23.1	2.15	2.78	1.75	39.4	0.63	55R-1, 33-35	802.13	18.9	2.24	2.69	1.88	34.8	0.50
36R-CC, 4-6	622.85	22.6	2.16	2.77	1.76	39.0	0.61	55R-2, 22-24	803.52	26.4	2.12	2.76	1.68	43.2	0.71
37R-1, 36-38	628.96	25.8	2.12	2.79	1.68	42.3	0.70	55R-3, 14-16	804.94	20.4	2.22	2.68	1.85	36.7	0.53
37R-1, 79-81	629.39	14.9	2.07	2.73	1.80	26.3	0.40	55R-4, 57-59	806.87	21.5	2.22	2.71	1.83	38.4	0.57
37R-2, 15-17	630.25	27.3	2.07	2.76	1.63	43.4	0.74	55R-5, 57-59	808.09	29.4	2.09	2.74	1.62	46.4	0.79
37R-2, 130-132	631.40	25.6	2.12	2.78	1.69	42.2	0.70	55R-6, 38-40	809.40	20.8	2.20	2.93	1.82	37.1	0.60
37R-3, 15-17	631.75	42.1	2.14	2.69	1.51	62.0	1.10	57R-1, 23-25	821.23	21.1	2.26	2.73	1.86	38.3	0.56
37R-3, 133-135	632.93	29.6	2.06	2.74	1.59	46.1	0.79	57R-1, 136-138	822.36	28.8	2.39	2.73	1.86	52.2	0.77
37R-4, 94-96	634.04	24.6	2.12	2.73	1.70	40.9	0.66	57R-2, 74-76	823.24	17.6	2.29	2.65	1.94	33.4	0.45
37R-5, 70-72	634.78	27.5	2.13	2.79	1.67	44.9	0.75	57R-3, 55-57	824.55	18.0	2.28	2.67	1.93	33.9	0.47
38R-1, 43-45	638.63	26.3	2.12	2.74	1.68	43.1	0.70	58R-1, 10-12	830.80	19.5	2.24	2.70	1.88	35.7	0.51
38R-1, 128-130	639.48	25.9	2.12	2.73	1.68	42.6	0.69	60R-1, 21-23	850.21	26.8	2.15	2.77	1.70	44.4	0.72
38R-2, 74-76	640.44	27.1	2.15	2.76	1.69	44.6	0.73	62R-1, 20-22	869.50	25.2	2.16	2.78	1.73	42.4	0.68
38R-2, 142-144	641.12	31.3	2.05	2.71	1.56	47.7	0.83	62R-1, 71-73	870.01	25.2	2.16	2.78	1.73	42.4	0.68
38R-3, 32-34	641.52	28.5	2.10	2.75	1.63	45.4	0.76	62R-2, 23-25	870.82	23.4	2.20	2.79	1.78	40.7	0.64
38R-3, 121-123	642.41	31.0	2.03	2.76	1.55	47.0	0.84	62R-2, 84-86	871.43	24.7	2.19	2.77	1.76	42.4	0.67
38R-4, 106-108	643.76	30.9	2.05	2.68	1.57	47.3	0.81	63R-1, 30-32	879.20	23.2	2.20	2.73	1.79	40.6	0.62
38R-5, 53-55	644.73	31.8	2.01	2.72	1.53	47.5	0.85	63R-1, 106-108	879.96	25.0	2.18	2.77	1.74	42.5	0.67
38R-6, 13-15	645.83	38.7	1.96	2.77	1.41	53.4	1.05	63R-2, 90-92	881.30	24.4	2.18	2.73	1.75	41.7	0.65
39R-1, 79-81	648.69	41.3	1.90	2.72	1.34	54.2	1.10	68R-1, 23-25	925.23	27.5	2.14	2.83	1.68	45.1	0.76
39R-1, 140-142	649.30	41.1	1.91	2.67	1.35	54.2	1.07	68R-1, 87-89	925.87	44.2	1.92	2.77	1.33	57.5	1.19
39R-2, 96-98	650.36	37.8	1.94	2.77	1.41	52.0	1.02	72R-1, 54-56	964.24	21.3	2.25	2.80	1.85	38.5	0.58
39R-3, 55-57	651.45	40.7	1.89	2.70	1.34	53.4	1.07	74R-CC, 6-8	983.82	10.2	2.49	2.73	2.26	22.4	0.27
39R-4, 92-94	653.32	40.3	1.92	2.72	1.37	54.0	1.07	75R-1, 37-39	992.67	22.5	2.25	2.81	1.84	40.4	0.62
39R-5, 83-85	654.73	43.6	1.89	2.67	1.32	56.1	1.13	75R-2, 41-43	994.21	19.3	2.28	2.81	1.91	36.0	0.53
39R-6, 61-63	656.01	41.5	1.89	2.76	1.33	54.1	1.12	75R-2, 90-92	994.70	18.8	2.25	2.73	1.90	34.8	0.50
40R-1, 43-45	657.93	41.0	1.89	2.68	1.34	53.7	1.07	75R-3, 73-75	996.03	13.3	2.40	2.76	2.12	27.5	0.36
40R-2, 131-133	660.31	38.4	1.96	2.70	1.41	53.0	1.01	75R-4, 21-23	996.51	18.2	2.30	2.76	1.94	34.5	0.49
40R-3, 112-114	661.62	37.0	1.97	2.67	1.44	51.9	0.96	76R-1, 2-4	1002.02	29.3	2.36	2.42	1.83	52.2	0.69
40R-4, 118-120	663.18	41.6	1.90	2.78	1.34	54.6	1.13	76R-1, 94-96	1002.94	11.8	2.41	2.74	2.16	24.8	0.32
40R-5, 69-71	664.19	49.6	1.82	2.69	1.22	59.0	1.30	77R-1, 51-53	1012.11	19.6	2.24	2.74	1.87	35.8	0.52
40R-6, 28-30	664.78	40.6	1.92	2.68	1.36	54.1	1.06	78R-1, 46-48	1021.66	13.8	2.37	2.74	2.08	28.2	0.37
41R-1, 74-76	667.94	44.3	1.84	2.72	1.27	55.1	1.18	79R-1, 38-40	1031.28	9.2	2.15	2.71	1.97	17.6	0.24
41R-2, 120-122	669.90	42.1	1.89	2.72	1.33	54.6	1.12	80R-1, 18-20	1040.78	31.3	2.31	2.76	1.76	53.8	0.84
41R-3, 85-87	671.05	41.0	1.94	2.77	1.37	55.0	1.11	80R-1, 74-76	1041.34	21.3	2.15	2.66	1.77	36.8	0.55
41R-4, 104-106	672.74	42.1	1.91	2.75	1.35	55.3	1.13	83R-1, 51-53	1070.11	24.0	2.10	2.70	1.69	39.7	0.63
41R-5, 76-78	673.96	41.5	1.95	2.74	1.38	56.0	1.11	83R-1, 114-116	1070.74	22.4	2.21	2.73	1.80	39.5	0.60
41R-6, 28-30	674.98	48.1	1.83	2.71	1.23	58.0	1.27	84R-1, 41-43	1079.71	19.9	2.18	2.75	1.81	35.3	0.53
42R-1, 30-32	677.10	37.7	1.92	2.68	1.40	51.4	0.99	84R-1, 61-63	1079.91	18.4	2.28	2.79	1.93	34.6	0.50
42R-1, 124-126	678.04	39.2	1.93	2.72	1.38	53.0	1.04	84R-1, 80-82	1080.10	19.7	2.24	2.74	1.87	35.9	0.53
42R-2, 66-68	678.96	39.3	1.94	2.70	1.39	53.4	1.04	89R-1, 96-98	1128.36	22.4	2.24	2.77	1.83	40.1	0.61
42R-3, 43-45	680.23	35.4	1.96	2.78	1.45	50.2	0.96	90R-2, 79-81	1138.23	34.9	1.99	2.65	1.48	50.2	0.90
42R-3, 142-144	681.22	40.4	1.91	2.76	1.36	53.8	1.09	90R-3, 21-23	1139.15	39.3	1.89	2.53	1.36	52.2	0.97
42R-4, 65-67	681.95	39.6	1.93	2.74	1.38	53.3	1.06	90R-3, 54-56	1139.48	47.2	1.80	2.61	1.22	56.3	1.20
42R-4, 137-139	682.67	40.5	1.89	2.68	1.35	53.2	1.06	91R-1, 24-26	1146.74	40.6	1.87	2.64	1.33	52.8	1.05
42R-5, 29-31	683.09	41.9	1.88	2.70	1.32	54.1	1.10	91R-1, 95-97	1147.45	52.1	1.80	2.55	1.18	60.1	1.30
42R-5, 140-142	684.20	40.0	1.91	2.71	1.36	53.2	1.06	92R-1, 41-43	1156.61	47.9	1.65	3.35	1.12	52.2	1.56
42R-6, 97-99	685.27	47.3	1.84	2.68	1.25	57.6	1.24	92R-1, 95-97	1157.15	79.3	1.82	2.38	1.01	78.5	1.84
44R-1, 59-61	696.69	44.1	1.89	2.71	1.31	56.5	1.17	93R-1, 69-71	1166.49	69.5	1.68	2.80	0.99	67.1	1.90
44R-1, 129-131	697.39	42.9	1.87	2.65	1.31	54.9	1.11	93R-1, 133-135	1167.13	34.6	1.88	2.24	1.39	47.1	0.76
44R-2, 68-70	698.28	42.8	1.86	2.70	1.30	54.5	1.13	93R-2, 47-49	1167.77	31.1	2.04	2.67	1.55	47.2	0.81
44R-3, 56-58	699.66	43.8	1.89	2.59	1.31	56.3	1.11	94R-1, 97-99	1176.37		3.01				
44R-4, 106-108	701.66	45.9	1.87	2.68	1.28	57.3	1.20	94R-2, 47-49	1177.20		3.01				
44R-5, 77-79	702.87	50.2	1.83	2.71	1.22	59.6	1.33	95R-2, 35-37	1181.15	20.6	2.16	2.93	1.79	36.1	0.59
47R-2, 52-54	725.72	51.3	1.81	2.72	1.20	60.0	1.36	95R-3, 78-80	1183.08	52.1	2.16	2.28	1.42	72.4	1.16
47R-2, 145-147	726.65	45.5	1.89	2.75	1.30	57.8	1.22	96R-1, 31-33	1185.41	18.6	2.27	2.72	1.92	34.9	0.50
51R-1, 70-72	763.90	43.3	1.90	2.65	1.32	56.0	1.12	96R-2, 14-16	1185.86	44.4	1.71	2.88	1.18	51.4	1.25
51R-2, 46-48	765.16	40.4	1.91	2.66	1.36	53.8	1.05	96R-2, 107-109	1186.79	41.5	1.63	2.77	1.15	46.6	1.12
51R-2, 108-110	765.78	38.7	1.97	2.71	1.42	53.8	1.02	96R-3, 53-55	1187.75	58.4	1.73	2.67	1.09	62.3	1.52
51R-3, 77-79	766.97	40.9	1.94	2.63	1.38	54.9	1.05	97R-2, 13-15	1195.08	25.0	2.28	2.98	1.83	44.5	0.73
51R-4, 35-37	768.05	39.1	1.95	2.60	1.40	53.4	0.99	97R-2, 23-25	1195.18	222.9	4.20	1.63	1.30	283.0	3.54
51R-4, 143-145	769.13	42.2	1.91	2.67	1.34	55.2	1.10	97R-2, 136-138	1196.31	28.2	2.21	3.07	1.72	47.5	0.84
51R-5, 76-78	769.96	49.2	1.86	2.66	1.24	59.8	1.28	97R-3, 92-94	1197.37	25.4	2.24	2.96	1.79	44.3	0.73
51R-6, 75-77	771.45	41.8	1.92	2.62	1.36	55.4	1.07	97R-4, 138-140	1199.33	27.8	2.15	2.91	1.69	45.7	0.79
52R-1, 61-63	773.51	34.8	1.99	2.68	1.48	50.2	0.91	97R-5, 72-74	1200.07	24.5	2.17	2.91	1.74	41.7	0.70
52R-2, 25-27	774.65	37.8	1.96	2.72	1.										

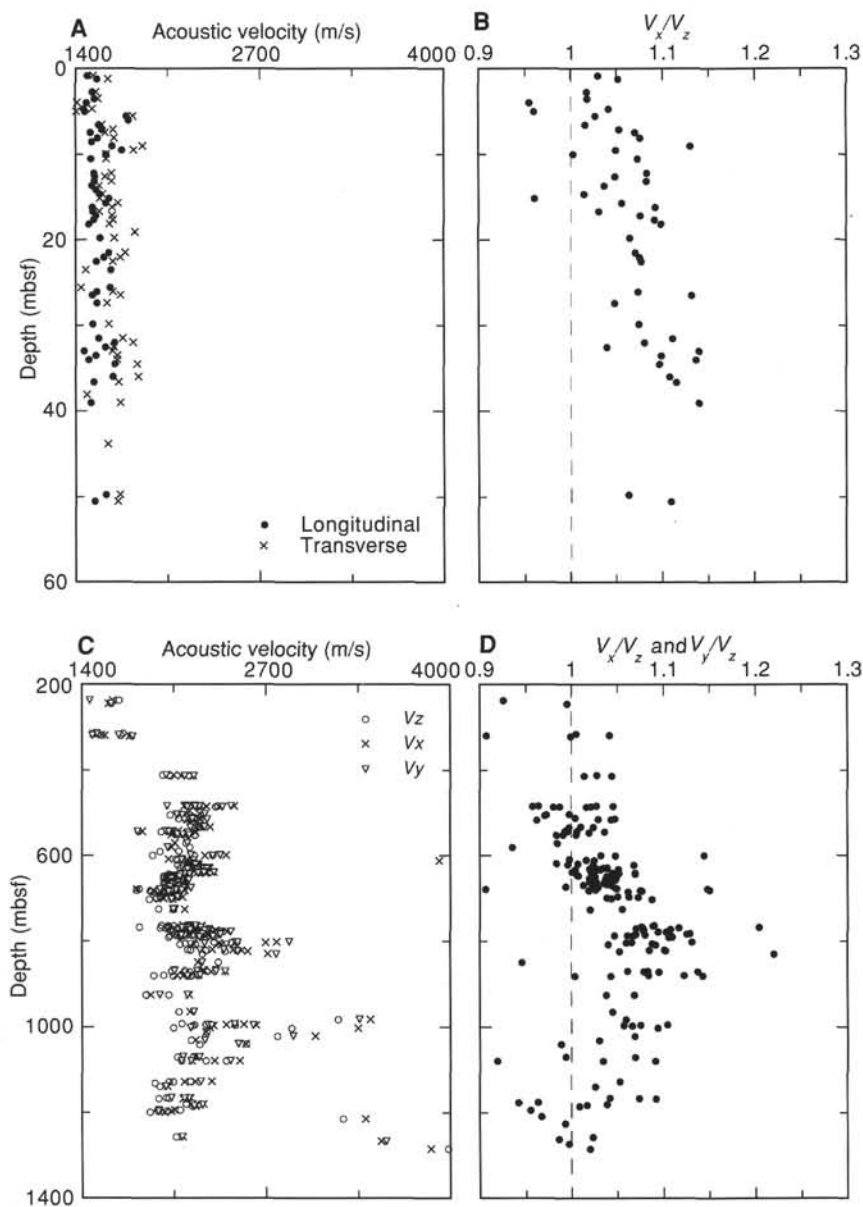


Figure 54. **A.** Discrete (DSV) longitudinal and transverse sonic velocity for the uppermost 50 mbsf of sediments recovered at Hole 918A. **B.** The anisotropic relationship ( $V_x/V_z$ ) between discrete (DSV) longitudinal ( $V_z$ ) and transverse ( $V_x$ ) sonic velocities for the uppermost 50 mbsf of sediments recovered at Site 918. **C.** Discrete (Hamilton Frame) longitudinal ( $V_z$ ) and transverse ( $V_x$  and  $V_y$ ) sonic velocities from the sediments below 200 mbsf at Site 918. **D.** The anisotropic relationship ( $V_x/V_z$  and  $V_y/V_z$ ) between discrete (Hamilton Frame) longitudinal ( $V_z$ ) and transverse ( $V_x$  and  $V_y$ ) sonic velocities for the sediments recovered below 200 mbsf at Site 918.

612.38 mbsf). A well-defined zone having relatively low velocities (2050 m/s, compared to 2200 m/s above and 2300 m/s below) are observed in the interval from 645 to 770 mbsf.  $V_x$  and  $V_y$  generally exceed  $V_z$ , and a tendency clearly exists for the difference to increase with depth (Fig. 54D). This interval corresponds to mechanical Unit M10 (Fig. 53), which is defined principally by variations in MST and index property data (i.e., high porosity, this section).

For Unit M11 (790–1170 mbsf), acoustic velocities fall between 2000 and 2500 m/s, with a few samples exceeding 3000 m/s.  $V_x$  and  $V_y$  tend to be higher than  $V_z$  in the upper part of the interval, but the difference diminishes with depth. The wider scatter in acoustic velocity data is consistent with the variability of the MST and index property data.

Acoustic velocities found in Core 152-918D-94R basalts range from 5350 to 5625 m/s. These values should probably be considered as maximum values because they are measured on massive samples, which may not be representative for the whole rock unit. The velocities measured in the sequence of basalts in the interval from 1195 to 1294 mbsf (Cores 152-918D-97R to -112R) range from 2100 m/s in strongly weathered zones to 5650 m/s in the unweathered, more massive units.

### Undrained Shear Strength

Owing to equipment failure, no shear-strength vane readings were done at Site 918.

### Thermal Conductivity and Electrical Resistivity

Thermal conductivities were measured for the sediments (two or three sections per core in lithologic Units I to III) and basalts (three samples) recovered at Site 918. For soft sediments, the full-space thermal conductivity method was employed, whereas for basalts, the half-space method was used (see "Physical Properties" section, "Explanatory Notes" chapter, this volume). The results are tabulated in Tables 16 and 17 and illustrated in Figure 55. Considerable scatter is seen in the thermal conductivity data. Mean thermal conductivity increases from  $1.34 \pm 0.15$  W/(m·K) at the seabed to a maximum of  $1.70 \pm 0.28$  W/(m·K) at the base of lithologic Unit IE. A prominent thermal conductivity minimum ( $\approx 1.1 \pm 0.16$  W/(m·K)) correlates with the middle of lithologic Unit II ( $\approx 700$ –800 mbsf). Conductivity varies from  $1.5 \pm 0.21$  W/(m·K) to  $1.8 \pm 0.15$  W/(m·K) in the basalts

Table 15. P-wave velocity measurements for Site 918.

Core, section, interval (cm)	Depth (mbsf)	DSV velocity		Hamilton Frame velocity			Core, section, interval (cm)	Depth (mbsf)	DSV velocity		Hamilton Frame velocity		
		V <sub>z</sub> (m/s)	V <sub>x</sub> (m/s)	V <sub>z</sub> (m/s)	V <sub>x</sub> (m/s)	V <sub>y</sub> (m/s)			V <sub>z</sub> (m/s)	V <sub>x</sub> (m/s)	V <sub>y</sub> (m/s)		
152-918A-													
1H-1, 87	0.87	1481	1525				2H-4, 25	11.55	1630	1847			
1H-2, 26	1.26	1548	1628				2H-4, 76	12.06	1686	1759			
2H-1, 95	2.75	1519	1546				2H-4, 128	12.58	1680	1728			
2H-2, 25	3.55	1534	1562				2H-5, 22	13.02	1690	1743			
2H-2, 70	4.00	1479	1413				2H-5, 86	13.66	1476	1616			
2H-2, 140	4.70	1458	1519				2H-5, 125	14.05	1482	1643			
2H-3, 25	5.05	1466	1408				2H-6, 36	14.66	1518	1668			
2H-3, 75	5.55	1759	1807				2H-6, 74	15.04	1609	1779			
2H-3, 125	6.05	1772					2H-6, 125	15.55	1484	1613			
2H-4, 36	6.61	1563	1588				3H-2, 30	18.10	1567	1640			
2H-4, 88	7.13	1583	1667				3H-2, 58	18.38	1569	1665			
2H-4, 125	7.50	1505	1611				3H-3, 45	19.75		1716			
2H-5, 30	8.10	1556	1674				3H-3, 79	20.09	1241	1306			
2H-5, 75	8.55	1512					3H-3, 126	20.56		1783			
2H-5, 125	9.05	1657	1873				3H-4, 31	21.11	1594	1407			
2H-6, 25	9.55	1726	1811				3H-4, 75	21.55	1440	1632			
2H-6, 75	10.05	1613	1618				3H-4, 124	22.04	1593	1747			
2H-7, 25	10.55	1507	1617				3H-5, 20	22.50	1426	1878			
3H-2, 28	12.23	1528	1655				3H-5, 75	23.05	1617	1661			
3H-2, 69	12.64	1533	1607				3H-5, 125	23.55		1672			
3H-2, 125	13.20	1530	1656				3H-6, 8	23.88	1578	1771			
3H-3, 25	13.70	1513	1568				3H-6, 83	24.63		1622			
3H-3, 75	14.20	1543	1291				3H-6, 134	25.14	1423	1728			
3H-3, 125	14.70	1569	1592				3H-7, 25	25.55	1548	1686			
3H-4, 25	15.20	1634	1570				152-918C-						
3H-4, 75	15.70	1610	1700				1H-1, 135	27.15	1569	1665			
3H-4, 125	16.20	1518	1658				1H-2, 20	27.50	1567	1672			
3H-5, 25	16.70	1520	1567				1H-2, 77	28.07	1560	1731			
3H-5, 75	17.20	1541	1658				1H-2, 125	28.55		1671			
3H-5, 125	17.70	1525	1664				1H-3, 75	29.55	1447	1795			
3H-6, 24	18.19	1494	1641				1H-3, 120	30.00	1534	1679			
3H-6, 115	19.10		1821				1H-4, 29	30.59	1502	1602			
3H-7, 34	19.79	1573	1675				1H-4, 76	31.06		1675			
4H-1, 75	21.55	1636	1752				1H-4, 125	31.55		1668			
4H-1, 125	22.05	1599	1719				1H-5, 70	32.50		1847			
4H-2, 25	22.55	1545	1664				1H-5, 125	33.05	1572	1905			
4H-2, 123	23.53	1649	1471				1H-6, 37	33.67		1896			
4H-4, 33	25.63	1643	1440				1H-6, 132	34.62	1558	1759			
4H-4, 78	26.08	1550	1664				1H-7, 25	35.05	1544	1716			
4H-4, 118	26.48	1518	1718				152-918D-						
4H-5, 62	27.42	1550	1624				14R-1, 13-15	412.93			1969	2049	1996
4H-7, 11	29.91	1521	1634				14R-1, 120-122	414.00			2158	2185	2190
5H-1, 124	31.54	1560	1733				14R-2, 54-56	414.84			2025	2102	2125
5H-2, 25	32.05	1673	1807				22R-1, 22-24	484.02			2248	2202	2131
5H-2, 77	32.57	1608	1671				22R-1, 69-71	484.49			2158	2236	2196
5H-2, 125	33.05	1458	1661				22R-1, 139-141	485.19			2157	2125	2005
5H-3, 28	33.58	1541	1693				22R-2, 20-22	485.50			2359	2477	2454
5H-3, 74	34.04	1490	1693				22R-2, 76-78	486.06			2211	2284	2232
5H-3, 125	34.55	1675	1837				22R-2, 127-129	486.57			2225	2189	2204
5H-4, 125	36.05	1665	1845				22R-3, 31-33	487.11			2345	2370	2395
5H-5, 35	36.65	1528	1704				22R-3, 88-90	487.68			2212	2190	2146
5H-6, 35	38.15		1482				24R-1, 72-74	503.92			2258	2236	2269
5H-6, 129	39.09	1507	1718				24R-2, 40-42	505.10			2158	2125	2073
6H-3, 110	43.90		1627				24R-2, 106-108	505.76			2025		
7H-1, 48	49.78	1610	1711				24R-3, 45-47	506.46			2167	2094	2112
7H-1, 125	50.55	1531	1698				25R-1, 37-39	513.17			2157	2178	2153
27R-2, 42-44	237.10			1663	1620	1458	25R-2, 49-51	514.29			2084	2189	2175
28R-2, 14-16	245.70			1607	1591	1607	25R-3, 98-100	515.35			2146	2235	2181
37R-1, 28-30	315.40			1690		1505	25R-4, 54-56	516.48			2166	2234	2285
37R-2, 8-10		316.70		1486	1480	1507	25R-5, 54-56	517.48			2236	2179	2124
37R-3, 35-37	318.50			1537	1541	1660	27R-1, 79-81	532.89			2225	2236	2258
37R-4, 41-43	320.00			1676	1564	1477	27R-2, 35-37	533.95			2235	2307	2268
37R-6, 25-27	322.40			1750	1738	1758	27R-3, 70-72	535.80			2190	2201	2167
152-918B-													
1H-2, 26	1.76	1500	1580				28R-1, 98-100	542.78			2054	2084	1996
1H-2, 75	2.25	1549	1640				28R-2, 55-57	543.85			1800	1827	1794
1H-2, 118	2.68	1499	1623				28R-2, 113-115	544.43			2034	2024	2024
1H-3, 32	3.32	1534	1647				28R-3, 71-73	545.51			1960	2044	2016
1H-3, 75	3.75	1514	1590				28R-4, 41-43	546.71			2135	2202	2148
1H-3, 131	4.31	1489	1697				29R-1, 56-58	551.96			2074	2035	2074
1H-4, 31	4.81	1435	1679				29R-1, 93-95	552.33			2115	2136	2114
1H-4, 75	5.25	1420	1363				29R-2, 31-33	553.21			2199	2168	2157
1H-4, 132	5.82	1476	1626				31R-1, 78-80	571.48			2136	2057	2147
1H-5, 25	6.25	1502	1606				32R-1, 91-93	581.21			2160	2033	2006
1H-5, 74	6.74	1514	1646				33R-1, 100-102	591.00			1951		
2H-1, 111	7.91	1534	1405				33R-1, 33-35	590.33			2084		
2H-2, 25	8.55		1812				34R-1, 20-22	599.80			2323	2417	2377
2H-2, 75	9.05	1699	1724				34R-1, 48-50	600.08			4440	4486	4582
2H-2, 125	9.55	1644	1646				34R-1, 92-94	600.52			1898	2173	2170
2H-3, 35	10.15	1507	1599				34R-2, 46-48	601.56			2192	2270	2323
2H-3, 84	10.64	1777	1766				35R-1, 17-19	609.37			2065	2014	2105
2H-3, 130	11.10						35R-1, 135-137	610.55			2075	2110	2105
							35R-2, 75-77	611.45			2115	2144	2190
							35R-CC, 6-8	612.38			4221	3925	4350

Table 15 (continued).

Core, section, interval (cm)	Depth (mbsf)	DSV velocity		Hamilton Frame velocity			Core, section, interval (cm)	Depth (mbsf)	DSV velocity		Hamilton Frame velocity		
		V <sub>z</sub> (m/s)	V <sub>x</sub> (m/s)	V <sub>z</sub> (m/s)	V <sub>x</sub> (m/s)	V <sub>y</sub> (m/s)			V <sub>z</sub> (m/s)	V <sub>x</sub> (m/s)	V <sub>y</sub> (m/s)		
36R-1, 38-40	619.28			2203	2155	2178	53R-4, 57-59	787.57			2025	2168	2128
36R-1, 114-116	620.04			2181	2214	2177	53R-4, 70-72	787.70			2178	2334	2315
36R-2, 121-123	621.61			2190	2170	2191	53R-4, 124-126	788.24			2073	2236	2104
36R-3, 54-56	622.44			2159	2204	2214	53R-5, 104-106	789.54			2104	2272	
36R-CC, 4-6	622.85			2074	2225	2203	53R-6, 46-48	790.46			2094	2319	2327
37R-1, 36-38	628.96			2192	2298	2254	53R-7, 4-6	791.54			2015	2225	2232
37R-1, 79-81	629.39			2214	2276	2261	55R-1, 33-35	802.13			2494	2777	2864
37R-1, 132-134	629.92			2214	2284	2296	55R-2, 23-25	803.53			2332	2483	2485
37R-2, 16-18	630.26			2094	2152	2147	55R-3, 14-16	804.94			2454	2698	2500
37R-2, 79-81	630.89			2181	2299	2226	55R-4, 57-59	806.87			2131	2370	2266
37R-2, 130-132	631.40			2237	2300	2261	55R-5, 58-60	808.10			2094	2189	2166
37R-3, 16-18	631.76			2136	2218	2191	55R-6, 38-40	809.40			2202	2386	2420
37R-3, 134-136	632.94			2136	2205	2284	57R-1, 25-27	821.25			2146	2321	2404
37R-4, 23-25	633.33			2158	2248	2203	57R-1, 136-138	822.36			2168	2468	2234
37R-4, 94-96	634.04			2158	2185	2147	57R-2, 75-77	823.25			2273	2527	2484
37R-5, 69-71	634.77			2169	2237	2214	57R-3, 55-57	824.55			2410	2572	2500
38R-1, 42-44	638.62			2147	2122	2261	58R-1, 11-13	830.81			2249	2715	2772
38R-1, 127-129	639.47			2238	2248	2229	60R-1, 20-22	850.20			2363	2221	2249
38R-2, 74-76	640.44			2226	2334	2334	62R-1, 7-9	869.37			2126	2254	2348
38R-2, 142-144	641.12			2094	2214	2262	62R-1, 20-22	869.50			2035	2264	2054
38R-3, 33-35	641.53			2159	2284	2224	62R-1, 71-73	870.01			2034	2413	2214
38R-3, 120-122	642.40			2136	2272	2220	62R-2, 23-25	870.82			2133	2253	2348
38R-4, 107-109	643.77			2095	2157	2126	62R-2, 84-86	871.43			2157	2311	2413
38R-5, 54-56	644.74			2015	2146	2162	63R-1, 30-32	879.20			1978	2225	2214
38R-6, 15-17	645.85			2063	2054	2095	63R-1, 87-89	879.77			1978	2072	2214
39R-1, 79-81	648.69			2025	2034	2044	63R-1, 106-108	879.96			1906	2120	2236
39R-1, 141-143	649.31			1978	2064	2043	63R-2, 32-34	880.72			2170	2198	2157
39R-2, 96-98	650.36			2006	2083	2031	63R-2, 90-92	881.30			2044	2116	2147
39R-3, 55-57	651.45			1996	2063	2091	68R-1, 23-25	925.23			2015	2159	2146
39R-4, 94-96	653.34			1978	2114	2034	68R-1, 88-90	925.88			1849	1886	1951
39R-5, 83-85	654.73			2006	2053	2035	72R-1, 54-56	964.24			2084	2163	2190
39R-6, 62-64	656.02			1996	2104	2034	74R-CC, 5-7	982.70			3208	3436	3359
40R-1, 43-45	657.93			2044	2125	2155	75R-1, 35-37	992.65			2104	2480	
40R-2, 129-131	660.29			2024	2115	2105	75R-2, 41-43	994.21			2274	2542	2479
40R-3, 112-114	661.62			2025	2074	2054	75R-2, 90-92	994.70			2192	2419	2292
40R-4, 118-120	663.18			2025	2074	2084	75R-3, 74-76	996.04			2480	2632	2609
40R-5, 70-72	664.20			1978	2044	2064	75R-4, 30-32	996.60			2178	2330	2313
40R-6, 29-31	664.79			2015	2094	2076	76R-1, 2-4	1002.02			2044	2304	2166
41R-1, 77-79	667.97			1987	2083	2042	76R-1, 94-96	1002.94			2878	3349	
41R-2, 119-121	669.89			2034	2053	2066	77R-1, 50-52	1012.10			2278	2276	
41R-3, 85-87	671.05			2025	2125	2102	78R-1, 45-47	1021.65			2780	3048	2892
41R-4, 104-106	672.74			2054	2115	2084	79R-1, 36-38	1031.26			2169	2201	2267
41R-5, 74-76	673.94			2114	2115	2086	80R-1, 19-21	1040.79			2560	2557	2503
41R-6, 29-31	674.99			1987	2064	2023	80R-1, 73-75	1041.33			2228		
42R-1, 30-32	677.10			2044	2113	2169	83R-1, 51-53	1070.11			2184	2227	2113
42R-1, 123-125	678.03			2006	2093	2115	83R-1, 114-116	1070.74			2073	2201	2230
42R-2, 66-68	678.96			1803	2054	2084	84R-1, 43-45	1079.73			2415	2336	2103
42R-3, 43-45	680.23			2064	1790	1951	84R-1, 62-64	1079.92			2273	2512	2447
42R-3, 142-144	681.22			1942	1988	1996	84R-1, 81-83	1080.11			2103	2177	2171
42R-4, 65-67	681.95			1786	2043	2064	89R-1, 98-100	1128.38			2046	2202	
42R-4, 137-139	682.67			1969	2125	2105	89R-1, 98-100	1128.38			2016	2125	
42R-5, 29-31	683.09			1933	1904	2034	89R-1, 14-46	1127.54			2167	2319	2242
42R-5, 139-141	684.19			1881	2033	2015	89R-4, 34-36	1131.74			1917		
42R-6, 98-100	685.28			1890	1996	2015	90R-3, 83-85	1139.77			1951	2006	1996
44R-1, 59-61	696.69			1951	2032	2064	93R-1, 19-21	1165.99			1996	2124	2034
44R-1, 129-131	697.39			1951	2061	2084	93R-1, 133-135	1167.13			2015	2167	2159
44R-2, 69-71	698.29			1951	2110	2074	93R-2, 47-49	1167.77			1942	2115	2126
44R-3, 57-59	699.67			1924	1969	2025	94R-1, 97-99	1176.37			5628	5348	5498
44R-4, 106-108	701.66			1924	1979	2034	94R-2, 47-49	1177.20			5858	5485	5550
44R-5, 77-79	702.87			1873	2039	2034	95R-2, 36-38	1181.16			2136	2258	2179
47R-2, 52-54	725.72			1941	2042	2054	95R-3, 78-80	1183.08			2191	2202	2253
47R-2, 144-146	726.64			2044	2126	2044	96R-1, 31-33	1185.41			2179	2202	2192
51R-1, 71-73	763.91			1960	2113	2157	97R-2, 23-25	1195.18			2094	2054	1946
51R-2, 47-49	765.17			2006	2178	2191	97R-2, 94-96	1195.89			1934		
51R-2, 109-111	765.79			2044	2245	2203	97R-3, 92-94	1197.37			1941		1942
51R-3, 77-79	766.97			2015	2188	2147	97R-3, 115-117	1197.60			1996	2034	
51R-4, 36-38	768.06			1802	2212	2126	97R-4, 138-140	1199.33			1881	1987	
51R-4, 143-145	769.13			2006	2242	2237	99R-4, 27-30	1209.87			4507	4415	4301
51R-5, 76-78	769.96			1951	2100	2104	100R-3, 24-26	1215.68			3242	3402	
51R-6, 75-77	771.45			1996	2124	2147	101R-4, 68-70	1226.37			5035	4954	5045
52R-1, 62-64	773.52			2064	2272	2298	105R-3, 37-39	1250.78				4632	4712
52R-2, 26-28	774.66			2025	2201	2164	106R-4, 56-58	1257.08			2063	2114	2107
52R-3, 2-4	775.92			2146	2345	2282	108R-1, 59-62	1262.79			5602	5416	5633
52R-3, 59-61	776.49			2044	2260	2264	109R-1, 70-72	1267.60				3513	3549
52R-4, 140-142	778.80			2212	2426	2452	110R-1, 121-123	1273.11			5095	5172	4988
52R-5, 56-58	779.46			2157	2346	2374	111R-3, 46-48	1284.81			3985	3865	4263
53R-1, 22-24	782.72			2083	2319	2382	112R-3, 18-20	1293.95			3538	3267	3339
53R-1, 129-131	783.79			2054	2260	2362							
53R-2, 76-78	784.76			2126	2295	2254							
53R-3, 55-57	786.05			2189	2348	2379							

Note: Data were calculated according to Method B or Method C, as defined in "Physical Properties" section, "Explanatory Notes" chapter (this volume).

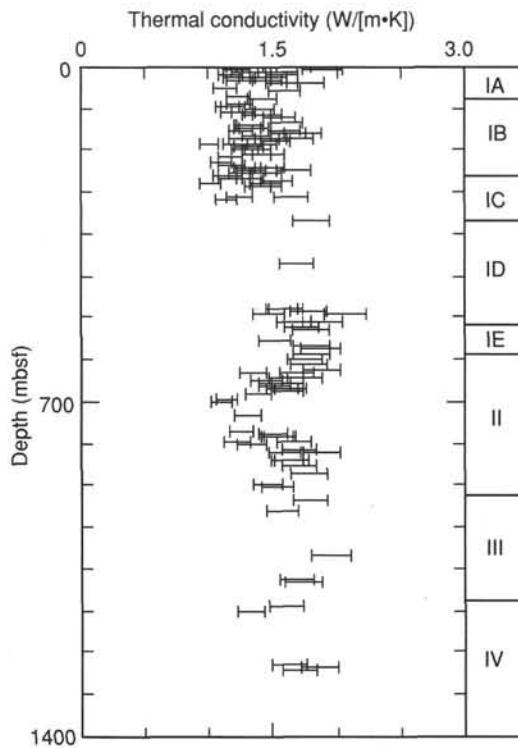


Figure 55. Thermal conductivity data for sediments recovered at Site 918.

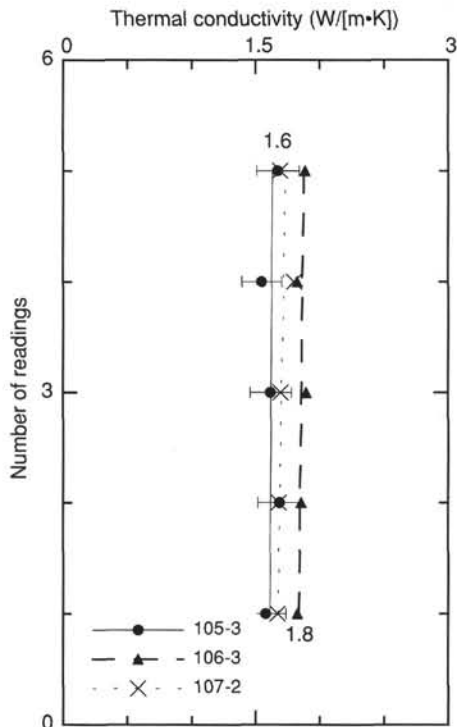


Figure 56. Thermal conductivities of basalt samples from Hole 918D in lithologic Unit IV.

Table 16. Summary of thermal conductivity measurements for sediments from Site 918.

Core, section, interval (cm)	Depth (mbsf)	Thermal conductivity (W/[m·K])	Core, section, interval (cm)	Depth (mbsf)	Thermal conductivity (W/[m·K])
152-918A-			3H-1, 60	16.90	1.149
1H-1, 75	0.75	1.220	3H-3, 75	20.05	1.315
2H-1, 75	2.55	1.229	3H-5, 75	23.05	1.439
3H-2, 80	12.75	1.288	152-918C-		
4H-1, 60	21.4	1.486	1H-1, 80	26.60	1.237
5H-2, 80	32.60	1.580	1H-3, 75	29.55	1.590
6H-2, 80	42.10	1.253	1H-5, 80	32.60	1.764
7H-2, 80	51.6	1.591	152-918D-		
8H-2, 80	61.1	1.230	14R-1, 70	413.50	1.689
9H-1, 100	69.3	1.411	24R-1, 82	504.02	1.608
9H-6, 75	76.55	1.242	24R-3, 16	506.17	1.579
10H-2, 75	80.05	1.231	25R-1, 43	513.23	1.787
10H-4, 75	83.05	1.182	25R-3, 96	515.33	1.471
10H-6, 75	86.05	1.157	25R-4, 41	516.35	2.068
11H-2, 75	89.55	1.397	27R-1, 120	533.37	1.669
11H-4, 75	92.55	1.192	27R-3, 60	535.7	1.891
11H-6, 75	95.55	1.275	28R-1, 54	542.30	1.731
12H-1, 130	98.10	1.374	28R-3, 50	545.30	1.727
12H-3, 75	100.55	1.458	29R-1, 63	552.03	1.809
12H-7, 30	105.60	1.549	31R-1, 78	571.48	1.508
14H-1, 75	116.55	1.613	32R-1, 97	581.27	1.996
14H-4, 75	121.05	1.322	33R-1, 70	590.70	2.029
14H-5, 66	122.46	1.317	34R-1, 93	600.53	1.910
15H-1, 75	126.05	1.356	35R-1, 71	609.91	1.869
15H-3, 75	129.05	1.310	36R-1, 118	620.08	1.879
15H-5, 75	132.05	1.592	37R-2, 94	631.04	2.009
16H-2, 75	135.55	1.253	38R-1, 24	638.44	1.912
16H-4, 75	138.55	1.624	38R-2, 30	640.00	1.681
16H-6, 75	141.55	1.735	39R-1, 60	648.50	1.607
17H-2, 75	145.05	1.384	39R-3, 60	651.50	1.753
17H-4, 75	148.05	1.495	40R-1, 55	658.05	1.450
17H-6, 75	151.05	1.696	40R-3, 60	661.10	1.613
18H-1, 75	153.05	1.263	40R-4, 10	662.10	1.515
18H-3, 75	156.05	1.520	41R-1, 60	667.80	1.515
18H-5, 75	159.05	1.426	41R-3, 60	670.80	1.634
19H-1, 80	162.60	1.210	41R-4, 96	672.66	1.572
19H-2, 75	164.05	1.002	42R-1, 60	677.40	1.610
19H-4, 75	167.05	1.316	42R-5, 60	683.40	1.386
19H-6, 75	170.05	1.281	44R-1, 50	696.60	1.140
20X-1, 60	171.90	1.381	44R-3, 59	699.69	1.106
20X-3, 60	174.90	1.389	47R-2, 100	726.20	1.306
21X-1, 40	181.90	1.469	51R-1, 80	764.00	1.251
21X-2, 70	183.70	1.382	51R-4, 70	768.40	1.502
22X-1, 66	191.56	1.169	51R-6, 25	770.95	1.543
23X-1, 90	200.70	1.120	52R-1, 130	774.20	1.552
23X-3, 60	203.40	1.165	53R-1, 60	783.10	1.219
23X-5, 65	206.45	1.181	53R-3, 60	786.10	1.672
24X-1, 70	209.40	1.310	53R-5, 58	789.08	1.337
24X-3, 75	212.00	1.476	55R-1, 60	802.40	1.708
24X-5, 75	215.45	1.658	55R-3, 65	805.45	1.883
25X-1, 100	218.60	1.338	55R-5, 60	808.12	1.595
25X-3, 65	221.25	1.449	57R-1, 60	821.60	1.651
25X-5, 75	224.35	1.249	57R-3, 85	824.85	1.611
26X-1, 75	227.25	1.135	58R-1, 90	831.60	1.708
26X-3, 75	230.25	1.168	60R-1, 22	850.22	1.787
26X-5, 75	233.25	1.001	62R-1, 76	870.06	1.457
27X-1, 75	235.95	1.327	63R-1, 118	880.08	1.532
27X-3, 75	238.95	1.534	66R-1, 22	905.92	1.791
27X-5, 85	242.05	1.451	68R-1, 60	925.60	1.571
28X-1, 50	244.60	0.913	78R-1, 36	1021.56	1.964
28X-3, 50	247.60	1.386	83R-1, 55	1070.15	1.683
28X-5, 50	250.60	1.460	84R-1, 58	1079.88	1.742
31X-3, 73	274.33	1.651	89R-2, 110	1130.00	1.605
31X-5, 73	277.33	1.086	90R-3, 69	1139.63	1.325
37X-5, 40	321.50	1.811			
152-918B-					
1H-2, 70	2.20	1.659			
1H-4, 70	5.20	1.196			
2H-2, 75	9.05	1.568			
2H-4, 60	11.90	1.377			
2H-6, 75	15.05	1.568			

Note: SD = standard drift in degrees/min (see "Physical Properties" section, "Explanatory Notes" chapter, this volume).

(Tables 16 and 17). Figure 56 illustrates mean values of thermal conductivity readings taken from three basalt samples.

Electrical resistance measurements for sediments recovered from Site 918, and calculated resistivity and formation factor values are tabulated in Table 18. Resistivities have been plotted as a function of depth in Figure 57. Although resistivity remains roughly constant

**Table 17. Thermal conductivity measurements performed for three basalt samples from Hole 918D in lithologic Unit IV.**

Core, section, interval (cm)	Depth (mbsf)	Thermal conductivity (W/(m-K))				
		1	2	3	4	5
152-918D-						
105R-3, 8–15 (Piece 1)	1250.49	1.577	1.688	1.620	1.551	1.675
106R-3, 87–97 (Piece 2B)	1253.47	1.825	1.853	1.897	1.823	1.885
107R-2, 64–73 (Piece 9B)	1259.30	1.617	1.682	1.696	1.800	1.691

Note: Half-space method was used.

( $\approx 0.7 \Omega\text{m}$ ), a break and local maximum is apparent for mechanical Unit 3 ( $\approx 70$  mbsf). This break correlates with an increase in the porosity data (Fig. 53A), suggesting the positive relationship between resistivity and porosity correlation.

### Summary

We suggest that the physical properties of the sediments at Site 918 can be best understood within a framework of 12 mechanical units (M1–M12). These units are principally defined by the continuous MST and discrete index property data sets and are supported by velocimetry, thermal conductivity, and electrical resistivity measurements. Note that many of these mechanical units do not correlate with lithological boundaries.

An important result is the use of physical properties data in providing absolute depths for seismic reflectors in the upper 80 mbsf of Hole 918A, with MST GRAPE bulk density and *P*-wave velocity being particularly valuable.

### HEAT FLOW

Four attempts were made in Hole 918A to measure the in-situ temperature using the water sampling temperature probe (WSTP) device. These measurements were performed simultaneously with extraction of in-situ pore fluid. The successful retrieval of pore fluids serves as a reliable indicator of the potential success of the temperature measurement because their composition, which mirrors that of pore fluids sampled at the same horizon using the shipboard squeezing technique, indicates the correct insertion of the probe inside the sediments. Below, a summary of the temperature measurements is presented, and an attempt is made to estimate the heat flow at this site on the basis of the temperature information and thermal heat conductivity measurements on core materials.

An attempt to measure in-situ temperature with the ADARA tool in Hole 918C led to a failure to penetrate the sediment.

### Temperature Measurements

The temperatures determined during the various runs of the WSTP are presented in Figures 58, 59, 60, and 61. The data indicate some difficulties with the upper two deployments. At 49.3 mbsf, the in-situ pore waters indicated that the probe was inserted into the sediments, but the thermal record is noisy, as shown by a gradual increase in temperature with time after an initial, almost isothermal, interval (Figs. 58A and 58B). We suppose that this is the result of the movement of the tool in the formation, which caused gradual frictional heating of the tip of the probe. On the basis of the first part of the record, we estimate as a tentative temperature the value of 6.3°C at 49.3 mbsf. That the record at 98.6 mbsf has been compromised is indicated not only by the in-situ pore fluid, which represents borehole fluid, but also by the very low temperature, which is only about 1°C above the mudline temperature (Figs. 59A and 59B). The temperature

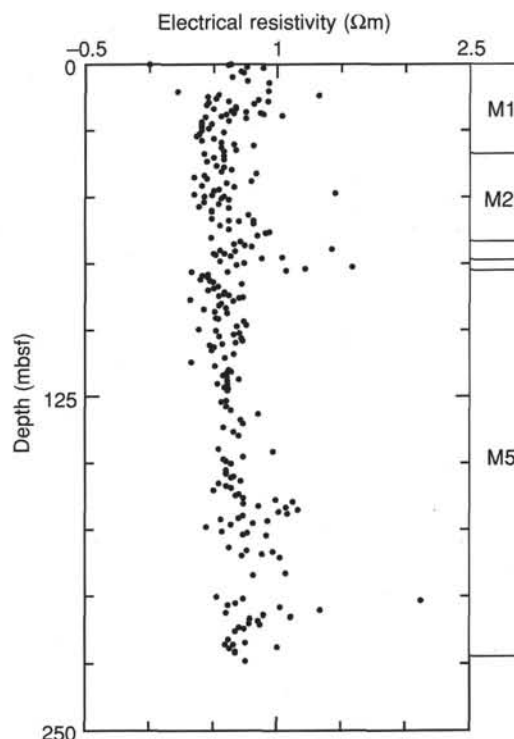


Figure 57. Profile of calculated electrical resistivity corresponding with the mechanical units in the sediments from Site 918.

and pore fluid data at 142.8 (Figs. 60A and 60B) and at 190.9 mbsf (Figs. 61A and 61B) indicate that good quality data were obtained. These data can be summarized as follows:

Depth (mbsf)	Temperature (°C)	Comments
49.3	6.3	Good pore fluid; tentative temperature
98.6	(6.39)	Tool not in formation
142.8	1.42	Good record
190.9	13.68	Good record

Temperature data also are presented in Figure 62 as a function of depth. The gradient of temperature, which fits the two deepest points and the bottom-water temperature of 3.2°C (Sverdrup et al., 1942), indicates a slope of 5.56°C/100 m. Thermal conductivity data in the upper 400 m depth range are presented in Figure 63. These data yield an average of  $1.31 \pm 0.15$  W/(m-K). Thus, a heat-flow value of about  $74.5 \pm 8$  mWm<sup>-2</sup> is obtained. Below 400 mbsf, thermal conductivities average about 1.81 W/(m-K), thus leading to a slightly different temperature gradient. This then leads to the temperature gradient presented in Figure 62B. In principle, a correction might be necessary

**Table 18. Electric resistance measurements and calculated resistivity and formation factor in sediments recovered from Site 918.**

Core, section, interval (cm)	Depth (mbsf)	Resistance (Ω)	Resistivity (Ωm)	Formation factor	Core, section, interval (cm)	Depth (mbsf)	Resistance (Ω)	Resistivity (Ωm)	Formation factor
152-918A-					8H-3, 30	62.10	53.50	1.03698	4.61082
1H-1, 11	0.11	11.40	0.220963	0.98249	8H-3, 117	62.97	45.40	0.879977	3.91273
1H-2, 26	1.26	28.00	0.542717	2.41314	8H-4, 25	63.55	28.30	0.548532	2.43899
1H-CC, 8	1.68	23.60	0.457433	2.03393	8H-4, 110	64.40	38.20	0.740421	3.29221
2H-1, 96	2.76	27.00	0.523334	2.32695	8H-5, 40	65.20	35.20	0.682273	3.03366
2H-2, 25	3.55	32.00	0.620248	2.75787	8H-5, 120	66.00	81.80	1.58551	7.04981
2H-2, 100	4.30	24.00	0.465186	2.06840	8H-6, 25	66.55	62.70	1.21530	5.40370
2H-3, 25	5.05	23.00	0.445803	1.98222	8H-6, 120	67.50	55.20	1.06993	4.75733
2H-3, 125	6.05	35.00	0.678396	3.01642	9H-1, 20	68.50	17.00	0.329507	1.46512
2H-4, 30	6.55	26.00	0.503952	2.24077	9H-1, 124	69.54	23.50	0.455495	2.02531
2H-4, 125	7.50	33.00	0.639631	2.84405	9H-2, 16	69.96	21.40	0.414791	1.84433
2H-5, 30	8.10	34.00	0.659014	2.93024	9H-2, 33	70.13	23.45	0.454526	2.02100
2H-5, 125	9.05	31.00	0.600865	2.67169	9H-2, 124	71.04	20.40	0.395408	1.75814
2H-6, 25	9.55	29.00	0.562100	2.49932	9H-2, 135	71.15	24.40	0.472939	2.10288
2H-6, 75	10.05	22.50	0.436112	1.93913	9H-3, 20	71.50	25.70	0.498137	2.21492
2H-7, 25	10.55	32.00	0.620248	2.75787	9H-3, 86	72.16	37.20	0.721039	3.20603
3H-1, 30	11.60	21.00	0.407038	1.80985	9H-3, 130	72.60	27.76	0.538065	2.39245
3H-2, 50	12.45	25.00	0.484569	2.15459	9H-4, 37	73.17	25.90	0.502013	2.23215
3H-2, 110	13.05	21.00	0.407038	1.80985	9H-4, 117	73.97	23.70	0.459371	2.04255
3H-3, 50	13.95	24.00	0.465186	2.06840	9H-5, 36	74.66	30.20	0.585359	2.60274
3H-3, 110	14.55	21.00	0.407038	1.80985	9H-5, 115	75.45	30.00	0.581483	2.58550
3H-4, 50	15.45	30.00	0.581483	2.58550	9H-6, 36	76.16	27.90	0.540779	2.40452
3H-4, 110	16.05	20.00	0.387655	1.72367	9H-6, 112	76.92	32.10	0.622186	2.76649
3H-5, 50	16.95	19.00	0.368272	1.63749	9H-7, 37	77.67	36.20	0.701656	3.11984
3H-5, 110	17.55	26.00	0.503952	2.24077	9H-CC, 15	78.11	37.60	0.728792	3.24050
3H-6, 50	18.45	21.00	0.407038	1.80985	10H-1, 17	77.97	16.50	0.319815	1.42203
3H-6, 110	19.05	29.00	0.562100	2.49932	10H-1, 128	79.08	33.90	0.657075	2.92162
3H-7, 25	19.70	34.00	0.659014	2.93024	10H-2, 13	79.43	29.00	0.562100	2.49932
3H-7, 50	19.95	42.00	0.814076	3.61971	10H-2, 80	80.10	28.20	0.546594	2.43037
4H-1, 60	21.40	29.00	0.562100	2.49932	10H-3, 05	80.85	31.00	0.600865	2.67169
4H-1, 110	21.90	35.00	0.678396	3.01642	10H-3, 50	81.30	21.90	0.424482	1.88742
4H-2, 25	22.55	30.00	0.581483	2.58550	10H-3, 112	81.92	26.50	0.513643	2.28386
4H-2, 110	23.40	22.00	0.426421	1.89604	10H-4, 31	82.61	31.50	0.610557	2.71478
4H-3, 40	24.20	30.00	0.581483	2.58550	10H-4, 113	83.43	26.90	0.521396	2.31834
4H-3, 110	24.90	26.00	0.503952	2.24077	10H-5, 38	84.18	28.00	0.542717	2.41314
4H-4, 40	25.70	30.00	0.581483	2.58550	10H-5, 125	85.05	38.18	0.740034	3.29049
4H-4, 110	26.40	23.00	0.445803	1.98222	10H-6, 37	85.67	39.10	0.757866	3.36977
4H-5, 40	27.20	27.00	0.523334	2.32695	10H-6, 113	86.43	35.40	0.686150	3.05090
4H-5, 110	27.90	30.00	0.581483	2.58550	10H-7, 38	87.18	20.10	0.389593	1.73229
4H-6, 40	28.70	33.00	0.639631	2.84405	10H-7, 15	86.95	26.90	0.521396	2.31834
4H-6, 110	29.40	29.00	0.562100	2.49932	10H-CC, 14	87.64	36.40	0.705532	3.13708
4H-7, 40	30.20	43.00	0.833458	3.70589	11H-1, 22	87.52	34.15	0.661921	2.94317
5H-1, 40	30.70	22.00	0.426421	1.89604	11H-1, 125	88.55	28.10	0.544655	2.42176
5H-1, 110	31.40	18.00	0.348890	1.55130	11H-2, 25	89.05	37.10	0.719100	3.19741
5H-2, 40	32.20	23.00	0.445803	1.98222	11H-2, 125	90.05	37.70	0.730730	3.24912
5H-2, 110	32.90	41.00	0.794693	3.53352	11H-3, 25	90.55	34.70	0.672582	2.99057
5H-3, 38	33.68	31.00	0.600865	2.67169	11H-3, 125	91.55	29.38	0.569465	2.53207
5H-3, 110	34.40	21.00	0.407038	1.80985	11H-4, 20	92.00	24.46	0.474102	2.10805
5H-4, 38	35.18	34.00	0.659014	2.93024	11H-4, 120	93.00	26.20	0.507828	2.25801
5H-4, 110	35.90	28.00	0.542717	2.41314	11H-5, 20	93.50	25.00	0.484569	2.15459
5H-5, 40	36.70	26.00	0.503952	2.24077	11H-6, 60	95.40	34.00	0.659014	2.93024
5H-6, 40	38.20	18.00	0.348890	1.55130	11H-6, 88	95.68	30.60	0.593112	2.63721
5H-6, 110	38.90	25.00	0.484569	2.15459	11H-7, 25	96.55	16.80	0.325630	1.44788
5H-7, 40	39.70	30.00	0.581483	2.58550	12H-1, 125	98.05	26.36	0.510929	2.27180
6H-1, 70	40.50	22.00	0.426421	1.89604	12H-2, 30	98.60	32.06	0.621411	2.76304
6H-1, 130	41.10	29.00	0.562100	2.49932	12H-2, 125	99.55	33.00	0.639631	2.84405
6H-2, 42	41.72	32.00	0.620248	2.75787	12H-3, 36	100.16	31.20	0.604742	2.68892
6H-2, 124	42.54	22.00	0.426421	1.89604	12H-3, 125	101.05	29.80	0.577606	2.56827
6H-3, 25	43.05	28.00	0.542717	2.41314	12H-4, 27	101.57	31.18	0.604354	2.68720
6H-3, 127	44.07	20.00	0.387655	1.72367	12H-4, 110	102.40	36.00	0.697779	3.10261
6H-4, 25	44.55	32.00	0.620248	2.75787	12H-5, 29	103.09	31.50	0.610557	2.71478
6H-4, 124	45.54	25.00	0.484569	2.15459	12H-5, 109	103.89	27.40	0.531088	2.36143
6H-5, 25	46.05	25.00	0.484569	2.15459	12H-6, 32	104.62	31.50	0.610557	2.71478
6H-5, 125	47.05	40.00	0.775310	3.44734	12H-6, 91	105.21	30.40	0.589236	2.61998
6H-6, 30	47.60	25.00	0.484569	2.15459	12H-7, 32	105.62	31.90	0.618310	2.74925
6H-6, 120	48.50	32.00	0.620248	2.75787	12H-CC, 34	106.27	31.70	0.614433	2.73202
6H-7, 20	49.00	36.00	0.697779	3.10261	13H-1, 125	107.55	31.00	0.600865	2.67169
6H-7, 55	49.35	42.00	0.814076	3.61971	13H-2, 125	109.05	29.00	0.562100	2.49932
6H-CC, 12	49.65	42.00	0.814076	3.61971	13H-3, 125	110.55	31.00	0.600865	2.67169
7H-1, 40	49.70	28.51	0.552602	2.45709	13H-4, 125	112.05	33.00	0.639631	2.84405
7H-1, 110	50.40	32.00	0.620248	2.75787	13H-5, 125	113.55	44.00	0.852841	3.79207
7H-2, 20	51.00	48.46	0.939288	4.17645	13H-6, 125	115.05	37.00	0.717162	3.18879
7H-2, 110	51.90	47.00	0.910990	4.05062	13H-7, 35	115.65	38.00	0.736545	3.27497
7H-3, 20	52.50	43.52	0.843538	3.75071	14H-1, 36	116.16	30.00	0.581483	2.58550
7H-3, 120	53.50	24.82	0.481080	2.13907	14H-1, 125	117.05	34.00	0.659014	2.93024
7H-4, 20	54.00	36.65	0.710378	3.15862	14H-2, 35	117.65	36.00	0.697779	3.10261
7H-4, 120	55.00	34.06	0.660177	2.93541	14H-2, 127	118.57	28.00	0.542717	2.41314
7H-5, 20	55.50	38.50	0.746236	3.31806	14H-3, 35	119.15	50.00	0.969138	4.30917
7H-5, 120	56.50	41.40	0.802446	3.56800	14H-3, 127	120.07	38.00	0.736545	3.27497
7H-6, 120	58.00	28.49	0.552215	2.45537	14H-4, 35	120.65	30.00	0.581483	2.58550
7H-7, 55	58.85	34.48	0.668317	2.97161	14H-4, 128	121.58	31.00	0.600865	2.67169
7H-CC, 5	59.02	30.39	0.589042	2.61912	14H-5, 35	122.15	33.00	0.639631	2.84405
8H-1, 4	58.84	26.00	0.503952	2.24077	14H-5, 107	122.87	31.00	0.600865	2.67169
8H-1, 110	59.90	26.70	0.517520	2.30110	15H-1, 125	126.55	31.00	0.600865	2.67169
8H-2, 26	60.56	32.70	0.633816	2.81820	15H-2, 35	127.15	31.00	0.600865	2.67169

Table 18 (continued).

Core, section, interval (cm)	Depth (mbsf)	Resistance ( $\Omega$ )	Resistivity ( $\Omega$ m)	Formation factor	Core, section, interval (cm)	Depth (mbsf)	Resistance ( $\Omega$ )	Resistivity ( $\Omega$ m)	Formation factor
15H-3, 35	128.65	34.00	0.659014	2.93024	23X-5, 120	207.00	31.90	0.618310	2.74925
15H-4, 35	130.15	33.00	0.639631	2.84405	23X-6, 30	207.60	39.20	0.759804	3.37839
15H-5, 35	131.65	37.00	0.717162	3.18879	23X-6, 90	208.20	45.90	0.889668	3.95582
16H-1, 35	133.65	28.00	0.542717	2.41314	24X-1, 25	208.95	37.00	0.717162	3.18879
16H-2, 35	135.15	31.00	0.600865	2.67169	24X-1, 125	209.95	37.80	0.732668	3.25774
16H-3, 35	136.65	33.00	0.639631	2.84405	24X-2, 25	210.45	33.50	0.649322	3.88715
16H-4, 35	138.15	26.00	0.503952	2.24077	24X-2, 125	211.45	39.50	0.765619	3.40425
16H-5, 35	139.65	36.00	0.697779	3.10261	24X-3, 25	211.95	48.10	0.932311	4.14543
17H-2, 35	144.65	35.00	0.678396	3.01642	24X-3, 125	212.95	48.00	0.930372	4.13681
17H-2, 125	145.55	38.00	0.736545	3.27497	24X-4, 25	215.05	68.30	1.323840	5.88633
17H-4, 35	147.65	51.00	0.988521	4.39536	24X-5, 115	215.85	44.00	0.852841	3.79207
17H-4, 125	148.55	58.00	1.12420	4.99864	24X-6, 78	216.98	48.00	0.930372	4.13681
17H-5, 35	149.15	38.00	0.736545	3.27497	24X-7, 53	217.73	42.30	0.819891	3.64556
17H-5, 125	150.05	44.00	0.852841	3.79207	25X-1, 25	217.85	35.00	0.678396	3.01642
18H-1, 20	152.50	55.00	1.06605	4.74009	25X-1, 125	218.85	39.00	0.755928	3.36116
18H-1, 119	153.49	60.00	1.16297	5.17101	25X-2, 25	219.35	45.00	0.872224	3.87826
18H-2, 29	154.09	52.30	1.01372	4.50740	25X-2, 125	220.35	46.00	0.891607	3.96444
18H-2, 120	155.00	56.00	1.08543	4.82628	25X-3, 30	220.90	53.50	1.036980	4.61082
18H-3, 22	155.52	38.00	0.736545	3.27497	25X-5, 30	223.90	39.00	0.755928	3.36116
18H-3, 127	156.57	36.00	0.697779	3.10261					
18H-4, 80	157.60	29.00	0.562100	2.49932	152-918B-				
18H-5, 25	158.55	48.00	0.930372	4.13681	1H-1, 1	0.01	20.98	0.484963	2.15634
18H-5, 104	159.34	42.00	0.814076	3.61971	1H-1, 52	0.52	12.92	0.298652	1.32793
18H-6, 44	160.24	33.00	0.639631	2.84405	1H-1, 120	1.20	14.40	0.332863	1.48004
18H-7, 22	161.52	23.00	0.445803	1.98222	1H-2, 20	1.70	13.40	0.309748	1.37726
19H-1, 25	162.05	29.50	0.571791	2.54241	1H-2, 120	2.70	15.70	0.362913	1.61366
19H-1, 125	163.05	39.60	0.767557	3.41287	1H-3, 27	3.27	12.00	0.277386	1.23337
19H-2, 40	163.70	38.00	0.736545	3.27497	1H-4, 45	4.95	16.50	0.381406	1.69588
19H-2, 113	164.43	47.30	0.916804	4.07648	1H-5, 30	6.30	17.50	0.404521	1.79866
19H-3, 25	165.05	32.40	0.628001	2.79234	2H-1, 30	7.10	17.50	0.404521	1.79866
19H-3, 125	166.05	39.41	0.763874	3.39649	2H-3, 30	10.10	18.50	0.427637	1.90144
19H-4, 20	166.50	50.10	0.971076	4.31779	2H-4, 50	11.80	22.00	0.508541	2.26118
19H-4, 124	167.54	45.70	0.885792	3.93859	2H-5, 77	13.57	19.00	0.439194	1.95283
19H-5, 30	168.10	37.50	0.726853	3.23188	2H-5, 128	14.08	22.40	0.517787	2.30229
19H-5, 123	169.03	52.80	1.02341	4.55049	2H-6, 75	15.05	24.60	0.568641	2.52841
19H-6, 37	169.67	55.20	1.06993	4.75733	3H-1, 60	16.90	18.85	0.435727	1.93742
19H-6, 125	170.55	42.00	0.814076	3.61971	3H-2, 26	18.06	20.20	0.466933	2.07617
19H-7, 20	171.00	27.30	0.529149	2.35281	3H-2, 65	18.45	23.70	0.547837	2.43590
19H-CC, 20	171.56	37.90	0.734606	3.26635	3H-2, 120	19.00	18.30	0.423014	1.88089
20X-1, 110	172.40	34.70	0.672582	2.99057	3H-3, 20	19.50	17.65	0.407989	1.81408
20X-2, 20	173.00	31.80	0.616372	2.74063	3H-3, 120	20.50	22.00	0.508541	2.26118
20X-2, 115	173.95	52.80	1.023410	4.55049	3H-5, 20	22.50	26.30	0.607938	2.70313
20X-3, 26	174.30	69.00	1.337410	5.94666	3H-5, 120	23.50	23.50	0.543214	2.41535
20X-3, 125	175.55	31.00	0.600865	2.67169	3H-6, 20	24.00	28.30	0.654169	2.90869
20X-4, 24	176.04	46.30	0.897422	3.99030	3H-6, 120	25.00	26.50	0.612561	2.72369
20X-4, 110	176.90	57.00	1.104820	4.91246	3H-7, 20	25.50	26.74	0.618108	2.74836
20X-CC, 4	177.02	40.70	0.788878	3.50767					
21X-1, 25	181.75	44.00	0.852841	3.79207	152-918C-				
21X-1, 125	182.75	40.50	0.785002	3.49043	1H-1, 45	26.25	24.60	0.621149	2.76188
21X-2, 25	183.25	45.00	0.872224	3.87826	1H-1, 120	27.00	25.80	0.651449	2.89660
21X-2, 125	184.25	36.40	0.705532	3.13708	1H-2, 20	27.50	22.00	0.555499	2.46997
21X-3, 23	184.73	38.60	0.748174	3.32668	1H-2, 120	28.50	19.30	0.487324	2.16684
21X-3, 98	185.48	35.00	0.678396	3.01642	1H-3, 25	29.05	27.50	0.694374	3.08747
22X-1, 48	191.38	32.00	0.620248	2.75787	1H-3, 72	29.52	35.10	0.886274	3.94073
22X-1, 125	192.15	39.00	0.755928	3.36116	1H-3, 124	30.04	21.40	0.540349	2.40261
23X-1, 29	200.09	30.70	0.595051	2.64583	1H-4, 30	30.60	19.20	0.484799	2.15561
23X-1, 123	201.03	34.00	0.659014	2.93024	1H-4, 110	31.40	26.00	0.656499	2.91906
23X-2, 34	201.64	51.80	1.004030	4.46430	1H-5, 10	31.90	24.00	0.605999	2.69452
23X-2, 120	202.50	32.60	0.631878	2.80958	1H-5, 25	32.05	27.00	0.681749	3.03133
23X-3, 40	203.20	35.00	0.678396	3.01642	1H-5, 73	32.53	31.00	0.782749	3.48042
23X-3, 110	203.90	35.00	0.678396	3.01642	1H-5, 110	32.90	17.00	0.429249	1.90861
23X-4, 90	205.20	38.90	0.753989	3.35254	1H-6, 25	33.55	24.00	0.605999	2.69452
23X-5, 25	206.05	32.80	0.635754	2.82682	1H-6, 87	34.17	22.60	0.570649	2.53734
					1H-CC, 10	35.31	39.00	0.984749	4.37859

because of cooling caused by the rapid sediment loading in the upper part of the hole. However, a 1-m.y. hiatus at about 70 mbsf would have minimized this loading effect.

## Discussion

The heat-flow estimate for Site 918 fits well with the regional estimates of heat flow in this region. During DSDP Legs 48 and 49, data were obtained both on the Rockall Plateau and in the Irminger Basin. During Leg 48, measurements were performed at Sites 403 and 406 on the Rockall Plateau, yielding values of 64.9 and 78.9  $\text{mWm}^{-2}$ , respectively. Sites 407 and 408 in the Irminger Basin indicated heat-flow values of 66.4 and 60.2  $\text{mWm}^{-2}$  for Sites 407 and 408. For a 55-m.y.-old crust, a theoretical value of 60 to 70  $\text{mWm}^{-2}$  has been estimated (Parsons and Sclater, 1977; Stein and Stein, 1992). Thus, if

the age of the basalts of Site 918 is about 55 Ma, then the heat flow is somewhat high. However, the observed heat-flow values at Site 918 are consistent with the thermal asymmetric models of seafloor spreading in the Norwegian-Greenland Sea (Langseth and Zielinski, 1974) and are relatively lower than heat-flow values observed along the transtensional volcanic margins of the eastern Norwegian-Greenland Sea (Okay and Crane, 1993; Okay, 1994). In addition, if fluid movement occurs through the sandstones below 825 mbsf (as suggested by the pore water chemistry, see "Inorganic Geochemistry" section, this chapter), then, of course, these fluids might be slightly higher in temperature and thus cause a slightly higher temperature gradient than expected (4.85°C/100 m).

## Ms 152IR-111

**NOTE:** For all sites drilled, core-description forms ("barrel sheets") can be found in Section 4, beginning on page 303. Forms containing smear-slide data can be found in Section 5, beginning on page 925. Thin-section data are given in Section 6, beginning on page 947. GRAPE, Index property, MAGSUS and Natural gamma-ray data are presented on CD-ROM (back pocket).

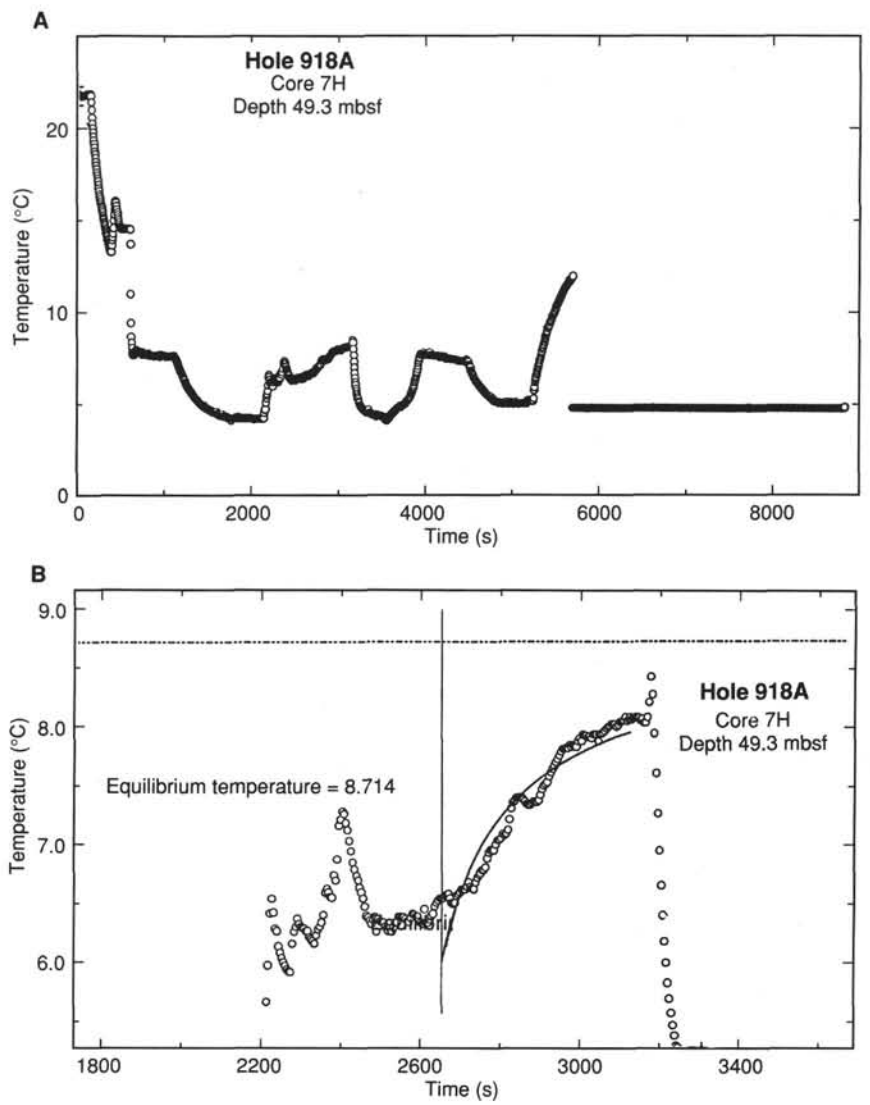


Figure 58. **A.** Temperature record of WSTP at 49.3 mbsf. **B.** Expanded temperature record at 49.3 mbsf; please note irregular behavior of temperature in later part of the record.

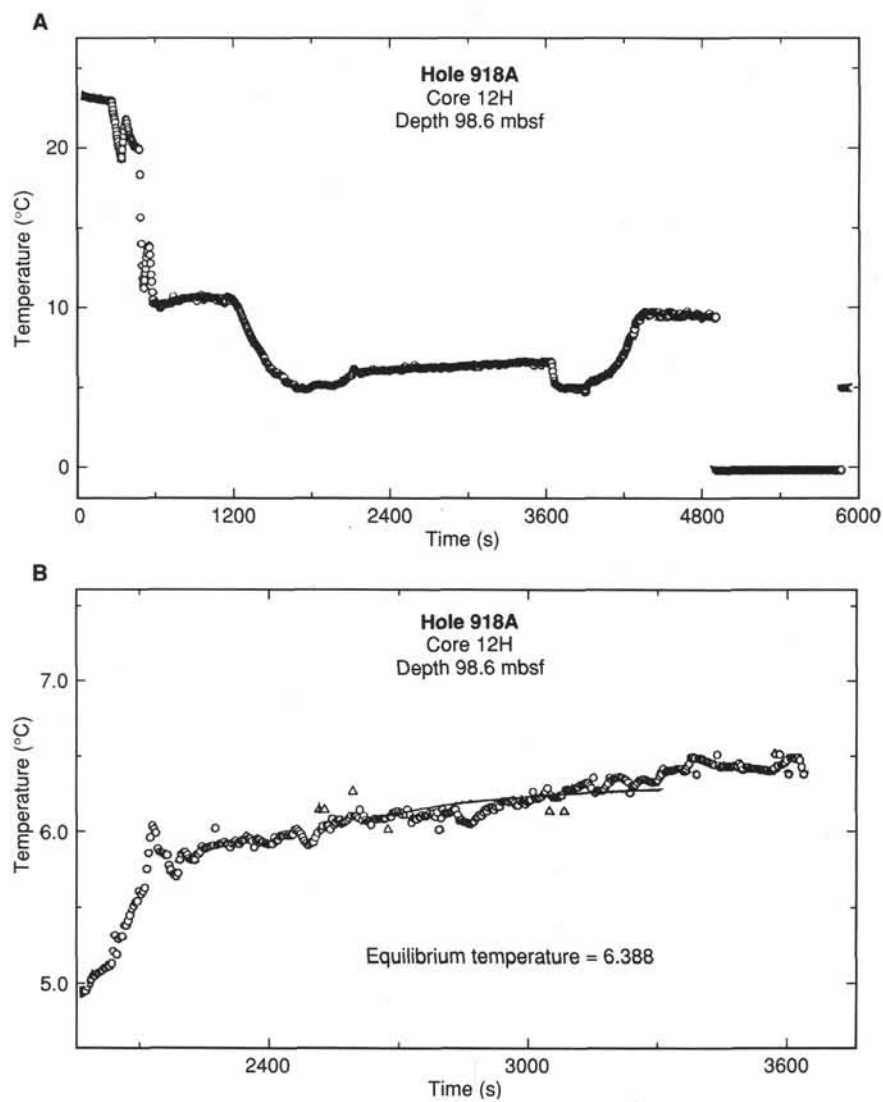


Figure 59. A. Temperature record of WSTP at 98.6 mbsf. B. Expanded temperature record at 98.6 mbsf.

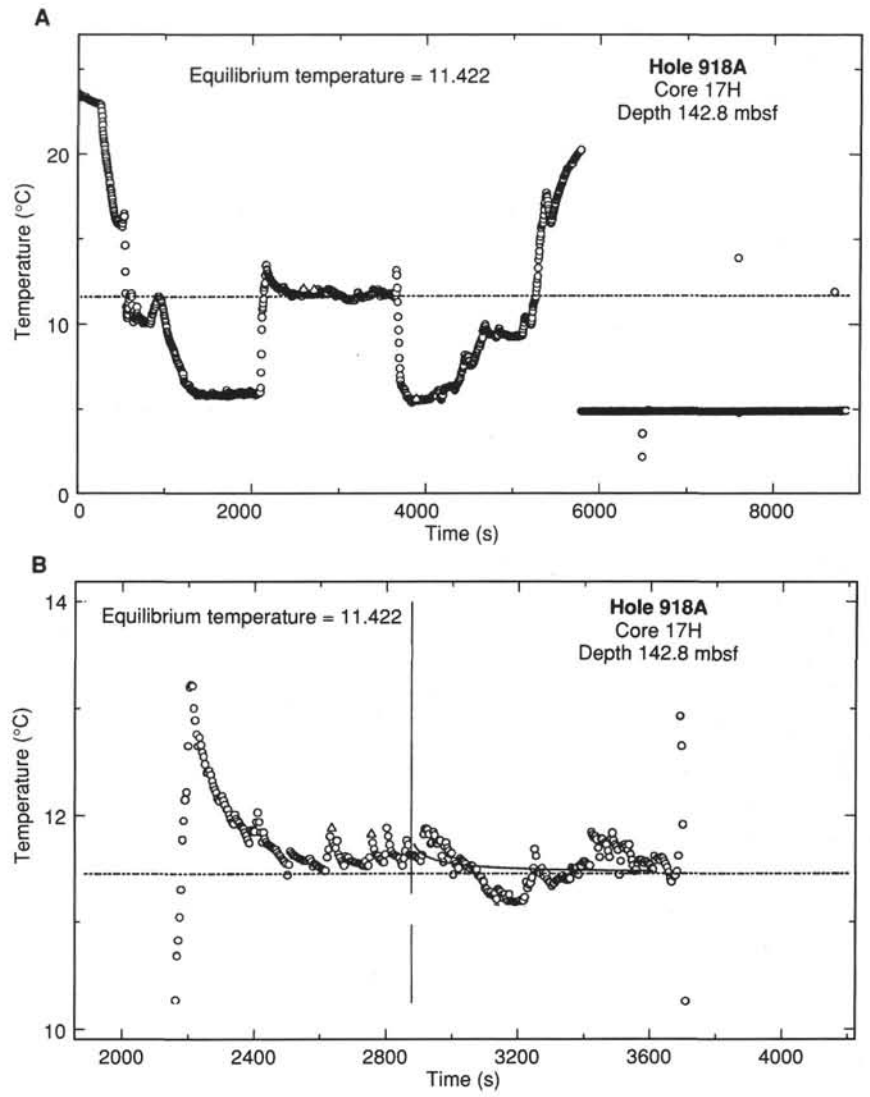


Figure 60. A. Temperature record of WSTP at 142.8 mbsf. B. Expanded temperature record at 142.8 mbsf.

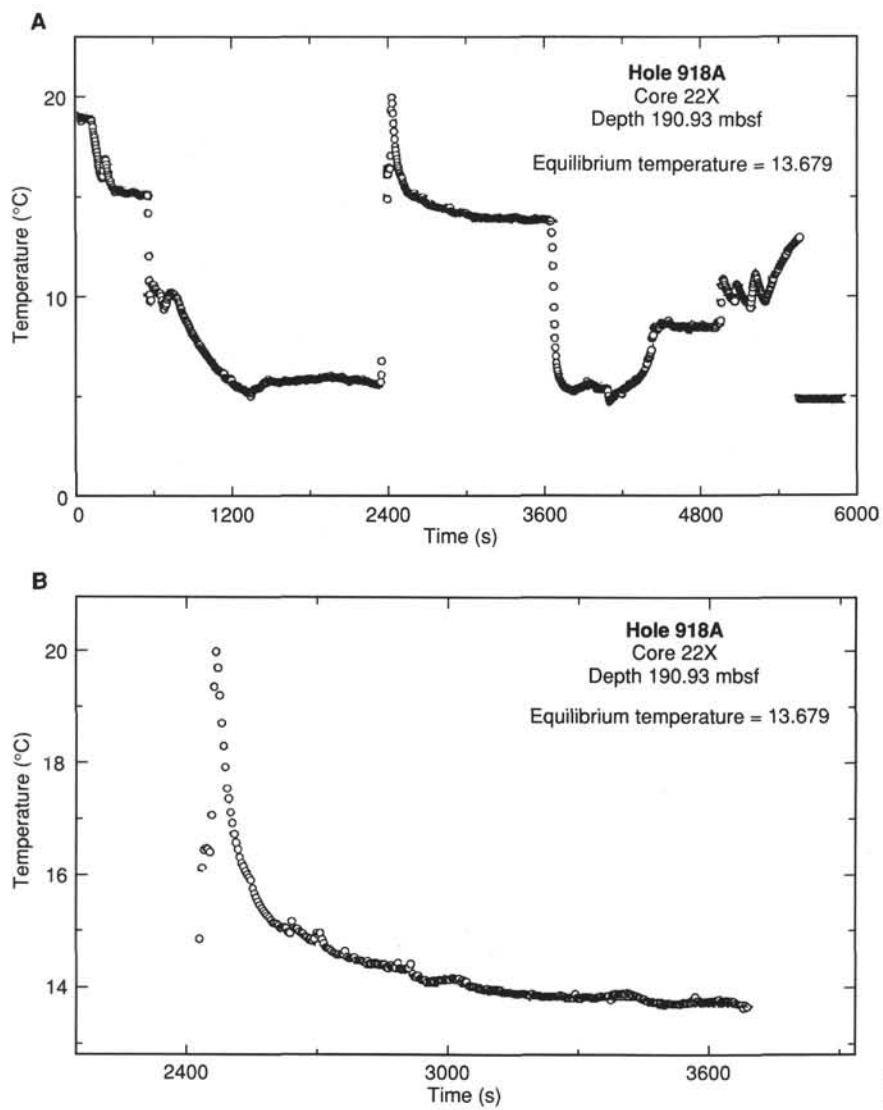


Figure 61. A. Temperature record of WSTP at 190.93 mbsf. B. Expanded temperature record at 190.93 mbsf.

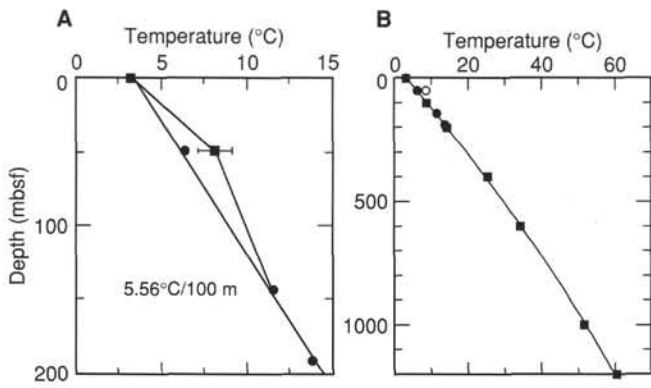


Figure 62. **A.** Profile of temperature vs. depth at Hole 918A. Note estimated temperature of 6.3°C at 49.3 mbsf (see text). **B.** Suggested temperature gradient at Site 918, estimated from constant heat flow and thermal conductivities. Open circle = rejected measurement at 49.3 mbsf (see Fig. 62A); closed circles = accepted data; squares = calculated data.

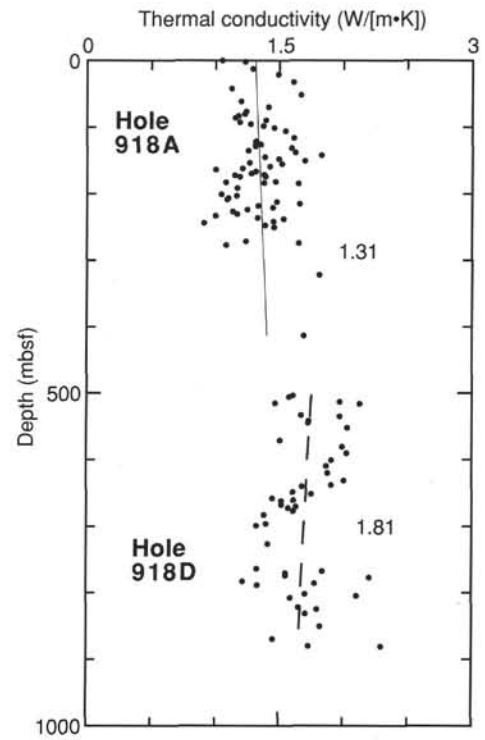


Figure 63. Measured thermal conductivities in Site 918 sediments, including average thermal conductivities in the depth ranges 0–400 and 400–900 mbsf.